Mono- and Dianionic Carbaborane Ligands and Their Transition Metal Complexes

Ewan J. M. Hamilton

Thesis Presented for the Degree of
Doctor of Philosophy
University of Edinburgh
1990

Declaration

Except where specific reference is made to other sources, the work presented in this thesis is the original work of the author. It has not been submitted, in whole or in part, for any other degree. Certain of the results have been published, or have been accepted for publication (see Appendix 2).

Ewan J. M. Hamilton

Dedicated to my parents and family for their unfailing support.

I devoted a day to a coarse sifting of the chicken shit, and another two trying to oxidize the acid contained in it into alloxan. The virtue and patience of ancient chemists must have been superhuman, or perhaps my inexperience with organic preparations was boundless. All I got were foul vapors, boredom, humiliation, and a black and murky liquid which irremediably plugged up the filters and displayed no tendency to crystallize, as the text declared it should. The shit remained shit, and the alloxan and its resonant name remained a resonant name. That was not the way to get out of the swamps: by what path would I therefore get out, I the discouraged author of a book which seemed good to me but which nobody read? Best to return among the colorless but safe schemes of inorganic chemistry.

Primo Levi, from *The Periodic Table*

Acknowledgements

First and foremost, I would like to thank my supervisor, Dr. Alan Welch, without whose assistance, encouragement, enthusiasm and optimism this work could not have been done.

Thanks are also due to John Millar, Heather Grant and Dr. David Reed, who obtained n.m.r. spectra, and Elaine M^{c}Dougall, who performed the elemental analyses.

The help of Dr. Ruth Sorbie and Ken Taylor was invaluable in obtaining and interpreting electrochemical and spectroelectrochemical data.

Assistance and encouragement have always been readily forthcoming from those who have worked over the years in laboratories 290-293, and although space limits a full "roll of honour" here, all help and advice has been greatly appreciated.

Finally, thanks are due to the University of Edinburgh for the use of facilities and to S.E.R.C. for financial support.

Abstract

Chapter 1 consists of a brief overview of transition metal cyclopentadienyl chemistry and of the chemistry of carbametallaborane species derived from [7,8-*nido*-$C_2B_9H_{11}$]$^{2-}$, with specific reference to the bonding modes commonly adopted by each ligand to transition metal fragments. The forms of the π-MO's of [C_5H_5]$^-$, [$C_2B_9H_{11}$]$^{2-}$ and of the monoanionic ligand [9-SMe_2-7,8-$C_2B_9H_{10}$]$^-$ (or [carb']$^-$), as obtained by extended Huckel molecular orbital (EHMO) calculations, are also presented.

In *Chapter 2*, the structure of [7,8-$C_2B_9H_{12}$]$^-$, **(1)**, is presented, showing an *endo* -H atom, rather than the commonly accepted μ-H, associated with the open ligand face.This result is supported by those of n.m.r. and theoretical studies. Isolobal replacement of the *endo*-terminal hydrogen atom by a {PPh_3Au^+} fragment leads to complex **(2)**, [10-*endo*-(PPh_3Au)-7,8-*nido*-$C_2B_9H_{11}$]$^-$, which has also been studied crystallographically. Structural trends within the series **(1)**, **(2)** and [$PPh_3Cu(C_2B_9H_{11})$]$^-$ have been rationalised *via* the results of EHMO calculations.

Chapter 3 presents the structure of [10,11-μ-H-9-SMe_2-7,8-*nido*-$C_2B_9H_{10}$], **(3)**, the protonated precursor to the monoanionic ligand [carb']$^-$. The molecule possesses an asymmetric bridging H atom on its open face, a structural feature whose origin may be traced using MO calculations at the extended Huckel level. The (triphenylphosphine)gold(I) and (triphenylphosphine)copper(I) derivatives of [carb']$^-$, **(4)** and **(5)**, have been prepared, and their structures determined by *X*-ray methods. In all three compounds, the SMe_2 substituent appears to adopt a preferred conformation, and it is suggested that this is allied to an intramolecular electrostatic interaction. Analysis of structural patterns within **(3)**, **(4)** and **(5)** reveals different trends to those observed for the related series in the previous chapter. These differences may be rationalised by frontier MO considerations.

Chapter 4 comprises a comparative structural, spectral and theoretical study of the analogous complexes (carb')$Mn(CO)_3$, (**6**), and $CpMn(CO)_3$, (**7**). The net electronic properties of the anionic ligands in the two complexes are shown to be highly similar, by consideration of infra-red carbonyl stretching frequencies and C-O distances determined by *X*-ray experiments. Extended Huckel and extended Huckel/fragment MO calculations suggest that the very slightly lower ν_{CO} observed for (**6**) is a result of slightly greater e^--donation into (primarily) the *e* acceptor orbitals of the $\{Mn(CO)_3\}$ fragment by the carbaborane ligand than by Cp. This results in limitation of σ-donation by the carbonyl ligands, giving the slightly lower ν_{CO} observed.

Chapter 5 details the preparation of the bis(carb') analogue of ferrocene, Fe(carb')$_2$, (**8**), and its structural characterisation as the *E*-isomer, where both (chiral) ligands are of the same optical isomer. The isomeric nature of (**8**) has been shown to be dependent on its method of preparation. Electrochemical work on Fe(carb')$_2$ again shows the net electron-donating properties of [carb'] to be comparable to those of Cp. (**8**) may also be readily oxidised chemically to give the monocation $[Fe(carb')_2]^+$. A second product, Fe(carb')$(C_2B_9H_{10}SMe)$, (**9**), has also been isolated and its structure determined as the *O*-isomer (where the two ligands are of opposite handedness). This, allied to the results of electrochemical studies, allow a mechanism for the formation of (**9**) to be proposed, involving loss of $\{Me^+\}$ from $[Fe(carb')_2]^+$.

Chapter 6 gives details of the experimental procedures leading to the results discussed in the body of the work, and comprises four sections: *1*. Synthetic Methods and Spectral Data, *2*. Crystallographic Techniques, *3*. Molecular Orbital Calculations, and *4*. Electrochemical and Spectroelectrochemical Techniques.

Abbreviations

AO	atomic orbital
BTMA	benzyltrimethylammonium
COSY	correlation spectroscopy
Cp	cyclopentadienyl
Cp^*	pentamethylcyclopentadienyl
dmso	dimethylsulphoxide
EHMO	extended Huckel molecular orbital
EHMO/FMO	extended Huckel/fragment molecular orbital
e.s.d.	estimated standard deviation
Et	ethyl
eV	electron volts
Fc	ferrocene
FMO	fragment molecular orbital
HOMO	highest occupied molecular orbital
LCAO	linear combination of atomic orbitals
LUMO	lowest unoccupied molecular orbital
Me	methyl
MO	molecular orbital
n.m.r.	nuclear magnetic resonance
Ph	phenyl
p.p.m.	parts per million
PSEPT	polyhedral skeletal electron pair theory
SEP	skeletal electron pair
TBA	tetra(n-butyl)ammonium
THF	tetrahydrofuran

Abbreviations for Specific Complexes

(1) $[7,8\text{-}nido\text{-}C_2B_9H_{12}]^-$

(2) $[10\text{-}endo\text{-}(PPh_3Au)\text{-}7,8\text{-}nido\text{-}C_2B_9H_{11}]^-$

(3) $[10,11\text{-}\mu\text{-}H\text{-}9\text{-}SMe_2\text{-}7,8\text{-}nido\text{-}C_2B_9H_{10}]$

(4) $[10,11\text{-}\mu\text{-}(PPh_3Au)\text{-}9\text{-}SMe_2\text{-}7,8\text{-}nido\text{-}C_2B_9H_{10}]$

(5) $[3\text{-}PPh_3\text{-}4\text{-}SMe_2\text{-}3,1,2\text{-}CuC_2B_9H_{10}]$

(6) $[3,3,3\text{-}(CO)_3\text{-}4\text{-}SMe_2\text{-}3,1,2\text{-}MnC_2B_9H_{10}]$

(7) $[(\eta\text{-}C_5H_5)Mn(CO)_3]$

(8) $[commo\text{-}3,3'\text{-}Fe\text{-}4,4'\text{-}(SMe_2)_2\text{-}1,1',2,2'\text{-}(C_2B_9H_{10})_2]$

(9) $[commo\text{-}3,3'\text{-}Fe\text{-}4\text{-}SMe_2\text{-}4'\text{-}SMe\text{-}1,1',2,2'\text{-}(C_2B_9H_{10})_2]$

Contents

Chapter 1

Introduction

Since the inception of carbametallaborane (or metallacarborane) chemistry in the mid-1960's [1,2], there has been drawn an analogy between the $[C_2B_9H_{11}]^{2-}$ (dicarbollide) ligand and the cyclopentadienide ($[C_5H_5]^-$ or Cp^-) anion. A more recent modification [3] of this analogy suggests that $[C_2B_9H_{11}]^{2-}$ may be better compared to the pentamethyl derivative of Cp^-, $C_5Me_5^-$ (or Cp^{*-}), on account of its steric requirements.

The basis of this long-standing analogy rests in the fact that both ions posess 6 π-electrons which occupy similar frontier orbitals associated with open pentagonal faces [4,5], and they therefore ought to show similar bonding capabilities towards (transition) metal fragments. (The π-molecular orbitals of the cyclopentadienyl and dicarbollide anions, as given by extended Hückel calculation (see Chapter 6, section 3) are presented in **Figure 1.5**).

Indeed, early communications, reporting the syntheses and characterisation of the first carbametallaborane species, were guided largely by attempts to prepare carbaborane-containing "versions" of well known cyclopentadienyl complexes, and some of the resulting complexes will be discussed later, by way of introduction to the carbametallaboranes.

The purpose of this introductory chapter is to outline the generally-used methods of synthesis of transition metal cyclopentadienyl and carbametallaborane complexes, and illustrate the types of bonding commonly adopted by each ligand

to transition metal fragments.

However, the validity of the analogy between $[C_2B_9H_{11}]^{2-}$ and Cp^- is ultimately questionable, for although the forms and occupations of the frontier orbitals are similar for each of the ligands, their overall charge differs by one unit. In order to truly compare carbametallaborane species with analogous cyclopentadienyl complexes, we require a *mono*anionic (or *charge compensated*) carbaborane ligand, which might be regarded as a more convincing analogue of Cp^-, given its single charge. Several such species are known [6,7], but the ligand on which attention is focussed in this work is $[9\text{-}SMe_2\text{-}7,8\text{-}C_2B_9H_{10}]^-$ or $[carb']^-$, which will be discussed more fully later in this chapter and, of course, in the body of the work itself.

Chemistry of the Cyclopentadienyl Ligand, $[C_5H_5]$

Introduction

The dramatic developments of the early 1950's, when the discovery of ferrocene, $Fe(\eta\text{-}C_5H_5)_2$, was announced to the world [8,9], made a permanent impact on the face of chemistry. Ferrocene remains to this day arguably the archetypal organometallic complex, and has been the subject of a great deal of investigation [10,11].

The massive interest in organometallic chemistry generated by this discovery led to rapid expansion of the field, which has now developed on a scale no doubt unimagined in the early days [12].

This explosive development is all the more noteworthy when one considers the manner in which the two initial (independent) syntheses of ferrocene were achieved. Both discoveries, made on either side of the Atlantic and published almost simultaneously, were (as is not uncommon in such monumentous cases) serendipitous, stumbled upon in pursuit of altogether different targets.

The group of Miller, Tebboth and Tremaine [8] in the United Kingdom, was attempting to react alkenes with nitrogen over an iron catalyst to give amines. One such experiment, with cyclopentadiene as substrate, resulted in an air-stable compound of empirical formula $C_{10}H_{10}Fe$, although the significance of this (to chemists in pursuit of a different goal) was not immediately recognised, and a few years elapsed before the work was completed and published.

Meanwhile in the U.S.A., Kealy and Pauson [9] were working on the synthesis of fulvalene. One synthetic strategy involved reaction of cyclopentadienylmagnesiumbromide with $FeCl_3$ (as an oxidising agent), with the intention of oxidative coupling of two of the organic groups to yield the desired product. Again however, a surprisingly stable organic compound of iron, undoubtedly of stoichiometry $C_{10}H_{10}Fe$, was obtained.

In neither of these original publications, however, was the correct structure proposed for bis(cyclopentadienyl)iron, but rather the structures postulated contained σ-bonded representations, in keeping with previously known organometallic species, such as phenyls, simple alkyls etc.. Very shortly after the initial communications, which had evidently aroused great interest, there appeared publications outlining the realisation of the true nature of the complex [13,14], *viz* $(\eta\text{-}C_5H_5)_2Fe$, with each cyclopentadienyl ligand bonded

equally through all five carbons to the iron, as shown in **Figure 1.1** .

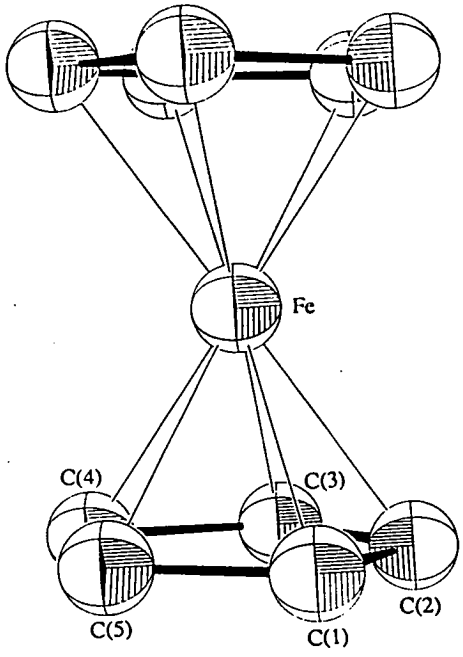

Figure 1.1

Research interest in ferrocene (and its derivatives and analogues) then diversified along two main paths: (i) Organic chemistry of the (aromatic) $[C_5H_5]^-$ ligands, and (ii) Extension of the principle of "sandwich bonding" to other transition metals and development of the chemistry of their η-cyclopentadienyl complexes.

Complexes of the cyclopentadienide anion, $(C_5H_5)^-$, comprise a massive wealth of published material, underlining the continuing interest in their chemistry. Any attempt to be remotely exhaustive in the description of this work is, to say the least, outwith the scope of this chapter. Therefore only a few complexes of specific interest will be discussed, in order to illustrate some aspects of transition metal cyclopentadienyl chemistry.

η-Bonded Cyclopentadienyl Ligands

Following the accidental discoveries of ferrocene, more direct methods of synthesis were soon developed for η-C_5H_5 complexes [15]. The most general synthetic strategy involves reaction of alkali metal cyclopentadienides with halides (or other complexes) of the appropriate (transition) metal, *e.g.*

$$2Na[C_5H_5] + MCl_2 \text{ ---> } [M(\eta\text{-}C_5H_5)_2] + 2NaCl$$

$$Na[C_5H_5] + W(CO)_6 \text{ ---> } Na[(\eta\text{-}C_5H_5)W(CO)_3]$$

η-ligation of cyclopentadienyl ligands to transition metals is still probably best exemplified by ferrocene and the other metallocenes.

Bis(cyclopentadienyl) complexes of a large number of transition metals were prepared in the early to mid-1950's [16-19], many of which do not obey the 18 electron rule. These include the first row complexes VCp_2 ($15e^-$), $CrCp_2$ ($16e^-$), $CoCp_2$ ($19e^-$) and $NiCp_2$ ($20e^-$), each of which is isostructural [20-23] at ambient temperature with the stable $18e^-$ ferrocene species. (The corresponding manganese complex differs from these, however, for although it possesses a sandwich-type structure [24], the bonding has been shown to be essentiallly ionic in character).

Analogous compounds of a number of 2nd and 3rd row metals are also known, for example ruthenocene [16], rhodocene [25], osmocene [26] and bis(cyclopentadienyl) iridium [25].

Metal-ligand bonding in the metallocenes is *via* interaction of the π-molecular

orbitals of the cyclopentadienide anions (details of which are presented and discussed later) with the metal valence orbitals.

The molecular orbital scheme for ferrocene [27] is shown in **Figure 1.2**, comprising interactions of the ligand group orbitals of $2(C_5H_5)$ (staggered conformation) with the iron 3d, 4s and 4p orbitals of appropriate symmetry.

As is easily seen in **Figure 1.2**, the 18 electrons in ferrocene occupy the 9 lowest (bonding) molecular orbitals, accounting for the stable structure observed. The relative instability (and greater reactivity) of the 19 and 20-electron cobaltocene and nickelocene species is readily understood, population of the antibonding a_{1g}" level being undesirable on a purely energetic basis.

Detailed analysis of these orbitals is not necessary at this stage, although the scheme serves to illustrate the nature of the bonding in $FeCp_2$ (and indeed in the metallocenes in general). The major contribution to the bonding between the metal and ligands is from the bonding e_{1g} and e_{1u} MO's. Filling of these orbitals in ferrocene represents, formally, electron donation from the ligands to the metal. The higher-lying (only weakly bonding) e_{2g} pair is derived from combination of the 2 metal *xy*-plane d-orbitals with empty orbitals of the $(Cp^-)_2$ ligand set, and occupation of this degenerate pair represents metal to ligand back-donation, *i.e.* slight π-acidity of the organic ligands.

The 18, 19 and 20-electron configurations of ferrocene, cobaltocene and nickelocene have clear effects on the chemistry each undergoes. The chemistry of $Fe(\eta\text{-}C_5H_5)_2$ is dominated by the organic chemistry of its cyclopentadienyl ligands, which are susceptible to a wide range of reactions typical of aromatic species, such as Friedel-Crafts acylation, alkylation etc..

Figure 1.2 Molecular Orbital Scheme for Ferrocene

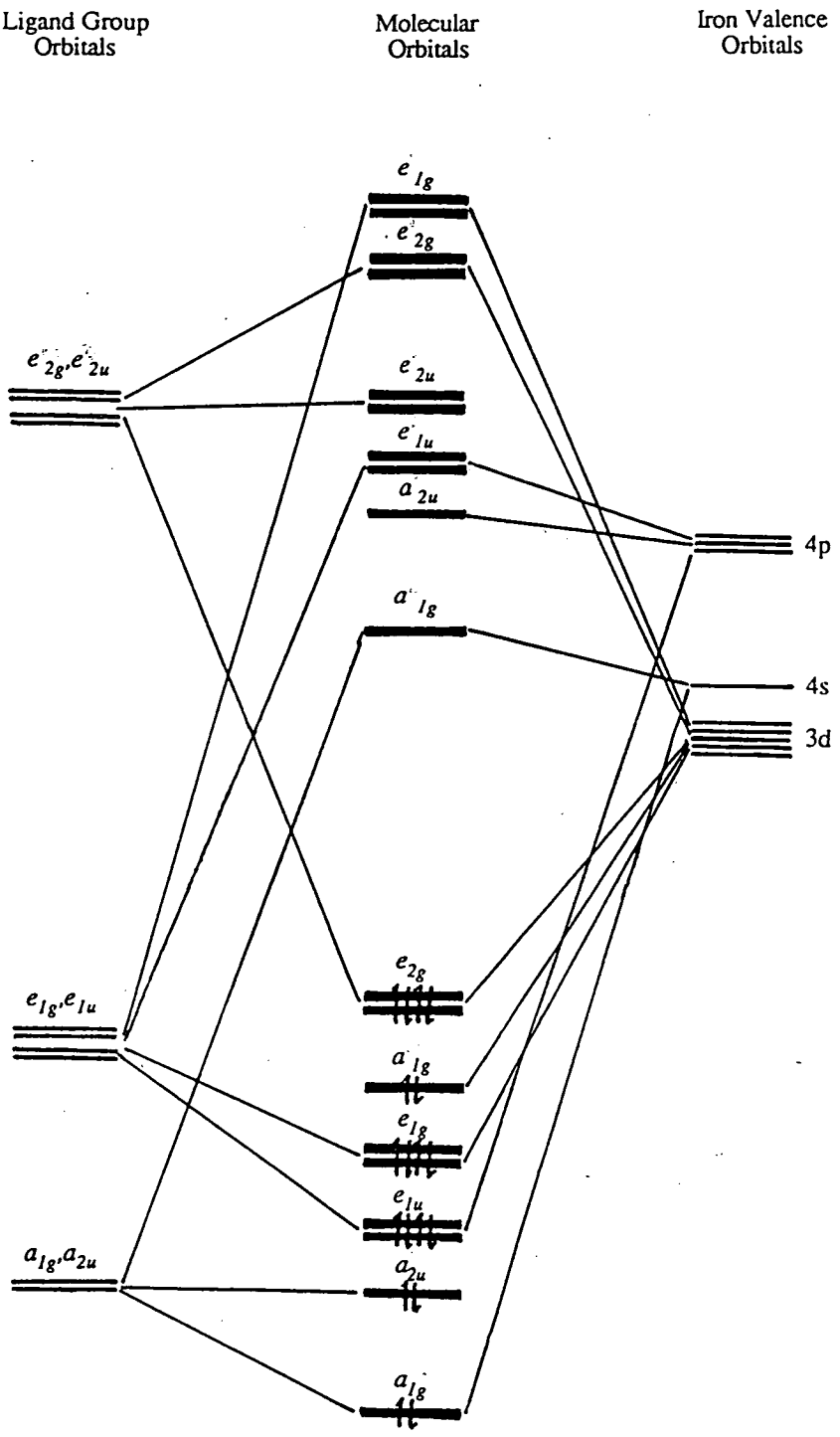

Similar aromatic behaviour has been demonstrated for a large number of other η-C_5H_5 complexes, such as $(\eta\text{-}C_5H_5)Mn(CO)_3$ [28], and $(\eta\text{-}C_5H_5)V(CO)_4$ [29]. Indeed, aromatic behaviour of η-bonded cyclopentadienyl ligands can normally be safely assumed, although certain complexes may not undergo specific reactions, as a particular metal centre may be capable of interfering with that reaction, *e.g.* oxidation to a cationic species would inhibit electrophilic attack or the specific conditions of a reaction might lead to decomposition of the organometalllic complex.

The "electron-rich" cobaltocene and nickelocene species each have a chemistry involving many reactions which result in 18-electron species. Indeed, in the nickel case, many of these reactions involve loss of at least one of the Cp ligands originally bonded to the metal. It is unsurprising that reactions of $CoCp_2$ and $NiCp_2$ yield products with $18e^-$ configurations, given that the 19^{th} and 20^{th} electrons in the bis(cyclopentadienyl) complexes reside in an orbital of antibonding character (a_{1g}), as is clear from **Figure 1.2.**

Having discussed the bonding in the bis(cyclopentadienyl) complexes, let us now turn our attention briefly to the "half-sandwich" species, *i.e.* those of the type $(\eta\text{-}C_5H_5)ML_n$.

These compounds constitute a massive volume of published material, testimony to the amount of attention which they have received over the years, and examples are known for elements ranging across all three transition series. Some well-known species of this type are the vanadium and manganese carbonyl complexes mentioned above, and the dimeric $[CpFe(CO)_2]_2$ [30], all of whose 4d and 5d metal analogues are also known.

The chemistry of the "half-sandwich" compounds has been widely developed, and involves both ligand replacement (with a wide range of other donors) or displacement reactions and organic transformations of the aromatic $[C_5H_5]$ group.

The bonding within the $CpML_n$ species is rather more difficult to describe than that in the metallocenes, as their symmetry is lower. Most treatments, however, adopt arguments based on the local symmetry of the $\{C_5H_5M\}$ (C_{5v}) and the $\{ML_n\}$ (whose symmetry varies with the nature of the L_n ligand set) fragments, and describe the bonding within each fragment separately.

η^3-ligation in Cyclopentadienyl Complexes

A very rare (but nonetheless known) mode of ligation in transition metal cyclopentadienyl complexes is that in which the ligand is bonded to the metal atom *via* only three of its five carbon atoms, akin to the bonding in π-allyl complexes.

The best-known example of a complex in which this type of ligation has been observed is $(\eta^3\text{-}C_5H_5)WCp(CO)_2$ [31]. Structural characterisation of this complex has confirmed the nature of the bonding present, and the structure is shown in **Figure 1.3**. It is of particular note that this complex contains 2 cyclopentadienyl ligands, each bonded to the tungsten atom in a different manner. As can be clearly seen, the η^3 ligand shows substantial deviation from planarity, thus foregoing the aromatic stabilisation associated with the planar conformation. It is interesting that this deformation is undergone in preference to expulsion of one of the carbonyl groups to allow the tungsten atom to attain a stable $18e^-$ configuration.

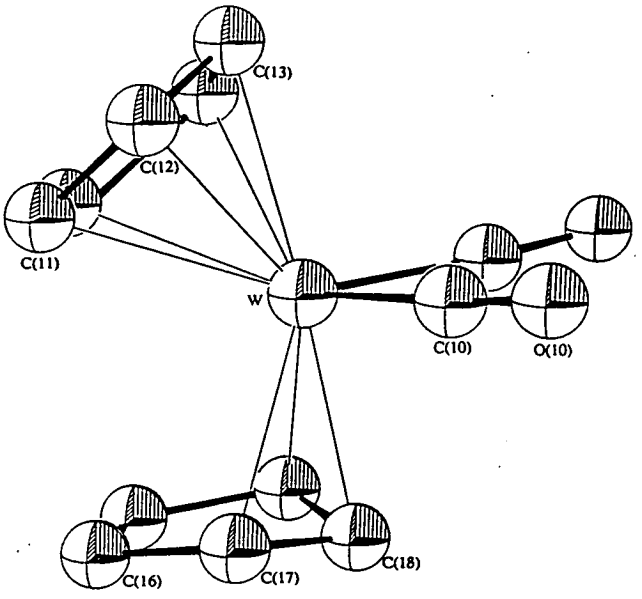

Figure 1.3

η^1-Cyclopentadienyl Complexes

A third mode of ligation known for the cyclopentadienyl ligand is where association with a transition metal atom is *via* a conventional 2 centre-2 electron bond, resulting in a σ-bonded organic moiety. Although more common than η^3-ligation, this type of bonding is still relatively rare, compared to the plethora of cases where "sandwich" or η-bonding is observed.

One interesting example of this type is $(\eta\text{-}C_5H_5)(\eta^1\text{-}C_5H_5)Fe(CO)_2$ [32], which is prepared by reaction of $(\eta\text{-}C_5H_5)Fe(CO)_2Cl$ with $Na[C_5H_5]$. ^1H n.m.r. spectroscopy shows a single sharp signal for the π-bonded Cp ring and a broader single resonance for the σ-bonded ligand at room temperature. On cooling to -80°C, however, this fluxionality is "frozen out" and a pattern consistent with a η^1-bonded $[C_5H_5]^-$ ligand is observed. Fluxionality of this type is common in σ-bonded cyclopentadienyl complexes [33]. The structure of this complex, as determined by *X*-ray methods, confirms the presence of two distinct Cp ligands,

as shown in **Figure 1.4** (below).

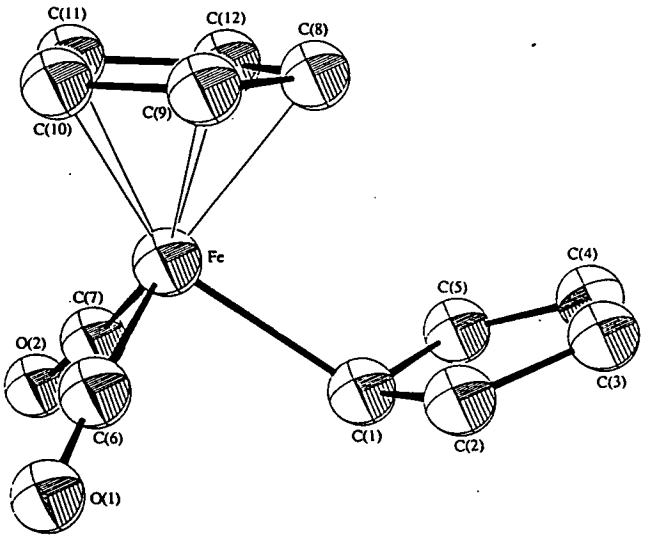

Carbametallaboranes: A Brief Introduction

The field of carbaborane and carbametallaborane chemistry has been developed extensively since the 1960's, encompassing a wide range of compounds of varying structural types.

While the initial carbametallaborane work concentrated on $\{C_2B_9M\}$ species, and these remain of great interest (and indeed the subject of the work contained in this thesis), there have also been developed synthetic routes to carbaborane and carbametallaborane clusters of varying sizes (usually between 5 and 12 atoms, although larger species are known) and containing differing numbers (between 1 and 4, but usually 2) of carbon vertices.

The $[C_2B_9H_{11}]^{2-}$ (dicarbollide) Anion

The work in this thesis concentrates upon $[C_2B_9]$ and $[C_2B_9M]$ species derived from 1,2-$C_2B_{10}H_{12}$ (*ortho*-carborane). 11-vertex ligands derived from 1,7-$C_2B_{10}H_{12}$ or *meta*-carborane, (a product of thermal rearrangement of 1,2-$C_2B_{10}H_{12}$) may be similarly used, although this area will not be addressed in the course of this work.

Formation of 11-vertex $[C_2B_9]$ carbaboranes from the parent icosahedral $C_2B_{10}H_{12}$ species may be achieved by partial (selective) cage degradation (or deboronation) of the *closo*-icosahedron in strongly basic alcoholic media [34,35], according to the equation below:

$$closo\text{-}1,2\text{-}C_2B_{10}H_{12} + RO^- + 2ROH \text{ ---> } [7,8\text{-}nido\text{-}C_2B_9H_{12}]^- + B(OR)_3 + H_2$$

Note that the different numbers given to the cage C atoms in the *closo* and *nido* compounds is not a function of any cage rearrangement, but rather an artefact of the conventional numbering schemes for each cluster type [36]. This conventional nomenclature will be used throughout the thesis, (except where otherwise indicated) and must be borne in mind during the discussions.

The $[7,8\text{-}C_2B_9H_{12}]^-$ anion produced by the above reaction is the precursor to the archetypal carbaborane ligand $[C_2B_9H_{11}]^{2-}$, which is obtained by deprotonation using strong bases, such as hydroxide, hydride etc. [1,2].

closo-Carbametallaborane from $[C_2B_9H_{11}]^{2-}$

It is fitting that the first known carbametallaborane species, prepared in 1965 [1] was the bis(dicarbollyl)iron complex $[Fe(C_2B_9H_{11})_2]^{2-}$, along with the monoanionic Fe^{III} species $[Fe(C_2B_9H_{11})_2]^-$. Thus, an historic parallel may be drawn between the preparation of the above complexes and the discovery of ferrocene, some 14 years before. The carbametallaborane compounds immediately following these [2] were also strongly allied to well-established η-Cp complexes, *e.g.* $[(C_2B_9H_{11})Mn(CO)_3]^-$ *versus* $[CpMn(CO)_3]$. Indeed, a number of "mixed sandwich" complexes of the type $[(C_5H_5)M(C_2B_9H_{11})]^{n-}$ were prepared, being regarded as metallocene analogues.

The preparative methods for carbametallaboranes have remained largely unchanged over the last 25 years, normally involving reaction of an alkali metal (or thallium) salt of the carbaborane anion with an appropriate metal reagent (often a halide), *e.g.*

$$2[C_2B_9H_{11}]^{2-} + FeCl_2 \longrightarrow [(C_2B_9H_{11})_2Fe]^{2-} \underset{\text{Na}}{\overset{[O]}{\rightleftharpoons}} [(C_2B_9H_{11})_2Fe]^-$$

$$[C_2B_9H_{11}]^{2-} + M(CO)_6 \xrightarrow{h\nu} [(CO)_3M(C_2B_9H_{11})]^{2-} + 3CO$$
$$\text{M=Cr, Mo, W}$$

This synthetic strategy is merely a modification of methods used in the closely related field of organometallic chemistry, which had been developing rapidly for a decade and a half before the advent of the carbametallaboranes.

Rationalisation of *closo*-[MC_2B_9] Structures

Carbametallaboranes in general may be thought of in two ways, namely (i) as metal/ligand complexes, *c.f.* transition metal Cp compounds, or (ii) as polyhedral cluster compounds, where the metal atom is a cluster vertex, like the B or C atoms. This apparent dubiety does not pose any problems, however, as each description is both internally consistent and entirely compatible with the other.

In order to illustrate the validity of the metal/ligand description, let us consider the *commo*-$M[C_2B_9]_2$ complexes. A molecular orbital scheme similar to that constructed for ferrocene (albeit in a lower symmetry point group) in **Figure 1.2** allows the sandwich structure of the molecule to be understood, the interactions of the carbaborane ligand π-MO's (see also **Figure 1.5**) with the metal valence orbitals producing 9 bonding orbitals, which accommodate the 18-electron configuration about the metal atom.

In order to rationalise carbametallaboranes in terms of their gross polyhedral structure, a different approach is required. The Polyhedral Skeletal Electron Pair (PSEP) Theory [37,38] has been successfully applied to a number of cluster types, the carbametallaboranes being but one of them.

PSEPT is, in essence, a set of electron-counting rules, which takes into account the size, atomic composition and overall charge of a cluster. The idea is then to divide the compound into its composite vertex fragments (such as {BH} and {CH}), and count the number of electrons each fragment has available for cluster bonding, *i.e.* for holding all of the fragments together *via* molecular orbitals delocalised over the polyhedron.

Fragments such as {BH} and {CH} have three orbitals available for cluster bonding, the 4th valence orbital of B or C being directed outwards from the polyhedral surface, to form a 2 centre-2 electron bond with the *exo*-H atom. This *exo* bond also "ties up" one valence electron from the main group element, and the result is that {BH} and {CH} fragments have 2 and 3 electrons respectively available for cluster bonding.

Extension of this to transition metal-containing fragments is relatively straightforward. The main difference here is that transition metals have 9 valence atomic orbitals, rather than 4 for the main group elements. The number of orbitals employed in skeletal bonding however is still 3 (although there are exceptions, but these undergo marked structural distortion, see later), with the other 6 orbitals used in bonding of *exo*-polyhedral ligands and in storage of non-bonding electron density. These six orbitals are usually filled, thus satisfying the 18-electron rule, and therefore the number of electrons available for cluster bonding, e, may be simply calculated by $e = v + x - 12$, where v is the number of metal valence electrons and x is the number of electrons donated by the *exo* -polyhedral ligands.

The total number of electrons available for skeletal bonding may now be counted, and is simply the sum of those for all vertex fragments, plus any electrons associated with "extra" (*e.g.* bridging) hydrogen atoms or overall charge on the cluster. Division by two gives the Skeletal Electron Pair (S.E.P.) count. For a cluster of **n** vertices, the following structural relationships apply:

N^o S.E.P.'s	N^o Vacant Vertices	Terminology
n+1	0	*closo*
n+2	1	*nido*
n+3	2	*arachno*
n+4	3	*hypho*

To illustrate the practical applicability of this, let us consider the known carbametallaborane species $[(CO)_3Mn(C_2B_9H_{11})]^-$. (The *X*-ray crystal structure of the Re analogue of this complex has been determined [39], showing a *closo* -icosahedral structure). The number of cluster vertices is 12 (Mn + 2C + 9B), and the skeletal electron pair count is calculated below.

Skeletal Electron Source		N° Electrons	
$\{Mn(CO)_3\}$		1	(7+6-12)
9 x {BH}		18	
2 x {CH}		6	
-ve charge		1	
	TOTAL	26	= 13 S.E.P.'s = (n + 1) S.E.P.'s => *closo*

Thus the geometry predicted by PSEPT is that of a *closo*-icosahedron, consistent with a $\{Mn(CO)_3^+\}$ fragment "filling" the vacant vertex site in $[C_2B_9H_{11}]^{2-}$ (which also has 13 S.E.P.'s but now only 11 vertices, and is therefore a *nido*-icosahedral fragment).

The "Slipped" Carbametallaboranes

The electron-counting rules discussed in the previous section predict *closo* -icosahedral geometry for 12-vertex, 26-electron clusters. It is noteworthy that this geometry can also be attained by clusters apparently possessing less than this number of skeletal electrons, an early example of which was the (supposedly) 25e⁻ $[(C_5H_5)Fe(C_2B_9H_{11})]$ cluster. An alternative (and probably more sensible) view of this species, however, is that it possesses only 5 "non-bonding" electrons (Fe^{III} in a *pseudo*-octahedral environment), and therefore the number of electrons available for cluster bonding must be calculated by $e = v + x - 11$,

which results in a S.E.P. count of 13, and thus does predict *closo* geometry.

On the other hand, the "electron rich" species of the form $[M(C_2B_9H_{11})_2]^{n-}$, where the metal, M, has more than six d-electrons (*e.g.* Ni^{II}, Pd^{II}, Cu^{II}, Cu^{III}, Au^{II}, Au^{III}) show a slip distortion of the metal atom from the pseudo fivefold axes of the open ligand faces, in each case *away* from the cage carbon atoms.

A simple explanation of this is that the metal atom slips to avoid the undesirable (> $18e^-$) configuration associated with a bis(η-bonded) structure. Consideration of a molecular orbital scheme of the type shown in **Figure 1.2** allows understanding of the reluctance of these complexes to adopt a symmmetrically-bonded sandwich structure, given that any electrons in excess of 18 would be forced to occupy an antibonding level.

Slipping of the metal atom from the centroid of the open face of the ligand is also observed for a second type of carbametallaborane cluster, where the metal atom is part of an angular $\{ML_2\}$ fragment derived from square planar geometry [40,41].

$\{ML_2\}$ is formally a 2-orbital donor to the carbaborane, and there is consequently a "mismatch" between these and the three filled π-MO's of $[C_2B_9H_{11}]^{2-}$. As a result of this, the metal fragment slips to maximise overlap with the two singly-noded cage π-orbitals (Ψ_2 and Ψ_3, see **Figure 1.5**).

σ-Bonded Carbametallaboranes

Although extremely uncommon, there does exist a mode of ligation in $[MC_2B_9]$ carbametallaboranes where the metal atom is attached to the carbaborane moiety

via an essentially η^1 or σ-bonding interaction which might, in effect, be viewed as the extreme case of the slipping distortions described above.

The only known (prior to the studies presented in Chapter 2, *vide infra*) example of such ligation to $[C_2B_9H_{11}]^{2-}$ is in the neutral species $[PPh_3Hg(C_2B_9H_{11})]$ [42], the formally Hg^{II} atom possessing a d^{10} configuration, and acting as a 1-orbital donor to the carbaborane ligand.

Although the $\{PPh_3Hg^{2+}\}$ fragment is essentially σ-bonded to the cage through only one boron atom (that opposite the C-C vector), there is retained at least slight interaction with the two other facial boron atoms, as is observed in the *endo* σ-bonded species **(1)** and **(2)** (see Chapter 2).

Exo-Polyhedral Agostic Bonding in Carbametallaboranes

A fourth general mode of bonding known for carbametallaboranes, normally seen in species containing more than one metal atom (although interesting monometallic species are also possible), involves 3 centre-2 electron (*agostic*) interactions between skeletal boron atoms, their terminal H atoms and an *exo* -polyhedral metal atom. In dimetallic complexes, these interactions help support the metal-metal bond from a facially bonded (*endo*-) metal atom to one outside the polyhedral surface, numerous examples being known for both *homo*- [43] and *hetero*dimetallic [44] complexes of $[C_2B_9H_{11}]^{2-}$ and related (carbon-substituted) dianionic carbaborane ligands.

Mononuclear complexes containing these *agostic* interactions are exemplified by the *exo-nido* rhodium (and iridium) species [45], although these are not strictly complexes of a dicarbollide *di*anion, and therefore are only mentioned as a point

of interest, rather than for any genuine comparative purpose.

The *Mono*anionic Carbaboranes, $[C_2B_9H_{10}L]^-$

Although there has been shown a broad similarity between the bonding capabilities of $[C_2B_9H_{11}]^{2-}$ and the cyclopentadienide anion, it is impossible to conduct any meaningful direct comparison between their chemistries, because of the different overall charge on each ligand.

For example, consider the hypothetical pair of related complexes $[(C_2B_9H_{11})ML_n]^{x-}$ and $[(\eta\text{-}C_5H_5)ML_n]^{y-}$. If the metal, M, is in the same oxidation state in both species and the ligand set L_n is common, the overall charge on the complexes must differ ($x = y + 1$). Conversely, if the net charge on the two compounds is to be the same ($x = y$) then either the oxidation state of the metal (M) or the composition of the ligand set (L_n) must differ.

With this in mind, investigation of the chemistry of *mono*anionic carbaborane ligands is of interest, with a view to gaining some true insight into the comparative bonding capabilities, donor/acceptor properties etc. of the carbaborane ligands with those of cyclopentadienyl ligands in genuinely analogous complexes.

A number of suitable (protonated) precursors to monoanionic carbaborane species have been prepared previously, each of general formula $[C_2B_9H_{11}L]$, where L is a $2e^-$ *exo*-polyhedral donor, bonded to a boron atom.

Published examples of the above type include those where L = pyridine [7], THF [7], $NCMe_3$ [7] and SMe_2 [6], although examples of ligation of the (deprotonated) anionic ligands to transition metal fragments are surprisingly

few [6,42], especially those where a full (structural) analysis of the product has been carried out [46,47].

The monoanionic ligands retain the same *nido* cage architecture as $[C_2B_9H_{11}]^{2-}$, because the *exo*-polyhedral ligand, L, provides both electrons for the B-L (*exo*) bond, where the H atom it replaces could donate only one. Thus the skeletal electron pair count (see section on PSEPT earlier) for $[C_2B_9H_{10}L]^-$ is the same as that for $[C_2B_9H_{11}]^{2-}$, but with the need to carry only a single overall negative charge.

This, however, raises the possibility of two different extreme representations of the charge-partitioning in the monoanionic ligands. One extreme form simply posesses a single negative charge on the facial atoms, where the second is zwitterionic, with the double negative charge on the $[C_2B_3]$ face offset by a positive charge on the *exo*-polyhedral group, L. Extended Hückel and extended Hückel/fragment molecular orbital calculations have been performed (see Chapter 4) in an attempt to ascertain which representation most accurately describes the partitioning of charge in ligands of this type.

The monoanionic carbaborane ligand on which attention has been focussed in this work is [9-SMe_2-7,8-*nido*-$C_2B_9H_{10}$]$^-$ (hereafter referred to as [carb']$^-$), the product of deprotonation of [10,11-μ-H-9-SMe_2-7,8-*nido*-$C_2B_9H_{10}$], (carb'H) [6].

Comparison of the π-Molecular Orbitals of $[C_5H_5]^-$, $[C_2B_9H_{11}]^{2-}$ and [carb']$^-$

As a prelude to the main body of the text, the results of extended Hückel molecular orbital calculations on (experimentally derived, see structures of complexes **(1)**, **(6)** and **(7)** in Chapters 2 and 4) models of each of the ligands are

presented, comprising **Figure 1.5**. These calculations were performed with charge iteration according to $H_{ii} = H_{ii}^{0} + (\text{sense})x(\text{charge})$. A general description of the method employed is given in Chapter 6, section 3.

The following points of interest arise from the results presented in **Figure 1.5**.

(i) The energies of corresponding orbitals for the two carbaborane ligands are similar, and lie consistently higher than those for the cyclopentadienide anion. This is perfectly reasonable, as the basis set of atomic orbitals for carbon lie deeper than those for boron, reflecting the differing electronegativities of the two elements.

This electronegativity difference also explains why the lowest lying (Ψ_1) π-MO for both carbaborane anions is predominantly carbon-based, while the orbitals of greater energy (Ψ_2-Ψ_5) are localised primarily on boron.

(ii) The nodal planes of the orbitals of $[carb']^-$ are rotated with respect to those of the other two ligands, suggesting that the SMe_2 substituent, as well as simply lowering the symmetry of the ligand (and hence of the orbitals) also perturbs the orbitals markedly, and therefore is perhaps not the "innocent" electron-provider initially assumed. Despite the rotation of the nodal planes in the $[carb']^-$ orbitals, the number of nodes within each orbital is the same as in the corresponding orbital in the other two ligands.

The π-molecular orbitals in **Figure 1.5** will be referred to from various parts of the main text, where structural parameters of complexes of all three ligands are discussed in terms of frontier MO interactions.

Figure 1.5 π-MO's of $[C_5H_5]^-$, $[C_2B_9H_{11}]^{2-}$ and $[carb']^-$

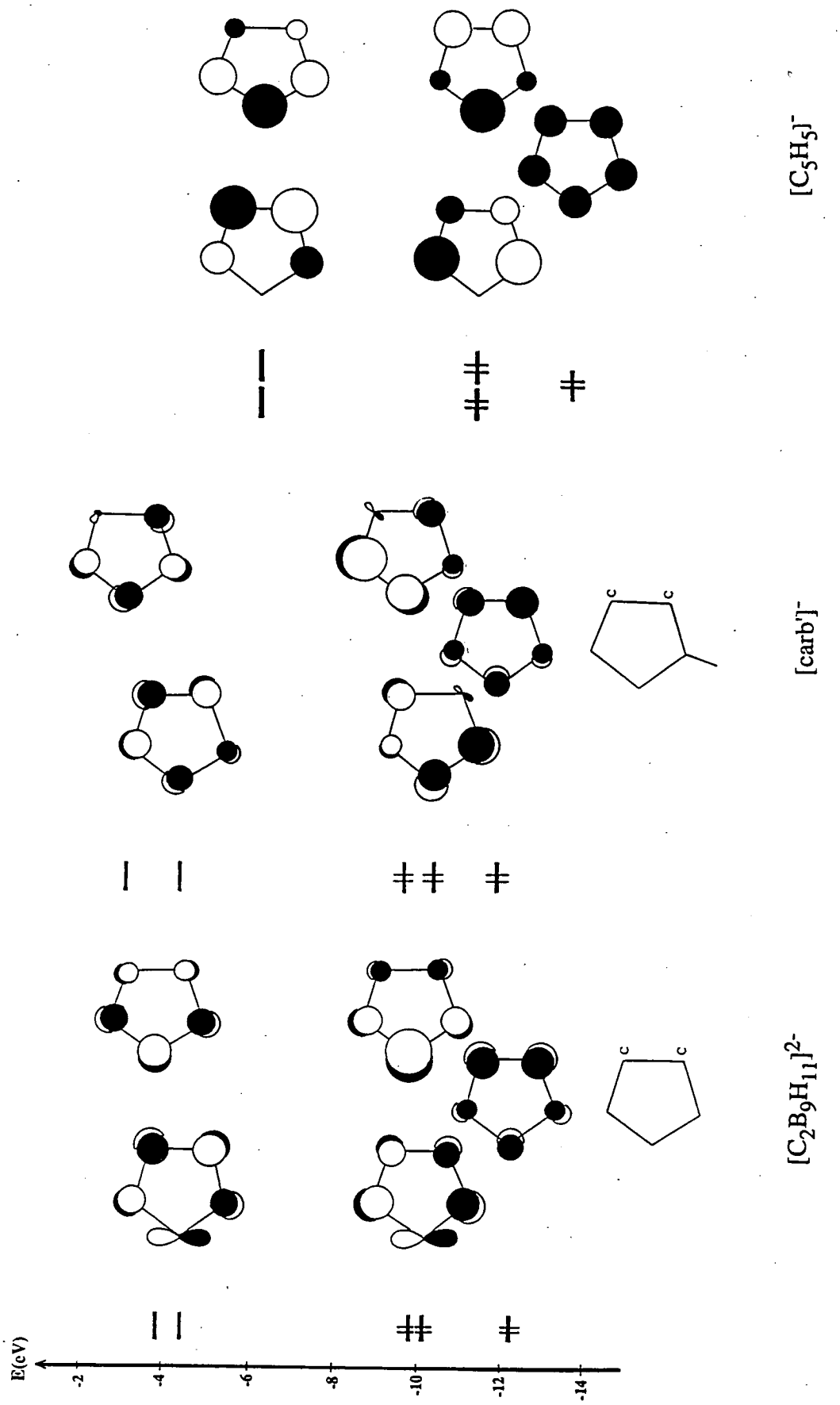

Scope of the Work Presented

The studies presented in this thesis investigate the electronic properties and bonding capabilities of $[carb']^-$, with comparison to those of the cyclopentadienyl and $[C_2B_9H_{11}]^{2-}$ ligands.

This initial work allows the validity of the isolobal analogy between the ligands to be assessed, by consideration of structural, spectral, and electrochemical evidence.

Ultimately, wider studies of the transition metal chemistry of $[carb']^-$ might be expected to move into the following general areas:

(i) Homogeneous catalysis. This has been a fruitful area of research in recent years, concentrating chiefly on hydrido-carbametallaborane complexes of rhodium, iridium and ruthenium which have been shown to be catalytically active in, for example, alkene hydrogenation and isomerisation, and deuterium exchange reactions in carbaborane systems [48,49].

(ii) Boron Neutron Capture Therapy (BNCT) [50]. Ongoing research into this medical application of boron cluster chemistry has opened up the possibility of several approaches to the problem of delivering sufficient quantities of boron (^{10}B) *selectively* to tumour tissue. One such approach might involve incorporation of carbametallaboranes containing *exo*-polyhedral amino acid ligands *into* the tumour, rather than simply attachment to its surface, the suggested mode of association for the currently most widely used BNCT agent $[B_{12}H_{11}SH]^{2-}$, BSH.

With potential applications such as those above, there is evident need for fundamental research into the chemistry of carbaboranes and carbametallaboranes, such as that presented herein.

Chapter 2

$[7,8\text{-}C_2B_9H_{12}]^-$ and Group Ib Derivatives

Introduction

The $[7,8\text{-}nido\text{-}C_2B_9H_{12}]^-$ anion, **(1)**, the precursor to the ubiquitous $[C_2B_9H_{11}]^{2-}$ (dicarbollide) ligand, has been prepared by the well-known partial cage degradation of $1,2\text{-}C_2B_{10}H_{12}$ (*o*-carborane) in alcoholic hydroxide solution [34,35].

It is well accepted that $[C_2B_9H_{12}]^-$ has a *nido*-icosahedral cage architecture, following the Polyhedral Skeletal Electron Pair (PSEP) Theory, although its actual structure has never been accurately determined.

The PSEPT and spectroscopic considerations allow a structure to be proposed for the non-hydrogen skeleton of **(1)**, but the point of chief interest, namely the position and bonding mode of the 12^{th} H atom associated with the cage, could not be fully addressed. In an early communication, Hawthorne [35] considered a number of possible sites for this 12^{th} hydrogen atom, (including an *endo* site, which is in fact the correct one, see later). It has since been generally accepted, however, that this atom occupies a bridging position on one of the (otherwise symmetry-equivalent) B-B connectivites on the open face of the ligand.

Recent structural determinations [51,52] for *nido*-$[3,4\text{-}Et_2\text{-}3,4\text{-}C_2B_5H_6]^-$ and *nido*-$[B_{11}H_{14}]^-$ have confirmed the presence of discrete $\{BH_2\}$ units in these *nido* carbaborane and borane species, where such functions have been more commonly

associated with more open (*arachno* and *hypho*) structures. With this in mind, detailed study of [7,8-*nido*-$C_2B_9H_{12}$]$^-$ has been carried out, *via* multinuclear, multidimensional n.m.r. work, single crystal *X*-ray crystallography and extended Hückel molecular orbital calculations.

[$PhCH_2NMe_3$][7,8-$C_2B_9H_{12}$], [BTMA](1)

Synthesis

[BTMA](1) was prepared by mixing aqueous solutions of equimolar quantities of [$PhCH_2NMe_3$]Br and K[$C_2B_9H_{12}$], as described in Chapter 6, section 1. The compound was crystallised by slow diffusion of n-hexane into a dichloromethane solution at -30^{0}C.

Characterisation of [BTMA](1)

The compound was characterised by elemental (C,H) microanalysis and ^{11}B, ^{11}B(COSY), ^{11}B-{^{1}H}, ^{1}H and ^{1}H-{^{11}B selective} n.m.r. studies.

The microanalytical results obtained were fully consistent with the proposed formulation of the compound.

N.m.r. Studies

The ^{1}H spectrum shows a multiplet resonance at δ 7.50-7.65 p.p.m., arising from the phenyl protons of the [BTMA]$^+$ counter ion, and singlet resonances at δ 4.43 and 3.13 p.p.m. assignable to its methylene and methyl protons resectively. A broad signal at δ 1.90 p.p.m. corresponds to the carbaborane C-H's.

The ^{11}B-{^{1}H} spectrum of [BTMA](1) exhibits 5 signals, of relative integrals 2:3:2:1:1, and retention of proton coupling in the ^{11}B spectrum reveals that all B nuclei have an associated *exo*-polyhedral H atom, as all five signals show clear doublet coupling, with J_{BH} in the range 125-150 Hz. In addition to this, the second-lowest frequency resonance (δ -32.54 p.p.m.) shows a smaller (*ca*. 50 Hz) coupling, thus appearing as a doublet of doublets. The additional structure on this resonance was noted on a very early ^{11}B spectrum of **(1)**. This resonance was assigned to the symmetry-unique B(10) atom in the open face of the ligand.

With this assignment having been made, the other signals were assigned *via* a ^{11}B(COSY) spectrum, a plot of which is shown in **Figure 2.1**, which also gives the assignments made.

Table 2.1 lists these assignments and also those for ^{1}H shifts obtained by a series of ^{1}H-{^{11}B selective} experiments.

Table 2.1 Assignment of ^{11}B and ^{1}H Chemical Shifts in **(1)**

Position	δ(^{11}B)	δ(^{1}H)
9,11	-10.38	1.94
3 (5,6)	-16.46	1.77 (1.24)
2,4	-21.29	1.26
10	-32.54	0.11(*exo*) -2.80(*endo*)
1	-37.17	0.55

A signal is observed for a low-frequency hydrogen atom, [δ -2.80 p.p.m., H(12)], significant enhancement of which is observed upon irradiation of the ^{11}B resonance at δ -32.54 p.p.m. (B(10)), and much weaker enhancement observed on irradiation of the B(9),B(11) resonance (δ -10.38 p.p.m.).

Figure 2.1 ^{11}B (COSY) Plot of $[7,8\text{-}C_2B_9H_{12}]^-$, **(1)**

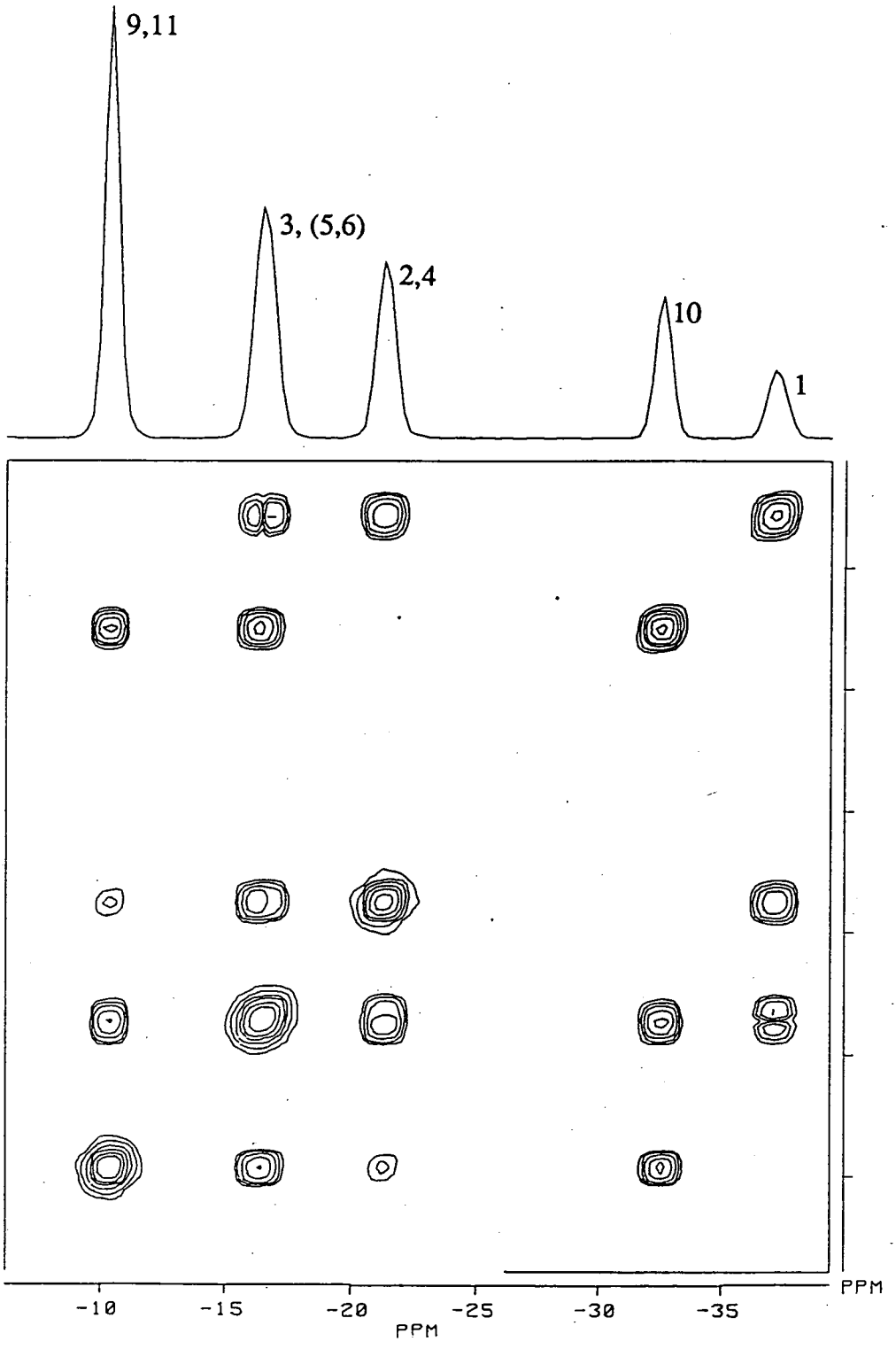

This information suggests that at ambient temperature, H(12) is strongly associated with B(10), the interaction with the other facial boron atoms B(9) and B(11) being much weaker. The association of H(12) with B(9) and B(11) is evidently extremely small, as it does not manifest itself in the form of additional structure, or even broadening, in the B(9),B(11) resonance (δ -10.38 p.p.m.) in the ^{11}B spectrum.

The ^{11}B and ^{11}B-{^{1}H} spectra remain essentially unchanged on cooling down to -78°C. This has the implication that the structure of **(1)** is most accurately described either by a form **(i)** which contains a discrete {BH_2} function and in which there is a small but detectable (and real) interaction between the *endo* H atom and B(9) and B(11), or by the asymmetrically-bridged form **(ii)**, whose rapid fluxionality could not be stopped within the limits of our n.m.r. experiment.

[dmsoH.dmso][7,8-$C_2B_9H_{12}$], [dmsoH.dmso](1)

Synthesis and Characterisation

[dmsoH.dmso]**(1)** was synthesised by addition of conc. H_2SO_4 to an aqueous mixture of K[$C_2B_9H_{12}$] and dimethylsulphoxide at 0°C, without stirring, as described in chapter 6, section 1, and was crystallised by the same method as for [BTMA]**(1)**, giving diffraction-quality crystals.

Microanalytical results were consistent with the $C_6H_{25}B_9O_2S_2$ formulation. ^{11}B and ^{11}B-{^{1}H} n.m.r. spectra were recorded, the results of which were identical to those for [BTMA]**(1)**, which have already been discussed in detail. The ^{1}H spectrum exhibits a broad signal at δ 6.5-7.0 p.p.m., corresponding to the dmso-solvated proton of the cation. Other signals at δ 2.73 and 1.88 p.p.m.

correspond to the 12 H atoms of the dmso solvent molecules and the cage C-H's respectively.

Structural Study of (1)

Introduction

In order to ascertain the nature of the 12^{th} H atom position in **(1)**, and therefore to distinguish between the two proposed forms **(i)** and **(ii)**, an accurate low temperature crystallographic study was undertaken, as the $[dmsoH.dmso]^+$ salt.

Initial attempts to determine the structure of **(1)** were frustrated by disorder in the carbaborane anion. Although good quality single crystals of $[PhCH_2NMe_3]$**(1)** were grown and diffraction data collected, subsequent analysis of this data revealed that, although the benzyltrimethylammonium counter-ions were ordered, both crystallographically independent $[C_2B_9]$ cages were randomly disordered over all 12 sites, appearing as *closo*-icosahedra, a form of disorder not uncommon in this type of system.

It was not possible to model this disorder satisfactorily, and so work on this structure was terminated. Details of crystal data, data collection and processing, and structure solution and refinement procedures for the disordered structure of [BTMA]**(1)** may be found in chapter 6, section 2.

However, by extreme fortune, it was discovered that if the synthesis of 9-SMe_2-7,8-$C_2B_9H_{11}$ (carb'H, **(3)**, see chapter 3) is carried out at too low a temperature, and with insufficient stirring, then the compound [dmsoH.dmso][7,8-$C_2B_9H_{12}$] is obtained in high yield. This compound may be

easily crystallised as described earlier, to give large single crystals, suitable for structural analysis.

Diffraction data for [dmsoH.dmso]**(1)** were collected at low-temperature, and crystal data and details of structure solution and refinement procedures may be found in chapter 6, section 2.

Discussion

The crystallographic study in the first instance confirms the chemical identity of the compound, which exists as [7,8-*nido*-$C_2B_9H_{12}$]$^-$ anions and protonated dimethylsulphoxide molecules, each of the latter being associated with a second dmso molecule *via* a hydrogen bonding interaction.

Positional parameters for all atoms, together with equivalent isotropic thermal parameters for non-hydrogen atoms are given in **Table 2.2**. Interatomic distances are presented in **Table 2.3**, and **Table 2.4** is comprised of selected interbond angles. Anisotropic thermal parameters for non-H atoms are to be found in **Table 2.5**. For both ions, non-hydrogen atoms are represented by thermal ellipsoids at the 50% probability level, and H atoms are given an artificial radius of 0.1Å for clarity.

The [dmsoH.dmso]$^+$ cation is shown in **Figure 2.2**, giving the appropriate numbering scheme. The cation consists of an O-protonated dimethylsulphoxide molecule, with a second dmso molecule associated to this through a hydrogen bonding interaction, *via* the O(1)-H(O)...O(2) bridge. This hydrogen bond is of a conventional type [53], with the following structural parameters: O(1)-H(O) = 0.95(4)Å, and O(2)...H(O) = 1.45(4)Å. The O(1)-H(O)...O(2) angle is 172(4)^o.

Figure 2.2 The [dmsoH.dmso]$^{+}$ Cation

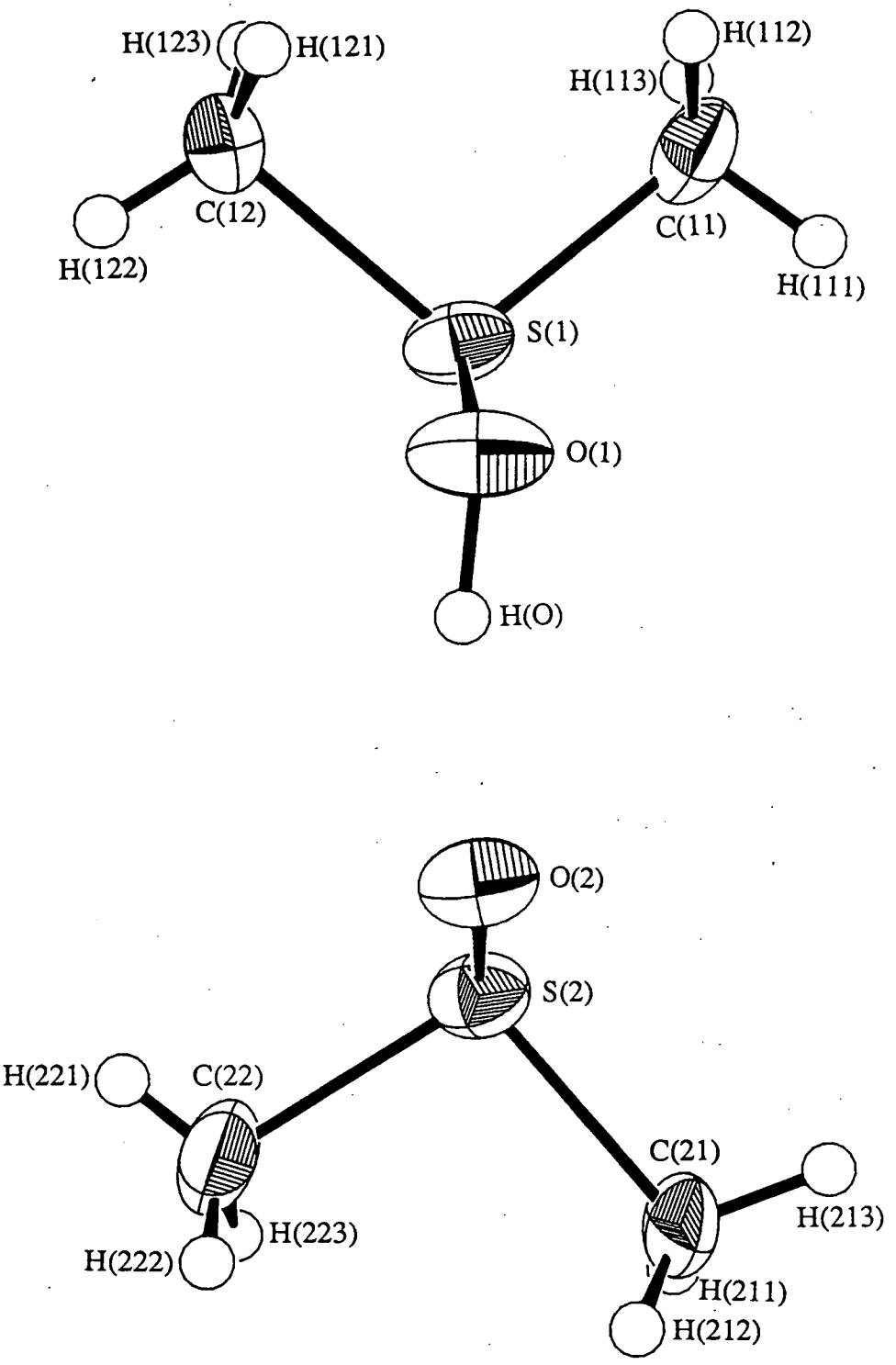

Figure 2.3 Plan View of $[7,8\text{-}C_2B_9H_{12}]^-$, **(1)**

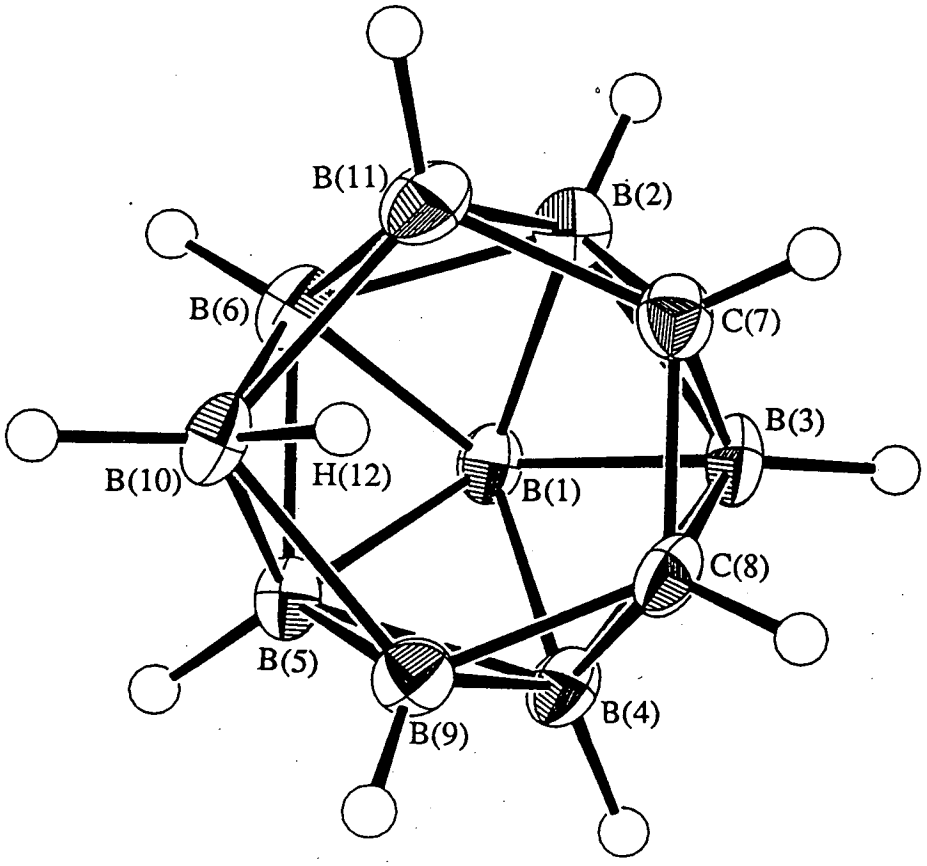

Table 2.2 Positional Parameters of Refined Atoms and Equivalent Isotropic Thermal Parameters in [dmsoH.dmso][7,8-*nido*-$C_2B_9H_{12}$], [dmsoH.dmso](1)

	x	y	z	Ueq
S(1)	0.67515(6)	0.31781(4)	0.38941(3)	0.0307(4)
S(2)	0.31787(6)	0.13183(4)	0.28430(3)	0.0316(4)
O(1)	0.52807(19)	0.38738(13)	0.34418(10)	0.0398(9)
O(2)	0.30872(16)	0.26974(13)	0.27500(9)	0.0341(9)
MC(11)	0.6944(3)	0.37984(22)	0.47988(13)	0.0350(13)
MC(12)	0.8461(3)	0.38545(21)	0.35948(14)	0.0347(12)
MC(21)	0.1145(3)	0.09026(25)	0.29071(14)	0.0433(14)
MC(22)	0.3221(4)	0.07756(24)	0.19265(16)	0.0462(15)
B(1)	0.35011(24)	0.28174(18)	0.58954(12)	0.0225(11)
B(2)	0.4006(3)	0.15025(20)	0.64327(14)	0.0262(12)
B(3)	0.4222(3)	0.15221(19)	0.54849(14)	0.0258(12)
B(4)	0.26004(25)	0.23734(20)	0.49757(12)	0.0246(11)
B(5)	0.1321(3)	0.28414(18)	0.55951(13)	0.0226(11)
B(6)	0.2197(3)	0.22831(20)	0.65211(13)	0.0255(11)
C(7)	0.32146(22)	0.03677(17)	0.58313(11)	0.0248(10)
C(8)	0.24401(23)	0.08355(17)	0.50477(11)	0.0233(10)
B(9)	0.0758(3)	0.15604(19)	0.50337(13)	0.0229(11)
B(10)	0.0413(3)	0.16088(20)	0.59958(13)	0.0246(11)
B(11)	0.2150(3)	0.06871(20)	0.64694(13)	0.0276(12)
H(111)	0.599(4)	0.3590(24)	0.4945(15)	
H(112)	0.709(3)	0.465(3)	0.4779(15)	
H(113)	0.789(3)	0.3411(24)	0.5129(16)	
H(121)	0.825(3)	0.471(3)	0.3648(15)	
H(122)	0.845(3)	0.3602(24)	0.3159(17)	
H(123)	0.938(4)	0.3636(24)	0.3972(16)	
H(211)	0.132(3)	0.007(3)	0.3001(15)	
H(212)	0.038(3)	0.1295(23)	0.2452(16)	
H(213)	0.091(3)	0.1155(25)	0.3353(16)	
H(221)	0.402(3)	0.091(3)	0.1832(15)	
H(222)	0.232(4)	0.1071(25)	0.1590(16)	
H(223)	0.313(3)	-0.012(3)	0.1978(15)	
H(O)	0.448(4)	0.336(3)	0.3160(19)	
H(1)	0.425(3)	0.3657(19)	0.6034(13)	
H(2)	0.499(3)	0.1329(23)	0.6826(15)	
H(3)	0.538(3)	0.1407(23)	0.5291(15)	
H(4)	0.282(3)	0.2833(24)	0.4474(14)	
H(5)	0.061(3)	0.3671(23)	0.5518(14)	
H(6)	0.211(3)	0.2843(23)	0.6991(15)	
H(7)	0.384(3)	-0.0343(24)	0.5809(14)	
H(8)	0.264(3)	0.0312(23)	0.4650(15)	
H(9)	-0.014(3)	0.1551(23)	0.4635(16)	
H(10)	-0.078(3)	0.1737(21)	0.6170(15)	
H(11)	0.210(3)	0.0102(23)	0.6944(14)	
H(12)	0.049(3)	0.0648(24)	0.5762(15)	

Table 2.3 Interatomic Distances (Å) in [dmsoH.dmso][7,8-*nido*-$C_2B_9H_{12}$], [dmsoH.dmso](1)

Anion

B(1) - B(2)	1.762(3)	B(5) - B(6)	1.816(3)
B(1) - B(3)	1.768(3)	B(5) - B(9)	1.761(3)
B(1) - B(4)	1.772(3)	B(5) -B(10)	1.775(3)
B(1) - B(5)	1.794(3)	B(5) - H(5)	1.09(3)
B(1) - B(6)	1.799(3)	B(6) -B(10)	1.777(3)
B(1) - H(1)	1.122(23)	B(6) -B(11)	1.771(3)
B(2) - B(3)	1.759(3)	B(6) - H(6)	1.07(3)
B(2) - B(6)	1.763(3)	C(7) - C(8)	1.542(3)
B(2) - C(7)	1.717(3)	C(7) -B(11)	1.613(3)
B(2) -B(11)	1.796(3)	C(7) - H(7)	0.95(3)
B(2) - H(2)	1.01(3)	C(8) - B(9)	1.606(3)
B(3) - B(4)	1.764(3)	C(8) - H(8)	0.96(3)
B(3) - C(7)	1.707(3)	B(9) -B(10)	1.817(3)
B(3) - C(8)	1.726(3)	B(9) - H(9)	0.94(3)
B(3) - H(3)	1.09(3)	B(10) -B(11)	1.849(3)
B(4) - B(5)	1.754(3)	B(10) -H(10)	1.10(3)
B(4) - C(8)	1.716(3)	B(10) -H(12)	1.15(3)
B(4) - B(9)	1.793(3)	B(11) -H(11)	1.08(3)
B(4) - H(4)	1.09(3)		

Cation

S(1) - O(1)	1.5498(17)	C(11) -H(113)	1.00(3)
S(1) -C(11)	1.7594(24)	C(12) -H(121)	0.97(3)
S(1) -C(12)	1.7708(25)	C(12) -H(122)	0.84(3)
S(2) - O(2)	1.5377(16)	C(12) -H(123)	0.96(3)
S(2) -C(21)	1.771(3)	C(21) -H(211)	0.94(3)
S(2) -C(22)	1.773(3)	C(21) -H(212)	1.04(3)
O(1) - H(O)	0.95(4)	C(21) -H(213)	0.91(3)
O(2)...H(O)	1.45(4)	C(22) -H(221)	0.73(3)
C(11) -H(111)	0.91(3)	C(22) -H(222)	0.94(3)
C(11) -H(112)	0.95(3)	C(22) -H(223)	1.00(3)

Table 2.4 Selected Interbond Angles (°) in [dmsoH.dmso][7,8-*nido*-$C_2B_9H_{12}$], [dmsoH.dmso](1)

O(1)	S(1)	MC(11)	103.45(10)	C(8)	B(4)	B(9)	54.43(12)
O(1)	S(1)	MC(12)	103.01(10)	B(1)	B(5)	B(4)	59.93(12)
MC(11)	S(1)	MC(12)	100.03(11)	B(1)	B(5)	B(6)	59.77(12)
O(2)	S(2)	MC(21)	103.67(11)	B(4)	B(5)	B(9)	61.34(12)
O(2)	S(2)	MC(22)	104.06(11)	B(6)	B(5)	B(10)	59.30(12)
MC(21)	S(2)	MC(22)	98.58(13)	B(9)	B(5)	B(10)	61.84(13)
S(1)	O(1)	H(O)	113.4(21)	B(1)	B(6)	B(2)	59.27(12)
S(2)	O(2)	H(O)	115.2(14)	B(1)	B(6)	B(5)	59.50(12)
O(1)	H(O)	O(2)	172.2(35)	B(2)	B(6)	B(11)	61.09(13)
B(2)	B(1)	B(3)	59.76(13)	B(5)	B(6)	B(10)	59.20(12)
B(2)	B(1)	B(6)	59.34(12)	B(10)	B(6)	B(11)	62.82(13)
B(3)	B(1)	B(4)	59.77(12)	B(2)	C(7)	B(3)	61.82(13)
B(4)	B(1)	B(5)	58.90(12)	B(2)	C(7)	B(11)	65.18(13)
B(5)	B(1)	B(6)	60.73(12)	B(3)	C(7)	C(8)	63.93(13)
B(1)	B(2)	B(3)	60.31(13)	B(3)	C(8)	B(4)	61.68(12)
B(1)	B(2)	B(6)	61.40(13)	B(3)	C(8)	C(7)	62.68(13)
B(3)	B(2)	C(7)	58.80(12)	B(4)	C(8)	B(9)	65.22(13)
B(6)	B(2)	B(11)	59.68(13)	B(4)	B(9)	B(5)	59.13(12)
C(7)	B(2)	B(11)	54.61(12)	B(4)	B(9)	C(8)	60.35(12)
B(1)	B(3)	B(2)	59.93(13)	B(5)	B(9)	B(10)	59.47(12)
B(1)	B(3)	B(4)	60.23(12)	B(5)	B(10)	B(6)	61.50(13)
B(2)	B(3)	C(7)	59.38(13)	B(5)	B(10)	B(9)	58.69(12)
B(4)	B(3)	C(8)	58.89(12)	B(6)	B(10)	B(11)	58.42(12)
C(7)	B(3)	C(8)	53.39(11)	H(10)	B(10)	H(12)	109.7(19)
B(1)	B(4)	B(3)	60.00(12)	B(2)	B(11)	B(6)	59.24(13)
B(1)	B(4)	B(5)	61.18(12)	B(2)	B(11)	C(7)	60.21(13)
B(3)	B(4)	C(8)	59.43(12)	B(6)	B(11)	B(10)	58.75(12)
B(5)	B(4)	B(9)	59.53(12)				

Table 2.5 Anisotropic Thermal Parameters ($Å^2$) in [dmsoH.dmso][7,8-*nido*-$C_2B_9H_{12}$], [dmsoH.dmso]**(1)**

	U11	U22	U33	U23	U13	U12
S(1)	0.0296(3)	0.0224(3)	0.0379(4)	0.0050(2)	-0.0004(3)	-0.0043(2)
S(2)	0.0310(4)	0.0296(4)	0.0325(4)	0.0041(2)	0.0019(3)	-0.0050(2)
O(1)	0.0357(8)	0.0288(7)	0.0498(12)	0.0036(7)	-0.0134(7)	-0.0032(7)
O(2)	0.0311(7)	0.0281(8)	0.0405(10)	0.0029(6)	-0.0013(7)	-0.0027(5)
C(11)	0.0259(11)	0.0474(13)	0.0316(14)	0.0111(10)	0.0098(10)	-0.0022(9)
C(12)	0.0397(12)	0.0404(12)	0.0239(13)	-0.0023(10)	0.0112(11)	-0.0047(9)
C(21)	0.0483(13)	0.0511(14)	0.0323(14)	-0.0060(11)	0.0239(12)	-0.0212(11)
C(22)	0.0424(13)	0.0492(15)	0.0491(17)	-0.0087(12)	0.0291(12)	-0.0095(11)
B(1)	0.0191(10)	0.0229(10)	0.0256(13)	-0.0021(8)	0.0084(9)	-0.0019(7)
B(2)	0.0250(11)	0.0256(10)	0.0273(14)	-0.0018(9)	0.0048(10)	-0.0008(8)
B(3)	0.0219(11)	0.0243(10)	0.0321(14)	-0.0026(9)	0.0144(10)	0.0018(8)
B(4)	0.0256(10)	0.0256(10)	0.0231(13)	0.0012(8)	0.0111(9)	-0.0024(8)
B(5)	0.0216(9)	0.0199(9)	0.0263(13)	-0.0031(8)	0.0087(8)	0.0004(7)
B(6)	0.0283(11)	0.0271(10)	0.0214(12)	-0.0057(9)	0.0107(10)	-0.0026(8)
C(7)	0.0263(9)	0.0195(8)	0.0283(12)	-0.0006(7)	0.0079(8)	0.0011(7)
C(8)	0.0300(10)	0.0208(9)	0.0193(11)	-0.0052(7)	0.0106(8)	0.0007(7)
B(9)	0.0222(10)	0.0243(9)	0.0214(13)	-0.0005(9)	0.0039(10)	-0.0017(8)
B(10)	0.0225(10)	0.0270(10)	0.0250(13)	-0.0049(9)	0.0126(10)	-0.0044(8)
B(11)	0.0313(11)	0.0267(10)	0.0252(13)	0.0036(9)	0.0112(10)	-0.0048(8)

There is a small (0.1Å), but statistically significant difference in S=O bond lengths, that to the protonated oxygen (O(1)) being the longer, (S(1)-O(1) = 1.5498(17)Å, S(2)-O(2) = 1.5377(16)Å). (In such cases, two measurements are normally regarded as significantly different if the difference between them is greater than twice the estimated standard deviation (e.s.d.) on that difference, a condition which holds true for the above measurements). Although O-protonation of a molecule such as dmso is conventionally thought of as a proton/lone-pair interaction, the above observation suggests that the MO involved possesses some bonding character between S and O, which is lessened upon interaction with H^+.

The [7,8-*nido*-$C_2B_9H_{12}$]$^-$ anion, **(1)**, is shown in **Figure 2.3** from a position above the open [C_2B_3] face, and the appropriate molecular numbering scheme is also given. *Exo* H atoms have the same number as the boron or carbon to which they are bonded.

The *nido*-icosahedral nature of the cage is clearly seen, with each vertex bearing an *exo*-polyhedral hydrogen atom (N.B. H(1) is completely obscured in this view by B(1)).

The open [C(7)C(8)B(9)B(10)B(11)] face of the anion is not planar, but is slightly folded into an envelope conformation about the B(9)..B(11) vector, such that B(10) and the C(7)-C(8) connectivity both dip towards the lower 5-boron belt (defined by B(2)B(3)B(4)B(5)B(6)), which is planar (σ = 0.0126Å). The [B(9)B(10)B(11)] and [B(11)C(7)C(8)B(9)] portions of the open face make fold angles [54] of $\phi = 2.34^o$ and $\theta = 1.88^o$ with the lower pentagonal plane. This type of folding in the upper face is commonly observed for complexes of [$C_2B_9H_{11}$]$^{2-}$

and related ligands [54].

The major result of the crystallographic study is the location of the 12th hydrogen atom, H(12), associated with the carbaborane anion. It is clearly seen from **Figure 2.3** that this atom occupies an *endo*-terminal site, bonded to B(10), giving the anion overall effective (though not crystallographically employed) C_s symmetry in the solid state.

In order to check that H(12) is ordered in this structure (and not disordered over two possible bridging positions on the B(9)-B(10) and B(10)-B(11) connectivities), a least-squares refinement was performed with H(12) and (for comparison) H(10) removed from the model. The two largest peaks in the resulting ΔF synthesis correspond to H(10) (0.83eÅ^{-3}) and H(12) (0.53eÅ^{-3}) respectively. The third highest peak (0.39eÅ^{-3}), *ca*. 1Å from S(2) is assigned to a sulphur lone pair.

The H(10)-B(10)-H(12) angle, at 109.7(19)^{o} is, within the limits of the experiment, the tetrahedral ideal, and the distances from H(12) to B(9) and B(11) are equal, at 1.71(3)Å. The lengths of the B(9)-B(10) and B(10)-B(11) edges are typical of those for unbridged connectivities [55].

Consistent with the structural results for other {BH_2}-containing *nido* species [51,52], the *endo* B-H bond appears a little longer than *exo* B-H bonds involving similarly-connected boron atoms, although the e.s.d.'s on these distances are sufficiently large (even in this relatively accurate structure) to make significant discussion of this (apparent) difference impossible.

Extended Hückel Molecular Orbital Calculations

Introduction

The key finding of the structural analysis, *viz* the determination of an *endo* H atom in **(1)**, rather than a μ-H atom, has been further studied by theoretical methods.

By simple consideration of the HOMO of $[7,8\text{-}nido\text{-}C_2B_9H_{11}]^{2-}$ and the LUMO (i.e. the only MO) of H^+, we can attempt to rationalise the observed structure, by predicting the preferred site of protonation of the $\{7,8\text{-}C_2B_9H_{11}\}^{2-}$ fragment.

Discussion

The frontier MO's of $[C_2B_9H_{11}]^{2-}$ have been reported previously [40], but these EHMO calculations have been repeated for the present purpose, with charge iteration according to $H_{ii} = [H_{ii}^{\ 0} + (\text{sense}) \times (\text{charge})]$ and using the experimental geometry of the $\{C_2B_9H_{12}\}^{2-}$ fragment, derived from the crystallographically-determined model of **(1)** by removal of H(12). These results are given in **Figure 1.5**.

The HOMO of the $\{7,8\text{-}C_2B_9H_{11}\}^{2-}$ fragment calculated by extended Hückel methods is an *a'* orbital, which is localised chiefly on B(10) (41%), with smaller in-phase coefficients on B(9) and B(11) (13% on each).

The HOMO is sketched below in **Figure 2.4**, showing the contributions from the boron atoms in the open face of the carbaborane fragment. These components are s-p hybrids, directed upwards and slightly inwards from the open face.

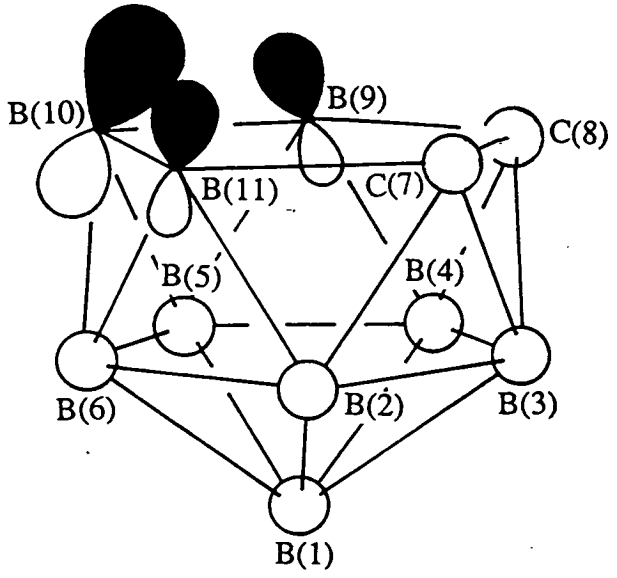

Figure 2.4 HOMO of $[7,8\text{-}C_2B_9H_{11}]^{2-}$

It is obvious from the form of this HOMO that interaction with the empty 1s orbital of H^+ (its LUMO) will result in protonation above B(10), within the projection of the open pentagonal face of the molecule to give the *endo* H atom located by the accurate crystallographic experiment.

This rationalisation of the structural features of **(1)** is only part of the use to which EHMO calculations on this system may be put. For example, the results of such calculations also allow understanding of the relative magnitudes of *exo* and *endo* B-H coupling constants to be gained.

This may be achieved by comparison of the results of calculations on two different $\{C_2B_9H_{11}\}^{2-}$ fragments, the first, **(a)**, derived by the removal of H(12), and the second **(b)**, by removal of H(10) from the crystallographically determined structure of $[7,8\text{-}C_2B_9H_{12}]^-$.

The composition of the HOMO's of these two fragments is presented in tabular form in **Table 2.6** (below).

Table 2.6 Composition of HOMO's of $\{C_2B_9H_{11}\}^{2-}$ Fragments

Fragment	HOMO localisation	B(2s) character	B(2p) character
(a) H(12) removed	B(10) 41%	12%	88%
	B(9) 13%	9%	91%
	B(11) 13%	10%	90%
(b) H(10) removed	B(10) 89%	23%	77%

For model **(b)**, the HOMO is clearly a true "sp^3 hybrid" localised on B(10), pointing outward from the carbaborane framework. The magnitude of the coupling constant $J_{B(10)H(10)}$, 134 ± 5 Hz, is typical of that for a 2 centre-2 electron *exo*-terminal B-H bond.

The HOMO produced by the calculation on fragment **(a)**, with H(12) removed from B(10), is rather different to that described above. Not only is the HOMO more delocalised, but it also possesses less percentage B(2s) character. The *endo* coupling constant, $J_{B(10)H(12)}$, is 50 ± 5 Hz, and it has been suggested that the low magnitudes of such coupling constants may be related to the relatively small amounts of B(2s) character in B-H *endo* bonds as compared to *exo* 2c-2e bonds. This assertion is fully supported by the above (**Table 2.6**) results of our calculations.

Finally, in earlier discussion of the n.m.r. spectra of **(1)**, a small but real interaction between H(12) and B(9),B(11) was implied by the ^1H-{^{11}B selective} experiment. This may now be rationalised by the form of the HOMO of **(a)**, showing in-phase contributions from B(9) and B(11) which possess some (9-10%)

B(2s) character, thus allowing a degree of interaction between the H(12) and the B(9) and B(11) nuclei in **(1)**.

[BTMA][10-*endo*-(PPh_3Au)-7,8-*nido*-$C_2B_9H_{11}$], [BTMA](2)

Introduction

The *X*-ray structural determination for the [7,8-*nido*-$C_2B_9H_{12}$]$^-$ anion, **(1)**, and the rationalisation of the position of its *endo* H atom H(12) by EHMO calculation have prompted investigation of complex **(2)**, [$PPh_3AuC_2B_9H_{11}$]$^-$. The interest in **(2)** is a result of the well-known isolobal analogy between the proton and the {PR_3Au^+} fragment [56].

After having succesfully synthesised and characterised the complex, its structure was determined by *X*-ray methods, to allow comparison to be made with **(1)** and with the copper (I) analogue [3-PPh_3-3,1,2-$CuC_2B_9H_{11}$]$^-$ [43] (see later).

Synthesis and Characterisation of [BTMA](2)

The complex was prepared by addition of dichloromethane to a mixture of equimolar quantities of solid Tl[$TlC_2B_9H_{11}$], PPh_3AuCl and [BTMA]Cl and stirring overnight. After filtration, the compound was purified by slow diffusion of n-hexane into a CH_2Cl_2 solution at -30^{0}C. This yielded large colourless needle-shaped crystals suitable for *X*-ray study. A more detailed description of the experimental procedure is given in Chapter 6, section 1.

Chemical characterisation was by means of elemental (C,H,N) microanalysis, infra-red spectroscopy and multielement n.m.r. spectroscopy.

The microanalytical results were consistent with the proposed formulation of the salt, along with an associated dichloromethane molecule of solvation (as found by the *X*-ray experiment).

The major feature of the infra-red spectrum of [BTMA]**(2)** is the B-H stretching envelope, centred on $2540cm^{-1}$.

^{1}H, ^{11}B, ^{11}B-{^{1}H} and ^{31}P n.m.r. spectra were recorded as CD_2Cl_2 solutions at ambient temperature, each serving to confirm the postulated structure of the molecule.

The ^{1}H spectrum shows a complicated multiplet between δ 7.40 and 7.75 p.p.m. corresponding to the H atoms of the PPh_3 group and the phenyl H's of the cation. Singlet resonances at δ 4.41 and 3.05 correspond to the methylene and methyl protons of the $[BTMA]^+$ counter-ion respectively.

The proton-decoupled ^{11}B spectrum exhibits 5 resonances, of relative intensity 3:2:1:2:1. (The highest frequency peak, at δ -16.19 p.p.m., having relative intensity 3, arises from an accidental co-incidence of 2 resonances in the ratio 2:1). All of the signals show doublet coupling in the ^{11}B spectrun, indicating that each B environment has an associated *exo* proton.

The ^{31}P spectrum shows only 1 peak, as expected, which occurs at δ 41.3 p.p.m..

Structural Study of [BTMA](2)

Introduction

Following the discovery of the *endo* H atom in **(1)** and the calculation of the HOMO of [7,8-*nido*-$C_2B_9H_{11}$]$^{2-}$ showing the 4 centre-2 electron nature of the interaction of H(12) with the carbaborane, the structural investigation of the isolobally-substituted species **(2)** should shed some light on the relative magnitudes of the interaction between the ligand HOMO and the LUMO of each of the incoming cationic fragments.

Discussion

4 ion-pairs of [BTMA]**(2)** crystallise in the monoclinic space group $P2_1/c$, along with one CH_2Cl_2 solvate molecule per molecule of carbametallaborane. Final coordinates of refined atoms are given in **Table 2.7** along with equivalent isotropic thermal parameters for non-hydrogen atoms. Relevant interatomic distances and interbond angles are presented in **Tables 2.8** and **2.9** respectively. Anisotropic thermal parameters are given in **Table 2.10**. Calculated coordinates of (non-refined) hydrogen atoms comprise **Table 2.11**.

Distances and angles pertinent to the [BTMA]$^+$ ion and the dichloromethane molecule are in good agreement with other structurally characterised examples [55,57], and are therefore unexceptional.

The anion **(2)** is viewed in projection in **Figure 2.5**, giving the numbering scheme adopted. Note that the anion has been numbered as a *nido* species, following its relationship to **(1)**.

Figure 2.5 Perspective View of [10-*endo*-(PPh_3Au)-7,8-*nido*-$C_2B_9H_{11}$]$^-$, **(2)**

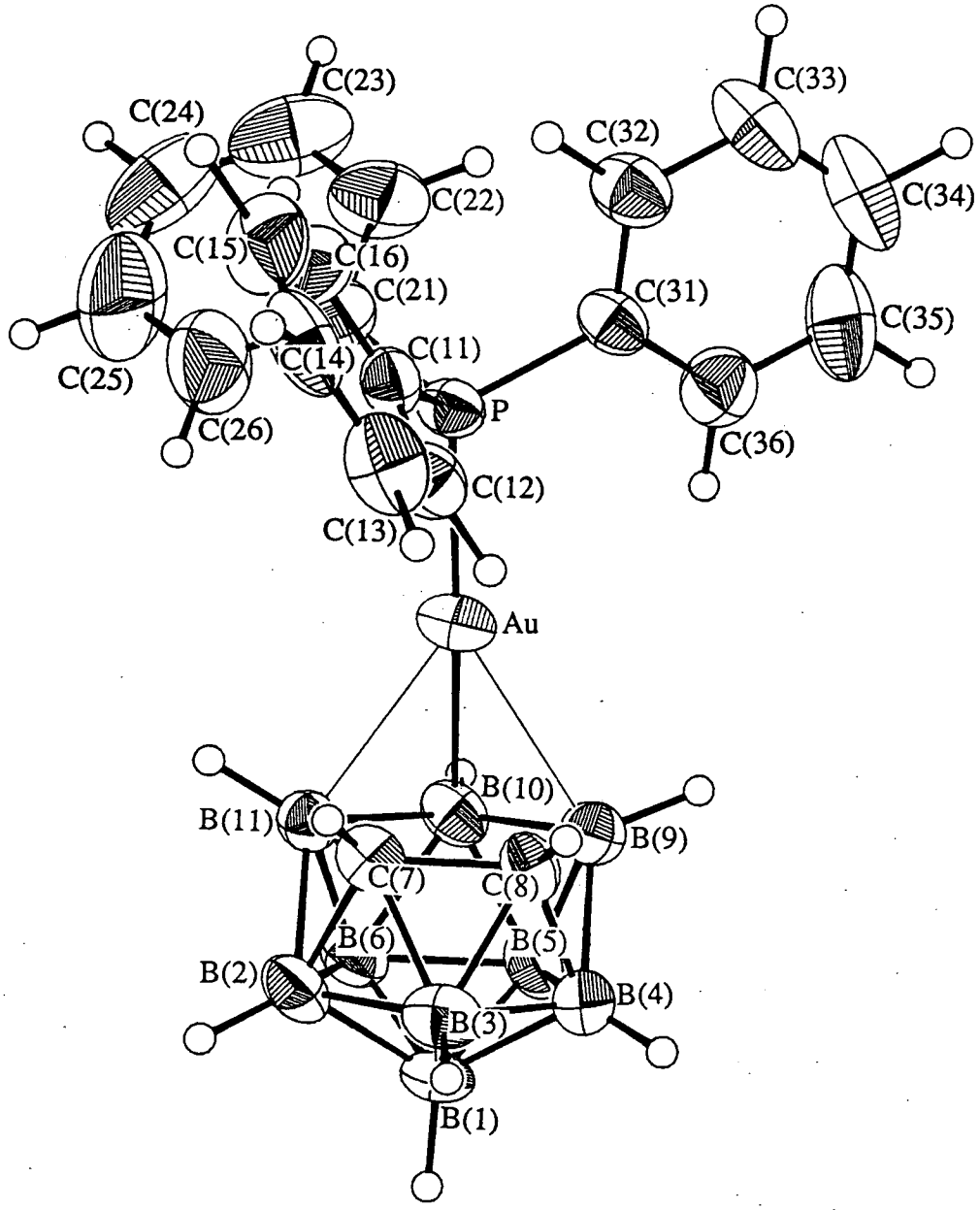

Figure 2.6 Alternative View of Central Fragment of [10-*endo*-(PPh_3Au)-7,8-*nido*-$C_2B_9H_{11}$]$^-$, **(2)**

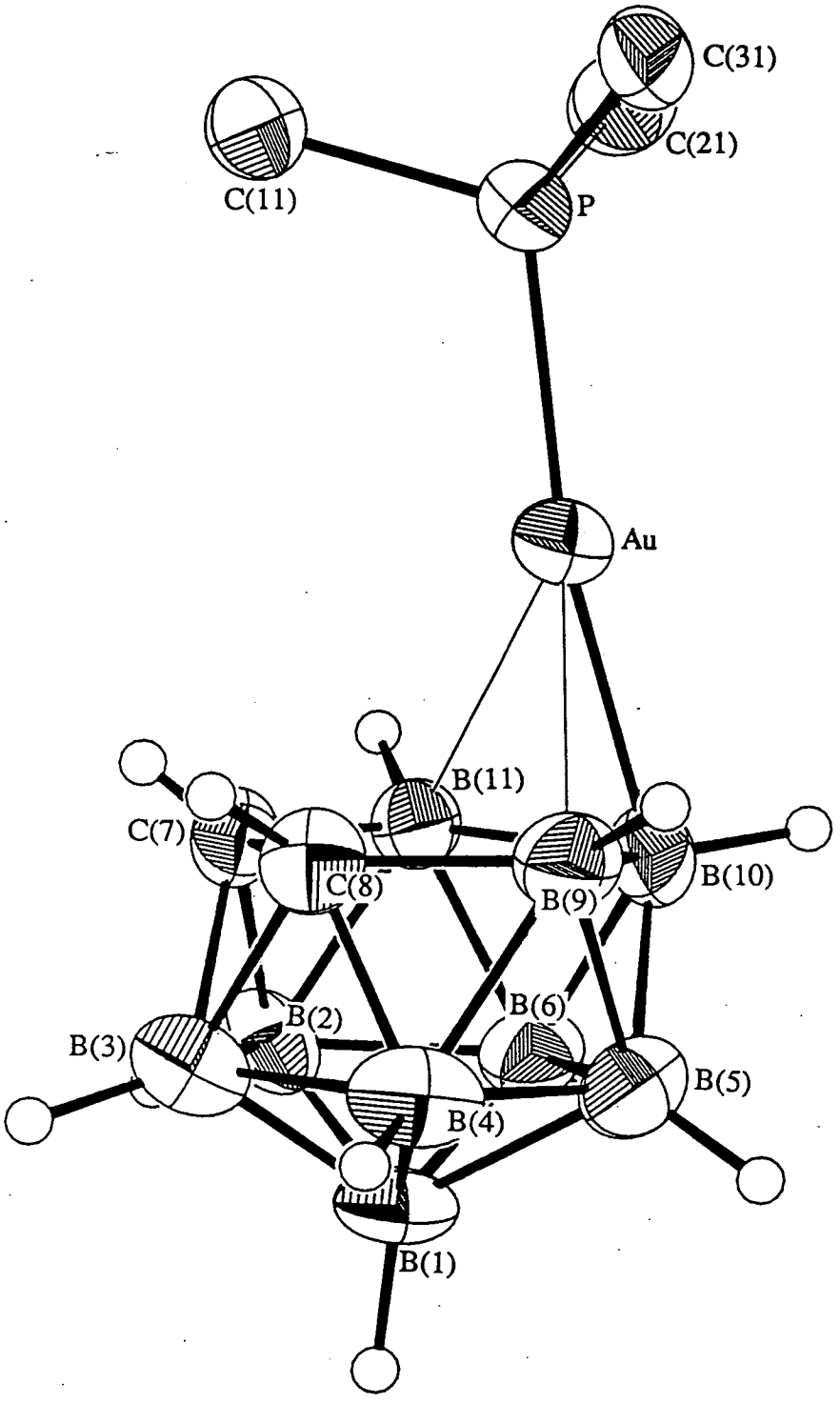

Table 2.7 Coordinates of Refined Atoms and Equivalent Isotropic Thermal Parameters ($Å^2$) for [BTMA][10-*endo*-(PPh_3Au)-7,8-*nido*-$C_2B_9H_{11}$], [BTMA]**(2)**

	x	y	z	Ueq
Au	0.16427(3)	0.31862(2)	0.89926(2)	0.0503(2)
P	0.09092(21)	0.41596(10)	0.84682(10)	0.0436(11)
C(11)	0.1842(6)	0.43290(20)	0.7692(3)	0.045(4)
C(12)	0.2228	0.37584	0.7302	0.054(5)
C(13)	0.2904	0.38605	0.6690	0.071(6)
C(14)	0.3193	0.45332	0.6468	0.068(6)
C(15)	0.2806	0.51038	0.6858	0.077(7)
C(16)	0.2130	0.50017	0.7470	0.065(6)
C(21)	0.1165(6)	0.4926(4)	0.8976(3)	0.059(5)
C(22)	0.0097	0.5403	0.9098	0.085(7)
C(23)	0.0355	0.5979	0.9509	0.108(10)
C(24)	0.1680	0.6079	0.9797	0.112(10)
C(25)	0.2748	0.5602	0.9674	0.140(13)
C(26)	0.2491	0.5026	0.9264	0.111(10)
C(31)	-0.0920(6)	0.41649(25)	0.8208(3)	0.047(4)
C(32)	-0.1488	0.46924	0.7806	0.061(6)
C(33)	-0.2918	0.46967	0.7653	0.081(7)
C(34)	-0.3780	0.41735	0.7903	0.095(8)
C(35)	-0.3213	0.36459	0.8305	0.092(8)
C(36)	-0.1783	0.36416	0.8457	0.068(6)
B(1)	0.3963(10)	0.1128(5)	0.9348(5)	0.052(6)
B(2)	0.4947(9)	0.1867(5)	0.9146(4)	0.051(5)
B(3)	0.4061(11)	0.1387(5)	0.8507(5)	0.058(6)
B(4)	0.2487(11)	0.1116(5)	0.8834(5)	0.055(6)
B(5)	0.2288(10)	0.1416(5)	0.9659(5)	0.051(6)
B(6)	0.3874(9)	0.1895(5)	0.9861(4)	0.049(5)
C(7)	0.3905(8)	0.2270(4)	0.8559(4)	0.044(5)
C(8)	0.2558(7)	0.1854(4)	0.8392(3)	0.044(4)
B(9)	0.1430(10)	0.1876(5)	0.8989(5)	0.050(5)
B(10)	0.2248(10)	0.2326(5)	0.9686(5)	0.047(6)
B(11)	0.3899(9)	0.2623(4)	0.9312(4)	0.043(5)
H(1)	0.453(10)	0.065(5)	0.951(4)	
H(2)	0.606(10)	0.186(5)	0.906(4)	
H(3)	0.458(10)	0.110(5)	0.807(5)	
H(4)	0.218(10)	0.071(5)	0.853(5)	
H(5)	0.177(10)	0.110(5)	1.001(5)	
H(6)	0.430(10)	0.192(5)	1.036(5)	
H(7)	0.426(11)	0.253(5)	0.829(5)	
H(8)	0.234(11)	0.187(5)	0.792(5)	
H(9)	0.029(11)	0.179(5)	0.891(5)	
H(10)	0.169(10)	0.251(5)	1.015(5)	
H(11)	0.450(10)	0.314(5)	0.934(5)	
C(41)	0.8220(5)	0.2713(3)	0.6193(4)	0.063(6)
C(42)	0.6935	0.2499	0.6447	0.076(7)
C(43)	0.6883	0.2142	0.7059	0.106(10)
C(44)	0.8117	0.1998	0.7416	0.113(10)
C(45)	0.9403	0.2212	0.7162	0.122(11)

C(46)	0.9454	0.2569	0.6550	0.095(8)
C(47)	0.8272(9)	0.3102(4)	0.5525(5)	0.063(6)
C(48)	0.9307(8)	0.4171(5)	0.6067(5)	0.067(6)
C(49)	0.6784(8)	0.4085(5)	0.5911(5)	0.069(6)
C(50)	0.8289(11)	0.4204(5)	0.4921(5)	0.078(7)
N	0.8171(7)	0.3894(4)	0.5610(4)	0.056(4)
Cl(1)	-0.3109(5)	0.6811(3)	0.84302(20)	0.183(4)
Cl(2)	-0.3810(8)	0.5613(4)	0.9116(5)	0.315(9)
C(99)	-0.3908(20)	0.6441(8)	0.9083(7)	0.162(15)

Table 2.8 Interatomic Distances (Å) in [BTMA][10-*endo*-(PPh_3Au)-7,8-*nido*-$C_2B_9H_{11}$], [BTMA]**(2)**

Au	- P	2.2485(20)	B(4)	- H(4)	1.02(10)
Au	- B(9)	2.528(9)	B(5)	- B(6)	1.813(13)
Au	-B(10)	2.222(9)	B(5)	- B(9)	1.785(13)
Au	-B(11)	2.486(9)	B(5)	-B(10)	1.751(13)
P	-C(11)	1.816(5)	B(5)	- H(5)	1.05(9)
P	-C(21)	1.799(7)	B(6)	-B(10)	1.790(13)
P	-C(31)	1.815(6)	B(6)	-B(11)	1.773(13)
B(1)	- B(2)	1.752(13)	B(6)	- H(6)	1.07(10)
B(1)	- B(3)	1.744(14)	C(7)	- C(8)	1.548(10)
B(1)	- B(4)	1.729(14)	C(7)	-B(11)	1.640(12)
B(1)	- B(5)	1.808(14)	C(7)	- H(7)	0.81(10)
B(1)	- B(6)	1.792(13)	C(8)	- B(9)	1.611(12)
B(1)	- H(1)	1.12(9)	C(8)	- H(8)	0.96(10)
B(2)	- B(3)	1.774(14)	B(9)	-B(10)	1.798(13)
B(2)	- B(6)	1.759(13)	B(9)	- H(9)	1.11(10)
B(2)	- C(7)	1.707(12)	B(10)	-B(11)	1.841(13)
B(2)	-B(11)	1.798(13)	B(10)	-H(10)	1.14(9)
B(2)	- H(2)	1.08(9)	B(11)	-H(11)	1.14(10)
B(3)	- B(4)	1.725(14)	C(41)	-C(47)	1.522(11)
B(3)	- C(7)	1.708(13)	C(47)	- N	1.536(11)
B(3)	- C(8)	1.706(13)	C(48)	- N	1.502(11)
B(3)	- H(3)	1.14(9)	C(49)	- N	1.505(11)
B(4)	- B(5)	1.747(14)	C(50)	- N	1.495(12)
B(4)	- C(8)	1.670(12)	Cl(1)	-C(99)	1.669(17)
B(4)	- B(9)	1.805(14)	Cl(2)	-C(99)	1.595(18)

Table 2.9 Selected Interbond Angles (°) in [BTMA][10-*endo*-(PPh_3Au)-7,8-*nido*-$C_2B_9H_{11}$], [BTMA]**(2)**

P	- Au	- B(9)	143.53(21)	B(1)	- B(5)	- B(4)	58.2(5)
P	- Au	-B(10)	169.29(24)	B(1)	- B(5)	- B(6)	59.3(5)
P	- Au	-B(11)	138.08(21)	B(4)	- B(5)	- B(9)	61.5(5)
Au	- P	-C(11)	112.79(18)	B(6)	- B(5)	-B(10)	60.3(5)
Au	- P	-C(21)	112.62(23)	B(9)	- B(5)	-B(10)	61.1(5)
Au	- P	-C(31)	115.41(19)	B(1)	- B(6)	- B(2)	59.1(5)
C(11)	- P	-C(21)	105.2(3)	B(1)	- B(6)	- B(5)	60.2(5)
C(11)	- P	-C(31)	103.81(25)	B(2)	- B(6)	-B(11)	61.2(5)
C(21)	- P	-C(31)	106.1(3)	B(5)	- B(6)	-B(10)	58.2(5)
P	-C(11)	-C(12)	117.7(4)	B(10)	- B(6)	-B(11)	62.2(5)
P	-C(11)	-C(16)	122.3(4)	B(2)	- C(7)	- B(3)	62.6(5)
P	-C(21)	-C(22)	122.8(5)	B(2)	- C(7)	-B(11)	65.0(5)
P	-C(21)	-C(26)	117.2(5)	B(3)	- C(7)	- C(8)	63.0(5)
P	-C(31)	-C(32)	122.1(4)	B(3)	- C(8)	- B(4)	61.4(6)
P	-C(31)	-C(36)	117.8(4)	B(3)	- C(8)	- C(7)	63.1(5)
B(2)	- B(1)	- B(3)	61.0(6)	B(4)	- C(8)	- B(9)	66.7(6)
B(2)	- B(1)	- B(6)	59.5(5)	B(4)	- B(9)	- B(5)	58.2(5)
B(3)	- B(1)	- B(4)	59.6(6)	B(4)	- B(9)	- C(8)	58.2(5)
B(4)	- B(1)	- B(5)	59.1(5)	B(5)	- B(9)	-B(10)	58.5(5)
B(5)	- B(1)	- B(6)	60.5(5)	Au	-B(10)	- B(9)	77.1(4)
B(1)	- B(2)	- B(3)	59.3(5)	Au	-B(10)	-B(11)	74.8(4)
B(1)	- B(2)	- B(6)	61.4(5)	Au	-B(10)	-H(10)	98.7(48)
B(3)	- B(2)	- C(7)	58.7(5)	B(5)	-B(10)	- B(6)	61.6(5)
B(6)	- B(2)	-B(11)	59.8(5)	B(5)	-B(10)	- B(9)	60.4(5)
C(7)	- B(2)	-B(11)	55.7(5)	B(6)	-B(10)	-B(11)	58.4(5)
B(1)	- B(3)	- B(2)	59.8(5)	B(2)	-B(11)	- B(6)	59.0(5)
B(1)	- B(3)	- B(4)	59.8(6)	B(2)	-B(11)	- C(7)	59.3(5)
B(2)	- B(3)	- C(7)	58.7(5)	B(6)	-B(11)	-B(10)	59.3(5)
B(4)	- B(3)	- C(8)	58.2(5)	C(41)	-C(47)	- N	112.9(6)
C(7)	- B(3)	- C(8)	53.9(5)	C(47)	- N	-C(48)	111.8(6)
B(1)	- B(4)	- B(3)	60.6(6)	C(47)	- N	-C(49)	110.0(6)
B(1)	- B(4)	- B(5)	62.7(6)	C(47)	- N	-C(50)	106.8(6)
B(3)	- B(4)	- C(8)	60.3(5)	C(48)	- N	-C(49)	107.9(6)
B(5)	- B(4)	- B(9)	60.3(5)	C(48)	- N	-C(50)	110.3(7)
B(8)	- B(4)	- B(9)	55.1(5)	C(49)	- N	-C(50)	110.0(7)
				Cl(1)	-C(99)	-Cl(2)	115.4(10)

Table 2.10 Anisotropic Thermal Parameters ($Å^2$) in [BTMA][10-*endo*-(PPh_3Au)-7,8-*nido*-$C_2B_9H_{11}$], [BTMA]**(2)**

	U11	U22	U33	U23	U13	U12
Au	0.0522(2)	0.0505(2)	0.0484(2)	0.0076(2)	0.0032(1)	0.0165(2)
P	0.0393(12)	0.0440(11)	0.0474(11)	0.0034(9)	0.0042(9)	0.0067(9)
C(12)	0.0490(52)	0.0632(51)	0.0484(46)	-0.0070(39)	-0.0028(40)	0.0072(41)
C(13)	0.0558(60)	0.0997(74)	0.0564(54)	-0.0115(51)	0.0057(46)	-0.0013(53)
C(14)	0.0329(48)	0.1221(83)	0.0498(50)	0.0111(55)	0.0041(39)	-0.0048(54)
C(15)	0.0644(66)	0.0916(70)	0.0757(65)	0.0229(54)	0.0194(54)	-0.0230(55)
C(16)	0.0653(61)	0.0612(52)	0.0681(57)	0.0110(43)	0.0120(48)	-0.0051(45)
C(11)	0.0338(43)	0.0506(43)	0.0517(44)	0.0016(35)	-0.0002(35)	-0.0032(34)
C(22)	0.0932(81)	0.0728(64)	0.0905(72)	-0.0207(56)	0.0138(61)	0.0296(60)
C(23)	0.172(14)	0.0714(73)	0.0826(79)	-0.0166(59)	0.0187(85)	0.0269(81)
C(24)	0.203(16)	0.0667(69)	0.0652(70)	-0.0165(54)	0.0240(88)	-0.0322(88)
C(25)	0.137(13)	0.146(13)	0.138(12)	-0.046(10)	-0.034(10)	-0.043(11)
C(26)	0.0912(96)	0.1060(91)	0.135(11)	-0.0419(81)	-0.0254(83)	-0.0051(73)
C(21)	0.0584(59)	0.0585(51)	0.0587(52)	0.0078(40)	-0.0001(48)	-0.0020(43)
C(32)	0.0512(57)	0.0715(58)	0.0618(53)	0.0102(45)	0.0058(44)	0.0082(45)
C(33)	0.0478(62)	0.1215(89)	0.0728(64)	0.0127(61)	-0.0076(51)	0.0165(61)
C(34)	0.0466(65)	0.163(12)	0.0756(71)	-0.0078(73)	-0.0145(56)	-0.0048(72)
C(35)	0.0543(68)	0.139(10)	0.0825(74)	-0.0010(70)	0.0082(57)	-0.0343(68)
C(36)	0.0658(66)	0.0675(59)	0.0714(59)	0.0066(45)	0.0001(51)	-0.0068(49)
C(31)	0.0367(45)	0.0573(46)	0.0456(42)	0.0033(35)	0.0040(35)	0.0083(37)
B(1)	0.0507(63)	0.0402(48)	0.0641(61)	0.0105(43)	-0.0115(50)	0.0135(44)
B(2)	0.0305(47)	0.0642(53)	0.0580(51)	-0.0061(49)	-0.0002(39)	0.0105(47)
B(3)	0.0550(67)	0.0513(56)	0.0687(67)	-0.0021(48)	0.0000(54)	0.0123(49)
B(4)	0.0461(62)	0.0438(51)	0.0763(69)	0.0020(46)	-0.0141(53)	-0.0030(44)
B(5)	0.0330(56)	0.0609(60)	0.0587(61)	0.0195(47)	-0.0046(47)	-0.0040(45)
B(6)	0.0428(52)	0.0527(51)	0.0502(48)	0.0127(45)	-0.0063(41)	0.0061(46)
C(7)	0.0424(48)	0.0540(46)	0.0361(41)	0.0020(33)	0.0038(35)	0.0034(37)
C(8)	0.0384(43)	0.0562(42)	0.0370(35)	-0.0013(39)	-0.0100(32)	-0.0009(40)
B(9)	0.0410(54)	0.0462(45)	0.0621(51)	0.0098(50)	0.0023(43)	-0.0017(47)
B(10)	0.0371(55)	0.0598(57)	0.0455(52)	0.0028(42)	0.0050(43)	0.0063(43)
B(11)	0.0362(52)	0.0455(48)	0.0473(51)	0.0053(39)	0.0043(42)	0.0008(40)
C(42)	0.0537(66)	0.0765(63)	0.0987(79)	0.0125(57)	-0.0107(58)	-0.0100(52)
C(43)	0.111(11)	0.0885(79)	0.120(10)	0.0115(74)	0.0130(84)	-0.0202(74)
C(44)	0.152(13)	0.0889(86)	0.0971(87)	0.0205(67)	-0.0234(94)	-0.0022(87)
C(45)	0.098(10)	0.143(12)	0.124(11)	0.0532(91)	-0.0521(87)	-0.0171(88)
C(46)	0.0664(73)	0.1045(83)	0.1134(93)	0.0164(71)	-0.0447(68)	0.0004(62)
C(41)	0.0718(67)	0.0575(52)	0.0610(57)	-0.0053(40)	-0.0069(52)	0.0105(47)
C(47)	0.0563(57)	0.0582(56)	0.0749(59)	-0.0038(44)	-0.0100(46)	0.0031(43)
C(48)	0.0306(50)	0.0897(66)	0.0820(64)	-0.0178(52)	-0.0189(45)	-0.0047(46)
C(49)	0.0338(51)	0.0692(58)	0.1039(74)	-0.0119(52)	0.0085(49)	0.0020(43)
C(50)	0.0760(71)	0.0807(65)	0.0773(66)	0.0199(54)	-0.0130(57)	-0.0035(55)
N	0.0298(38)	0.0639(43)	0.0750(48)	-0.0028(37)	-0.0069(34)	0.0006(32)
Cl(1)	0.1709(42)	0.2866(64)	0.0921(24)	-0.0104(33)	0.0319(26)	-0.0675(41)
Cl(2)	0.2682(80)	0.1698(59)	0.510(13)	-0.0419(67)	0.2092(88)	0.0065(50)
C(99)	0.247(20)	0.139(14)	0.100(11)	-0.0231(92)	0.043(12)	0.032(13)

Table 2.11 Calculated Positions of Non-refined Hydrogen Atoms in [BTMA][10-*endo*-(PPh_3Au)-7,8-*nido*-$C_2B_9H_{11}$], [BTMA]**(2)**

	x	y	z
H(120)	0.2005	0.3238	0.7473
H(130)	0.3203	0.3419	0.6387
H(140)	0.3716	0.4612	0.5994
H(150)	0.3029	0.5625	0.6686
H(160)	0.1831	0.5444	0.7772
H(220)	-0.0929	0.5325	0.8875
H(230)	-0.0472	0.6348	0.9604
H(240)	0.1879	0.6525	1.0115
H(250)	0.3774	0.5680	0.9897
H(260)	0.3317	0.4657	0.9169
H(320)	-0.0820	0.5098	0.7613
H(330)	-0.3357	0.5105	0.7342
H(340)	-0.4887	0.4177	0.7785
H(350)	-0.3880	0.3241	0.8498
H(360)	-0.1343	0.3233	0.8768
H(420)	0.5979	0.2610	0.6170
H(430)	0.5888	0.1977	0.7256
H(440)	0.8077	0.1722	0.7890
H(450)	1.0358	0.2101	0.7439
H(460)	1.0450	0.2735	0.6353
H(471)	0.9248	0.2981	0.5282
H(472)	0.7408	0.2930	0.5210
H(481)	1.0337	0.4056	0.5878
H(482)	0.9180	0.3929	0.6554
H(483)	0.9187	0.4727	0.6116
H(491)	0.5940	0.3874	0.5606
H(492)	0.6671	0.4642	0.5945
H(493)	0.6751	0.3862	0.6411
H(501)	0.8242	0.4763	0.4874
H(502)	0.7474	0.3972	0.4612
H(503)	0.9297	0.4022	0.4755
HC(1)	-0.5002	0.6583	0.9058
HC(2)	-0.3442	0.6646	0.9541

Non-hydrogen atoms are represented by thermal ellipsoids at the 50% probabilty level. Hydrogen atoms have been given an artificial radius of 0.1Å for clarity. Cage H atoms carry the same number as the B or C to which they are bonded, and phenyl H's bonded to C(*ij*) are numbered H(*ij*0).

An alternative view is shown in **Figure 2.6**, showing more clearly the mode of ligation of the gold atom to the carbaborane cage. Phenyl rings are represented only by C(x1) where x = 1-3, *i.e.* the P-bonded carbons.

Initially apparent from **Figures 2.5** and **2.6** is the *endo* position adopted by the gold(I)phoshine fragment with respect to the carbaborane cage. The bonding mode is essentially σ in character, as discussed previously for **(1)**. There is also a strong similarity between the structure determined for **(2)** and that of the neutral $[PPh_3Hg(C_2B_9H_{11})]$ [42], where again an *endo*-type σ-bond was observed.

The Au-B(10) distance is 2.222(9)Å with the longer secondary interactions of the gold atom with B(9) and B(11) 2.528(9) and 2.486(9)Å respectively.

This slight asymmetry in the essentially C_S geometry of the anion is also evident in the P-Au-B(9) and P-Au-B(11) angles, which are 143.53(21) and 138.08(21)^o respectively. This represents a tilting of the Au-P vector from the symmetric position by *ca.* 2.7^o.

The open $[C_2B_3]$ face of the carbaborane is slightly folded into an envelope conformation about the B(9)..B(11) vector, with the C(7)-C(8) connectivity and B(10) both dipping towards the lower 5-boron belt, resulting in fold angles of θ = 3.15 and ϕ = 3.28^o. The gold atom is situated 2.062Å vertically above the open face, with the slip parameter, Δ [54], relative to the centroid of the lower 5B plane

calculated at 0.87Å.

The Au-B(10)-H(10) angle is 98.7(48)°, while the corresponding [H(12)-B(10)-H(10)] angle in **(1)** is, within experimental error, tetrahedral. The apparent narrowing of the angle in **(2)** is explained if we consider the acceptor orbital of the (triphenylphosphine)gold fragment to point towards where H(12) was located in **(1)**. This idea is also supported by the (apparent) non-linearity about the Au atom [P-Au-B(10) 169.29(24)Å]. We can imagine however, a linear arrangement between the phosphorous atom, the gold atom and the centre of the $\{PPh_3Au^+\}/\{C_2B_9H_{11}^{2-}\}$ LUMO/HOMO interaction, which would retain effective tetrahedral coordination about B(10).

Intra-cage distances and angles are within the accepted ranges for such parameters. Detailed analysis of facial B-B, B-C and C-C distances is contained in the following discussion on structural trends within the series $[C_2B_9H_{11}X]^-$, where X = H^+, $\{PPh_3Au^+\}$ and $\{PPh_3Cu^+\}$.

Structural Patterns in (1), (2) and $[PPh_3CuC_2B_9H_{11}]^-$

The structure of the $[3\text{-}PPh_3\text{-}3,1,2\text{-}CuC_2B_9H_{11}]^-$ anion has been determined previously [43] showing, unlike those of **(1)** or **(2)**, an essentially *closo* structure, with the copper atom slightly closer to the facial boron atoms than to the carbons. This results in a slip parameter [54], Δ, of 0.27Å. The structure is shown in **Figure 2.7** (overleaf). **Table 2.12** compares Δ, average B-B_{facial}, average B-C_{facial}, and C-C for **(1)**, **(2)** and $[PPh_3CuC_2B_9H_{11}]^-$.

Figure 2.7 Perspective View of $[3\text{-}PPh_3\text{-}3,1,2\text{-}CuC_2B_9H_{11}]^-$

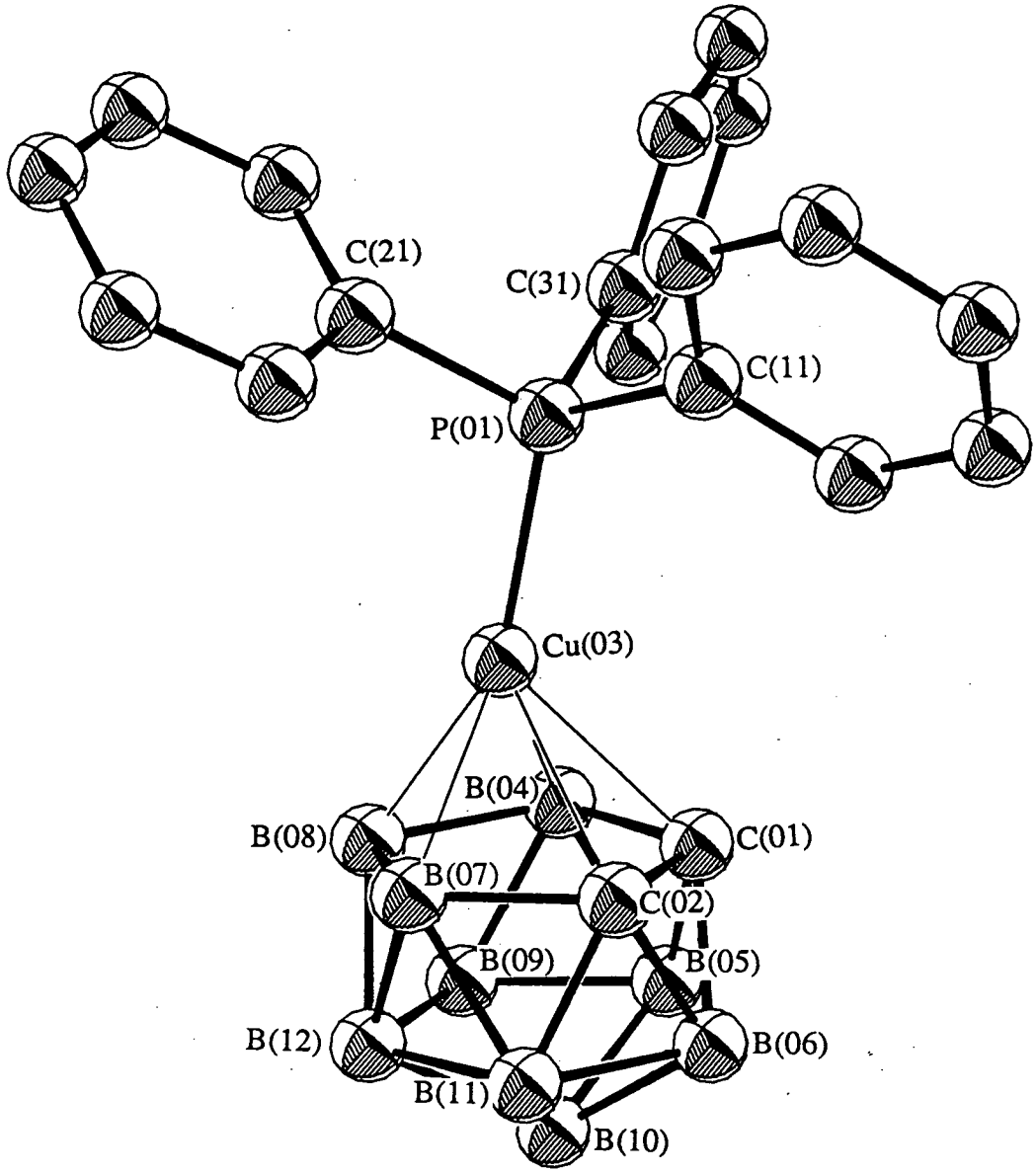

Table 2.12 Key Molecular Parameters (Å) in **(1)**, **(2)** and $[PPh_3CuC_2B_9H_{11}]^-$

$\{C_2B_9H_{11}\}^{2-}$	$\{H^+\}$	$\{PPh_3Au^+\}$	$\{PPh_3Cu^+\}$
Δ	0.91	0.87	0.27
Av. B-B_{facial}	1.833(3)	1.820(13)	1.768(10)
Av B-C_{facial}	1.610(3)	1.626(12)	1.666(10)
C-C	1.542(2)	1.548(10)	1.586(9)

Identifiable trends in going from H^+ to $\{PPh_3Au^+\}$ to $\{PPh_3Cu^+\}$ are:

(i) Δ, the slip parameter, decreases, (ii) Av. B-$B_{fac.}$ shortens, (iii) Av. B-$C_{fac.}$ lengthens, and (iv) C-C lengthens.

These changes are small between the protonated species **(1)** and the gold(I)phosphine analogue **(2)**, but are greatly magnified on going to the triphenylphosphinecopper(I) species. In order to gain some understanding of these structural patterns, let us consider the frontier molecular orbitals of the component parts of the three species.

All three complexes may be notionally divided into a common {7,8-*nido*-$C_2B_9H_{11}\}^{2-}$ fragment and H^+, $\{PPh_3Au^+\}$ and $\{PPh_3Cu^+\}$ cationic fragments respectively, and the observed structures rationalised in terms of the interactions of the frontier MO's of these fragments.

The π-MO's of the $[C_2B_9H_{11}]^{2-}$ anion (as calculated by charge-iterated extended Hückel methods on the experimentally-derived geometry, by removal of H(12) from **(1)**) have been presented in the previous chapter (see **Figure 1.5**). The filled π-MO's are sketched in **Figure 2.8**.

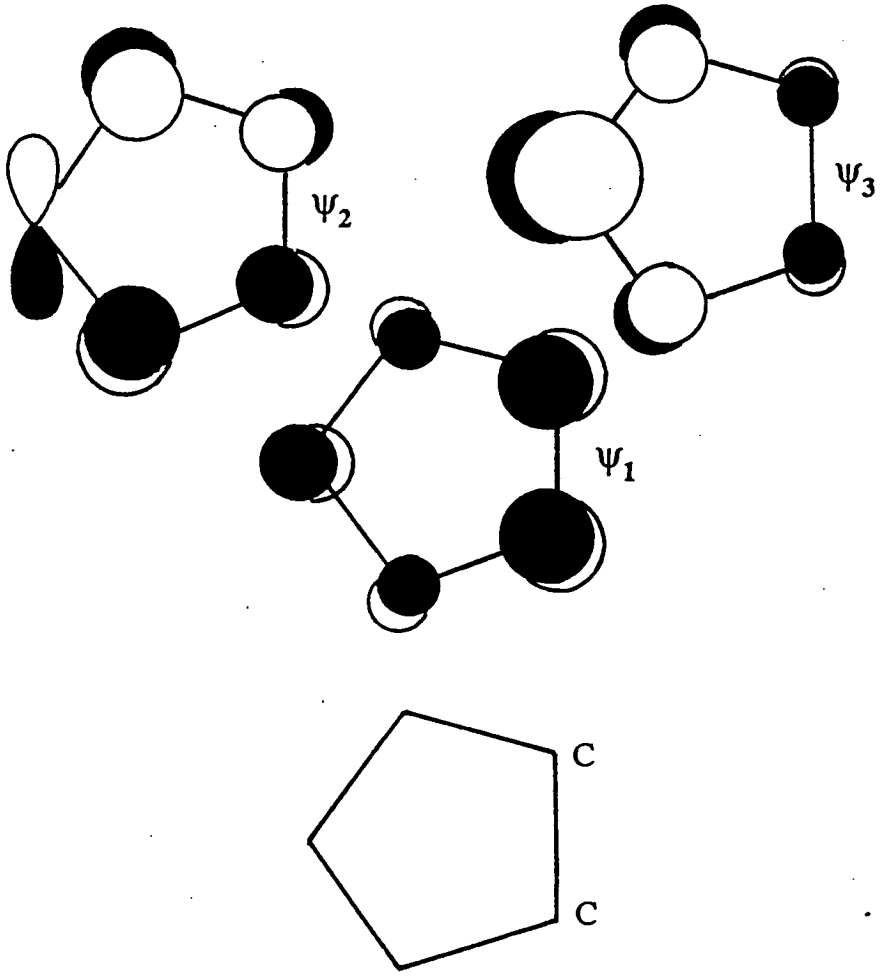

Figure 2.8

The trends in structural parameters observed are therefore related to the nature of the unfilled frontier molecular orbitals of the incoming cationic fragments and their ability to overlap with and depopulate the filled π-MO's of the carbaborane moiety.

H^+ has only one orbital (its 1s) which is, of course, empty. The frontier orbitals of $\{H_3PAu^+\}$ and $\{H_3PCu^+\}$ have been investigated previously by entended Hückel calculations [58]. In the gold case, these comprise a $6s/6p_z$ hybrid orbital of a_1 symmetry which is of suitable energy for bonding and a higher-lying *e* pair ($6p_x$,$6p_y$) which are of too high energy to act as efficient acceptor orbitals. Thus the isolobal analogy between the proton and the $\{R_3PAu^+\}$ fragment, and

the tendency for gold(I) to form linear $14e^-$ species such as PPh_3AuCl and **(2)**.

In the case of $\{H_3PCu^+\}$, the empty frontier orbitals are similar to those above, a $4s/4p_z$ hybrid (a_1) orbital and a degenerate $4p_x,4p_y$ (e) pair. In this case, however, unlike the phosphinegold(I) species, all three of these orbitals are of suitable energy to interact efficiently with filled orbitals of other ligands, accounting for the preference of Cu(I) for tetrahedral coordination.

The unfilled frontier molecular orbitals of $\{H_3PAu^+\}$ and $\{H_3PCu^+\}$ are shown in **Figure 2.9** (below).

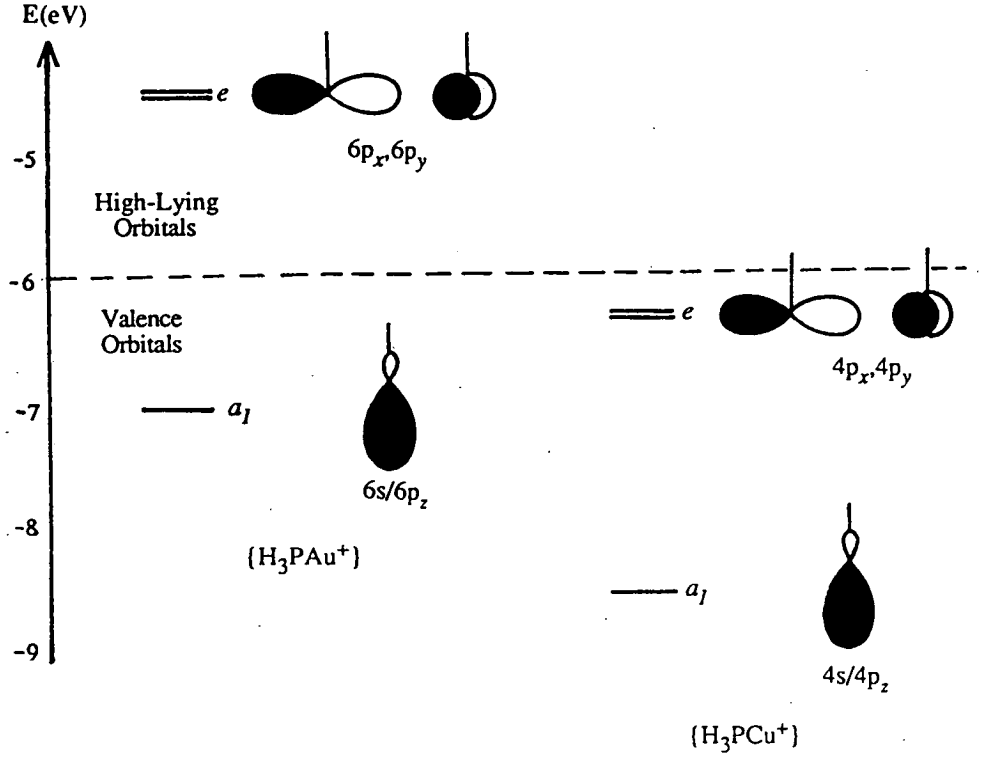

In order to understand the observed patterns, let us envisage the expected effects on the degree of depopulation of the filled carbaborane π-MO's of moving from interaction with the H(1s) orbital to the empty $\{H_3PCu^+\}$ frontier orbital set.

As discussed in some detail earlier, the key interaction in the bonding of H^+ to $[C_2B_9H_{11}]^{2-}$ (to form **(1)**) is a HOMO/LUMO overlap of Ψ_3 with H(1s). (Anion

(2) is formed by a similar HOMO/LUMO interaction of Ψ_3 with the $6s/6p_z$ hybrid orbital of the $\{Ph_3PAu^+\}$ fragment).

Upon moving to $\{PPh_3Cu^+\}$, the relative accessibility of the $4p_x$,$4p_y$ orbitals results in an attempt to maximise overlap with all three π-MO's of the $\{C_2B_9H_{11}\}^{2-}$ fragment with the copper acceptor orbitals, the most obvious result of which is the more central positioning of the copper atom in $[Ph_3PCuC_2B_9H_{11}]^-$ than of H(12) or Au in **(1)** or **(2)**.

Specifically, in addition to depopulation of Ψ_3, there is depopulation of Ψ_2 and Ψ_1, and the effects of these interactions are as follows:

(i) Ψ_3 (HOMO) is less depopulated than in the H^+ case, as a result of the slippage of the Cu atom to a more central position, and this will lead primarily to shortening of the facial B-B connectivites, a lesser lengthening effect on the B-C *fac.* distances and a small effect on the C-C distance. (Note that the predicted magnitudes are a function of the degree of localisation of the orbital on each of the atoms).

(ii) Depopulation of Ψ_2 will lead to (in decreasing order of importance), lengthening of B-C_{facial} and shortening of C-C.

(iii) Depopulation of Ψ_1 has a lengthening effect on all three types of bond, with the primary effect on the C-C distance, as the orbital is localised predominantly on the (more electronegative) carbon atoms.

The net result of the above three interactions on the B-B, B-C and C-C distances will be:

(a) B-B_{facial} shortens, because the major effect is the decreased depopulation of the HOMO (Ψ_3), which is chiefly localised on the facial boron atoms.

(b) B-C_{facial} lengthens, as all three changes in depopulation act in concert.

(c) The net effect on C-C is a lengthening, the depopulation of Ψ_1 (carbon-based) overriding the effects of changes in depopulation of the boron-based HOMO and 2nd HOMO.

All of the trends described above are as observed in the experimentally determined structures (relevant parameters are in **Table 2.12**, see before). The values for $[PPh_3AuC_2B_9H_{11}]^-$, **(2)**, lie very close to those for **(1)**, underlining the isolobal relationship, although the fact that they lie towards those for the copper(I) species suggests that there is at least some involvement of the relatively high-lying Au $6p_x$,$6p_y$ pair, as has been suggested previously by analysis of the structures of some small gold clusters [58].

Having previously discussed the isolobal analogy between $[7,8\text{-}C_2B_9H_{11}]^{2-}$ and the cyclopentadienide ion, it is of interest to contrast the effects upon intra-ring distances in $\{PPh_3Au^+\}$ and $\{PPh_3Cu^+\}$ complexes of $[C_5H_5]^-$ and its derivatives.

$PPh_3Au(C_5H_5)$ has been shown by n.m.r. study [59,60] to possess essentially a Au-C σ-bond, and is fluxional at room temperature. For reasons of instability, this complex was not characterised crystallographically, but the tetraphenylcyclopentadienyl complex $PPh_3Au(Ph_4C_5H)$ has been synthesised and studied by *X*-ray methods [61], the structure being shown in **Figure 2.10** with the phenyl rings, except for the P- and Cp-bonded carbon atoms, omitted for clarity.

Figure 2.10 Structures of $[PPh_3Au(Ph_4C_5H)]$ and $[PPh_3Cu(C_5H_5)]$

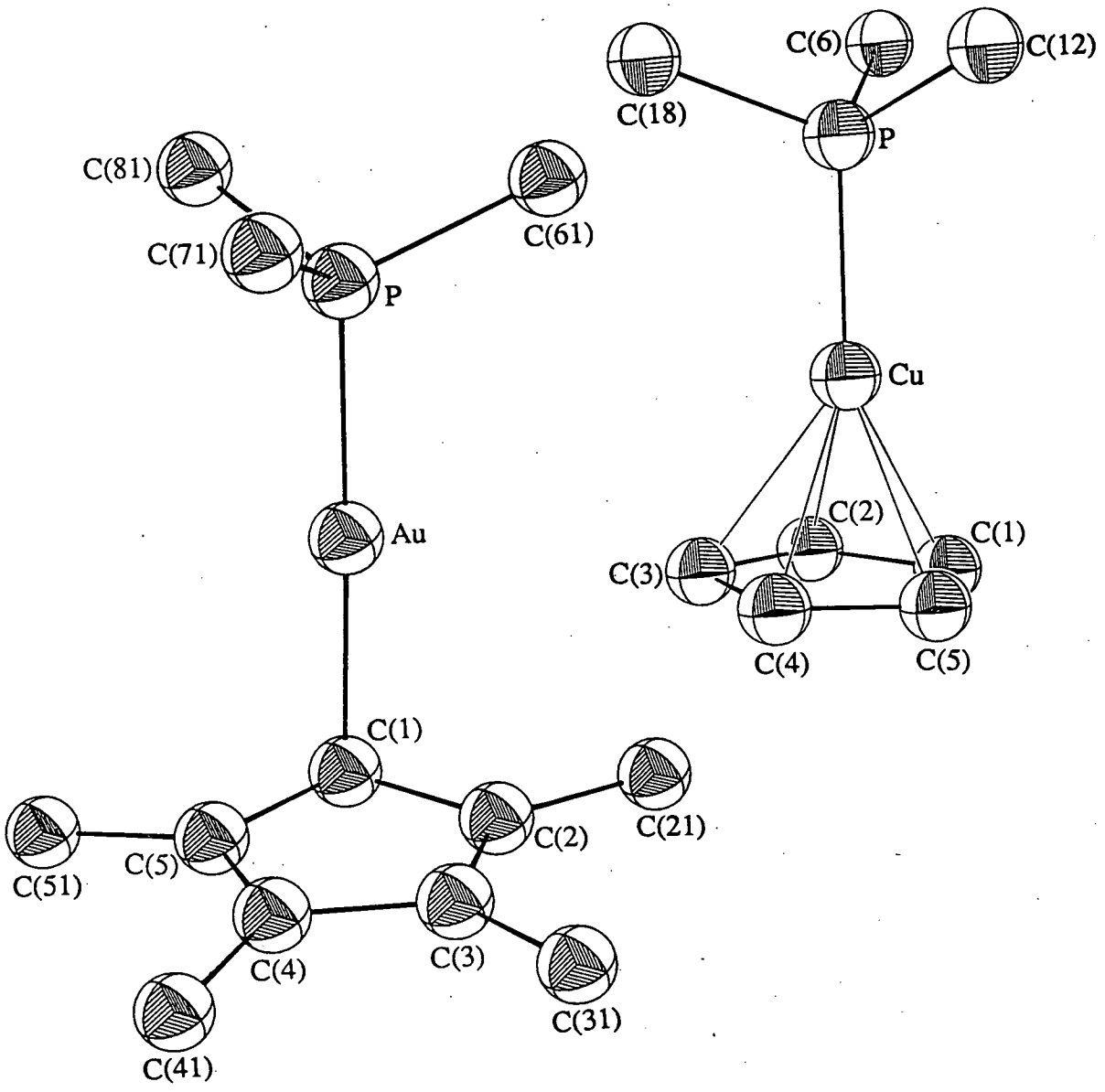

The essentially σ Au-C(1) interaction is clearly seen, with the additional interactions of the gold atom with C(2) and C(5), *c.f.* those of H(12) or Au with B(9) and B(11) in complexes **(1)** and **(2)**. Relevant distances are Au-C(1) = 2.15(1)Å, Au-C(2) = 2.67(1)Å and Au-C(5) = 2.76(1)Å.

The structure of the triphenylphosphinecopper(I) derivative of Cp^- was determined approximately 20 years ago [62], and is also shown in **Figure 2.10.** Again, phenyl rings are represented only by C(x1), where x = 1-3. For reasons similar to those discussed above for the carbaborane complex, the organic ligand adopts an essentially symmetrical η^5 bonding mode to the Cu atom.

Comparison of equivalent intra-facial C-C distances on moving from $\{PPh_3Au^+\}$ to $\{PPh_3Cu^+\}$ gives the following results:

The C(1)-C(2) and C(1)-C(5) bonds (≡ B-B_{facial}) shorten, the C(2)-C(3) and C(4)-C(5) bonds (≡ B-C_{facial}) lengthen, and C(3)-C(4) (≡ C-C) shortens.

These structural patterns, different to those observed for the analogous dicarbollide species, may be readily understood by bearing in mind the homocyclic nature of the cyclopentadienyl ligand, and the resultant set of π-MO's from extended Hückel calculation (see **Figure 1.5**, in the previous chapter).

Conclusions

The structure of $[7,8\text{-}C_2B_9H_{12}]^-$, **(1)**, has been determined, showing an *endo*-H atom, rather than the widely accepted μ-H and this result is supported by the results of n.m.r. and theoretical studies.

Moreover, isolobal replacement of the *endo*-terminal hydrogen atom by a (triphenylphoshine)gold(I) fragment leads to complex **(2)**, which has also been studied crystallographically.

Structural trends within the series **(1)**, **(2)** and the previously-known $[PPh_3Cu(C_2B_9H_{11})]^-$ species have been rationalised *via* the results of molecular orbital calculations.

Chapter 3

Carb'H and Group Ib Derivatives

[10,11-μ-H-9-SMe_2-7,8-*nido*-$C_2B_9H_{10}$], (carb'H), (3)

Introduction

The above compound was first prepared in the mid-1970's (along with a number of other structural isomers [6]), as a potential source, upon deprotonation, of the monoanionic carbaborane ligand [9-SMe_2-7,8-*nido*-$C_2B_9H_{10}$]$^-$, [carb']$^-$, as discussed in Chapter 1.

The compound was synthesised according to a modified version of a literature method, as described in Chapter 6, section 1.

Characterisation of (3)

Elemental (C,H) analysis was carried out, the results of which were consistent with the proposed $C_4H_{17}B_9S$ formulation of the compound.

N.m.r spectroscopy was also used to confirm the identity of the species. The results of the ^1H, ^{11}B and ^{11}B-{^1H} n.m.r studies confirmed the proposed structure of the compound, with -SMe_2 substitution at the B(9) position of the [7,8-C_2B_9] polyhedron, the resonance at δ -4.30 p.p.m. remaining as a singlet on retention of proton coupling in the ^{11}B spectrum.

The chief features of the ^1H n.m.r. spectrum are the 2 signals arising from the protons of the sulphur-bonded methyl groups. It was stated in the original report

of the characterisation of **(3)** that two different signals for these groups indicated a restricted degree of rotation about the S-B(9) bond. It is clear, however, that this spectral data gives no information whatever on the degree of rotation of the pendant dimethylsulphide group in solution, as the 2 methyl groups will always be magnetically inequivalent, no matter what the torsion about the S-B(9) bond, assuming no inversion of configuration occurs at sulphur. Initially, we considered that any restriction of rotation about the boron-sulphur bond at ambient temperature would be unlikely [63], but subsequent crystallographic work upon **(3)** and a number of its metal derivatives (see later) have called this early assertion into question, as in the solid state, at least, there appears to be a preferred orientation adopted by the dimethylsulphide group with respect to the carbaborane cage. It is not possible to say, however, whether or not this conformation persists in the solution phase.

The boron spectra were (partially) assigned by Hermanek *et al* [6], by comparison with those of the [7,8-*nido*-$C_2B_9H_{12}$]$^-$ anion. The second lowest frequency resonance was noted to have a smaller (30-45 Hz) coupling in the ^{11}B spectrum (in addition to the $J_{BH(exo)}$ coupling which is observed for all boron atoms except B(9)), and this was attributed to the presence of a μ-H atom on the B(9)-B(10) or B(10)-B(11) connectivity, i.e always retaining an interaction with the B(10) atom. This argument has also been put forward and widely upheld [64] with respect to the 12th H atom of [7,8-*nido*-$C_2B_9H_{12}$]$^-$ itself, but as discussed in Chapter 2, this cannot necessarily be taken as evidence for a bridging hydrogen, as it could also be interpreted in terms of a discrete {BH_2} unit within the carbaborane framework [51,52].

Structural study on (3)

Introduction

In view of the specific interest in **(3)** as the (protonated) precursor to the monoanionic carbaborane ligand [9-SMe_2-7,8-*nido*-$C_2B_9H_{10}$]$^-$, [carb']$^-$, it was notable that both the position and bonding mode of the 11th H atom (presumably that which is removed upon deprotonation) were not unambiguously determined by spectroscopic methods. To this end, an accurate, low-temperature *X*-ray crystallographic study of **(3)** was undertaken, the experimental details of which are to be found in Chapter 6, section 2.

Discussion of the Structure of (3)

The crystallographic study of **(3)** in the first instance confirms the identity of the compound, showing the *nido*-icosahedral nature of the 11-vertex cage and the SMe_2 function bonded to boron atom B(9), as inferred from the spectroscopic work.

The compound exists as 2 crystallographically independent molecules, *a* and *b*, in the asymmetric fraction of the unit cell. These molecules differ from each other only in the torsion angle about the S-B(9) bond, and this will be discussed more fully later in this chapter. Apart from the dimethylsulphide-B(9) torsion angle both molecules *a* and *b* exhibit the same general structural features.

Figure 3.1 shows a perspective view of molecule *a* of carb'H, with the appropriate molecular numbering scheme, and **Figure 3.2** is a view from above the open 5-atom face of the same molecule, showing the conformation of the

pendant SMe_2 ligand. In both figures, non-hydrogen atoms are represented by ellipsoids at the 50% probability level, and H atoms have been given artificial radii of 0.1Å for clarity. Cage *exo*-H atoms carry the same number as the boron or carbon atom to which they are attached.

In molecule *b* the S-B(9) torsion angle differs by around 23^{o} from that in molecule *a*, resulting in a conformation with nearer complete eclipsing of the sulphur lone pair and the B(9)-C(8) connectivity.

Table 3.1 gives the final atomic coordinates for all atoms (in both molecules) and (for non-H atoms) equivalent isotropic thermal parameters.

Interatomic distances are given in **Table 3.2**, interbond angles are contained in **Table 3.3**, and anisotropic thermal parameters for non-hydrogen atoms are given in **Table 3.4**.

The initial major point of interest from the structural determination is the site and bonding mode of the 11^{th} H atom associated with the polyhedron, labelled H(*), which is clearly shown to adopt a bridging position between B(10) and B(11) on the open 5-atom face of the carbaborane. It is noticeable that the bridge is significantly asymmetric in both molecules of carb'H; specifically H(*a)-B(10a) is 1.11(3)Å and H(*a)-B(11a) is 1.31(3)Å, where H(*b)-B(10b) is 1.22(3)Å and H(*b)-B(11b) is 1.39(3)Å. It is of some interest that the B-H-B bridge in [8-SMe_2-7,9-*nido*-$C_2B_9H_{11}$] is symmetric [65], with H-B(10) = H-B(11) = 1.28Å. The difference between these two bridging H's can be rationalised by the following treatment:

Figure 3.1 Perspective View of carb'H, **(3)**, (molecule *a*)

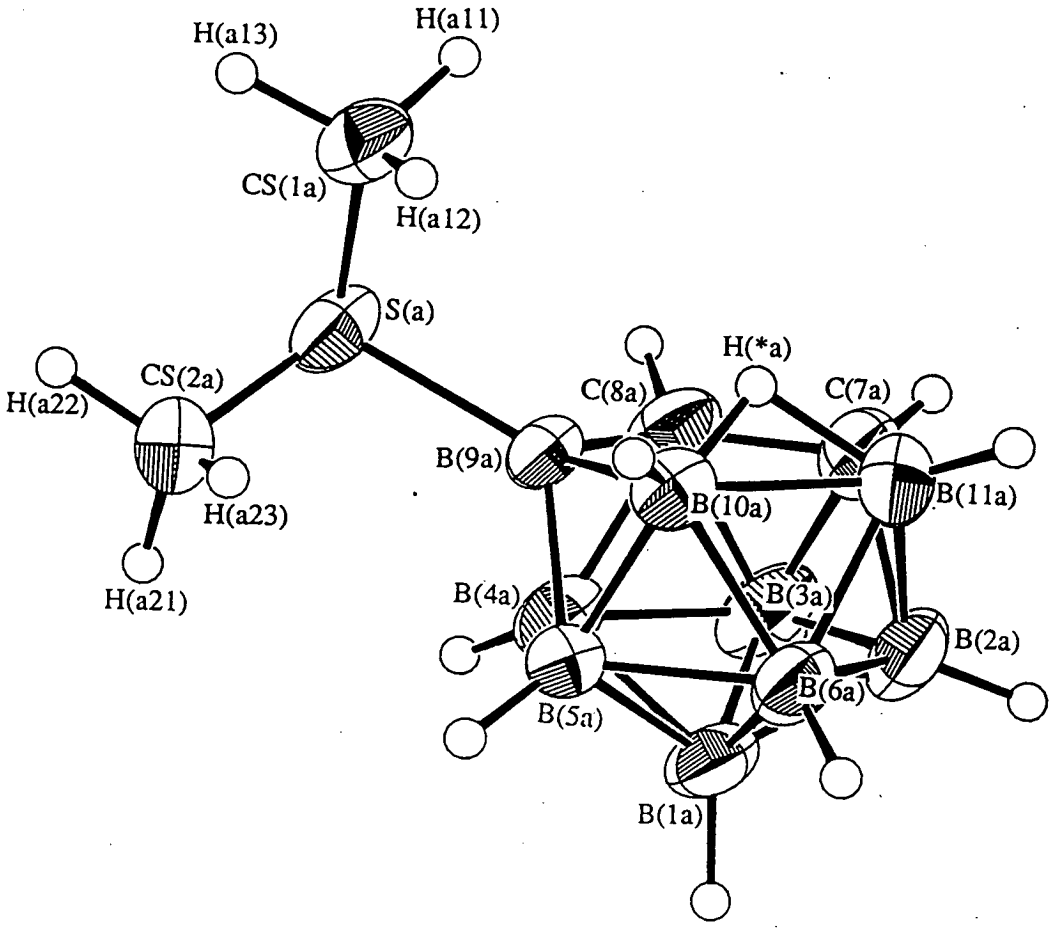

Figure 3.2 View From Above Open Face of carb'H, **(3)**, (molecule *a*)

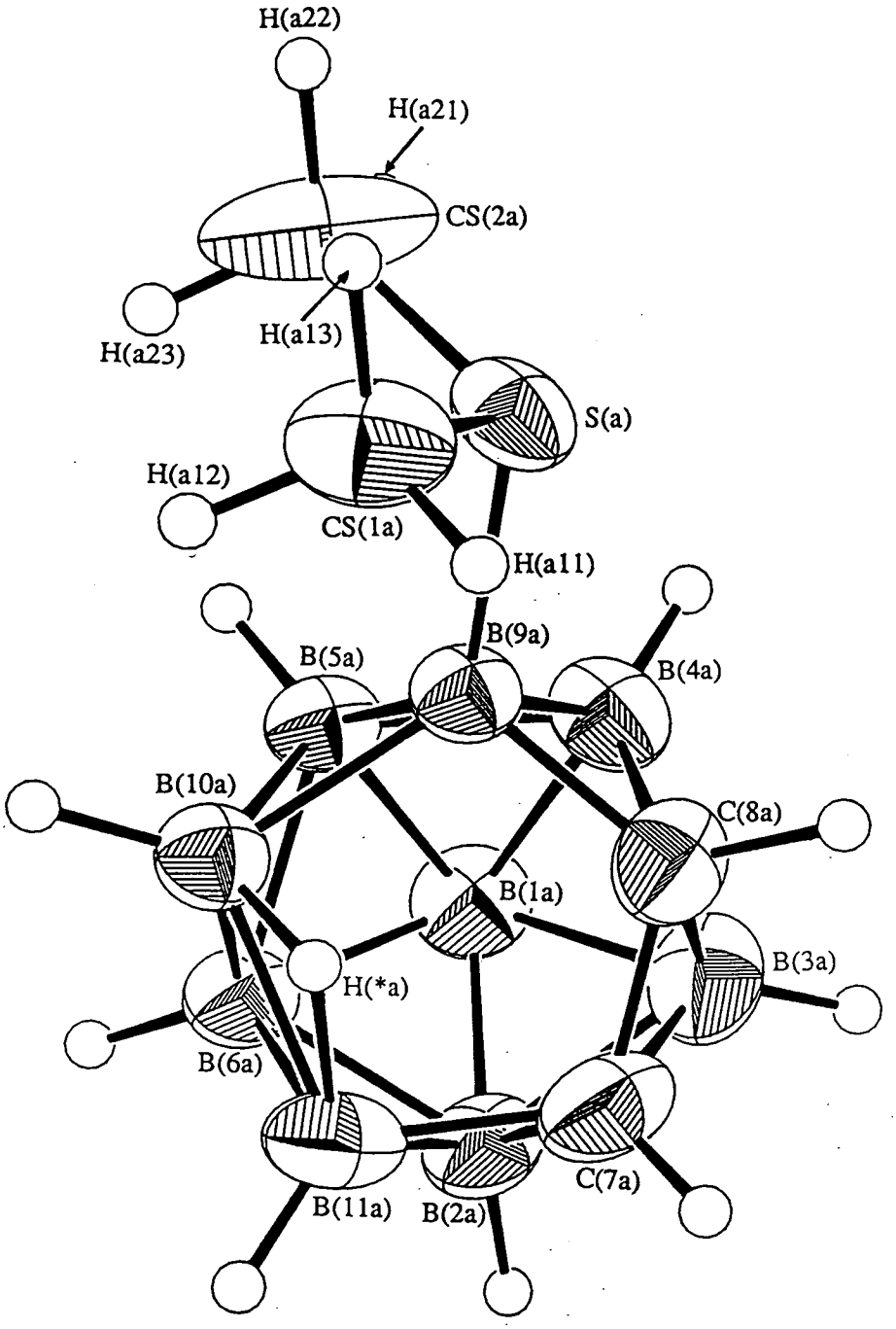

Table 3.1 Coordinates of Refined Atoms and Equivalent Isotropic Thermal Parameters ($Å^2$) in [10,11-μ-H-9-SMe_2-7,8-*nido*-$C_2B_9H_{10}$], carb'H, **(3)**

	x	y	z	Ueq
S(a)	0.28339(6)	0.50594(6)	0.74844(5)	0.0543(4)
CS(1a)	0.4092(3)	0.5721(3)	0.89584(21)	0.0680(19)
CS(2a)	0.3532(4)	0.6307(4)	0.7025(3)	0.125(4)
B(1a)	-0.2536(3)	0.4679(3)	0.6394(3)	0.0592(19)
B(2a)	-0.3199(3)	0.4313(3)	0.7506(3)	0.0651(21)
B(3a)	-0.2555(3)	0.3274(3)	0.6577(3)	0.0676(21)
B(4a)	-0.0869(3)	0.4149(3)	0.62429(25)	0.0571(19)
B(5a)	-0.0453(3)	0.57396(25)	0.70139(22)	0.0502(17)
B(6a)	-0.1908(3)	0.5851(3)	0.78330(25)	0.0562(18)
C(7a)	-0.1847(3)	0.37267(25)	0.8065(3)	0.0729(21)
C(8a)	-0.0531(3)	0.36857(23)	0.74344(24)	0.0630(18)
B(9a)	0.0701(3)	0.49794(23)	0.75785(21)	0.0453(16)
B(10a)	0.0197(3)	0.6129(3)	0.85526(23)	0.0501(17)
B(11a)	-0.1544(4)	0.5147(3)	0.8862(3)	0.0680(22)
S(b)	-0.22948(7)	0.87045(6)	0.66900(6)	0.0658(5)
CS(2b)	-0.3046(4)	0.9752(3)	0.6194(3)	0.0884(24)
CS(1b)	-0.2613(4)	0.7515(3)	0.5314(3)	0.0815(22)
B(1b)	0.2735(4)	1.1753(3)	0.8471(3)	0.0690(22)
B(2b)	0.3982(4)	1.0923(3)	0.8717(3)	0.0773(24)
B(3b)	0.2494(5)	1.0956(3)	0.9435(3)	0.0805(25)
B(4b)	0.0719(4)	1.0921(3)	0.8466(3)	0.0665(21)
B(5b)	0.1156(3)	1.08273(25)	0.71294(24)	0.0551(18)
B(6b)	0.3212(4)	1.0805(3)	0.7275(3)	0.0673(21)
C(7b)	0.2717(3)	0.9598(3)	0.8719(3)	0.0751(21)
C(8b)	0.0923(3)	0.95489(24)	0.85366(21)	0.0628(18)
B(9b)	0.0036(3)	0.94901(23)	0.72891(22)	0.0483(16)
B(10b)	0.1446(3)	0.9414(3)	0.64557(25)	0.0579(19)
B(11b)	0.3233(4)	0.9442(3)	0.7531(4)	0.0776(25)
H(1a)	-0.347(4)	0.472(3)	0.564(3)	
H(2a)	-0.444(4)	0.397(3)	0.7522(25)	
H(3a)	-0.330(4)	0.236(3)	0.601(3)	
H(4a)	-0.064(4)	0.386(3)	0.545(3)	
H(5a)	-0.003(4)	0.644(3)	0.667(3)	
H(6a)	-0.238(4)	0.664(3)	0.800(3)	
H(7a)	-0.219(4)	0.310(3)	0.832(3)	
H(8a)	-0.012(4)	0.285(3)	0.731(3)	
H(10a)	0.107(4)	0.709(3)	0.913(3)	
H(11a)	-0.186(4)	0.547(3)	0.965(3)	
H(*a)	0.006(4)	0.545(3)	0.900(3)	
H(1b)	0.327(4)	1.274(3)	0.875(3)	
H(2b)	0.524(4)	1.127(3)	0.917(3)	
H(3b)	0.272(4)	1.130(3)	1.037(3)	
H(4b)	-0.024(4)	1.128(3)	0.883(3)	
H(5b)	0.064(4)	1.123(3)	0.653(3)	
H(6b)	0.399(4)	1.118(3)	0.670(3)	
H(7b)	0.303(4)	0.926(3)	0.922(3)	
H(8b)	0.031(4)	0.913(3)	0.893(3)	
H(10b)	0.116(4)	0.902(3)	0.548(3)	
H(11b)	0.416(4)	0.900(3)	0.727(3)	
H(*b)	0.170(4)	0.860(3)	0.677(3)	

Table 3.2 Interatomic Distances (Å) in [10,11-μ-H-9-SMe_2-7,8-*nido*-$C_2B_9H_{10}$], carb'H, **(3)**

S(a) -CS(1a)	1.768(3)
S(a) -CS(2a)	1.770(4)
S(a) -B(9a)	1.879(3)
B(1a) -B(2a)	1.740(5)
B(1a) -B(3a)	1.778(5)
B(1a) -B(4a)	1.774(4)
B(1a) -B(5a)	1.777(4)
B(1a) -B(6a)	1.795(4)
B(1a) -H(1a)	1.15(3)
B(2a) -B(3a)	1.740(5)
B(2a) -B(6a)	1.762(5)
B(2a) -C(7a)	1.690(5)
B(2a) -B(11a)	1.800(5)
B(2a) -H(2a)	1.06(3)
B(3a) -B(4a)	1.769(5)
B(3a) -C(7a)	1.712(5)
B(3a) -C(8a)	1.740(5)
B(3a) -H(3a)	1.05(3)
B(4a) -B(5a)	1.767(4)
B(4a) -C(8a)	1.752(4)
B(4a) -B(9a)	1.749(4)
B(4a) -H(4a)	1.03(3)
B(5a) -B(6a)	1.797(4)
B(5a) -B(9a)	1.736(4)
B(5a) -B(10a)	1.779(4)
B(5a) -H(5a)	1.07(3)
B(6a) -B(10a)	1.785(4)
B(6a) -B(11a)	1.775(5)
B(6a) -H(6a)	1.13(3)
C(7a) -C(8a)	1.525(4)
C(7a) -B(11a)	1.623(5)
C(7a) -H(7a)	0.91(3)
C(8a) -B(9a)	1.571(4)
C(8a) -H(8a)	1.14(3)
B(9a) -B(10a)	1.775(4)
B(10a)-B(11a)	1.843(5)
B(10a)-H(10a)	1.12(3)
B(10a)-H(*a)	1.11(3)
B(11a)-H(11a)	1.07(3)
B(11a)-H(*a)	1.31(3)

S(b) -CS(2b)	1.792(4)
S(b) -CS(1b)	1.797(3)
S(b) -B(9b)	1.889(3)
B(1b) -B(2b)	1.724(5)
B(1b) -B(3b)	1.769(5)
B(1b) -B(4b)	1.777(5)
B(1b) -B(5b)	1.768(5)
B(1b) -B(6b)	1.793(5)
B(1b) -H(1b)	1.07(3)
B(2b) -B(3b)	1.728(6)
B(2b) -B(6b)	1.757(5)
B(2b) -C(7b)	1.679(5)
B(2b) -B(11b)	1.796(5)
B(2b) -H(2b)	1.04(3)
B(3b) -B(4b)	1.768(5)
B(3b) -C(7b)	1.704(5)
B(3b) -C(8b)	1.738(5)
B(3b) -H(3b)	1.08(3)
B(4b) -B(5b)	1.771(5)
B(4b) -C(8b)	1.744(5)
B(4b) -B(9b)	1.757(4)
B(4b) -H(4b)	1.16(3)
B(5b) -B(6b)	1.790(5)
B(5b) -B(9b)	1.736(4)
B(5b) -B(10b)	1.776(4)
B(5b) -H(5b)	1.11(3)
B(6b) -B(10b)	1.788(5)
B(6b) -B(11b)	1.777(5)
B(6b) -H(6b)	1.19(3)
C(7b) -C(8b)	1.531(4)
C(7b) -B(11b)	1.613(5)
C(7b) -H(7b)	0.88(3)
C(8b) -B(9b)	1.582(4)
C(8b) -H(8b)	0.94(3)
B(9b) -B(10b)	1.773(4)
B(10b)-B(11b)	1.851(5)
B(10b)-H(10b)	1.12(3)
B(10b)-H(*b)	1.22(3)
B(11b)-H(11b)	1.14(3)
B(11b)-H(*b)	1.39(3)

Table 3.3 Interbond Angles (°) in [10,11-μ-H-9-SMe_2-7,8-*nido*-$C_2B_9H_{10}$], carb'H, **(3)**

CS(1a)-	S(a)	-CS(2a)	100.66(17)	B(1a) -B(4a)	-B(5a)	60.22(17)
CS(1a)-	S(a)	-B(9a)	104.34(13)	B(1a) -B(4a)	-H(4a)	121.8(19)
CS(2a)-	S(a)	-B(9a)	104.89(16)	B(3a) -B(4a)	-C(8a)	59.24(18)
S(a)	-CS(1a)	-H(a11)	109.5(3)	B(3a) -B(4a)	-H(4a)	123.3(19)
S(a)	-CS(1a)	-H(a12)	109.2(3)	B(5a) -B(4a)	-B(9a)	59.15(16)
S(a)	-CS(1a)	-H(a13)	109.7(3)	B(5a) -B(4a)	-H(4a)	120.7(19)
S(a)	-CS(2a)	-H(a21)	110.4(4)	C(8a) -B(4a)	-B(9a)	53.31(15)
S(a)	-CS(2a)	-H(a22)	109.6(4)	C(8a) -B(4a)	-H(4a)	130.9(19)
S(a)	-CS(2a)	-H(a23)	108.4(4)	B(9a) -B(4a)	-H(4a)	123.3(19)
B(2a)	-B(1a)	-B(3a)	59.26(19)	B(1a) -B(5a)	-B(4a)	60.07(17)
B(2a)	-B(1a)	-B(6a)	59.76(18)	B(1a) -B(5a)	-B(6a)	60.32(17)
B(2a)	-B(1a)	-H(1a)	119.5(17)	B(1a) -B(5a)	-H(5a)	119.4(17)
B(3a)	-B(1a)	-B(4a)	59.74(18)	B(4a) -B(5a)	-B(9a)	59.91(16)
B(3a)	-B(1a)	-H(1a)	123.2(17)	B(4a) -B(5a)	-H(5a)	123.0(17)
B(4a)	-B(1a)	-B(5a)	59.71(17)	B(6a) -B(5a)	-B(10a)	59.89(16)
B(4a)	-B(1a)	-H(1a)	124.8(17)	B(6a) -B(5a)	-H(5a)	119.2(17)
B(5a)	-B(1a)	-B(6a)	60.39(17)	B(9a) -B(5a)	-B(10a)	60.66(16)
B(5a)	-B(1a)	-H(1a)	122.9(17)	B(9a) -B(5a)	-H(5a)	127.0(17)
B(6a)	-B(1a)	-H(1a)	119.6(17)	B(10a)-B(5a)	-H(5a)	119.0(17)
B(1a)	-B(2a)	-B(3a)	61.46(19)	B(1a) -B(6a)	-B(2a)	58.55(17)
B(1a)	-B(2a)	-B(6a)	61.69(18)	B(1a) -B(6a)	-B(5a)	59.29(17)
B(1a)	-B(2a)	-H(2a)	127.1(17)	B(1a) -B(6a)	-H(6a)	121.0(17)
B(3a)	-B(2a)	-C(7a)	59.85(19)	B(2a) -B(6a)	-B(11a)	61.18(18)
B(3a)	-B(2a)	-H(2a)	116.6(17)	B(2a) -B(6a)	-H(6a)	122.3(17)
B(6a)	-B(2a)	-B(11a)	59.77(18)	B(5a) -B(6a)	-B(10a)	59.57(16)
B(6a)	-B(2a)	-H(2a)	129.1(17)	B(5a) -B(6a)	-H(6a)	121.7(17)
C(7a)	-B(2a)	-B(11a)	55.31(18)	B(10a)-B(6a)	-B(11a)	62.38(18)
C(7a)	-B(2a)	-H(2a)	118.0(17)	B(10a)-B(6a)	-H(6a)	119.5(17)
B(11a)-B(2a)		-H(2a)	119.6(17)	B(11a)-B(6a)	-H(6a)	122.8(17)
B(1a)	-B(3a)	-B(2a)	59.28(19)	B(2a) -C(7a)	-B(3a)	61.50(19)
B(1a)	-B(3a)	-B(4a)	60.02(18)	B(2a) -C(7a)	-B(11a)	65.77(20)
B(1a)	-B(3a)	-H(3a)	127.9(19)	B(2a) -C(7a)	-H(7a)	121.0(21)
B(2a)	-B(3a)	-C(7a)	58.65(19)	B(3a) -C(7a)	-C(8a)	64.76(20)
B(2a)	-B(3a)	-H(3a)	125.9(19)	B(3a) -C(7a)	-H(7a)	113.3(21)
B(4a)	-B(3a)	-C(8a)	59.91(18)	C(8a) -C(7a)	-H(7a)	116.5(21)
B(4a)	-B(3a)	-H(3a)	120.8(19)	B(11a)-C(7a)	-H(7a)	121.0(21)
C(7a)	-B(3a)	-C(8a)	52.43(17)	B(3a) -C(8a)	-B(4a)	60.85(18)
C(7a)	-B(3a)	-H(3a)	123.8(19)	B(3a) -C(8a)	-C(7a)	62.81(19)
C(8a)	-B(3a)	-H(3a)	123.3(19)	B(3a) -C(8a)	-H(8a)	112.1(17)
B(1a)	-B(4a)	-B(3a)	60.24(18)	B(4a) -C(8a)	-B(9a)	63.25(17)
B(4a)	-C(8a)	-H(8a)	117.3(17)	B(2b) -B(1b)	-H(1b)	119.5(18)
C(7a)	-C(8a)	-H(8a)	115.9(17)	B(3b) -B(1b)	-B(4b)	59.81(21)
B(9a)	-C(8a)	-H(8a)	121.1(17)	B(3b) -B(1b)	-H(1b)	124.0(18)
S(a)	-B(9a)	-B(4a)	114.15(17)	B(4b) -B(1b)	-B(5b)	59.94(19)
S(a)	-B(9a)	-B(5a)	125.54(18)	B(4b) -B(1b)	-H(1b)	125.2(18)
S(a)	-B(9a)	-C(8a)	116.73(18)	B(5b) -B(1b)	-B(6b)	60.35(19)
S(a)	-B(9a)	-B(10a)	126.57(18)	B(5b) -B(1b)	-H(1b)	122.3(18)
B(4a)	-B(9a)	-B(5a)	60.95(16)	B(6b) -B(1b)	-H(1b)	118.6(18)
B(4a)	-B(9a)	-C(8a)	63.44(17)	B(1b) -B(2b)	-B(3b)	61.68(22)

B(5a) -B(9a) -B(10a)	60.88(16)	B(1b) -B(2b) -B(6b)	62.03(21)
B(5a) -B(10a)-B(6a)	60.54(16)	B(1b) -B(2b) -H(2b)	127.8(19)
B(5a) -B(10a)-B(9a)	58.46(15)	B(3b) -B(2b) -C(7b)	59.99(21)
B(5a) -B(10a)-H(10a)	118.6(17)	B(3b) -B(2b) -H(2b)	121.6(19)
B(6a) -B(10a)-B(11a)	58.55(17)	B(6b) -B(2b) -B(11b)	60.01(21)
B(6a) -B(10a)-H(10a)	120.6(17)	B(6b) -B(2b) -H(2b)	123.7(19)
B(9a) -B(10a)-H(10a)	125.7(17)	C(7b) -B(2b) -B(11b)	55.19(20)
B(11a)-B(10a)-H(10a)	127.4(17)	C(7b) -B(2b) -H(2b)	120.3(19)
B(11a)-B(10a)-H(*a)	44.9(17)	B(11b)-B(2b) -H(2b)	116.1(19)
H(10a)-B(10a)-H(*a)	114.4(24)	B(1b) -B(3b) -B(2b)	59.05(22)
B(2a) -B(11a)-B(6a)	59.05(18)	B(1b) -B(3b) -B(4b)	60.30(21)
B(2a) -B(11a)-C(7a)	58.92(19)	B(1b) -B(3b) -H(3b)	131.0(18)
B(2a) -B(11a)-H(11a)	118.0(18)	B(2b) -B(3b) -C(7b)	58.60(21)
B(6a) -B(11a)-B(10a)	59.07(17)	B(2b) -B(3b) -H(3b)	125.9(18)
B(6a) -B(11a)-H(11a)	116.9(18)	B(4b) -B(3b) -C(8b)	59.66(19)
C(7a) -B(11a)-H(11a)	128.0(18)	B(4b) -B(3b) -H(3b)	122.3(18)
B(10a)-B(11a)-H(11a)	121.8(18)	C(7b) -B(3b) -C(8b)	52.82(18)
B(10a)-B(11a)-H(*a)	36.7(14)	C(7b) -B(3b) -H(3b)	121.0(18)
H(11a)-B(11a)-H(*a)	115.1(23)	C(8b) -B(3b) -H(3b)	120.8(18)
B(10a)-H(*a) -B(11a)	98.4(24)	B(1b) -B(4b) -B(3b)	59.89(21)
CS(2b)- S(b) -CS(1b)	100.54(15)	B(1b) -B(4b) -B(5b)	59.79(19)
CS(2b)- S(b) -B(9b)	106.03(14)	B(1b) -B(4b) -H(4b)	129.9(17)
CS(1b)- S(b) -B(9b)	103.84(14)	B(3b) -B(4b) -C(8b)	59.32(19)
S(b) -CS(2b)-H(b21)	109.5(3)	B(3b) -B(4b) -H(4b)	120.0(17)
S(b) -CS(2b)-H(b22)	109.6(3)	B(5b) -B(4b) -B(9b)	58.95(17)
S(b) -CS(2b)-H(b23)	109.3(3)	B(5b) -B(4b) -H(4b)	128.7(17)
S(b) -CS(1b)-H(b11)	109.5(3)	C(8b) -B(4b) -B(9b)	53.74(17)
S(b) -CS(1b)-H(b12)	109.3(3)	C(8b) -B(4b) -H(4b)	120.7(17)
S(b) -CS(1b)-H(b13)	109.6(3)	B(9b) -B(4b) -H(4b)	119.9(17)
B(2b) -B(1b) -B(3b)	59.28(22)	B(1b) -B(5b) -B(4b)	60.27(19)
B(2b) -B(1b) -B(6b)	59.88(20)	B(1b) -B(5b) -B(6b)	60.53(19)
B(1b) -B(5b) -H(5b)	122.3(17)	B(4b) -C(8b) -H(8b)	119.6(21)
B(4b) -B(5b) -B(9b)	60.12(18)	C(7b) -C(8b) -H(8b)	116.3(21)
B(4b) -B(5b) -H(5b)	124.2(17)	B(9b) -C(8b) -H(8b)	120.1(21)
B(6b) -B(5b) -B(10b)	60.16(18)	S(b) -B(9b) -B(4b)	114.29(19)
B(6b) -B(5b) -H(5b)	119.3(17)	S(b) -B(9b) -B(5b)	124.40(19)
B(9b) -B(5b) -B(10b)	60.63(17)	S(b) -B(9b) -C(8b)	118.12(19)
B(9b) -B(5b) -H(5b)	124.5(17)	S(b) -B(9b) -B(10b)	125.47(19)
B(10b)-B(5b) -H(5b)	115.9(17)	B(4b) -B(9b) -B(5b)	60.93(18)
B(1b) -B(6b) -B(2b)	58.09(20)	B(4b) -B(9b) -C(8b)	62.73(18)
B(1b) -B(6b) -B(5b)	59.13(19)	B(5b) -B(9b) -B(10b)	60.82(17)
B(1b) -B(6b) -H(6b)	125.5(16)	B(5b) -B(10b)-B(6b)	60.31(18)
B(2b) -B(6b) -B(11b)	61.10(21)	B(5b) -B(10b)-B(9b)	58.55(17)
B(2b) -B(6b) -H(6b)	126.9(16)	B(5b) -B(10b)-H(10b)	119.4(17)
B(5b) -B(6b) -B(10b)	59.53(18)	B(6b) -B(10b)-B(11b)	58.43(19)
B(5b) -B(6b) -H(6b)	120.3(16)	B(6b) -B(10b)-H(10b)	118.4(17)
B(10b)-B(6b) -B(11b)	62.57(20)	B(9b) -B(10b)-H(10b)	128.2(17)
B(10b)-B(6b) -H(6b)	114.1(16)	B(11b)-B(10b)-H(10b)	125.8(17)
B(11b)-B(6b) -H(6b)	121.1(16)	B(11b)-B(10b)-H(*b)	48.5(16)
B(2b) -C(7b) -B(3b)	61.42(22)	H(10b)-B(10b)-H(*b)	104.3(23)
B(2b) -C(7b) -B(11b)	66.08(23)	B(2b) -B(11b)-B(6b)	58.89(21)
B(2b) -C(7b) -H(7b)	121.6(22)	B(2b) -B(11b)-C(7b)	58.73(21)
B(3b) -C(7b) -C(8b)	64.74(21)	B(2b) -B(11b)-H(11b)	118.9(17)
B(3b) -C(7b) -H(7b)	110.5(22)	B(6b) -B(11b)-B(10b)	59.00(19)
C(8b) -C(7b) -H(7b)	113.6(22)	B(6b) -B(11b)-H(11b)	120.1(17)

B(11b)-C(7b) -H(7b)	123.6(22)	C(7b) -B(11b)-H(11b)	125.4(17)
B(3b) -C(8b) -B(4b)	61.02(20)	B(10b)-B(11b)-H(11b)	123.4(17)
B(3b) -C(8b) -C(7b)	62.45(20)	B(10b)-B(11b)-H(*b)	41.1(14)
B(3b) -C(8b) -H(8b)	115.1(21)	H(11b)-B(11b)-H(*b)	104.8(22)
B(4b) -C(8b) -B(9b)	63.53(18)	B(10b)-H(*b) -B(11b)	90.3(21)

Table 3.4 Anisotropic Thermal Parameters ($Å^2$) in [10,11-μ-H-9-SMe_2-7,8-*nido*-$C_2B_9H_{10}$], carb'H, **(3)**

	U11	U22	U33	U23	U13	U12
S(a)	0.0329(3)	0.0606(4)	0.0498(3)	0.0084(3)	0.0101(2)	0.0215(3)
CS(1a)	0.0370(12)	0.0906(19)	0.0524(14)	0.0263(13)	0.0061(11)	0.0190(12)
CS(2a)	0.0532(17)	0.1861(39)	0.1227(28)	0.1171(30)	0.0459(18)	0.0477(21)
B(1a)	0.0351(13)	0.0643(17)	0.0599(16)	0.0253(14)	0.0051(12)	0.0209(12)
B(2a)	0.0348(13)	0.0577(17)	0.0886(21)	0.0356(16)	0.0254(14)	0.0208(12)
B(3a)	0.0354(14)	0.0512(16)	0.0903(22)	0.0184(16)	0.0082(14)	0.0126(12)
B(4a)	0.0379(13)	0.0631(18)	0.0493(15)	0.0116(13)	0.0069(11)	0.0208(12)
B(5a)	0.0373(12)	0.0525(15)	0.0499(14)	0.0278(12)	0.0144(11)	0.0190(11)
B(6a)	0.0393(13)	0.0527(16)	0.0662(17)	0.0298(14)	0.0217(12)	0.0251(12)
C(7a)	0.0505(14)	0.0632(16)	0.0951(20)	0.0523(16)	0.0333(14)	0.0261(12)
C(8a)	0.0418(12)	0.0485(14)	0.0826(17)	0.0287(13)	0.0154(12)	0.0223(11)
B(9a)	0.0293(11)	0.0472(14)	0.0472(13)	0.0191(11)	0.0110(10)	0.0168(10)
B(10a)	0.0411(13)	0.0479(15)	0.0479(14)	0.0191(12)	0.0140(11)	0.0193(11)
B(11a)	0.0520(16)	0.0761(20)	0.0659(18)	0.0399(16)	0.0332(14)	0.0323(15)
S(b)	0.0424(3)	0.0670(4)	0.0714(4)	0.0402(4)	0.0172(3)	0.0142(3)
CS(2b)	0.0581(16)	0.0836(20)	0.1051(23)	0.0509(18)	0.0216(16)	0.0371(15)
CS(1b)	0.0602(17)	0.0573(17)	0.0867(20)	0.0136(15)	-0.0152(15)	0.0080(13)
B(1b)	0.0720(20)	0.0426(16)	0.0612(18)	0.0164(14)	-0.0039(15)	0.0037(14)
B(2b)	0.0524(17)	0.0657(20)	0.0811(22)	0.0358(18)	-0.0102(16)	0.0009(15)
B(3b)	0.0892(25)	0.0684(21)	0.0483(17)	0.0218(15)	-0.0058(16)	0.0074(18)
B(4b)	0.0757(20)	0.0522(17)	0.0498(16)	0.0144(13)	0.0150(15)	0.0225(15)
B(5b)	0.0503(15)	0.0455(15)	0.0511(15)	0.0234(12)	0.0067(12)	0.0105(12)
B(6b)	0.0448(15)	0.0572(18)	0.0770(20)	0.0346(16)	0.0116(14)	0.0036(13)
C(7b)	0.0580(16)	0.0668(17)	0.0785(18)	0.0462(15)	0.0003(14)	0.0160(13)
C(8b)	0.0605(15)	0.0575(15)	0.0516(14)	0.0294(12)	0.0127(12)	0.0136(12)
B(9b)	0.0423(13)	0.0430(14)	0.0446(13)	0.0180(11)	0.0116(11)	0.0120(11)
B(10b)	0.0473(15)	0.0536(16)	0.0537(16)	0.0205(13)	0.0172(12)	0.0107(12)
B(11b)	0.0453(16)	0.0643(19)	0.1024(26)	0.0402(18)	0.0188(16)	0.0198(14)

Bridging H atoms are regarded as protonic in character (*i.e.* they react with bases), (although it is of some note that ^{1}H n.m.r. shifts of such atoms would lead one to assume a more hydridic nature than is chemically observed), and cage carbon atoms are more electronegative than either these H atoms or their neighbouring boron atoms in carbaboranes. Hence one might adopt an extremely simple viewpoint that a boron atom adjacent to the cage carbon atoms (in this case B(11)) would possess a more positive charge than a more remote boron atom such as B(10), and that the μ-H atom would therefore bond more strongly to B(10) than to B(11). Additionally, differences in electronegativity cause carbon-bonded H atoms to bear a greater δ^+ than those bonded to boron, the importance of which will become apparent during this discussion.

To investigate this idea further, charge-iterated extended Hückel molecular orbital calculations have been carried out on idealised models of [9-SH_2-7,8-*nido*-$C_2B_9H_{10}$]$^-$ (lowest energy conformer - see later) and [7,8-*nido*-$C_2B_9H_{11}$]$^{2-}$. The models used in these calculations may be found in Chapter 6, section 3.

The net charges calculated for atoms B(10) and B(11) were as follows: In [$C_2B_9H_{11}$]$^{2-}$, B(10) bears a net charge of -0.153 and B(11) carries a charge of -0.003. In the SH_2-substituted model, [9-SH_2-$C_2B_9H_{10}$]$^-$, B(10) is calculated to have a charge of -0.030, where B(11) is again more positive at +0.022.

The results of the calculations suggest that in both models, B(10) is, as predicted on a simplistic basis, substantially more negative than B(11), and that the similarity in the two results leads to the conclusion that the observed asymmetry of the μ-H site in carb'H, with the bridging proton favouring the more negatively-charged boron B(10), is a function of the cage carbon atom positions,

rather than any effect of the exo-polyhedral SMe_2 group.

The structural difference between molecules *a* and *b* of carb'H, which was alluded to earlier, can be best illustrated by means of a *Root Mean Square Misfit* calculation [66].

For two (crystallographically determined) fragments with the same numbering scheme, a geometrical calculation can be performed which superimposes the centres of gravity of the fragments, then maps every numbered pair of atoms (e.g B[1] with B[1']), and calculates the square root of the mean of the squares of the difference in the distances from the centre of gravity of the atoms within each pair. This technique can be applied to whole (or parts of) molecules, to gain information on the degree of gross similarity of the molecular structure, and can be especially useful in the case of delocalised systems, such as boranes and heteroboranes [67].

In the case of compound **(3)**, *r.m.s. misfit* calculations were performed between **(i)** The $\{C_2B_9S\}$ fragments of molecules *a* and *b* and **(ii)** The $\{C_2B_9SC_{(methyl)2}\}$ fragments of the 2 conformers. For calculation **(i)**, the *r.m.s. misfit* between the two fragments was only 0.016Å, denoting practically identical $\{C_2B_9S\}$ geometries in the two molecules. The inclusion of the methyl carbon atoms in calculation **(ii)**, however, causes the *r.m.s. misfit* between the fragments to increase to 0.209Å. Hence the geometric difference between molecules *a* and *b* lies in the orientation of the pendant SMe_2 group with respect to the carbaborane framework. More specifically, the lone pair-S(a)-B(9a)-C(8a) torsion angle (calculated from the available CS(1a)-S(a)-B(9a)-C(8a) and CS(2a)-S(a)-B(9a)-C(8a) torsions) is 27.29°, and the corresponding angle in

molecule *b* is 4.04°.

Of further interest with respect to the bonding of the dimethylsulphide ligand to the polyhedron are the interbond angles between S-B(9)-C(8) and S-B(9)-B(10). The former angle has been determined as 116.73° (molecule *a*) and 118.12° (molecule *b*), where the latter is consistently wider, at 126.57° and 125.47° for molecules *a* and *b* respectively.

Taken together, the above pieces of information, (i) orientation of SMe_2 function about S-B(9) bond so as to give small lone pair-S-B(9)-C(8) torsion angles and (ii) S-B(9)-C(8) angles more acute than S-B(9)-B(10) angles might suggest some interaction between the sulphur lone pair and $C(8)\text{-}H^{\delta+}$.

A series of EHMO calculations has been carried out on idealised models of $[9\text{-}SH_2\text{-}7,8\text{-}nido\text{-}C_2B_9H_{10}]^-$, where the torsion angle between the SH_2 group and the carbaborane cluster has been varied and the resultant total energy of the molecule mapped. The models used in each of the calculations are given in Chapter 6, section 3. The only variables between each of the models are the positions of the sulphur-bonded hydrogen atoms, the coordinates of which are given for each nominal value of the lone pair-S-B(9)-C(8) torsion angle, along with the positions of the other atoms, which are invariant between calculations.

The energies so calculated are given in **Table 3.5**, and are also presented in graphical form in **Figure 3.3**. It can be clearly seen from **Fig. 3.3** that the minimum energy calculated results when the sulphur lone pair exactly eclipses the B(9)-C(8) connectivity, i.e. when the torsion angle is 0°. This supports the results of the structural study and the idea that these might be traced to an intramolecular electrostatic interaction of the type S(lone pair)..$H(8)^{\delta+}$.

Table 3.5 Calculated Conformational Energies for [9-SH_2-7,8-*nido*-$C_2B_9H_{10}$]$^-$

S(l.p.)-S-B(9)-C(8) Torsion Angle	Total Energy (eV)
-180	-841.318954
-150	-841.281107
-120	-841.116519
-90	-841.034324
-60	-841.171367
-30	-841.332933
0	-841.391246
30	-841.330169
60	-841.184423
90	-841.029070
120	-841.028301
150	-841.195170
180	-841.318954

Figure 3.3 Energy Profile for Rotation about S-B(9) Bond

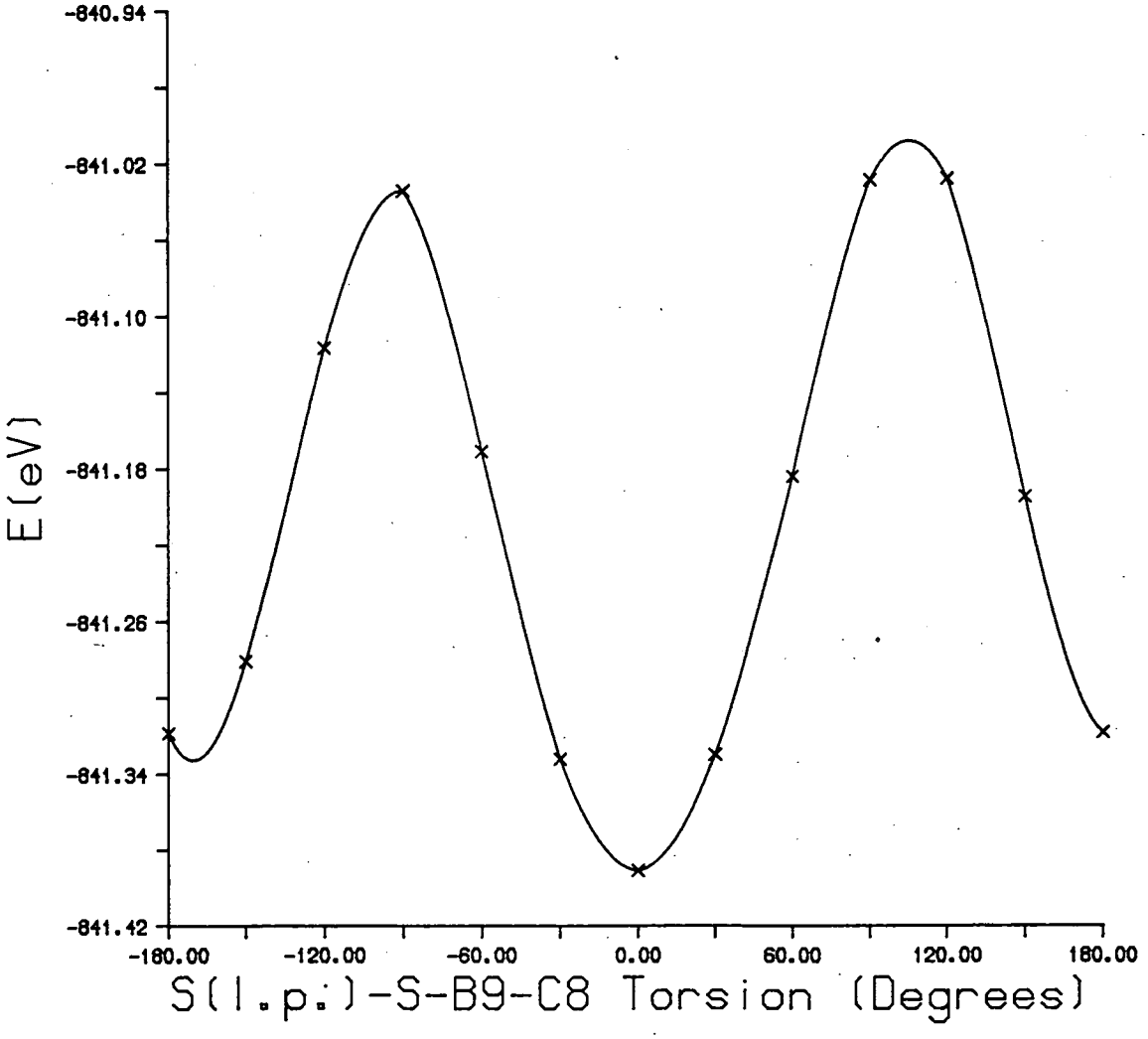

Other experimentally determined features of the molecule do not differ substantially from those expected for such a compound. Specifically, the five atoms which define the open face of the carbaborane [C(7), C(8), B(9), B(10) and B(11)] can be fitted to a plane from which no atom deviates by more than 0.024Å in molecule *a* and 0.023Å in molecule *b*. The angles made by this plane and the S-B(9) vector are 27.08^{o} and 26.26^{o} in molecules *a* and *b*, which are in full accord with the geometrically preferred angle of inclination (26^{o}) for a substituent on an 11-vertex *nido* species such as carb'H. The sulphur-boron distances in molecules *a* and *b* are 1.879Å and 1.889Å respectively, which are in good agreement with values already published for similar bonds in related species [65,68,69]. It can also be seen that the longest of the boron-boron connectivities in both molecules is B(10)-B(11), i.e. that which supports the μ-H atom, the reasons for the lengthening of such connectivities being well documented [55].

Deprotonation of carb'H

As discussed previously, the purpose of studying carb'H was to ascertain the position of the 11th "cage" H atom; that having been achieved, the next step was to effect deprotonation of the neutral carbaborane to give the monoanionic ligand [9-SMe_2-7,8-*nido*-$C_2B_9H_{10}$]$^-$, [carb']$^-$.

The compound does not undergo facile deprotonation with Lewis bases such as triethylamine, NEt_3, as does for example [70] decaborane(14). Instead, slightly more forcing conditions must be used for its successful deprotonation, namely excess KOH, which leads to the formation of the readily soluble species K^+[carb']$^-$, which may then be used *in situ* for reactions with transition metal salts and metal complexes containing halide ligands. This method was used to

synthesise compounds **(6)**, **(8)** and **(9)**, which are discussed in Chapters 4 and 5.

It is also possible to prepare and isolate the thallium(I) complex of [carb']$^-$, viz. Tl[9-SMe_2-7,8-*nido*-$C_2B_9H_{10}$], which is a pale yellow-green, slightly light-sensitive compound. The compound was prepared from carb'H in an analogous manner to the preparation of Tl[$TlC_2B_9H_{11}$], using KOH/TlOAc in appropriate proportions. A typical synthesis is described in Chapter 6, section 1.

Because of its inherent insolubility, the only available method of characterisation of Tl[carb'] is elemental (C,H) microanalysis, which was performed, giving results fully consistent with the proposed formulation.

Further evidence for the identity of the species may be taken from its subsequent chemical behaviour, acting as a synthetic equivalent of [carb']$^-$ in later reactions (see syntheses of compounds **(4)** and **(5)**, Chapter 6, section 1). Such reactions may be crudely followed by monitoring the solubilisation of the carbaborane function, which manifests itself in the infra-red spectrum in the form of a B-H stretching envelope, centred around 2500cm^{-1}.

[10,11-μ-(PPh_3Au)-9-SMe_2-7,8-*nido*-$C_2B_9H_{10}$], PPh_3Au(carb'), (4)

Introduction

Further to the work in Chapter 2 and on carb'H, **(3)**, synthetic, spectroscopic and *X* -ray crystallographic studies have been carried out upon the above compound, **(4)**, where isolobal substitution of the bridging H atom by (triphenylphoshine)gold (I) has been effected, as part of the overall investigation of the bonding capabilities of the [9-SMe_2-7,8-*nido*-$C_2B_9H_{10}$]$^-$ ligand to metal fragments.

Synthesis and Characterisation of (4)

[10,11-μ-(PPh_3Au)-9-SMe_2-7,8-*nido*-$C_2B_9H_{10}$], **(4)**, was synthesised by reaction of equimolar quantities of Tl[carb'] and PPh_3AuCl in dichloromethane, as described in Chapter 6, section 1, and chemical characterisation was achieved by infra-red spectroscopy, elemental microanalysis and multinuclear n.m.r. spectroscopy.

Infra-red Spectroscopy

The chief features of interest in the infra-red spectrum of **(4)** are the absorption centred at 2540cm^{-1}, due to B-H stretching, and the Au-P stretch, which occurs at 535cm^{-1}.

N.m.r. Spectroscopy

^1H, ^{31}P, ^{11}B and ^{11}B-{^1H} spectra were recorded, each consistent with the expected nature of the molecule. In the ^1H spectrum, 2 signals were observed at δ 2.35 and 2.39 p.p.m., arising from the protons of the inequivalent methyl groups of the dimethylsulphide ligand, and a complex multiplet at δ 7.4-7.7 p.p.m. due to the H atoms of the triphenylphosphine group.

The ^{31}P n.m.r. spectrum displayed only the expected one (broad) signal at δ 41.0 p.p.m., the broadening of the resonance being an indication of the bonding of the phosphorous-containing moiety (albeit through the gold atom) to the carbaborane system [71,72].

The ^{11}B-{^1H} spectrum confirmed the presence of 9 boron atoms (8

resonances, with 1 accidental coincidence leading to one signal possessing a relative integral double that of the other seven). The highest frequency resonance (δ -10.31 p.p.m.) was the only peak which did not display doublet coupling in the proton-coupled boron spectrum, and was hence assigned as arising from the B(9) nucleus.

Structural Study on (4)

Introduction

The structural work on **(4)** was carried out to investigate any differences in molecular geometry produced by the isolobal replacement of the asymmetrically-bridging H atom by the $\{PPh_3Au^+\}$ fragment. Diffraction-quality crystals were grown by slow diffusion of n-hexane into a dichloromethane solution of the compound, as described in Chapter 6, section 1. Details of the crystallographic procedures and crystal data for the structure may be found in Chapter 6, section 2.

Discussion

Compound **(4)**, $PPh_3Au(carb')$, crystallises with a molecule of dichloromethane of crystallisation per molecule of carbaauraborane. This does not result in any unusual solvent-carbametallaborane interactions however, hence any structural differences between **(3)** and **(4)** are attributable solely to intramolecular effects.

A perspective view of the $PPh_3Au(carb')$ molecule is shown in **Figure 3.4**, which also shows the appropriate molecular numbering scheme. Carbaborane H atoms have the same number as the B or C atom to which they are bonded and

phenyl H's bonded to C(*ij*) are numbered as H(*ij*0).

Final coordinates of refined atoms and (for non-H's) equivalent isotropic thermal parameters are given in **Table 3.6**. Interatomic distances comprise **Table 3.7**, and **Table 3.8** gives selected interbond angles. **Table 3.9** consists of anisotropic thermal parameters and **Table 3.10** shows calculated H atom coordinates. It is initially obvious from **Figure 3.4** that the replacement of the μ-H atom in carb'H leads to a bridging $\{PPh_3Au^+\}$ fragment on the same (B(10)-B(11)) connectivity.

This change between molecules **(3)** and **(4)** does not however lead to a sizeable effect upon the polyhedral geometry. In order to monitor this, *r.m.s. misfit* calculations were again performed, this time between the $\{C_2B_9\}$ fragments of carb'H and PPh_3Au(carb'). The resulting *misfit* of only 0.028Å (molecule *a* of carb'H) and 0.026Å (molecule *b*) indicates a minimal difference between the geometries of the fragments. Upon inclusion of the sulphur atoms in the calculations, i.e. comparison of the $\{C_2B_9S\}$ portions of the molecules, the *misfits* rise to 0.043Å and 0.045Å for comparison of **(4)** with molecules *a* and *b* of carb'H respectively. The poorer fit when sulphur is included in the calculations is a reflection of the fact that the S atom in **(4)** is depressed below its preferred angle of inclination to the plane defined by C(7), C(8), B(9), B(10) and B(11), an angle of 21.9° being formed between this plane and the S(1)-B(9) vector. This angle is in comparison with those in carb'H of 27.1° molecule *a* and 26.3° molecule *b* .

Figure 3.4 Perspective View of [10,11-μ-(PPh_3Au)-9-SMe_2-7,8-*nido*-$C_2B_9H_{10}$], PPh_3Au(carb'), **(4)**

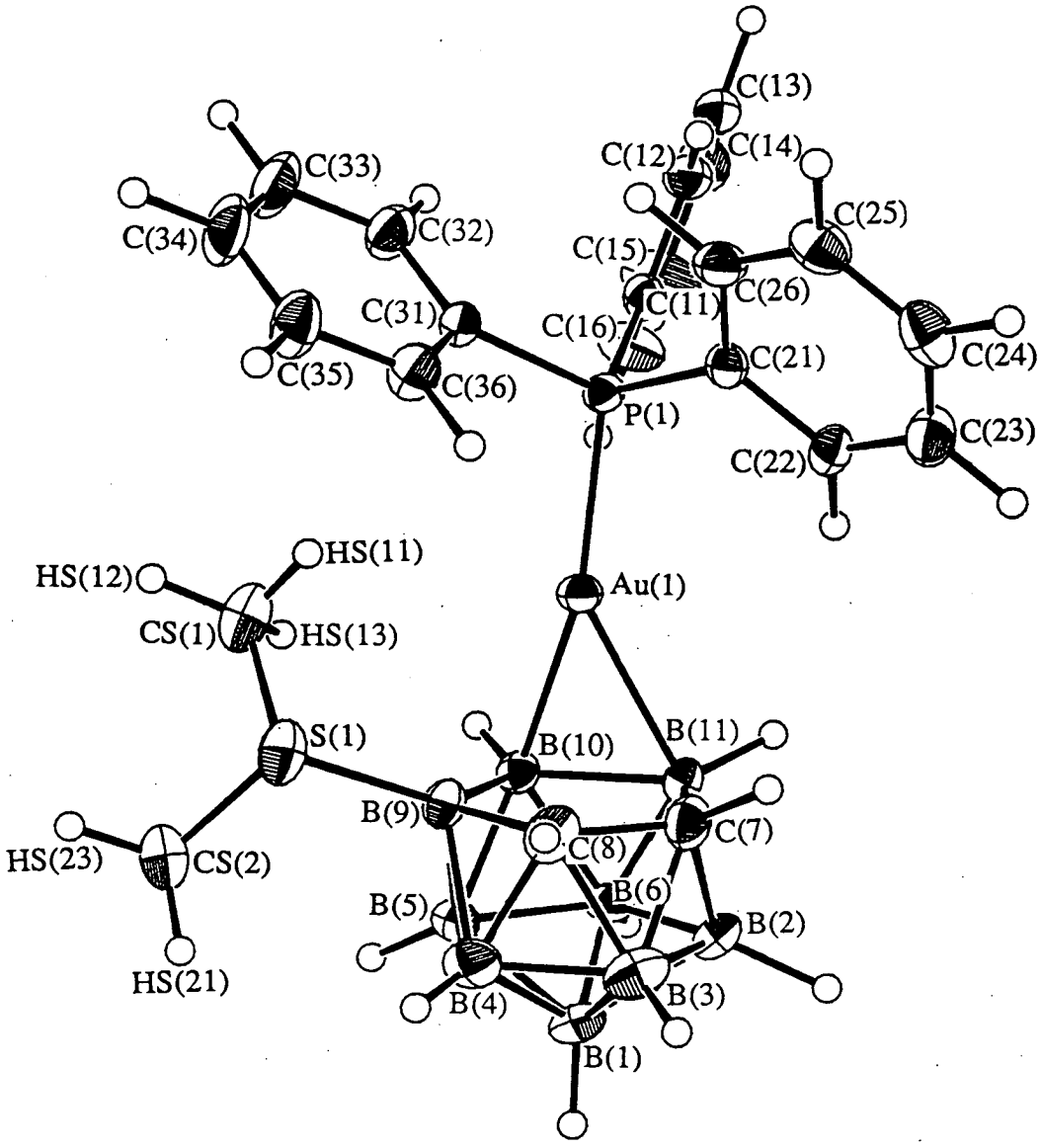

Table 3.6 Coordinates of Refined Atoms and Equivalent Isotropic Thermal Parameters ($Å^2$) in [10,11-μ-(PPh_3Au)-9-SMe_2-7,8-*nido*-$C_2B_9H_{10}$], PPh_3Au(carb'), **(4)**

	x	y	z	Ueq
Au(1)	1.01420(1)	-0.01384(1)	0.26048(1)	0.0245(1)
P(1)	0.97619(8)	0.14105(9)	0.31099(8)	0.0224(7)
S(1)	1.25651(10)	-0.12742(12)	0.39521(9)	0.0409(9)
CS(1)	1.1821(5)	-0.1163(6)	0.4547(4)	0.065(5)
CS(2)	1.3061(5)	-0.2595(6)	0.4311(4)	0.058(5)
C(12)	0.81444	0.23904	0.32052	0.032(3)
C(13)	0.72217	0.23711	0.31744	0.034(3)
C(14)	0.67245	0.13920	0.30328	0.040(3)
C(15)	0.71501	0.04324	0.29219	0.057(4)
C(16)	0.80728	0.04518	0.29527	0.043(4)
C(11)	0.85700(20)	0.14308(19)	0.30943(22)	0.025(3)
C(22)	0.97103	0.24894	0.16663	0.029(3)
C(23)	0.98162	0.33811	0.12035	0.040(3)
C(24)	1.00748	0.43911	0.15982	0.042(4)
C(25)	1.02276	0.45094	0.24558	0.037(3)
C(26)	1.01217	0.36176	0.29187	0.031(3)
C(21)	0.98631(24)	0.26076(20)	0.25239(17)	0.024(3)
C(32)	1.02232	0.1679	0.48704	0.040(3)
C(33)	1.08620	0.1856	0.57005	0.052(4)
C(34)	1.18128	0.2042	0.58608	0.048(4)
C(35)	1.21249	0.2051	0.51908	0.042(4)
C(36)	1.14861	0.1874	0.43606	0.035(3)
C(31)	1.05353(17)	0.1688(3)	0.42004(20)	0.025(3)
B(1)	1.1502(4)	-0.2581(5)	0.1306(4)	0.034(4)
B(2)	1.0680(5)	-0.1581(5)	0.0729(4)	0.036(4)
B(3)	1.1885(5)	-0.1250(6)	0.1223(4)	0.044(4)
B(4)	1.2339(4)	-0.1937(5)	0.2194(4)	0.036(4)
B(5)	1.1420(4)	-0.2703(4)	0.2319(4)	0.028(3)
B(6)	1.0372(4)	-0.2460(4)	0.1398(4)	0.029(3)
C(7)	1.1014(4)	-0.0446(4)	0.1337(3)	0.035(3)
C(8)	1.1916(4)	-0.0643(4)	0.2152(3)	0.035(3)
B(9)	1.1704(4)	-0.1417(4)	0.2810(4)	0.026(3)
B(10)	1.0507(4)	-0.1837(4)	0.2378(3)	0.024(3)
B(11)	1.0084(4)	-0.1063(5)	0.1373(4)	0.029(3)
H(1)	1.174(5)	-0.329(6)	0.101(4)	
H(6)	0.986(5)	-0.305(5)	0.114(4)	
H(2)	1.034(5)	-0.155(5)	-0.010(4)	
H(3)	1.234(5)	-0.097(6)	0.088(4)	
H(4)	1.295(5)	-0.208(6)	0.243(4)	
H(5)	1.155(5)	-0.358(6)	0.268(4)	
H(7)	1.094(5)	0.037(6)	0.101(5)	
H(8)	1.252(6)	-0.009(5)	0.226(5)	
H(10)	1.012(5)	-0.213(6)	0.273(4)	
H(11)	0.929(5)	-0.073(6)	0.092(4)	
Cl(1)	0.57964(17)	-0.08676(18)	-0.03513(17)	0.0952(18)
Cl(2)	0.76077(21)	0.00140(20)	0.07526(18)	0.0989(20)
CM	0.6421(7)	0.0243(8)	0.0131(9)	0.122(10)

Table 3.7 Interatomic Distances (Å) in [10,11-μ-(PPh_3Au)9-SMe_2-7,8-*nido*-$C_2B_9H_{10}$], PPh_3Au(carb'), **(4)**

Au(1) - P(1)	2.2550(12)	B(2) -B(11)	1.790(9)
Au(1) -B(10)	2.233(6)	B(2) - H(2)	1.31(7)
Au(1) -B(11)	2.357(6)	B(3) - B(4)	1.746(10)
P(1) -C(11)	1.817(3)	B(3) - C(7)	1.730(9)
P(1) -C(21)	1.817(3)	B(3) - C(8)	1.732(9)
P(1) -C(31)	1.813(4)	B(3) - H(3)	1.11(7)
S(1) -CS(1)	1.796(8)	B(4) - B(5)	1.773(9)
S(1) -CS(2)	1.798(7)	B(4) - C(8)	1.709(9)
S(1) - B(9)	1.896(6)	B(4) - B(9)	1.798(9)
B(1) - B(6)	1.803(9)	B(4) - H(4)	0.88(7)
B(1) - B(2)	1.766(9)	B(5) - B(9)	1.763(8)
B(1) - B(3)	1.762(10)	B(5) -B(10)	1.791(8)
B(1) - B(4)	1.755(9)	B(5) - H(5)	1.21(7)
B(1) - B(5)	1.782(9)	C(7) - C(8)	1.558(8)
B(1) - H(1)	1.13(7)	C(7) -B(11)	1.636(8)
B(6) - B(2)	1.760(9)	C(7) - H(7)	1.13(8)
B(6) - B(5)	1.791(8)	C(8) - B(9)	1.594(8)
B(6) -B(10)	1.775(8)	C(8) - H(8)	1.10(9)
B(6) -B(11)	1.769(8)	B(9) -B(10)	1.772(8)
B(6) - H(6)	1.03(7)	B(10) -B(11)	1.844(8)
B(2) - B(3)	1.760(10)	B(10) -H(10)	1.05(7)
B(2) - C(7)	1.694(9)	B(11) -H(11)	1.23(7)
Cl(1)- CM	1.689(12)	Cl(2)- CM	1.742(12)

Table 3.8 Selected Interbond Angles (°) in [10,11-μ-(PPh_3Au)-9-SMe_2-7,8-*nido*-$C_2B_9H_{10}$], PPh_3Au(carb'), **(4)**

P(1)	-Au(1)	-B(10)	166.80(15)	B(1) - B(6) - B(5)	59.5(3)
P(1)	-Au(1)	-B(11)	144.99(15)	B(2) - B(6) -B(11)	61.0(4)
B(10)	-Au(1)	-B(11)	47.30(21)	B(5) - B(6) -B(10)	60.3(3)
Au(1)	- P(1)	-C(11)	114.25(11)	B(10) - B(6) -B(11)	62.7(3)
Au(1)	- P(1)	-C(21)	112.68(11)	B(1) - B(2) - B(6)	61.5(4)
Au(1)	- P(1)	-C(31)	112.71(12)	B(1) - B(2) - B(3)	60.0(4)
C(11)	- P(1)	-C(21)	106.08(15)	B(6) - B(2) -B(11)	59.8(4)
C(11)	- P(1)	-C(31)	105.83(16)	B(3) - B(2) - C(7)	60.1(4)
C(21)	- P(1)	-C(31)	104.51(16)	C(7) - B(2) -B(11)	55.9(3)
CS(1)	- S(1)	-CS(2)	98.9(3)	B(1) - B(3) - B(2)	60.2(4)
CS(1)	- S(1)	- B(9)	104.0(3)	B(1) - B(3) - B(4)	60.0(4)
CS(2)	- S(1)	- B(9)	107.6(3)	B(2) - B(3) - C(7)	58.1(4)
S(1)	-CS(1)	-HS(11)	102.6(7)	B(4) - B(3) - C(8)	58.9(4)
S(1)	-CS(1)	-HS(12)	118.5(7)	C(7) - B(3) - C(8)	53.5(3)
S(1)	-CS(1)	-HS(13)	107.0(7)	B(1) - B(4) - B(3)	60.4(4)
S(1)	-CS(2)	-HS(21)	108.7(6)	B(1) - B(4) - B(5)	60.7(4)
S(1)	-CS(2)	-HS(22)	110.8(6)	B(3) - B(4) - C(8)	60.2(4)
S(1)	-CS(2)	-HS(23)	108.9(6)	B(5) - B(4) - B(9)	59.2(3)
P(1)	-C(11)	-C(12)	121.94(24)	C(8) - B(4) - B(9)	54.0(3)
P(1)	-C(11)	-C(16)	118.06(24)	B(1) - B(5) - B(6)	60.6(3)
P(1)	-C(21)	-C(22)	118.34(23)	B(1) - B(5) - B(4)	59.1(4)
P(1)	-C(21)	-C(26)	121.61(23)	B(6) - B(5) -B(10)	59.4(3)
P(1)	-C(31)	-C(32)	122.8(3)	B(4) - B(5) - B(9)	61.1(3)
P(1)	-C(31)	-C(36)	117.2(3)	B(9) - B(5) -B(10)	59.8(3)
B(6)	- B(1)	- B(2)	59.1(4)	B(2) - C(7) - B(3)	61.9(4)
B(6)	- B(1)	- B(5)	59.9(3)	B(2) - C(7) -B(11)	65.0(4)
B(2)	- B(1)	- B(3)	59.9(4)	B(3) - C(7) - C(8)	63.3(4)
B(3)	- B(1)	- B(4)	59.5(4)	B(3) - C(8) - B(4)	61.0(4)
B(4)	- B(1)	- B(5)	60.2(4)	B(3) - C(8) - C(7)	63.2(4)
B(1)	- B(6)	- B(2)	59.4(4)	B(4) - C(8) - B(9)	65.8(4)
S(1)	- B(9)	- B(4)	108.1(4)	B(6) -B(10) - B(5)	60.3(3)
S(1)	- B(9)	- B(5)	121.2(4)	B(6) -B(10) -B(11)	58.5(3)
S(1)	- B(9)	- C(8)	114.6(4)	B(5) -B(10) - B(9)	59.3(3)
S(1)	- B(9)	-B(10)	131.0(4)	Au(1) -B(11) -B(10)	62.83(25)
B(4)	- B(9)	- B(5)	59.7(3)	B(6) -B(11) - B(2)	59.3(3)
B(4)	- B(9)	- C(8)	60.2(4)	B(6) -B(11) -B(10)	58.8(3)
B(5)	- B(9)	-B(10)	60.9(3)	B(2) -B(11) - C(7)	59.1(4)
Au(1)	-B(10)	-B(11)	69.9(3)	Cl(1)- CM -Cl(2)	115.5(7)

Table 3.9 Anisotropic Thermal Parameters ($Å^2$) in [10,11-μ-(PPh_3Au)-9-SMe_2-7,8-*nido*-$C_2B_9H_{10}$], PPh_3Au(carb') , **(4)**

	U11	U22	U33	U23	U13	U12
Au(1)	0.0227(1)	0.0226(1)	0.0241(1)	-0.0039(1)	0.0091(1)	0.0010(1)
P(1)	0.0204(6)	0.0231(6)	0.0199(6)	-0.0029(4)	0.0067(5)	0.0005(4)
S(1)	0.0382(8)	0.0480(8)	0.0264(7)	0.0005(6)	0.0021(6)	-0.0034(6)
Cs(1)	0.0782(51)	0.0778(51)	0.0291(34)	0.0091(32)	0.0165(35)	0.0196(40)
Cs(2)	0.0556(42)	0.0700(46)	0.0355(34)	0.0094(31)	0.0059(33)	0.0254(34)
C(12)	0.0280(28)	0.0318(27)	0.0298(27)	-0.0031(21)	0.0107(24)	0.0033(20)
C(13)	0.0310(28)	0.0381(29)	0.0275(27)	-0.0004(22)	0.0119(24)	0.0078(22)
C(14)	0.0236(27)	0.0505(34)	0.0401(32)	0.0019(25)	0.0131(25)	0.0016(23)
C(15)	0.0332(32)	0.0401(33)	0.0896(52)	-0.0112(33)	0.0275(35)	-0.0112(26)
C(16)	0.0307(29)	0.0292(28)	0.0635(39)	-0.0067(27)	0.0207(29)	-0.0010(22)
C(11)	0.0197(24)	0.0297(25)	0.0223(24)	0.0012(19)	0.0054(21)	0.0012(18)
C(22)	0.0277(27)	0.0337(27)	0.0201(25)	0.0002(20)	0.0056(22)	-0.0003(20)
C(23)	0.0417(32)	0.0426(32)	0.0294(29)	0.0068(23)	0.0131(26)	0.0035(24)
C(24)	0.0361(31)	0.0345(30)	0.0492(35)	0.0148(26)	0.0160(28)	0.0042(23)
C(25)	0.0326(28)	0.0268(27)	0.0453(33)	-0.0019(23)	0.0124(26)	-0.0009(21)
C(26)	0.0301(26)	0.0261(26)	0.0319(28)	-0.0052(21)	0.0109(23)	0.0020(19)
C(21)	0.0184(23)	0.0255(24)	0.0217(25)	-0.0012(18)	0.0038(20)	0.0006(18)
C(32)	0.0339(29)	0.0565(36)	0.0251(29)	0.0018(24)	0.0135(25)	0.0062(25)
C(33)	0.0487(37)	0.0804(48)	0.0200(29)	0.0018(28)	0.0112(29)	0.0094(33)
C(34)	0.0380(34)	0.0730(44)	0.0213(29)	-0.0007(27)	-0.0026(27)	0.0021(29)
C(35)	0.0306(30)	0.0593(37)	0.0277(29)	-0.0004(26)	0.0022(26)	-0.0033(25)
C(36)	0.0214(26)	0.0488(33)	0.0295(28)	-0.0001(23)	0.0088(23)	-0.0010(22)
C(31)	0.0276(25)	0.0239(24)	0.0193(23)	0.0011(18)	0.0074(21)	0.0021(18)
B(1)	0.0332(33)	0.0362(33)	0.0307(32)	-0.0078(25)	0.0195(29)	-0.0017(24)
B(6)	0.0258(30)	0.0226(27)	0.0322(32)	-0.0086(23)	0.0098(26)	0.0010(21)
B(2)	0.0437(37)	0.0396(34)	0.0211(30)	-0.0049(24)	0.0135(29)	0.0033(27)
B(3)	0.0461(39)	0.0431(38)	0.0411(38)	-0.0072(29)	0.0267(34)	-0.0064(29)
B(4)	0.0203(29)	0.0446(36)	0.0380(34)	-0.0060(28)	0.0122(28)	-0.0009(25)
B(5)	0.0259(29)	0.0248(28)	0.0290(30)	-0.0013(22)	0.0108(26)	0.0021(21)
C(7)	0.0428(31)	0.0294(27)	0.0265(27)	0.0043(21)	0.0120(25)	-0.0002(23)
C(8)	0.0324(29)	0.0359(29)	0.0305(28)	-0.0027(22)	0.0132(25)	-0.0114(22)
B(9)	0.0240(28)	0.0292(29)	0.0201(27)	-0.0023(21)	0.0038(24)	-0.0036(21)
B(10)	0.0249(28)	0.0220(27)	0.0217(28)	-0.0025(21)	0.0074(24)	-0.0017(20)
B(11)	0.0309(31)	0.0311(30)	0.0178(27)	-0.0023(22)	0.0045(25)	0.0044(23)
Cl(1)	0.0832(15)	0.0647(13)	0.1167(19)	0.0056(12)	0.0294(14)	0.0017(11)
Cl(2)	0.0847(18)	0.0996(18)	0.0882(18)	0.0362(13)	0.0120(15)	0.0183(12)
CM	0.0618(62)	0.0697(61)	0.203 (14)	-0.0150(70)	0.0321(77)	0.0030(45)

Table 3.10 Calculated Coordinates of Hydrogen Atoms in [10,11-μ-(PPh_3Au)-9-SMe_2-7,8-*nido*-$C_2B_9H_{10}$], $PPh_3Au(carb')$, **(4)**

	x	y	z
HS(11)	1.1519	-0.0362	0.4377
HS(12)	1.2141	-0.1234	0.5231
HS(13)	1.1273	-0.1768	0.4297
HS(21)	1.3491	-0.2829	0.3963
HS(22)	1.2511	-0.3191	0.4208
HS(23)	1.3496	-0.2551	0.4981
H(120)	0.8529	0.3148	0.3315
H(130)	0.6892	0.3114	0.3260
H(140)	0.6010	0.1377	0.3009
H(150)	0.6765	-0.0326	0.2812
H(160)	0.8402	-0.0291	0.2867
H(220)	0.9510	0.1708	0.1361
H(230)	0.9698	0.3290	0.0540
H(240)	1.0157	0.5082	-0.1240
H(250)	1.0428	0.5291	0.2761
H(260)	1.0240	0.3709	0.3583
H(320)	0.9487	0.1535	0.4746
H(330)	1.0620	0.1849	0.6219
H(340)	1.2307	0.2180	0.6504
H(350)	1.2861	0.2195	0.5315
H(360)	1.1728	0.1881	0.3842
HC(1)	0.6706	0.1043	0.0346
HC(2)	0.5885	0.0054	0.0376

This depression of the SMe_2 group by ca. 5^0 in the gold complex presumably arises as an effect of steric interaction between the CS(1) methyl group of the dimethylsulphide ligand and the C(31)-C(36) phenyl ring which approaches most closely in the solid state structure.

As discussed earlier in this chapter, it appears that the sulphur lone pair has a tendency to almost eclipse the B(9)-C(8) connectivity, giving small lone pair-S-B(9)-C(8) torsion angles. In the case of **(4)**, this torsion is observed to be 4.4^0, in accord with those in carb'H (27.3^0 and 4.0^0 in molecules *a* and *b*).

It is noteworthy that the SMe_2 group in PPh_3Au(carb') does not adopt a torsion about the B(9)-S(1) bond which would alleviate the observed intramolecular crowding. The fact that it does not do so would tend to add weight to the assertion that the stereochemical preference of the SMe_2 group for the near-eclpised lone pair-C(8) torsion is indeed a very real one whose origin lies in the lone pair..$H(8)^{\delta+}$ interaction discussed earlier.

Further evidence for this interaction in **(4)** comes from the relative sizes of the S(1)-B(9)-C(8) and S(1)-B(9)-B(10) angles, 114.6^0 and 131.0^0 respectively. The narrowing of the former angle (also observed in **(3)**) is presumably a further effect of the coulombic interaction which leads to the preferred orientation of the pendant dimethylsulphide group.

The bridging $\{AuPPh_3^+\}$ fragment is asymmetric with respect to B(10) and B(11), favouring B(10), with bond lengths Au(1)-B(10) = 2.233(6)Å and Au(1)-B(11) = 2.357(6)Å. As with carb'H, **(2)**, this difference is statistically significant, and can again be traced to the charge difference between B(10) and B(11) in $[carb']^-$, B(10) being the more negative, as modelled by EHMO

calculations, and therefore having the greater affinity for the incoming positive gold phosphine fragment.

This result is in complete accord with the comparable structural parameters for carb'H, showing the same type of asymmetry, but the precision of the measurement (location of Au *versus* location of H) is obviously much greater. The measured Au(1)-B(10) and Au(1)-B(11) distances in **(4)** are in good agreement with previously published values for such connectivities in related species [73-75].

The sum of the angles at Au(1) (P(1)-Au(1)-B(10), P(1)-Au(1)-B(11) and B(10)-Au(1)-B(11)) is 359.09°, indicating planarity at the gold atom, with the subsequent implication that the orbital number [76] of Au in PPh_3Au(carb') is two, one orbital directed towards the PPh_3 ligand and the other towards the HOMO of the carbaborane, i.e. towards the B(10)-B(11) connectivity, favouring B(10), as indicated by the greater value of the P(1)-Au(1)-B(10) angle (166.80°) c.f. the P(1)-Au(1)-B(11) angle (144.99°). For a symmetric bridge, these two angles would be expected to be equal.

Other parameters within compound **(4)** are as expected for such a molecule, specifically the Au-P distance and angles around P and S are in reasonable agreement with published details of related species [68,69,73-75].

Determination of the structure of **(4)** affords the first opportunity to directly compare analogous metal complexes of the Cp^- and $[carb']^-$ ligands. The structure of the tetraphenylcyclopentadienyl complex was discussed earlier (see **Figure 2.10**), and possesses an essentially Au-C σ bond, unlike the bridging function found in **(4)**. These findings (and those for the carbaboranes **(1)** and **(3)**)

are entirely consistent with the differing forms of the HOMO's obtained by extended Hückel calculations, (see **Figure 1.5**).

[3-PPh_3-4-SMe_2-3,1,2-$CuC_2B_9H_{10}$], PPh_3Cu(carb'), (5)

Introduction

Following the structural comparisons drawn in Chapter 2 between the protonated and (triphenylphosphine)gold (I) derivatives of the $[7,8\text{-}C_2B_9H_{11}]^{2-}$ ligand with the $\{CuPPh_3^+\}$ derivative, it was decided to attempt a similar analysis for the related compounds of the monoanionic $[carb']^-$ ligand.

Unlike the (triphenylphosphine)copper (I) derivative of $[C_2B_9H_{11}]^{2-}$ however, the PPh_3Cu(carb') complex, **(5)**, had not been previously reported, and therefore details of its synthesis and characterisation will be presented prior to detailed discussion of the *X*-ray structural analysis.

Synthesis and Characterisation of (5)

[3-PPh_3-4-SMe_2-3,1,2-$CuC_2B_9H_{10}$], **(5)**, was prepared by reaction of dichloromethane suspensions of Tl[carb'] and $[PPh_3CuBr]_4$ in 4:1 molar ratio, as described in Chapter 6, section 1, and the product was purified by crystallisation, effected by diffusion of n-hexane into a dichloromethane solution at -30°C. This technique also produced crystals of suitable habit for structural study (see later).

The identity of the species was confirmed by elemental microanalysis and multinuclear n.m.r. spectroscopy. ^1H, ^{11}B, $^{11}B\text{-}\{^1H\}$ and ^{31}P n.m.r spectra were recorded at ambient temperature.

The ^{1}H spectrum shows a multiplet at δ 7.20-7.75 p.p.m., corresponding to the protons of the triphenylphoshine group. The two inequivalent methyl groups of the SMe_2 function appear as singlets at δ 2.33 and 2.24 p.p.m., and the carbon-bonded H atoms of the carbaborane show broader resonances centred at 2.26 and 2.01 p.p.m..

The $^{11}B-\{^{1}H\}$ spectrum displays 7 resonances, of relative integral 2:1:1:1:1:2:1. On retention of proton coupling in the ^{11}B spectrum, all resonances show doublet coupling except one of the components of the highest frequency coincidence at δ -15.37 p.p.m., thus assignable to B(4), the sulphur-bonded boron atom.

The ^{31}P spectrum obtained at room temperature was unfortunately of little use in identification of the species, as the compound had (at least partially) decomposed over the timescale of the experiment, and two resonances were observed (at δ 9.78 and -4.54 p.p.m.) where only one would be expected for the proposed (and found in the solid state, see later) structure. Further evidence for decomposition was taken from the change in colour of the sample from colourless to brown during the ^{31}P n.m.r. experiment.

Structural Study on (5)

Introduction

As has already been explained, the reason behind the structural analysis of **(5)** was to enable detailed comparisons to be drawn both with the *closo* -$[3\text{-}PPh_3\text{-}3,1,2\text{-}CuC_2B_9H_{11}]^-$ anion [43] and with the *nido* compounds **(3)** and **(4)** presented earlier in this chapter.

Details of data collection and processing, and of the crystallographic

procedures used in the solution and refinement of the structure may be found in Chapter 6, section 2.

Discussion

2 molecules of compound **(5)** crystallise in the triclinic space group $P\bar{1}$, with no unusually short intermolecular contacts.

A perspective view of $PPh_3Cu(carb')$ is shown in **Figure 3.5**, showing the numbering scheme employed. (The same problems arise here as in Chapter 2, because of the different numbering conventions for *closo* and *nido* species, and these must again be borne in mind during the discussion). Non-hydrogen atoms are represented by thermal ellipsoids at the 50% probability level and H atoms have been given artificial radii of 0.1Å for clarity. Phenyl H atoms bonded to C(*ij*) are numbered H(*ij*0), and cage hydrogens carry the same number as the vertex to which they are bonded.

Positional coordinates of refined atoms are given in **Table 3.11**, along with equivalent isotropic thermal parameters for non-hydrogen atoms. **Table 3.12** gives interatomic distances and interbond angles are given in **Table 3.13**. Anisotropic thermal parameters comprise **Table 3.14** and **Table 3.15** gives calculated coordinates of (non-refined) hydrogen atoms.

Figure 3.5 clearly shows the essential structural features of the complex. It is initially apparent that, unlike carb'H or $PPh_3Au(carb')$ the geometry of the polyhedron is, to a first approximation, icosahedral. The copper atom in **(5)** is regarded as a polyhedral vertex, and adopts a very similar position with respect to the cage framework as does Cu(03) in $[PPh_3Cu(C_2B_9H_{11})]^-$ (see **Figure 2.7**).

Figure 3.5 Perspective View of [3-PPh_3-4-SMe_2-3,1,2-$CuC_2B_9H_{10}$], PPh_3Cu(carb'), **(5)**

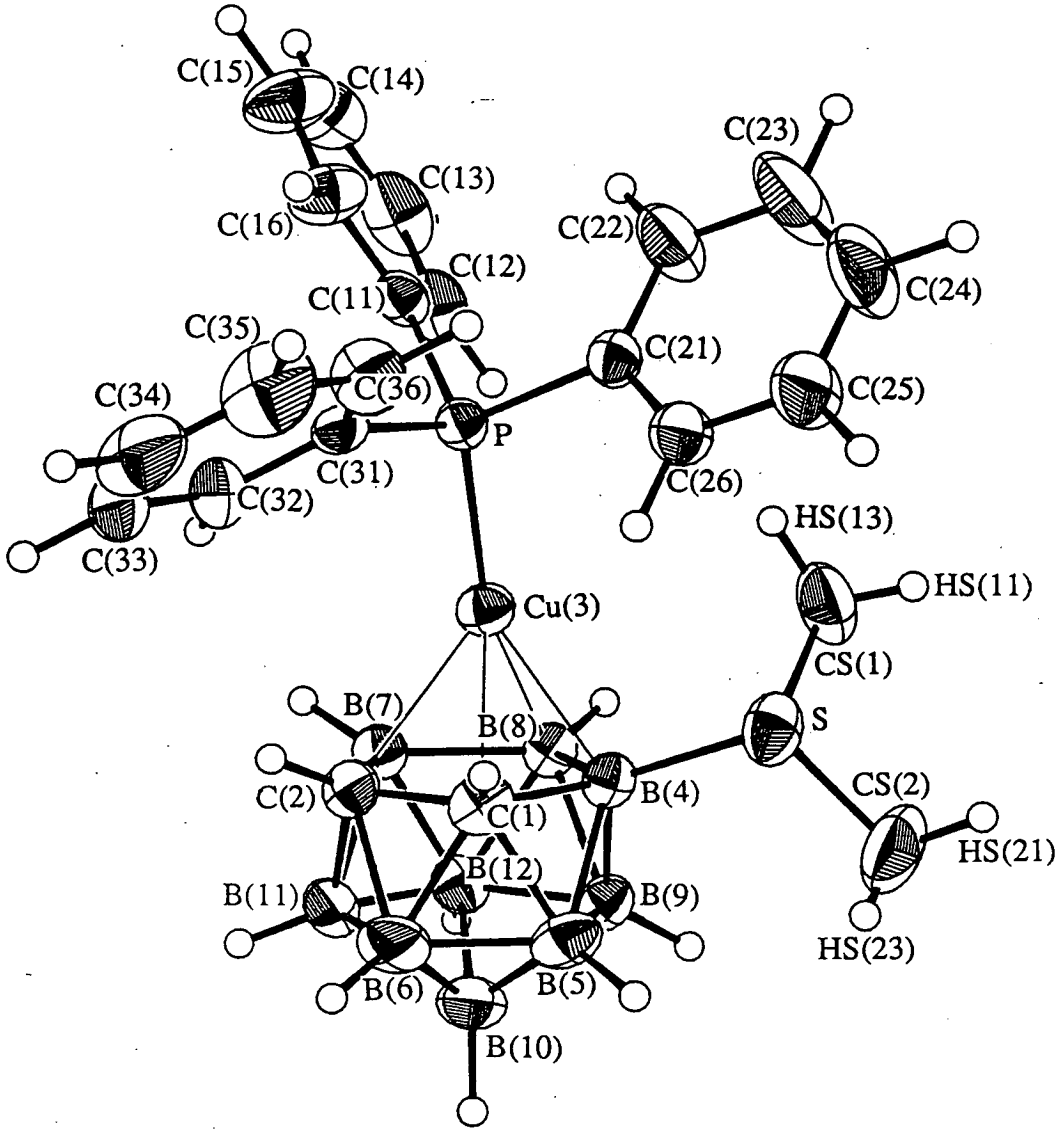

Table 3.11 Positional Coordinates of Refined Atoms in [3-PPh_3-4-SMe_2-3,1,2-$CuC_2B_9H_{10}$], PPh_3Cu(carb'), **(5)**

	x	y	z	Ueq
Cu(3)	0.22919(4)	0.75298(4)	0.24695(3)	0.0382(3)
P	0.15486(8)	0.83671(7)	0.35583(6)	0.0318(5)
S	-0.07947(9)	0.71203(9)	0.14353(7)	0.0543(6)
CS(1)	-0.0781(6)	0.5854(5)	0.2681(4)	0.074(4)
CS(2)	-0.1453(5)	0.6299(6)	0.0698(4)	0.091(4)
C(1)	0.1741(4)	0.8749(3)	0.06751(24)	0.0389(20)
C(2)	0.3411(4)	0.8711(3)	0.09192(23)	0.0396(20)
B(4)	0.1250(4)	0.7287(3)	0.1168(3)	0.0351(21)
B(5)	0.1493(5)	0.8059(4)	-0.0179(3)	0.047(3)
B(6)	0.2912(5)	0.9017(4)	-0.0330(3)	0.051(3)
B(7)	0.4229(4)	0.7221(3)	0.1623(3)	0.0370(22)
B(8)	0.2846(4)	0.6169(3)	0.1787(3)	0.0326(21)
B(9)	0.2234(4)	0.6407(4)	0.0524(3)	0.0415(24)
B(10)	0.3292(5)	0.7512(4)	-0.0412(3)	0.053(3)
B(11)	0.4531(5)	0.7995(4)	0.0276(3)	0.048(3)
B(12)	0.4142(4)	0.6381(4)	0.0796(3)	0.0433(24)
C(11)	0.25851(25)	0.77143(18)	0.47813(17)	0.0368(19)
C(12)	0.32171	0.64232	0.51621	0.0501(23)
C(13)	0.39843	0.58786	0.61110	0.061(3)
C(14)	0.41194	0.66252	0.66792	0.070(3)
C(15)	0.34873	0.79164	0.62984	0.075(3)
C(16)	0.27202	0.84610	0.53495	0.0559(25)
C(21)	-0.03736(23)	0.8212(3)	0.38964(13)	0.0381(19)
C(22)	-0.07771	0.7524	0.48991	0.070(3)
C(23)	-0.22596	0.7366	0.51082	0.109(4)
C(24)	-0.33387	0.7897	0.43147	0.093(4)
C(25)	-0.29351	0.8585	0.33121	0.068(3)
C(26)	-0.14526	0.8743	0.31029	0.0497(23)
C(31)	0.16471(21)	1.00960(22)	0.30489(18)	0.0360(19)
C(32)	0.29559	1.05228	0.25913	0.0564(25)
C(33)	0.30715	1.18428	0.21459	0.079(3)
C(34)	0.18783	1.27362	0.21583	0.082(3)
C(35)	0.05695	1.23095	0.26160	0.084(4)
C(36)	0.04539	1.09894	0.30613	0.0567(25)
HS(11)	-0.176(4)	0.563(3)	0.276(3)	
HS(12)	-0.018(4)	0.511(4)	0.272(3)	
HS(13)	-0.062(4)	0.615(4)	0.313(3)	
HS(21)	-0.253(4)	0.619(3)	0.085(3)	
HS(22)	-0.073(4)	0.558(4)	0.076(3)	
HS(23)	-0.138(4)	0.687(4)	0.010(3)	
H(1)	0.109(4)	0.947(3)	0.061(3)	
H(2)	0.365(4)	0.947(3)	0.096(3)	
H(5)	0.050(4)	0.844(3)	-0.073(3)	
H(6)	0.293(4)	0.996(3)	-0.090(3)	
H(7)	0.525(4)	0.715(3)	0.210(3)	
H(8)	0.280(4)	0.518(3)	0.239(3)	
H(9)	0.178(4)	0.564(3)	0.036(3)	
H(10)	0.354(4)	0.744(3)	-0.119(3)	
H(11)	0.548(4)	0.835(3)	0.001(3)	
H(12)	0.502(4)	0.555(3)	0.0764(25)	

Table 3.12 Interatomic Distances (Å) in [3-PPh_3-4-SMe_2-3,1,2-$CuC_2B_9H_{10}$], PPh_3Cu(carb'), **(5)**

Cu(3)	- P	2.1681(9)	B(4)	- B(5)	1.783(6)
Cu(3)	- C(1)	2.394(3)	B(4)	- B(8)	1.787(5)
Cu(3)	- C(2)	2.369(3)	B(4)	- B(9)	1.761(5)
Cu(3)	- B(4)	2.212(4)	B(5)	- B(6)	1.747(6)
Cu(3)	- B(7)	2.187(4)	B(5)	- B(9)	1.788(6)
Cu(3)	- B(8)	2.130(4)	B(5)	-B(10)	1.752(6)
P	-C(11)	1.8192(24)	B(5)	- H(5)	1.13(4)
P	-C(21)	1.8179(25)	B(6)	-B(10)	1.748(6)
P	-C(31)	1.8178(25)	B(6)	-B(11)	1.756(6)
S	-CS(1)	1.784(5)	B(6)	- H(6)	1.06(4)
S	-CS(2)	1.800(6)	B(7)	- B(8)	1.791(5)
S	- B(4)	1.911(4)	B(7)	-B(11)	1.792(6)
CS(1)	-HS(11)	0.95(4)	B(7)	-B(12)	1.784(6)
CS(1)	-HS(12)	0.93(4)	B(7)	- H(7)	1.13(4)
CS(1)	-HS(13)	0.85(4)	B(8)	- B(9)	1.789(5)
CS(2)	-HS(21)	1.02(4)	B(8)	-B(12)	1.781(5)
CS(2)	-HS(22)	0.96(4)	B(8)	- H(8)	1.11(4)
CS(2)	-HS(23)	0.85(4)	B(9)	-B(10)	1.792(6)
C(1)	- C(2)	1.555(5)	B(9)	-B(12)	1.779(6)
C(1)	- B(4)	1.643(5)	B(9)	- H(9)	1.11(4)
C(1)	- B(5)	1.710(5)	B(10)	-B(11)	1.770(6)
C(1)	- B(6)	1.718(6)	B(10)	-B(12)	1.801(6)
C(1)	- H(1)	0.93(4)	B(10)	-H(10)	1.15(4)
C(2)	- B(6)	1.721(5)	B(11)	-B(12)	1.764(6)
C(2)	- B(7)	1.670(5)	B(11)	-H(11)	1.00(4)
C(2)	-B(11)	1.695(5)	B(12)	-H(12)	1.17(4)
C(2)	- H(2)	0.94(4)			

Table 3.13 Selected Interbond Angles (^{o}) in [3-PPh_3-4-SMe_2-3,1,2-$CuC_2B_9H_{10}$], PPh_3Cu(carb'), **(5)**

P	-Cu(3)	- C(1)	119.33(8)	C(1)	- B(6)	- B(5)	59.15(23)
P	-Cu(3)	- C(2)	122.48(8)	C(2)	- B(6)	-B(11)	58.35(23)
P	-Cu(3)	- B(4)	135.38(10)	B(5)	- B(6)	-B(10)	60.16(25)
P	-Cu(3)	- B(7)	142.18(10)	B(10)	- B(6)	-B(11)	60.7(3)
P	-Cu(3)	- B(8)	161.74(10)	Cu(3)	- B(7)	- C(2)	74.44(18)
C(1)	-Cu(3)	- C(2)	38.11(11)	Cu(3)	- B(7)	- B(8)	63.86(17)
C(1)	-Cu(3)	- B(4)	41.56(12)	C(2)	- B(7)	-B(11)	58.50(22)
C(2)	-Cu(3)	- B(7)	42.78(13)	B(8)	- B(7)	-B(12)	59.76(21)
B(4)	-Cu(3)	- B(8)	48.55(14)	B(11)	- B(7)	-B(12)	59.11(23)
B(7)	-Cu(3)	- B(8)	48.99(14)	Cu(3)	- B(8)	- B(4)	68.12(17)
Cu(3)	- P	-C(11)	115.67(8)	Cu(3)	- B(8)	- B(7)	67.15(17)
Cu(3)	- P	-C(21)	113.77(8)	B(4)	- B(8)	- B(9)	59.00(21)
Cu(3)	- P	-C(31)	111.81(8)	B(7)	- B(8)	-B(12)	59.94(21)
C(11)	- P	-C(21)	104.86(11)	B(9)	- B(8)	-B(12)	59.78(22)
C(11)	- P	-C(31)	105.05(11)	B(4)	- B(9)	- B(5)	60.31(22)
C(21)	- P	-C(31)	104.67(11)	B(4)	- B(9)	- B(8)	60.44(21)
CS(1)	- S	-CS(2)	98.6(3)	B(5)	- B(9)	-B(10)	58.59(23)
CS(1)	- S	- B(4)	104.49(21)	B(8)	- B(9)	-B(12)	59.88(22)
CS(2)	- S	- B(4)	108.47(22)	B(10)	- B(9)	-B(12)	60.58(23)
Cu(3)	- C(1)	- C(2)	70.08(17)	B(5)	-B(10)	- B(6)	59.87(25)
Cu(3)	- C(1)	- B(4)	63.29(17)	B(5)	-B(10)	- B(9)	60.61(24)
C(2)	- C(1)	- B(6)	63.23(23)	B(6)	-B(10)	-B(11)	59.86(25)
B(4)	- C(1)	- B(5)	64.21(23)	B(9)	-B(10)	-B(12)	59.36(23)
B(5)	- C(1)	- B(6)	61.27(24)	B(11)	-B(10)	-B(12)	59.20(24)
Cu(3)	- C(2)	- C(1)	71.81(18)	C(2)	-B(11)	- B(6)	59.81(23)
Cu(3)	- C(2)	- B(7)	62.78(17)	C(2)	-B(11)	- B(7)	57.15(21)
C(1)	- C(2)	- B(6)	62.99(23)	B(6)	-B(11)	-B(10)	59.46(25)
B(6)	- C(2)	-B(11)	61.83(24)	B(7)	-B(11)	-B(12)	60.22(23)
B(7)	- C(2)	-B(11)	64.35(23)	B(10)	-B(11)	-B(12)	61.27(24)
Cu(3)	- B(4)	- C(1)	75.15(18)	B(7)	-B(12)	- B(8)	60.31(21)
Cu(3)	- B(4)	- B(8)	63.33(16)	B(7)	-B(12)	-B(11)	60.67(23)
C(1)	- B(4)	- B(5)	59.71(22)	B(8)	-B(12)	- B(9)	60.33(22)
B(5)	- B(4)	- B(9)	60.60(22)	B(9)	-B(12)	-B(10)	60.06(23)
B(8)	- B(4)	- B(9)	60.56(21)	B(10)	-B(12)	-B(11)	59.52(24)
C(1)	- B(5)	- B(4)	56.07(21)	P	-C(11)	-C(12)	118.37(17)
C(1)	- B(5)	- B(6)	59.58(23)	P	-C(11)	-C(16)	121.61(17)
B(4)	- B(5)	- B(9)	59.08(22)	P	-C(21)	-C(22)	122.21(18)
B(6)	- B(5)	-B(10)	59.97(25)	P	-C(21)	-C(26)	117.68(18)
B(9)	- B(5)	-B(10)	60.80(24)	P	-C(31)	-C(32)	117.45(18)
C(1)	- B(6)	- C(2)	53.78(21)	P	-C(31)	-C(36)	122.49(18)
S	- B(4)	- C(1)	118.16(24)	S	- B(4)	- B(8)	128.85(24)
S	- B(4)	- B(5)	110.24(23)	S	- B(4)	- B(9)	119.60(24)

Table 3.14 Anisotropic Thermal Parameters ($Å^2$) for [3-PPh_3-4-SMe_2-3,1,2-$CuC_2B_9H_{10}$], PPh_3Cu(carb'), **(5)**

	U11	U22	U33	U23	U13	U12
Cu(3)	0.0391(3)	0.0347(2)	0.0344(2)	-0.0151(2)	0.0014(2)	-0.0041(2)
P	0.0285(4)	0.0311(4)	0.0288(4)	-0.0096(3)	0.0004(3)	-0.0039(3)
S	0.0338(5)	0.0542(6)	0.0657(6)	-0.0299(5)	-0.0023(4)	-0.0025(4)
CS(1)	0.0656(30)	0.0678(30)	0.0780(32)	-0.0277(25)	0.0232(26)	-0.0366(24)
CS(2)	0.0448(26)	0.1164(48)	0.1014(37)	-0.0671(36)	-0.0097(29)	-0.0175(28)
C(1)	0.0441(19)	0.0253(16)	0.0381(18)	-0.0089(14)	-0.0081(15)	0.0052(14)
C(2)	0.0522(21)	0.0241(16)	0.0350(17)	-0.0065(14)	-0.0015(15)	-0.0107(15)
B(4)	0.0314(19)	0.0311(18)	0.0351(19)	-0.0111(15)	-0.0029(15)	-0.0021(15)
B(5)	0.0586(26)	0.0412(22)	0.0309(20)	-0.0107(17)	-0.0124(18)	0.0003(19)
B(6)	0.0730(30)	0.0389(22)	0.0276(19)	0.0005(17)	0.0007(19)	-0.0129(21)
B(7)	0.0351(20)	0.0326(19)	0.0351(19)	-0.0105(16)	-0.0005(16)	-0.0038(16)
B(8)	0.0347(19)	0.0228(17)	0.0321(18)	-0.0061(15)	-0.0046(15)	0.0010(15)
B(9)	0.0437(22)	0.0361(20)	0.0391(20)	-0.0185(17)	-0.0008(17)	-0.0064(17)
B(10)	0.0620(28)	0.0534(25)	0.0335(21)	-0.0165(19)	0.0065(19)	-0.0121(21)
B(11)	0.0464(24)	0.0457(23)	0.0427(22)	-0.0163(18)	0.0119(18)	-0.0164(19)
B(12)	0.0401(22)	0.0375(21)	0.0444(22)	-0.0174(18)	0.0058(17)	-0.0035(17)
C(12)	0.0445(21)	0.0402(20)	0.0499(21)	-0.0037(16)	-0.0042(17)	-0.0049(16)
C(13)	0.0445(22)	0.0531(24)	0.0601(25)	0.0092(20)	-0.0053(19)	-0.0009(18)
C(14)	0.0469(24)	0.0982(34)	0.0404(21)	-0.0056(22)	-0.0089(18)	0.0018(23)
C(15)	0.0645(27)	0.0993(34)	0.0481(23)	-0.0369(23)	-0.0190(20)	0.0099(25)
C(16)	0.0493(22)	0.0635(24)	0.0438(20)	-0.0245(18)	-0.0106(17)	0.0081(18)
C(11)	0.0276(16)	0.0407(18)	0.0322(16)	-0.0086(14)	0.0026(13)	-0.0049(14)
C(22)	0.0435(22)	0.1010(34)	0.0408(21)	0.0007(21)	0.0017(17)	-0.0236(22)
C(23)	0.0503(27)	0.1791(56)	0.0555(28)	0.0009(32)	0.0134(22)	-0.0436(32)
C(24)	0.0348(22)	0.1415(46)	0.0740(31)	-0.0219(30)	0.0077(21)	-0.0269(26)
C(25)	0.0353(21)	0.0913(31)	0.0591(25)	-0.0242(23)	-0.0025(18)	-0.0070(20)
C(26)	0.0332(18)	0.0608(23)	0.0441(19)	-0.0198(17)	-0.0012(15)	-0.0046(16)
C(21)	0.0321(17)	0.0393(18)	0.0348(17)	-0.0127(14)	-0.0002(14)	-0.0075(14)
C(32)	0.0564(23)	0.0491(22)	0.0556(22)	-0.0212(18)	0.0090(18)	-0.0235(18)
C(33)	0.1024(36)	0.0759(30)	0.0525(24)	-0.0265(22)	0.0193(23)	-0.0618(29)
C(34)	0.1399(45)	0.0392(22)	0.0579(26)	-0.0164(20)	-0.0056(28)	-0.0294(28)
C(35)	0.1093(39)	0.0361(23)	0.0912(34)	-0.0256(23)	-0.0047(29)	0.0005(24)
C(36)	0.0612(24)	0.0349(19)	0.0643(24)	-0.0213(17)	0.0062(19)	-0.0024(18)
C(31)	0.0427(18)	0.0345(17)	0.0249(15)	-0.0109(13)	-0.0004(13)	-0.0097(15)

Table 3.15 Calculated Coordinates of Non-refined Hydrogen Atoms in [3-PPh_3-4-SMe_2-3,1,2-$CuC_2B_9H_{10}$], PPh_3Cu(carb'), **(5)**

	x	y	z
H(120)	0.31125	0.58451	0.47222
H(130)	0.44736	0.48790	0.64058
H(140)	0.47133	0.62036	0.74138
H(150)	0.35919	0.84944	0.67382
H(160)	0.22308	0.94606	0.50547
H(220)	0.00583	0.7113	0.55134
H(230)	-0.25721	0.6833	0.58844
H(240)	-0.44865	0.7774	0.44765
H(250)	-0.37705	0.8996	0.26977
H(260)	-0.11402	0.9276	0.23267
H(320)	0.38797	0.98311	0.25817
H(330)	0.40847	1.21732	0.17916
H(340)	0.19677	1.37582	0.18136
H(350)	-0.03543	1.30011	0.26255
H(360)	-0.05593	1.06590	0.34156

The copper atom sits at a vertical distance of 1.721Å from the centroid of the ligated $[C_2B_3]$ face of the carbaborane, with the Cu(3)-C(1) and Cu(3)-C(2) distances averaging 2.382(3)Å. Cu(3) is consistently closer to the facial boron atoms than to the carbons, with distances from copper to B(4), B(7) and B(8) at 2.212(4), 2.187(4) and 2.130(4)Å respectively. This slippage of the Cu atom towards the B atoms may also be represented by the slip parameter, Δ [54], which is calculated in this case as +0.34Å.

The ligated face of the carbaborane is slightly folded into an envelope conformation about the B(4)-B(7) vector, resulting in fold angles of θ and ϕ of 2.11 and 1.15°. Such folding is a commonly observed structural feature of 3-metalla-1,2-dicarbaboranes such as **(5)** [54,77].

The above structural distortions of the molecule are entirely consistent with the greater degree of localisation of the carbaborane frontier M.O.'s on the facial boron atoms rather than the (more electronegative) carbons (as discussed in Chapters 1 & 2, and later in this chapter).

Although the structure of **(5)** is different in overall polyhedral architecture to those of **(3)** and **(4)**, there remain a number of strong structural similarities between the compounds, namely in the orientation of the dimethylsulphide group with respect to the $[C_2B_9]$ framework.

As observed in the structures of **(3)** and **(4)** (and in that of complex **(6)** in Chapter 4), the SMe_2 function takes up a preferred orientation, the reason for which has been traced to an intramolecular electrostatic interaction between the lone pair of the sulphur atom and the most proximate of the carbaborane $C\text{-}H^{\delta+}$ functions. As in the other examples where this has been observed, a narrowing of

the S-B(4)-C(1) angle ($118.16(24)^{o}$) is noted, along with a widening of the opposite (S-B(4)-B(8), $128.85(24)^{o}$) angle.

Intramolecular steric crowding is observed in **(5)** between one of the phenyl rings [C(21)-C(26)] of the PPh_3 moiety and the CS(1) methyl group of the SMe_2 function. This results in depression by *ca.* 5^{o} of the dimethylsulphide group from its preferred angle of inclination (approx. 26^{o} with respect to the ligated face of the carbaborane). Sharpening of the S-B(4)-B(5) angle to $110.24(23)^{o}$ provides another measure of this distortion.

A highly similar distortion was observed in the gold analogue **(4)**. Again, however, the favourable torsion angle about the S-B(4) bond is retained at the (evidently lesser) expense of this steric interaction.

Misfit calculations between **(5)** and **(3)** (both independent molecules *a* and *b*) and **(4)** illustrate this point, the individual misfit of the sulphur atoms being greater between the copper and protonated species, 0.105Å (average) than between the copper and gold complexes, 0.083Å.

Structural Patterns in (3), (4) and (5)

In Chapter 2, a successful rationalisation of facial distances in the series of complexes of $[C_2B_9H_{11}]^{2-}$ with H^+, $\{PPh_3Au^+\}$ and $\{PPh_3Cu^+\}$ was carried out, by consideration of frontier molecular orbital interactions. The analogous series of $[carb']^-$ complexes have been structurally characterised (**(3)**, **(4)** and **(5)**), and it is therefore of interest to attempt an analysis similar to that presented for the anions in the previous chapter.

As before, the values of relevant parameters are tabulated, in this case comprising **Table 3.16**. Note that Δ, the slip parameter, is not included in this analysis, because the proton and gold phosphine fragment located in structures **(3)** and **(4)** are not on (or very close to) the B(10)..C(7),C(8) midpoint vector, and therefore meaningful analysis of Δ values may prove difficult.

It should also be noted that because of the different numbering schemes [36] adopted for *nido* **(3)** and **(4)** and *closo* **(5)**, confusion could arise in comparing equivalent connectivities. For the purpose of clarity, the intrafacial distances in **(5)** appear in **Table 3.16** under a *nido*-type numbering system, whereby equivalent interatomic distances in all three complexes are similarly named.

Finally, it should be remembered that the symmetry of [carb']$^-$ (C_1) is lower than that of $[C_2B_9H_{11}]^{2-}$ (C_s), and therefore all 5 distances between adjacent atoms in the open face must be treated as separate parameters, and not averaged over the two B-B and B-C separations.

Table 3.16 Intra-facial Distances (Å) in (3), (4) and (5)

{carb'}$^-$	{H^+}*	{PPh_3Au^+}	{PPh_3Cu^+}
B(9)-B(10)	1.774(4)	1.772(8)	1.787(5)
B(10)-B(11)	1.847(5)	1.844(8)	1.791(5)
C(8)-B(9)	1.577(5)	1.594(8)	1.643(5)
C(7)-B(11)	1.618(4)	1.636(8)	1.670(5)
C(7)-C(8)	1.525(4)	1.558(8)	1.555(5)

*Average value for 2 independent molecules.

The general trends identifiable in going from H^+ to $\{PPh_3Au^+\}$ to $\{PPh_3Cu^+\}$ are as follows: (i) B(9)-B(10) lengthens, (ii) B(10)-B(11) shortens, (iii) C(8)-B(9) lengthens, (iv) C(7)-B(11) lengthens, and (v) C(7)-C(8) lengthens.

As observed in the similar analysis of Chapter 2, the magnitudes of the changes between the protonated and aurated species are small (except for the anomalously large effect upon the C(7)-C(8) distance). The B(9)-B(10) connectivity appears to be shortened, contrary to the general trend, although the magnitude of this effect is insignificant.

The differences observed between carb'H and the copper derivative are, however, much larger.

As before, these effects may be traced to differences in depopulation of the carbaborane filled π-MO's. These have been calculated for $[carb']^-$ by extended Hückel methods, using an experimentally-derived model (by removal of $\{Mn(CO)_3^+\}$ from the structure of complex **(6)**). The π-orbital set so obtained is shown in **Figure 1.5**, with the three filled π-MO's sketched in **Figure 3.6** (below).

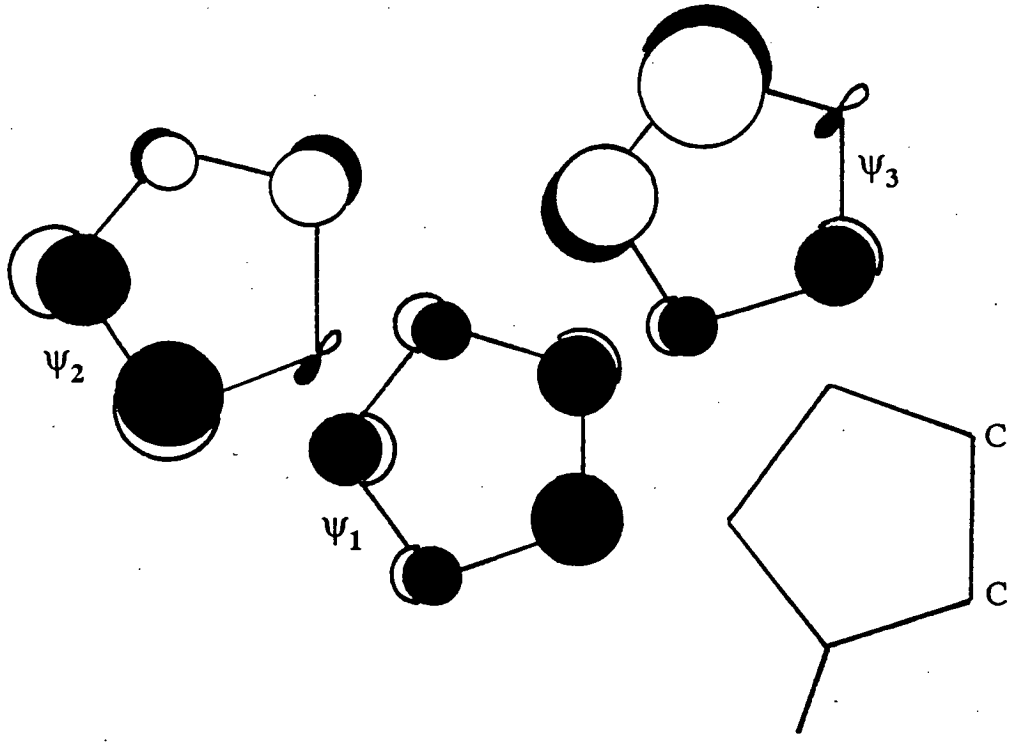

Note that the positions of the nodal planes are different to those in the corresponding orbitals of $[C_2B_9H_{11}]^{2-}$, the effects of which will become clear later in the discussion.

The structures of **(3)** and **(4)** are consistent with key interactions between H(1s) or Au 6s/6p_z orbitals with Ψ_3 (the HOMO) of [carb']$^-$.

In the copper case, however, as discussed previously for $[PPh_3CuC_2B_9H_{11}]^-$, the metal atom is almost symmetrically bonded to the $[C_2B_3]$ face of the ligand, to maximise overlap of all 3 accessible Cu acceptor orbitals with the three filled π-MO's of the carbaborane.

Again, let us look at the predicted changes in depopulation of Ψ_1, Ψ_2 and Ψ_3 on moving from H^+ (complex **(3)**) to $\{PPh_3Cu^+\}$ (complex **(5)**), and the results of these on interatomic distances within the open face of the ligand.

(i) Reduction in depopulation of Ψ_3 will have the following effects (in decreasing order of importance): shortening of B(10)-B(11), shortening of C(8)-B(9) and lengthening of B(9)-B(10).

(ii) Depopulation of Ψ_2 will lead to: lengthening of B(9)-B(10), lengthening of C(7)-B(11) and a shortening of B(10)-B(11).

(iii) Depopulation of the (all in-phase) Ψ_1 orbital will result in lengthening of all connectivities, with the predominant effect on C(7)-C(8) and a lesser influence on the two B-C distances. The B(9)-B(10) and B(10)-B(11) connectivities will scarcely be affected, as Ψ_1 is predominantly carbon-based and therefore of relatively low energy.

The net results of the above three changes in depopulation on the internuclear separations in the open face of the ligand are as follows:

(a) **B(9)-B(10)** will lengthen, as all three effects reinforce each other.

(b) **B(10)-B(11)** is chiefly affected by the depopulation of Ψ_3, with depopulation of Ψ_2 acting in the same sense, leading to a shortening of the connectivity.

(c) In the case of **C(8)-B(9)**, effects from Ψ_3 and Ψ_1 will act in opposite directions, making firm prediction of the net influence difficult. It would appear, however, from the experimental data (showing a longer bond in the copper complex) that the predominant influence is from the depopulation of the carbon-localised Ψ_1 orbital.

(d) **C(7)-B(11)** will be expected to show a lengthening, as a result of changes in depopulation of Ψ_2 and Ψ_1.

(e) **C(7)-C(8)** is influenced almost exclusively by depopulation of Ψ_1, which will cause the internuclear separation to increase.

The most interesting result of the above analysis is the understanding afforded of the different trends observed for the two independent B-B connectivities (one increasing, the other decreasing). This has undoubtedly been shown to be a function of the positions of the nodal planes of the π-MO's of [carb']$^-$, which are rotated with respect to those in $[C_2B_9H_{11}]^{2-}$, thus intersecting different connectivities.

Conclusions

[10,11-μ-H-9-SMe_2-7,8-*nido*-$C_2B_9H_{10}$], **(3)**, is the precursor to the monoanionic carbaborane ligand [carb']$^-$. Although **(3)** has been known for some considerable time, its structure had not been determined prior to this work.

The molecule possesses an asymmetric bridging hydrogen atom on its open face, a structural feature which has been rationalised by the results of extended Hückel molecular orbital calculations.

The (triphenylphosphine)gold(I) and (triphenylphosphine)copper(I) derivatives of [carb']$^-$ have been prepared and their structures determined. In all three species, there is a preferred orientation adopted by the dimethylsulphide group, a result of an intramolecular electrostatic interaction.

An analysis of structural patterns within the open [C_2B_3] face of the ligand shows different trends to those observed in the related series discussed in the previous chapter. These differences have been traced to the nature of the π-MO's of [carb']$^-$ compared to those of [$C_2B_9H_{11}$]$^{2-}$.

Chapter 4

(carb')$Mn(CO)_3$ versus $CpMn(CO)_3$: A Comparative Study

Introduction

In this chapter, the synthesis, characterisation and molecular structure of the carbamanganaborane [3,3,3-$(CO)_3$-4-SMe_2-3,1,2-$MnC_2B_9H_{10}$], (carb')$Mn(CO)_3$, **(6)**, are presented and discussed, along with the analogous cyclopentadienyl complex, [(η-C_5H_5)$Mn(CO)_3$], **(7)**. The structure of **(7)** has been determined previously, over 25 years ago [78], but was redetermined, in order to obtain parameters of sufficient accuracy as to allow meaningful discussion.

The electronic structures of both complexes, as investigated by extended Hückel and extended Hückel/fragment molecular orbital calculations are also discussed.

This pair of complexes was selected for study for the following reasons: (i) $CpMn(CO)_3$, **(7)**, is an extremely well known species and hence the analogous complex of the monoanionic carbaborane ligand [carb']$^-$ might be viewed as a suitable target molecule in order to test the analogy between the two ligands in terms of ease of synthesis of their complexes, their stability etc., and (ii) the common carbonyl ligands in the two complexes possess the potential to reflect the relative electronic (donor/acceptor) properties of carb' *versus* Cp in their C-O stretching frequencies [79] and/or in the bond lengths within the {$Mn(CO)_3$} fragments [80].

$[3,3,3\text{-}(CO)_3\text{-}4\text{-}SMe_2\text{-}3,1,2\text{-}MnC_2B_9H_{10}]$, (carb')$Mn(CO)_3$, (6)

Synthesis

The carbamanganaborane complex **(6)** was synthesised by reaction of equimolar quantities of $K^+[carb']^-$ and $[Mn(CO)_3(NCMe)_3]^+BPh_4^-$ in dichloromethane, with subsequent work-up involving preparative thin-layer chromatography, as described in Chapter 6, section 1.

(carb')$Mn(CO)_3$ was isolated in 30% yield, along with a smaller quantity of a second species of lower R_f value, full characterisation of which was frustrated by its relative instability. This second product will be discussed more fully later.

Characterisation of (6)

The compound was identified by means of infra-red spectroscopy, elemental analysis and n.m.r. spectroscopy.

Infra-red Spectroscopy

Of greatest interest in the infra-red spectrum of **(6)** are the carbonyl stretches occurring at 2020, 1950 and 1925cm^{-1}, and the B-H stretch, centred around 2525cm^{-1}. Further discussion of the C-O stretching frequencies will comprise a later part of this chapter, on the electronic structure of **(6)** in comparison with that of its cyclopentadienyl analogue, $CpMn(CO)_3$, **(7)**.

^{1}H, ^{11}B, ^{11}B-{^{1}H} and ^{13}C spectra were recorded, each consistent with the proposed identity of the compound.

In the ^{1}H spectrum, 2 signals were observed at δ 2.50 and 2.72 p.p.m., corresponding to the protons of the inequivalent methyl groups of the SMe_2 function.

The ^{11}B-{^{1}H} spectrum of **(6)** displayed 9 signals each of relative integral 1, eight of which display doublet coupling (J_{BH} 138-170 Hz) in the ^{11}B spectrum. The exception is the second highest frequency resonance (δ -4.05 p.p.m.) which is therefore assignable to the sulphur-bearing boron atom B(4).

An interesting feature of the ^{13}C spectrum was the resonance at δ 221.9 p.p.m., corresponding to the carbonyl carbon nuclei (see later).

The synthesis of **(6)** also gave an orange co-product in small yield. Although this compound was relatively unstable and decomposed to give carb'H, (3), an infra-red spectrum was obtained. This contained peaks at 2540cm^{-1} attributable to B-H stretching, 2015cm^{-1} tentatively assigned to Mn-H stretching because of its relatively low intensity and extreme sharpness, and two absorptions at 1937 and 1865cm^{-1} attributable to stretching of carbonyl groups, possibly of a bridging or semi-bridging nature.

The orange colour of the complex would suggest the Mn(I) oxidation state. This throws into some question the rôle of the carbaborane ligand, given the postulated presence of a hydride ligand.

X-Ray Crystallographic Study of (6)

Introduction

The structure of (carb')$Mn(CO)_3$, **(6)**, was determined at low temperature, in order not only to simply ascertain the stereochemistry of the complex but also to obtain accurate structural parameters which could be of later use in discussion of the electronic structure of the carbamanganaborane *versus* that of its well-known organometallic (cyclopentadienyl) analogue.

Diffraction-quality crystals of **(6)** were grown by slow diffusion of n-hexane into a CH_2Cl_2 solution of the compound, as described in Chapter 6, section 1.

Crystal data, details of data collection and processing, and details of procedures used in the structure solution and refinement may be found in Chapter 6, section 2.

Discussion

Figure 4.1 is a perspective view of a molecule of the compound, which shows the numbering scheme employed. This view clearly shows the cluster to be a *closo* -icosahedron, with the Mn atom occupying the 3-position, and cage C atoms at positions 1 and 2, in accordance with conventional nomenclature [36].

Figure 4.2 is a view of **(6)** from above the $\{Mn(CO)_3\}$ unit, illustrating the orientation of the tricarbonylmanganese moiety with respect to the carbaborane framework and the conformation adopted by the SMe_2 ligand about the S-B(4) bond.

Figure 4.1 Perspective View of $[3,3,3\text{-}(CO)_3\text{-}4\text{-}SMe_2\text{-}3,1,2\text{-}MnC_2B_9H_{10}]$, $(carb')Mn(CO)_3$, **(6)**

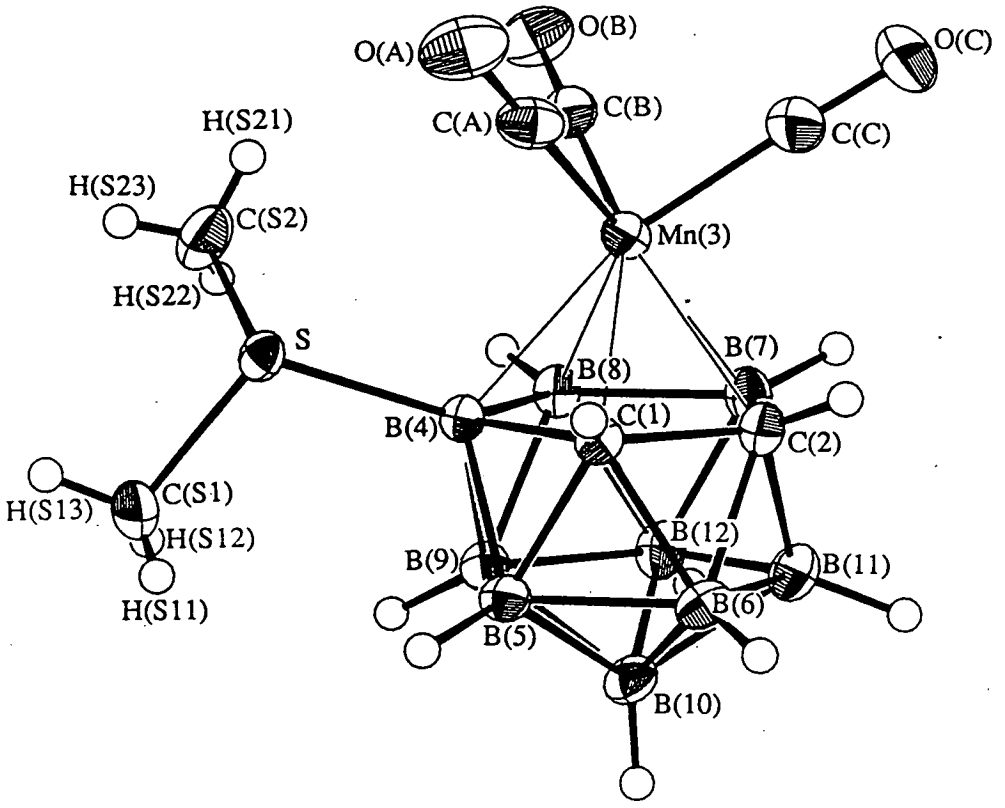

Figure 4.2 View of $[3,3,3\text{-}(CO)_3\text{-}4\text{-}SMe_2\text{-}3,1,2\text{-}MnC_2B_9H_{10}]$, $(carb')Mn(CO)_3$, **(6)**, from Above Mn Position

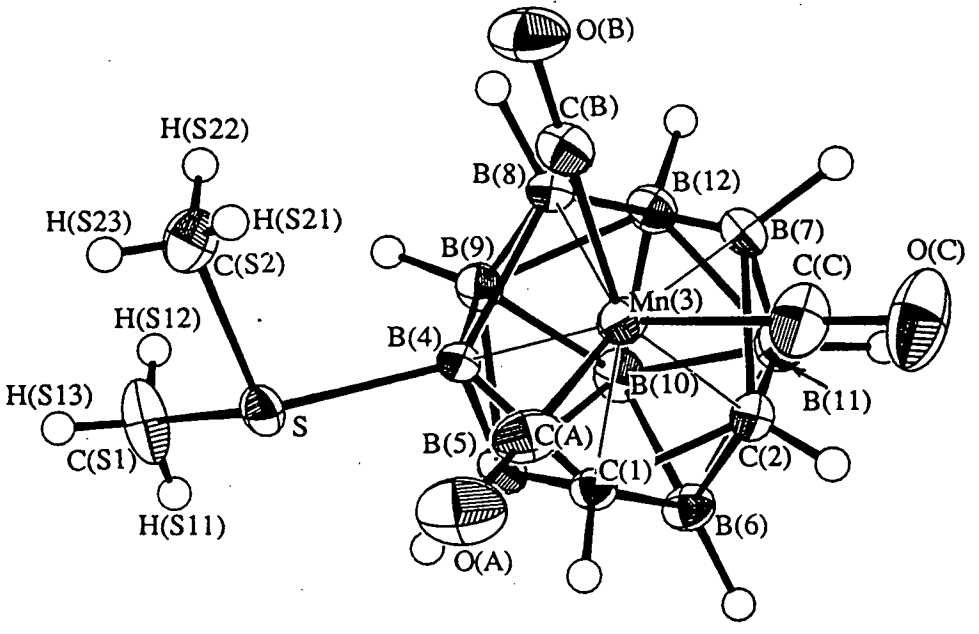

Table 4.1 Fractional Co-ordinates of Atoms in $[3,3,3\text{-}(CO)_3\text{-}4\text{-}SMe_2\text{-}3,1,2\text{-}MnC_2B_9H_{10}]$, $(carb')Mn(CO)_3$, **(6)**

	x	y	z
Mn(3)	0.20127(4)	0.12906(4)	0.84748(2)
S	0.27009(8)	-0.15568(5)	0.69886(4)
C(S1)	0.3293(5)	-0.1956(3)	0.57909(22)
C(S2)	0.0007(4)	-0.2671(3)	0.66932(23)
C(A)	0.2500(3)	-0.0289(3)	0.91973(16)
O(A)	0.2784(3)	-0.13069(24)	0.96441(15)
C(B)	-0.0661(3)	0.02095(25)	0.82698(16)
O(B)	-0.23858(25)	-0.04681(22)	0.81349(15)
C(C)	0.1913(4)	0.2326(3)	0.96380(19)
O(C)	0.1872(4)	0.3028(3)	1.03566(16)
C(1)	0.4903(3)	0.19644(22)	0.80137(14)
C(2)	0.4436(3)	0.35289(23)	0.83112(15)
B(4)	0.2977(3)	0.06749(23)	0.71054(15)
B(5)	0.5274(3)	0.1932(3)	0.67885(17)
B(6)	0.6241(3)	0.3783(3)	0.75971(18)
B(7)	0.2121(4)	0.3461(3)	0.76563(18)
B(8)	0.1112(3)	0.1590(3)	0.68204(17)
B(9)	0.2898(4)	0.17587(25)	0.60114(16)
B(10)	0.4916(4)	0.3695(3)	0.63164(18)
B(11)	0.4442(4)	0.4734(3)	0.73338(19)
B(12)	0.2381(4)	0.3504(3)	0.63586(18)
H(1)	0.574(4)	0.167(3)	0.8461(21)
H(2)	0.503(4)	0.409(3)	0.8949(21)
H(5)	0.624(4)	0.136(3)	0.6614(20)
H(6)	0.777(5)	0.443(4)	0.7976(25)
H(7)	0.134(5)	0.416(4)	0.7933(24)
H(8)	-0.044(4)	0.091(3)	0.6406(20)
H(9)	0.247(4)	0.115(3)	0.5245(22)
H(10)	0.564(4)	0.431(3)	0.5834(21)
H(11)	0.498(5)	0.605(4)	0.7492(24)
H(12)	0.159(5)	0.413(4)	0.5842(23)
H(S11)	0.454(7)	-0.143(5)	0.586(3)
H(S12)	0.263(5)	-0.166(4)	0.531(3)
H(S13)	0.296(5)	-0.299(4)	0.5706(23)
H(S21)	-0.047(5)	-0.268(4)	0.721(3)
H(S22)	-0.064(5)	-0.232(4)	0.617(3)
H(S23)	-0.013(5)	-0.357(4)	0.656(3)

Table 4.2 Interatomic Distances (Å) in [3,3,3-$(CO)_3$-4-SMe_2-3,1,2-$MnC_2B_9H_{10}$], (carb')$Mn(CO)_3$, **(6)**

Mn(3)	- C(A)	1.8059(23)	C(2)	- H(2)	0.92(3)
Mn(3)	- C(B)	1.7802(22)	B(4)	- B(5)	1.771(3)
Mn(3)	- C(C)	1.808(3)	B(4)	- B(8)	1.782(3)
Mn(3)	- C(1)	2.1686(20)	B(4)	- B(9)	1.768(3)
Mn(3)	- C(2)	2.1688(21)	B(5)	- B(6)	1.766(3)
Mn(3)	- B(4)	2.1988(21)	B(5)	- B(9)	1.772(3)
Mn(3)	- B(7)	2.2080(25)	B(5)	-B(10)	1.770(3)
Mn(3)	- B(8)	2.2298(23)	B(5)	- H(5)	1.05(3)
S	-C(S1)	1.792(3)	B(6)	-B(10)	1.775(4)
S	-C(S2)	1.792(3)	B(6)	-B(11)	1.761(4)
S	- B(4)	1.8995(22)	B(6)	- H(6)	1.06(3)
C(S1)	-H(S11)	0.83(5)	B(7)	- B(8)	1.797(3)
C(S1)	-H(S12)	0.82(4)	B(7)	-B(11)	1.791(4)
C(S1)	-H(S13)	0.85(3)	B(7)	-B(12)	1.780(4)
C(S2)	-H(S21)	0.83(4)	B(7)	- H(7)	1.07(3)
C(S2)	-H(S22)	0.88(3)	B(8)	- B(9)	1.805(3)
C(S2)	-H(S23)	0.77(4)	B(8)	-B(12)	1.797(3)
C(A)	- O(A)	1.144(3)	B(8)	- H(8)	1.09(3)
C(B)	- O(B)	1.146(3)	B(9)	-B(10)	1.777(3)
C(C)	- O(C)	1.139(4)	B(9)	-B(12)	1.772(3)
C(1)	- C(2)	1.585(3)	B(9)	- H(9)	1.08(3)
C(1)	- B(4)	1.687(3)	B(10)	-B(11)	1.771(4)
C(1)	- B(5)	1.711(3)	B(10)	-B(12)	1.783(4)
C(1)	- B(6)	1.719(3)	B(10)	-H(10)	0.97(3)
C(1)	- H(1)	0.88(3)	B(11)	-B(12)	1.764(4)
C(2)	- B(6)	1.713(3)	B(11)	-H(11)	1.08(3)
C(2)	- B(7)	1.704(3)	B(12)	-H(12)	1.09(3)
C(2)	-B(11)	1.702(3)			

Table 4.3 Selected Interbond Angles (°) in $[3,3,3\text{-}(CO)_3\text{-}4\text{-}SMe_2\text{-}3,1,2\text{-}MnC_2B_9H_{10}]$, (carb')$Mn(CO)_3$, **(6)**

C(A) -Mn(3) - C(B)	90.93(10)	C(1) - B(6) - B(5)	58.77(13)
C(A) -Mn(3) - C(C)	89.92(11)	C(2) - B(6) -B(11)	58.65(13)
C(B) -Mn(3) - C(C)	88.88(11)	B(5) - B(6) -B(10)	59.99(14)
C(1) -Mn(3) - C(2)	42.88(7)	B(10) - B(6) -B(11)	60.12(14)
C(1) -Mn(3) - B(4)	45.43(7)	Mn(3) - B(7) - C(2)	65.87(11)
C(2) -Mn(3) - B(7)	45.82(8)	Mn(3) - B(7) - B(8)	66.76(11)
B(4) -Mn(3) - B(8)	47.44(8)	C(2) - B(7) -B(11)	58.20(13)
B(7) -Mn(3) - B(8)	47.76(9)	B(8) - B(7) -B(12)	60.30(13)
C(S1) - S -C(S2)	99.98(14)	B(11) - B(7) -B(12)	59.18(14)
C(S1) - S - B(4)	107.00(12)	Mn(3) - B(8) - B(4)	65.37(10)
C(S2) - S - B(4)	104.60(11)	Mn(3) - B(8) - B(7)	65.49(11)
Mn(3) - C(A) - O(A)	178.93(22)	B(4) - B(8) - B(9)	59.05(12)
Mn(3) - C(B) - O(B)	179.13(21)	B(7) - B(8) -B(12)	59.40(13)
Mn(3) - C(C) - O(C)	177.67(24)	B(9) - B(8) -B(12)	58.95(13)
Mn(3) - C(1) - C(2)	68.57(10)	B(4) - B(9) - B(5)	60.02(13)
Mn(3) - C(1) - B(4)	68.23(10)	B(4) - B(9) - B(8)	59.82(12)
C(2) - C(1) - B(6)	62.30(13)	B(5) - B(9) -B(10)	59.84(13)
B(4) - C(1) - B(5)	62.81(13)	B(8) - B(9) -B(12)	60.30(13)
B(5) - C(1) - B(6)	61.97(13)	B(10)- B(9) -B(12)	60.33(14)
Mn(3) - C(2) - C(1)	68.55(10)	B(5) -B(10) - B(6)	59.74(13)
Mn(3) - C(2) - B(7)	68.30(11)	B(5) -B(10) - B(9)	59.95(13)
C(1) - C(2) - B(6)	62.69(13)	B(6) -B(10) -B(11)	59.54(14)
B(6) - C(2) -B(11)	62.07(14)	B(7) -B(10) -B(12)	60.10(14)
B(7) - C(2) -B(11)	63.46(14)	B(9) -B(10) -B(12)	59.70(14)
Mn(3) - B(4) - C(1)	66.33(10)	B(11)-B(10) -B(12)	59.49(14)
Mn(3) - B(4) - B(8)	67.19(10)	C(2) -B(11) - B(6)	59.28(13)
C(1) - B(4) - B(5)	59.25(12)	C(2) -B(11) - B(7)	58.34(13)
B(5) - B(4) - B(9)	60.12(13)	B(6) -B(11) -B(10)	60.35(14)
B(8) - B(4) - B(9)	61.13(13)	B(10)-B(11) -B(12)	60.59(14)
C(1) - B(5) - B(4)	57.93(12)	B(7) -B(12) - B(8)	60.29(13)
C(1) - B(5) - B(6)	59.26(13)	B(7) -B(12) -B(11)	60.72(14)
B(4) - B(5) - B(9)	59.86(13)	B(8) -B(12) - B(9)	60.76(13)
B(6) - B(5) -B(10)	60.27(14)	B(9) -B(12) -B(10)	59.97(14)
B(9) - B(5) -B(10)	60.21(13)	B(10) -B(12) -B(11)	59.91(14)
C(1) - B(6) - C(2)	55.01(12)		

Table 4.4 Isotropic and Anisotropic Thermal Parameters ($Å^2$) in $[3,3,3\text{-}(CO)_3\text{-}4\text{-}SMe_2\text{-}3,1,2\text{-}MnC_2B_9H_{10}]$, (carb')$Mn(CO)_3$, **(6)**

	U11	U22	U33	U23	U13	U12
Mn(3)	0.0181(1)	0.0230(1)	0.0185(1)	0.0006(1)	0.0037(1)	0.0065(1)
S	0.0255(2)	0.0155(2)	0.0220(2)	0.0042(2)	0.0054(2)	0.0102(2)
C(S1)	0.0634(18)	0.0221(10)	0.0384(13)	0.0043(9)	0.0275(13)	0.0189(11)
C(S2)	0.0289(11)	0.0199(9)	0.0449(14)	0.0001(9)	0.0059(10)	0.0025(8)
C(A)	0.0227(9)	0.0358(11)	0.0203(9)	0.0067(8)	0.0038(7)	0.0084(8)
O(A)	0.0397(10)	0.0463(10)	0.0382(9)	0.0216(8)	0.0068(8)	0.0162(8)
C(B)	0.0240(9)	0.0246(9)	0.0274(9)	0.0055(7)	0.0070(7)	0.0109(8)
O(B)	0.0195(7)	0.0398(9)	0.0485(10)	0.0116(8)	0.0078(7)	0.0074(7)
C(C)	0.0342(12)	0.0310(11)	0.0330(11)	-0.0022(9)	0.0144(10)	0.0032(9)
O(C)	0.0627(14)	0.0459(11)	0.0384(10)	-0.0138(8)	0.0243(10)	0.0030(10)
C(1)	0.0174(8)	0.0182(7)	0.0180(8)	0.0036(6)	0.0022(6)	0.0073(6)
C(2)	0.0210(8)	0.0180(8)	0.0229(8)	-0.0008(6)	0.0028(7)	0.0061(7)
B(4)	0.0161(8)	0.0162(8)	0.0173(8)	0.0018(6)	0.0016(7)	0.0074(7)
B(5)	0.0219(10)	0.0204(9)	0.0226(9)	0.0066(7)	0.0072(8)	0.0109(8)
B(6)	0.0181(9)	0.0204(9)	0.0259(10)	0.0043(7)	0.0042(8)	0.0034(8)
B(7)	0.0238(10)	0.0225(9)	0.0273(10)	0.0001(8)	0.0048(8)	0.0132(8)
B(8)	0.0171(9)	0.0209(9)	0.0218(9)	0.0004(7)	0.0002(7)	0.0093(7)
B(9)	0.0254(10)	0.0198(9)	0.0176(8)	0.0047(7)	0.0029(7)	0.0104(8)
B(10)	0.0293(11)	0.0195(9)	0.0248(10)	0.0081(8)	0.0073(9)	0.0084(8)
B(11)	0.0285(11)	0.0189(9)	0.0293(11)	0.0043(8)	0.0039(9)	0.0098(8)
B(12)	0.0279(11)	0.0221(9)	0.0260(10)	0.0040(8)	0.0011(8)	0.0139(8)
H(1)	0.024 (6)					
H(2)	0.028 (7)					
H(5)	0.025 (6)					
H(6)	0.044 (9)					
H(7)	0.039 (8)					
H(8)	0.026 (6)					
H(9)	0.032 (7)					
H(10)	0.027 (7)					
H(11)	0.044 (9)					
H(12)	0.036 (8)					
H(S11)	0.076 (14)					
H(S12)	0.040 (9)					
H(S13)	0.037 (8)					
H(S21)	0.049 (10)					
H(S22)	0.039 (8)					
H(S23)	0.047 (9)					

In both figures, non-hydrogen atoms are represented by thermal ellipsoids at the 50% probability level, while H atoms have been given an artificial radius of 0.1Å for clarity.

Fractional coordinates of atoms in (carb')$Mn(CO)_3$ are presented in **Table 4.1**, while **Table 4.2** gives interatomic distances and **Table 4.3** comprises selected interbond angles in the molecule. **Table 4.4** gives anisotropic thermal parameters for non-H atoms and individual isotropic thermal parameters for hydrogen atoms. The metal atom in compound **(6)** is 1.643Å from the best (least-squares) plane through the ligated atoms [C(1), C(2), B(4), B(7), B(8)]. This ligated 5-atom face is (albeit slightly) folded into an envelope conformation (unusually for *closo* 12-vertex 1,2-dicarba-3-metallaboranes) along the C(2)...B(8) vector, giving 3-atom and 4-atom portions, defined by C(2), B(7), B(8) and C(2), C(1), B(4), B(8) respectively. These portions give fold parameters [54] $\phi = -2.40^{o}$ and $\theta = -1.52^{o}$. The negative signs of these parameters denotes unusual folding of the 3- and 4-atom portions *towards* the Mn atom. Distances from the manganese atom to the ligated boron atoms, B(4), B(7) and B(8), average 2.212Å, whereas the average distance to the cage carbon atoms, C(1) and C(2), is less, at 2.169Å. In order to confirm that this is simply an effect of the smaller radius of carbon *versus* boron, and not a slippage of the Mn atom with respect to the facial atoms, a geometrical calculation was carried out, which shows no evidence of slip of the manganese atom relative to the lower pentagonal 5-boron plane [B(5), B(6), B(11), B(12), B(9)]. The tricarbonylmanganese fragment adopts an orientation which places one carbonyl group [C(B)O(B)] almost exactly *trans* to the mid-point of the C(1)-C(2) connectivity. The Mn(3)-C(B) bond (1.7802(22)Å) is significantly shorter than the Mn(3)-C(A) (1.8059(23)Å) and Mn(3)-C(C) (1.808(3)Å) bonds.

This phenomenon may be readily understood by consideration of the fact that the frontier molecular orbitals of [*nido*-C_2B_9] ligands are localised chiefly on the facial boron atoms (see discussions in earlier chapters), thus the carbon atoms in the open face exert the observed *trans* influence. It is a point of some interest (and surprise) that no such influence is observed [39] in the closely related anionic carbarhenaborane $[(C_2B_9H_{11})Re(CO)_3]^-$.

Bond lengths from Mn(3) to C(A) and C(C) are, within experimental error, equal, thus suggesting the *trans* influence of the {B(7)H(7)} and {B(4)SMe_2} functions are essentially the same. Although the data for the structure were collected carefully and at low temperature, and the e.s.d.'s on the derived measurements are consequently small, no statistically significant comment may be made on the relative C-O distances.

Bond angles within the {$Mn(CO)_3$} fragment are broadly as expected, with CO-Mn-CO angles averaging 89.91° and the average Mn-C-O angle being 178.58°.

Another feature of interest in the complex is the orientation of the SMe_2 function with respect to the carbametallaborane framework. As discussed in some detail in Chapter 3, there appears to be a preferred conformation for the dimethylsulphide unit in carb'H and the other complexes so far characterised, and the possible origin of this preference has been traced *via* the results of molecular orbital calculations (see Chapter 3).

In complex **(6)**, this preferred orientation can be clearly seen in **Figures 4.1** and **4.2**, with the sulphur lone pair almost exactly eclipsing the B(4)-C(1) connectivity. The lone pair-S-B(4)-C(1) torsion angle is calculated to be 4.1°.

Another structural similarity between (carb')$Mn(CO)_3$ and the other fully characterised [carb'] species is the narrowing of the S-B(4)-C(1) angle (117.82° in **(6)**), compared to the S-B(4)-B(8) angle (130.47° in **(6)**). This can be regarded as further evidence for an electrostatic interaction of the type lone pair..$H(1)^{\delta+}$, discussed previously.

$(\eta\text{-}C_5H_5)Mn(CO)_3$, $CpMn(CO)_3$, (7)

Synthesis

The previously known species $CpMn(CO)_3$ was synthesised following a modified version of a published method for the preparation of fluorenyl- and indenyl-manganesetricarbonyl [81], using the thallium (I) salt of Cp^- and manganese pentacarbonylbromide. Experimental details are to be found in Chapter 6, section 1.

Characterisation of (7)

The complex was characterised by elemental microanalysis, ^1H and ^{13}C n.m.r. spectroscopy and infra-red spectroscopy, each fully consistent with the proposed species.

Structural Study of (7)

Introduction

The structure of **(7)** has been determined previously [78], although this work was carried out in the early 1960's, and hence the precision of the measurements was relatively low, given the great advances in crystallography in recent years.

The structure of $CpMn(CO)_3$ was redetermined accurately (at low temperature) in order to obtain parameters of sufficient precision to allow meaningful comparison with those of (carb')$Mn(CO)_3$, **(6)**. The estimated standard deviations on molecular parameters from our redetermination are an order of magnitude smaller than those previously reported.

Crystals of sufficient habit for *X*-ray study were grown by slow diffusion of n-hexane into a CH_2Cl_2 solution of the compound. Crystal data, details of data collection and processing, and details of refinement procedures may be found in Chapter 6, section 2.

Discussion

A perspective view of the molecule is presented in **Figure 4.3**, with a second view from above the $\{Mn(CO)_3\}$ unit in **Figure 4.4**, clearly showing the orientation of the tricarbonylmanganese group with respect to the pentagonal ligand. Both figures show the appropriate molecular numbering scheme. Mn, C and O atoms are represented by thermal ellipsoids at the 50% probability level and hydrogen atoms have been given an artificial radius of 0.1Å for clarity. Hydrogen atoms carry the same number as the carbons to which they are attached.

Fractional coordinates of atoms are given in **Table 4.5**, and **Table 4.6** shows interatomic distances and interbond angles within the molecule. **Table 4.7** is comprised of anisotropic thermal parameters for non-hydrogen atoms.

The manganese atom sits symmetrically above the plane of the C_5 ligand (for the best plane through the 5 atoms, no atom deviates by more than 0.0008Å, denoting an extremely high degree of planarity).

Figure 4.3 Perspective View of $[(\eta\text{-}C_5H_5)Mn(CO)_3]$, $CpMn(CO)_3$, **(7)**

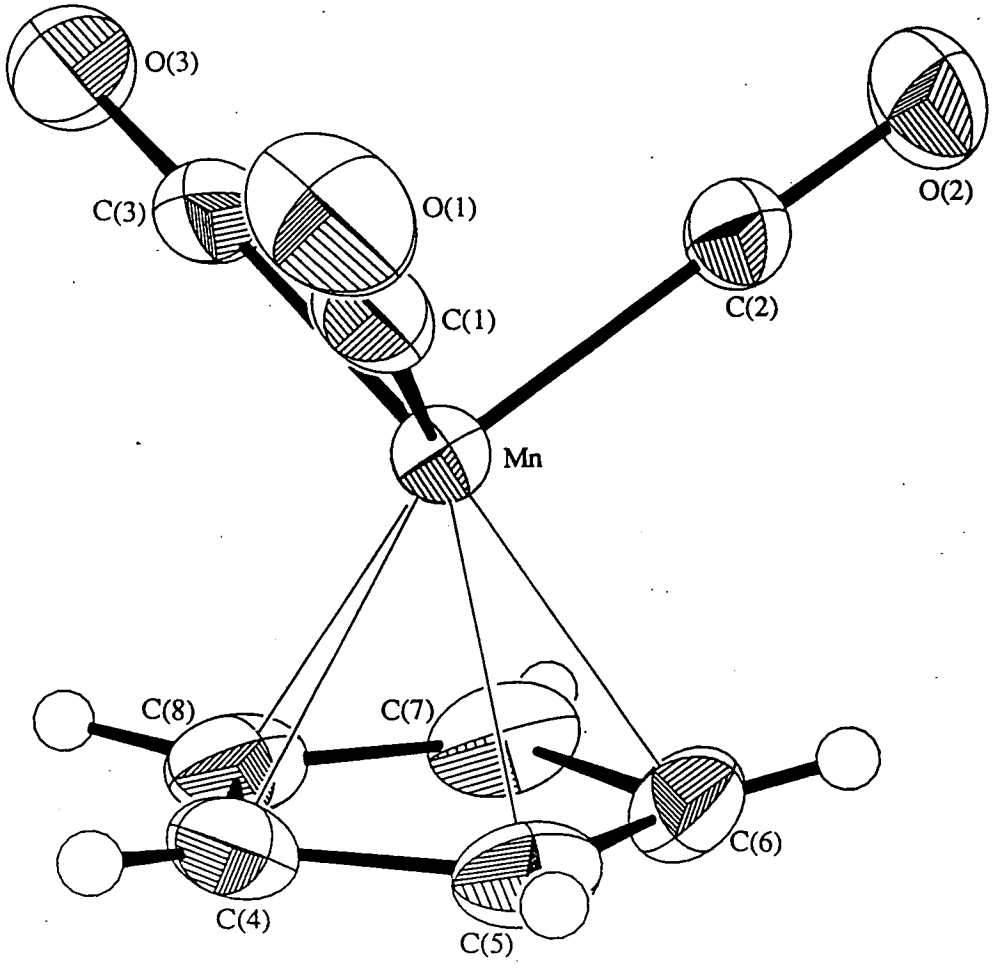

Figure 4.4 View of $[(\eta\text{-}C_5H_5)Mn(CO)_3]$, $CpMn(CO)_3$, **(7)**, from Above the Mn Position

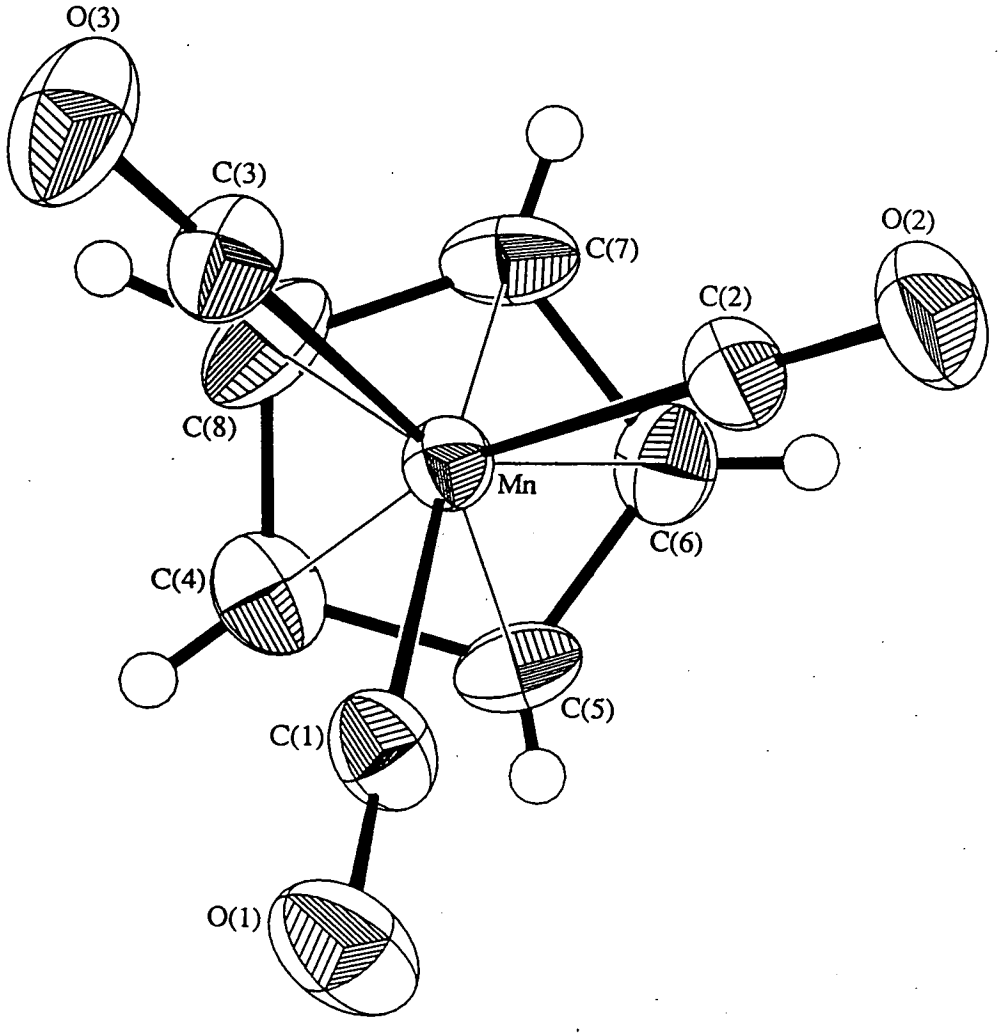

Table 4.5 Atomic Co-ordinates in $[(\eta\text{-}C_5H_5)Mn(CO)_3]$, $CpMn(CO)_3$, **(7)**

	x	y	z
Mn	0.28993(3)	0.00486(4)	0.26318(3)
O(1)	0.48324(18)	0.3074(3)	0.38259(24)
O(2)	0.08500(18)	0.2888(3)	0.14544(21)
O(3)	0.2672(3)	-0.0365(4)	0.52081(23)
C(1)	0.40814(21)	0.1887(3)	0.33768(25)
C(2)	0.16497(21)	0.1777(3)	0.19287(23)
C(3)	0.2757(3)	-0.0190(3)	0.4209(3)
C(4)	0.41172(25)	-0.2086(4)	0.2493(3)
C(5)	0.35952(25)	-0.0963(4)	0.1257(3)
C(6)	0.2281(3)	-0.1174(4)	0.05959(24)
C(7)	0.1977(3)	-0.2445(4)	0.1428(3)
C(8)	0.3114(3)	-0.2988(3)	0.2589(3)
H(4)	0.486(4)	-0.203(7)	0.309(5)
H(5)	0.398(5)	-0.032(6)	0.105(5)
H(6)	0.166(4)	-0.059(7)	-0.007(5)
H(7)	0.123(4)	-0.277(6)	0.129(5)
H(8)	0.333	-0.367	0.345

Table 4.6 Interatomic Distances (Å) and Interbond Angles (°) in $[(\eta\text{-}C_5H_5)Mn(CO)_3]$, $CpMn(CO)_3$, **(7)**

Mn	- C(1)	1.7947(25)	O(3)	- C(3)	1.137(4)
Mn	- C(2)	1.7876(25)	C(4)	- C(5)	1.416(4)
Mn	- C(3)	1.797(3)	C(4)	- C(8)	1.399(4)
Mn	- C(4)	2.136(3)	C(4)	- H(4)	0.81(5)
Mn	- C(5)	2.133(3)	C(5)	- C(6)	1.394(4)
Mn	- C(6)	2.141(3)	C(5)	- H(5)	0.75(6)
Mn	- C(7)	2.142(3)	C(6)	- C(7)	1.426(4)
Mn	- C(8)	2.139(3)	C(6)	- H(6)	0.85(5)
O(1)	- C(1)	1.148(3)	C(7)	- C(8)	1.401(4)
O(2)	- C(2)	1.148(3)	C(7)	- H(7)	0.86(5)

C(1)	- Mn	- C(2)	91.85(11)	Mn	- C(1)	- O(1)	178.58(24)
C(1)	- Mn	- C(3)	92.63(12)	Mn	- C(2)	- O(2)	178.68(23)
C(2)	- Mn	- C(3)	91.94(12)	Mn	- C(3)	- O(3)	179.1(3)
C(4)	- Mn	- C(5)	38.74(11)	C(5)	- C(4)	- C(8)	107.8(3)
C(4)	- Mn	- C(8)	38.21(11)	C(4)	- C(5)	- C(6)	108.46(25)
C(5)	- Mn	- C(6)	38.07(11)	C(5)	- C(6)	- C(7)	107.5(3)
C(6)	- Mn	- C(7)	38.89(11)	C(6)	- C(7)	- C(8)	107.8(3)
C(7)	- Mn	- C(8)	38.20(12)	C(4)	- C(8)	- C(7)	108.5(3)
C(5)	- C(4)	- H(4)	124.0(36)	C(5)	- C(6)	- H(6)	134.5(36)
C(8)	- C(4)	- H(4)	127.3(36)	C(7)	- C(6)	- H(6)	116.8(35)
C(4)	- C(5)	- H(5)	123.9(43)	C(6)	- C(7)	- H(7)	127.1(33)
C(6)	- C(5)	- H(5)	127.5(43)	C(8)	- C(7)	- H(7)	125.0(33)

Table 4.7 Anisotropic Thermal Parameters ($Å^2$) in $[(\eta\text{-}C_5H_5)Mn(CO)_3]$, $CpMn(CO)_3$, **(7)**

	U11	U22	U33	U23	U13	U12
Mn	0.0241(2)	0.0254(2)	0.0237(2)	0.0004(1)	0.0109(1)	0.0018(1)
O(1)	0.0350(9)	0.0371(9)	0.0621(12)	-0.0093(9)	0.0112(9)	-0.0052(8)
O(2)	0.0350(9)	0.0589(12)	0.0457(10)	0.0092(9)	0.0149(8)	0.0184(9)
O(3)	0.0762(16)	0.0648(12)	0.0418(11)	0.0152(9)	0.0398(12)	0.0270(11)
C(1)	0.0295(10)	0.0287(10)	0.0352(10)	-0.0015(8)	0.0105(9)	0.0060(8)
C(2)	0.0273(10)	0.0367(11)	0.0276(9)	0.0012(8)	0.0111(8)	0.0044(8)
C(3)	0.0446(14)	0.0353(12)	0.0333(11)	0.0042(8)	0.0225(11)	0.0098(9)
C(4)	0.0363(11)	0.0388(12)	0.0410(12)	-0.0060(10)	0.0180(10)	0.0096(10)
C(5)	0.0444(13)	0.0344(11)	0.0411(11)	-0.0058(9)	0.0311(11)	-0.0072(10)
C(6)	0.0439(13)	0.0408(12)	0.0252(9)	-0.0044(9)	0.0134(9)	-0.0014(10)
C(7)	0.0441(13)	0.0388(12)	0.0465(13)	-0.0136(10)	0.0276(11)	-0.0179(10)
C(8)	0.0731(17)	0.0233(10)	0.0434(13)	0.0023(9)	0.0379(13)	0.0046(11)

Mn-C distances lie between 2.133(3) and 2.142(3)Å. This gives a perpendicular distance from the 5-carbon plane to the metal atom of 1.772Å, greater than the Mn-ligand face distance in **(6)**, because of the relative sizes of the ligated faces in the Cp and carbaborane ligands [82].

The orientation of the $\{Mn(CO)_3\}$ over the Cp ligand is such that one of the carbonyl groups [C(2)O(2)] is essentially *trans* to a C-C edge of the cyclopentadienyl ligand.

It is of note that C(2) is significantly closer to the Mn centre (Mn-C(2) = 1.7876(25)Å) than are the other two carbonyl carbons [Mn-C(1) = 1.7947(25)Å and Mn-C(3) = 1.797(3)Å].(The complementary trend which might be expected in C-O distances is, however, not observed in this case).

The average OC-Mn-CO angle is 92.14^0, in accord with the prediction of an obtuse angle from the relative magnitudes of integrated absorption coefficients of the carbonyl stretching vibrations in the infra-red spectrum [83]. The average Mn-C-O angle is almost exactly linear, as expected, at 178.79^0.

As a result of the redetermination of the $CpMn(CO)_3$ structure, it is now also possible to report details of the H atom positions on the $(C_5H_5)^-$ ligand, which were not found by the earlier experiment. A common feature of the positions of these hydrogen atoms is that each is slightly bent out of the C_5 plane of the ligand, towards the metal atom, by the order of $3\text{-}9^0$. Calculations have been performed at the extended Hückel level on a range of metal-coordinated cyclic polyenes [82], and suggest the preferred angle of inclination of the H atoms in the C_5 case should be 0^0.

Structural and Spectral Comparison Between (6) and (7)

In terms of structural parameters derived from accurate, low-temperature crystallographic studies, and spectral characteristics, the carb' and cyclopentadienyl ligands in compounds **(6)** and **(7)** appear to behave in an electronically very similar manner, as manifested in the following parameters:

(i) C-O bond distances. The average C-O distances in compounds **(6)** and **(7)** are identical within the limits of the *X*-ray structural analysis.

(ii) $Mn\text{-}C_{(carbonyl)}$ distances. Again, the two average distances from each of the structures are extremely close, (1.798Å in **(6)** and 1.793Å in **(7)**), and taking into account the errors on the parameters (even from the accurate experiment performed) no statistically significant comment may be made on this very small difference.

(iii) C-O stretching frequencies. Although the difference in average ν_{CO} for compounds **(6)** and **(7)** is very small (*ca.* $7cm^{-1}$) there is, nonetheless, a measurable difference, although obviously there are no e.s.d.'s, as such, on this type of measurement. The carbonyl infra-red stretches for the Cp complex **(7)** occur at 2025 and $1945cm^{-1}$. The corresponding measurements for the carbamanganaborane species **(6)** are 2020, 1950 and $1925cm^{-1}$. (Note that the *e* vibration in the essentially C_{3v} $\{Mn(CO)_3\}$ fragment retains its degeneracy in the Cp complex, but that this degeneracy is lifted in the lower-symmetry carb' species, giving rise to three carbonyl absorptions, instead of two). In simplistic terms, this very small difference suggests slightly greater electron donation to the manganese atom by carb' than by Cp, resulting in a more electron-rich metal centre. This

leads to greater π back-donation into the carbonyl ligands, giving very slight weakening of the C-O bonds, and hence the lower average ν_{CO} observed.

(iv) ^{13}C n.m.r. shifts.There is a difference of only 3 p.p.m. between the shifts of the carbonyl carbon nuclei in the two complexes (δ 221.9 p.p.m. in **(6)** and 225.0 p.p.m. in **(7)**). This is not a significant difference and may be regarded as further evidence for similar carbonyl electronic environments in both molecules.

Electronic Structures of (6) and (7)

Introduction

As outlined in Chapter 1, $[carb']^-$ is regarded as a true analogue of the cyclopentadienyl anion in that their frontier orbitals are similar and that unlike $[C_2B_9H_{11}]^{2-}$, the charges on the ligands are the same.

The overall charge on $[carb']^-$ is undoubtedly 1^-, although we may envisage two extreme representations of the charge-partitioning in the ligand.

In the first form, I, we have the charge of 1- resident on the facial atoms of the carbaborane, as shown in **Figure 4.5** (below).

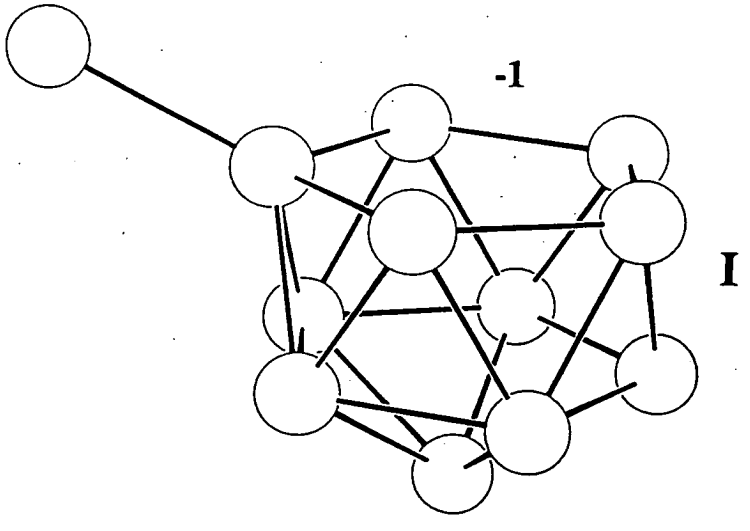

I

The second extreme representation, **II**, which is zwitterionic, may be drawn as in **Figure 4.6** below, where the increased negative charge (2-) on the facial atoms of the ligand is compensated by a positive charge on the pendant sulphur atom:

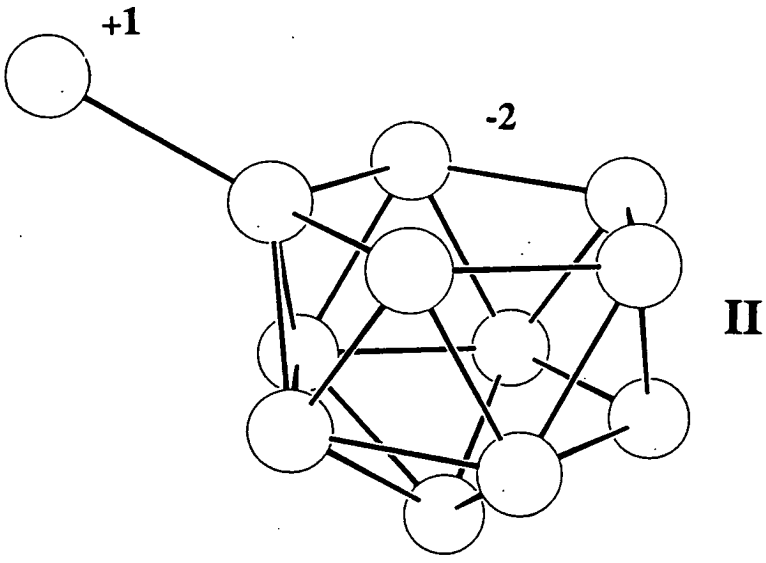

Figure 4.6

The very similar results for compounds **(6)** and **(7)** in terms of carbonyl parameters might lead us to suggest that, in the case of the tricarbonylmanganese complex at least, I is the more dominant of the two extreme forms of $[carb']^-$ in that it more closely approximates to the charge distribution in Cp^-, the metal atom ligating to a 5-atom face bearing a nominal net charge of 1-.

It was felt, however, that a more rigorous examination of the electronic properties of the $[carb']^-$ and Cp^- ligands in **(6)** and **(7)** must be carried out if a distinction between the two extreme representations of the (overall) monoanionic carbaborane ligand were to be made, affording a more accurate representation of the true charge-partitioning in the ligand.

For the abovementioned purpose, EHMO calculations, with full charge iteration on all atoms, were performed on the crystallographically derived models of compounds **(6)** and **(7)**.

Table 4.8 shows the calculated net charges for all atoms in (carb')$Mn(CO)_3$, and **Table 4.9** gives those for $[(\eta\text{-}C_5H_5)Mn(CO)_3]$.

The key results of these calculations may be summarised as follows: for (carb')$Mn(CO)_3$ the sum of the net charges for atoms in the $\{Mn(CO)_3\}$ moiety comes to -0.51. The corresponding summated charge for the cyclopentadienyl analogue is calculated to be only -0.20. This means that the carbaborane ligand in **(6)** transfers $1.51e^-$ to the $\{Mn(CO)_3^+\}$ unit, whereas net transfer from the Cp^- ligand in **(7)**is only $1.20e^-$.

The above results, showing $[carb']^-$ to be a stronger donor to the tricarbonylmanganese cation than the cyclopentadienyl anion by the order of approximately $0.3e^-$, may be readily understood by consideration of the atomic orbitals (AO's) contributing to the frontier orbitals of each of the η-ligands.

As discussed earlier, the frontier orbitals of carbaborane ligands contain greatest contributions from the AO's of the boron atoms (in particular the B 2p orbitals). The H_{ii}'s of these orbitals lie higher (i.e. are less negative) than the corresponding H_{ii}'s of the carbon AO's which constitute the frontier orbitals of the Cp^- ligand, hence the donor orbitals of carbaboranes are higher-lying than those of Cp^-, meaning that the former are "better donors".

Table 4.8 Calculated Net Charges for Atoms in $[3,3,3\text{-}(CO)_3\text{-}4\text{-}SMe_2\text{-}3,1,2\text{-}MnC_2B_9H_{10}]$, (carb')$Mn(CO)_3$, **(6)**

Atom	Net Charge
Mn(3)	0.14167
C(A)	0.05632
O(A)	-0.27504
C(B)	0.05603
O(B)	-0.28408
C(C)	0.06395
O(C)	-0.26753
S	0.26376
C(S1)	0.05450
C(S2)	0.05194
C(1)	0.00638
C(2)	0.00270
B(4)	0.11966
B(5)	0.08010
B(6)	0.10655
B(7)	0.04261
B(8)	0.02107
B(9)	0.03203
B(10)	0.03857
B(11)	0.06845
B(12)	0.02228
H(1)	0.00794
H(2)	0.00212
H(5)	-0.07417
H(6)	-0.06585
H(7)	-0.08732
H(8)	-0.09726
H(9)	-0.09083
H(10)	-0.07827
H(11)	-0.07817
H(12)	-0.09478
H(S11)	0.04246
H(S12)	0.04243
H(S13)	0.04016
H(S21)	0.04366
H(S22)	0.03440
H(S23)	0.05156

Table 4.9 Calculated Net Charges for Atoms in $[(\eta\text{-}C_5H_5)Mn(CO)_3]$, $CpMn(CO)_3$, **(7)**

Atom	Net Charge
Mn	0.20482
C(1)	0.09887
O(1)	-0.23968
C(2)	0.09947
O(2)	-0.24036
C(3)	0.10446
O(3)	-0.23146
C(4)	0.01519
C(5)	0.01789
C(6)	0.02189
C(7)	0.01700
C(8)	0.02544
H(4)	0.02360
H(5)	0.03061
H(6)	0.02206
H(7)	0.01878
H(8)	0.01141

This donor ability might initially appear to run contrary to the notion of boranes and carbaboranes as electron-deficient compounds [84]. One must bear in mind, however, that the electron-deficiency of boron, possessing less valence electrons than valence orbitals, (3 valence e^-'s, 4 valence AO's), has already been completely alleviated by clustering, hence the compounds are electron-precise for the physical and electronic structures they adopt.

It can be seen fom **Table 4.8** that the "extra" $0.3e^-$ which are donated to the metal centre by the carb' ligand are (partially) offset by a calculated charge on the sulphur atom of +0.26. This might suggest that the most accurate representation of the monoanionic carbaborane ligand is (in this case, at least) neither of the two extreme forms **I** or **II** introduced earlier, but in fact a third form, **III**, intermediate between the two, in which the five facial atoms carry a charge of -1.5 and the S atom partially balances the "extra" charge, as shown below in **Figure 4.7**.

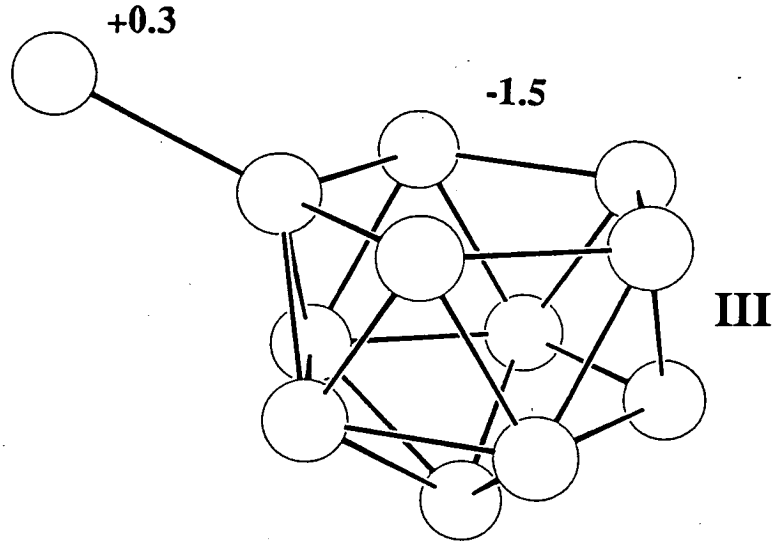

This intermediate form might be regarded as a resonance form of the ligand, of which the two extremes **I** and **II** are canonical forms, as frequently used in discussion of organic systems.

Extended Hückel/Fragment Molecular Orbital Calculations

Introduction

In order to investigate more fully the interaction between the $\{Mn(CO)_3\}$ fragment and the carb' and Cp ligands, a fragment molecular orbital (FMO) calculation was carried out for a model of each of complexes **(6)** and **(7)**.

In the FMO calculation a molecule is (arbitrarily) divided into component fragments and the interactions between the fragment orbitals are studied by the manner in which they combine to form the MO's of the complete molecule.

Of specific interest in this case are the degree of electron transfer between the $[\eta\text{-ligand}]^-$ and $\{Mn(CO)_3^+\}$ fragments upon interaction to form complexes **(6)** and **(7)**, the character of the orbitals which are populated and depopulated by this interaction, and the structural and physicochemical consequences thereof.

Results and Discussion

For ease of interpretation of results and for true comparability between the calculations, the models used were constructed by positioning and orienting an idealised C_{3v} $\{Mn(CO)_3^+\}$ fragment above the experimentally-derived ligand models, as found in the crystallographic studies. These models may be found in Chapter 6, section 3.

The H_{ii}'s used in the EHMO/FMO calculations were the averaged values of those calculated in the previous (charge-iterated) calculations, and are also to be found in Chapter 6, section 3.

The major results of the EHMO/FMO calculations fully support those of the earlier charge-iterated EHMO calculations, indicating that the $[carb']^-$ fragment is a stronger donor to the $\{Mn(CO)_3^+\}$ fragment than is Cp^-.

The carbaborane is calculated to donate $1.28e^-$ to the cationic tricarbonylmanganese fragment, whereas the net transfer between fragments in the $CpMn(CO)_3$ case was calculated to be only $0.62e^-$.

Inspection of the fragment orbitals of $\{Mn(CO)_3^+\}$ in the two calculations reveals that approximately 80% of the "extra" electron donation in the $(carb')Mn(CO)_3$ case over that in the $CpMn(CO)_3$ case goes into the *e* acceptor orbital set (LUMO) and that approximately 20% of the "extra" electrons reside in the acceptor orbital of a_1 symmetry (the 2^{nd} LUMO).

The *e* orbitals of the $\{Mn(CO)_3^+\}$ fragment are of the correct symmetry for σ-interaction with the highest occupied MO's of the carbonyl ligands. Thus build-up of electron density in the *e* orbitals (LUMO's) disfavours σ-donation from the carbonyl HOMO's to the manganese centre. These HOMO's are σ-antibonding between C and O, thus population of the $\{Mn(CO)_3^+\}$ LUMO prevents strengthening of the C-O bonds, giving weaker C-O interactions in $(carb')Mn(CO)_3$, **(6)**, *versus* $CpMn(CO)_3$, **(7)**.

The a_1 orbital (2^{nd} LUMO) of the cationic tricarbonylmanganese fragment, which is populated by $0.12e^-$ more in the carbaborane complex than in the cyclopentadienyl complex, is of appropriate symmetry for interaction with the π^* system of the carbonyl ligands. Population of the a_1 orbital then leads to back-donation into the C-O π^* orbitals, again contributing to weakening of the C-O bonds in the carb' complex *versus* those in the Cp species.

Figure 4.8 Acceptor Orbitals of $\{Mn(CO)_3^+\}$

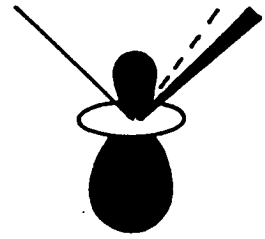

a_1

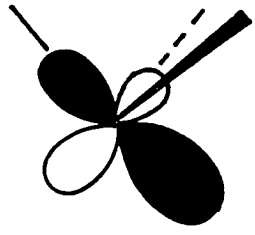

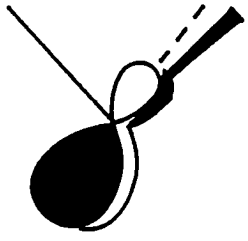

e

Symmetry-Allowed Overlap of e Orbitals with CO HOMO and a_1 Orbital with CO π^* Orbital

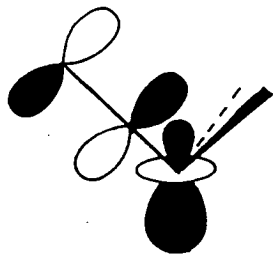

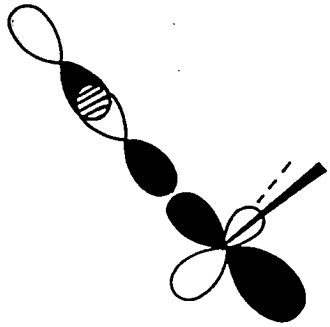

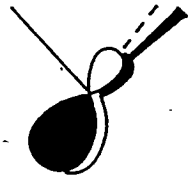

This orbital analysis suggests that the C-O bonds in complex **(6)** ought to be slightly weaker than those in **(7)**.

Of further relevance in the EHMO/FMO calculations are the C-O reduced overlap population elements, which are a measure of bond strength (and should also therefore be related to bond lengths and infra-red stretching frequencies). The overlap populations for C-O in (carb')$Mn(CO)_3$ are between 1.278 and 1.292, slightly lower than those for the $CpMn(CO)_3$ species, which are in the range 1.295-1.296.

Although the bonding within the $\{Mn(CO)_3^+\}$ moiety is shown by the crystallographic work to be indistinguishable, within the limits of the experiments, in the carbaborane and cyclopentadienyl cases, the previous discussion on infra-red carbonyl stretching frequencies detailed a slight, but measurable difference in average $\nu_{C\text{-}O}$'s for the two species. This difference is indeed very small (*ca.* $7cm^{-1}$), but is, however, in complete agreement with the theoretical results, being indicative of a slightly weaker C-O bond in the carbamanganaborane complex than in its Cp analogue.

Conclusions

The comparative study of analogous complexes **(6)** and **(7)** reveals that the net electronic properties of the cyclopentadienyl and monoanionic carbaborane ligands are highly similar.

This conclusion is reached as a result of the extreme similarity in infra-red carbonyl stretching frequencies and C-O bond distances observed for the complexes. Extended Hückel and extended Hückel/fragment MO calculations do

suggest, however, that the very slightly lower average ν_{CO} observed for the carbametallaborane species is a result of a slightly greater degree of e^--donation by [carb'] into (primarily) the *e* orbitals of the manganese tricarbonyl fragment. This leads to limitation of σ-donation by the carbonyls to the manganese atom and hence lower C-O stretching frequencies.

Chapter 5

The Bis(cage) Iron System

Introduction

The work in this chapter may be regarded essentially as an extension of that in Chapter 4, where [carb']$^-$ was bonded in an η^5 mode to a d^6 transition metal centre in an entirely analogous fashion to the cyclopentadienyl ligand. These results have shown the analogy between Cp^- and [carb']$^-$ to be a valid one, with highly similar structural and spectral parameters being determined for analogous complexes of the two ligands.

This knowledge prompted the investigation of the [carb']$^-$ analogue of another extremely well-known Cp^- complex, ferrocene, which created a great deal of interest when first described in the early 50's [8,9], and led to the development of modern organometallic chemistry.

[*commo*-3,3'-Fe-4,4'-$(SMe_2)_2$-1,1',2,2',-$(C_2B_9H_{10})_2$], Fe(carb')$_2$, (8)

Synthesis and Characterisation

Two separate methods of preparation were devised for **(8)**, each of which is fully described in Chapter 6, section 1.

The first of these (Method 1), is a modification of the procedure used to prepare ferrocene [85], involving *in situ* deprotonation of the ligand precursor and

dropwise addition of a solution of $FeCl_2.4H_2O$ to the mixture.

Subsequent chromatographic work-up of the pink/purple product reveals the presence of two identically coloured compounds, formed in unequal quantities. These two complexes are thought to be isomeric, the possible nature of this isomerism forming part of the discussion of the structure of **(8)** (and also of that of **(9)**, see later).

The major compound, of higher R_f value, accounts for approximately 90% of the total product formed and so was collected, while the minor compound was not present in sufficient amount to be of use in further study.

A second synthetic route (Method 2) was later devised, involving Tl[carb'] and $FeCl_2.4H_2O$. Again a pink/purple product was obtained, but in this case chromatographic purification yielded only a single band. This was removed from the silica and crystallisation effected by slow diffusion of n-hexane into a dichloromethane solution at -30°C. The crystals obtained, although small, were of sufficient habit for use in *X*-ray structural analysis. Later evidence suggests that this corresponds to the minor (uncollected) product from Method 1.

Chemical characterisation will be described for the (major) product obtained by the first synthetic route.

The complex was identified by elemental (C,H) microanalysis and ^1H, ^{11}B, $^{11}B\text{-}\{^1H\}$ and $^1H\text{-}\{^{11}B$ selective$\}$ n.m.r. studies.

Microanalytical results were in full accord with the proposed $C_8H_{32}B_{18}S_2Fe$ formulation for the ferrocene analogue **(8)**.

The major features of the ^{1}H spectrum are the two singlets at δ 2.82 and 2.86 p.p.m., assigned to the protons of each of the inequivalent methyl groups in the molecule. It must be noted that whatever the stereochemistry at iron, these methyl groups will give (excepting accidental coincidences) two signals, each signal comprising contributions from one of the CH_3 groups on each ligand, and that as observed for previously-discussed $[carb']^-$ complexes, the two methyl groups associated with each cage remain magnetically inequivalent whatever the torsion about the B-S bond.

The $^{11}B-\{^{1}H\}$ spectrum of $Fe(carb')_2$ displays 8 resonances of relative intensity 1:1:2:1:1:1:1:1. On retention of proton coupling in the ^{11}B spectrum, the highest frequency resonance (δ -2.56 p.p.m.) is the only one which does not show doublet coupling, being thus assignable to the sulphur-bonded boron nuclei [B(4), B(4')].

$^{1}H-\{^{11}B$ selective$\}$ n.m.r. experiments reveal the presence of 8 independent boron-bonded H atoms, consistent with the proposed structure.

Structural Study on (8)

Introduction

Diffraction-quality crystals of the *E* isomer (see later for definition) of **(8)** were grown by a CH_2Cl_2/n-hexane solvent diffusion experiment at -30°C. Crystal data, details of data collection and processing, and techniques employed in structure solution and refinement are to be found in Chapter 6, section 2.

Figure 5.1 shows a perspective view of the molecule, giving the appropriate molecular numbering scheme. Cage H atoms carry the same number as the B or C atom to which they are bonded. **Figure 5.2** is a plan view of both carbaborane [C_2B_3] faces, along with the Fe, S and methyl C atoms, which more clearly illustrates the *cisoid* conformation of the ligands.

Table 5.1 gives final coordinates of refined atoms and equivalent isotropic thermal parameters for non-H atoms. Interatomic distances and selected interbond angles are given in **Tables 5.2** and **5.3** respectively. Anisotropic thermal parameters may be found in **Table 5.4**. Hydrogen atom coordinates are presented in **Table 5.5**.

Figure 5.1 shows the *commo*-3,3'-Fe-$(C_2B_9)_2$ structure of **(8)**, which is clearly that of 2 vertex-fused approximate icosahedra, with the iron atom common to both. The pendant dimethylsulphide groups are bonded to the B(4) and B(4') atoms of the carbaborane ligands.

It can be seen that both cages have the same handedness in this structure, a feature clarified by the view given in **Figure 5.2**. In cases such as this where two chiral polyhedral ligands are present in the same molecule, there is no current convention of nomenclature, and it is therefore necessary to devise some system for this purpose.

The system which has been adopted is based simply on the relative (and not absolute) chirality of the ligands in a single molecule. If the two ligands are of the same optical isomer, then the complex is designated the prefix *Even* or *E*.

Figure 5.1 Perspecive View of *E*-[*commo*-3,3'-Fe-4,4'-$(SMe_2)_2$-1,1',2,2',-$(C_2B_9H_{10})_2$], *E*-[Fe(carb')$_2$], **(8)**

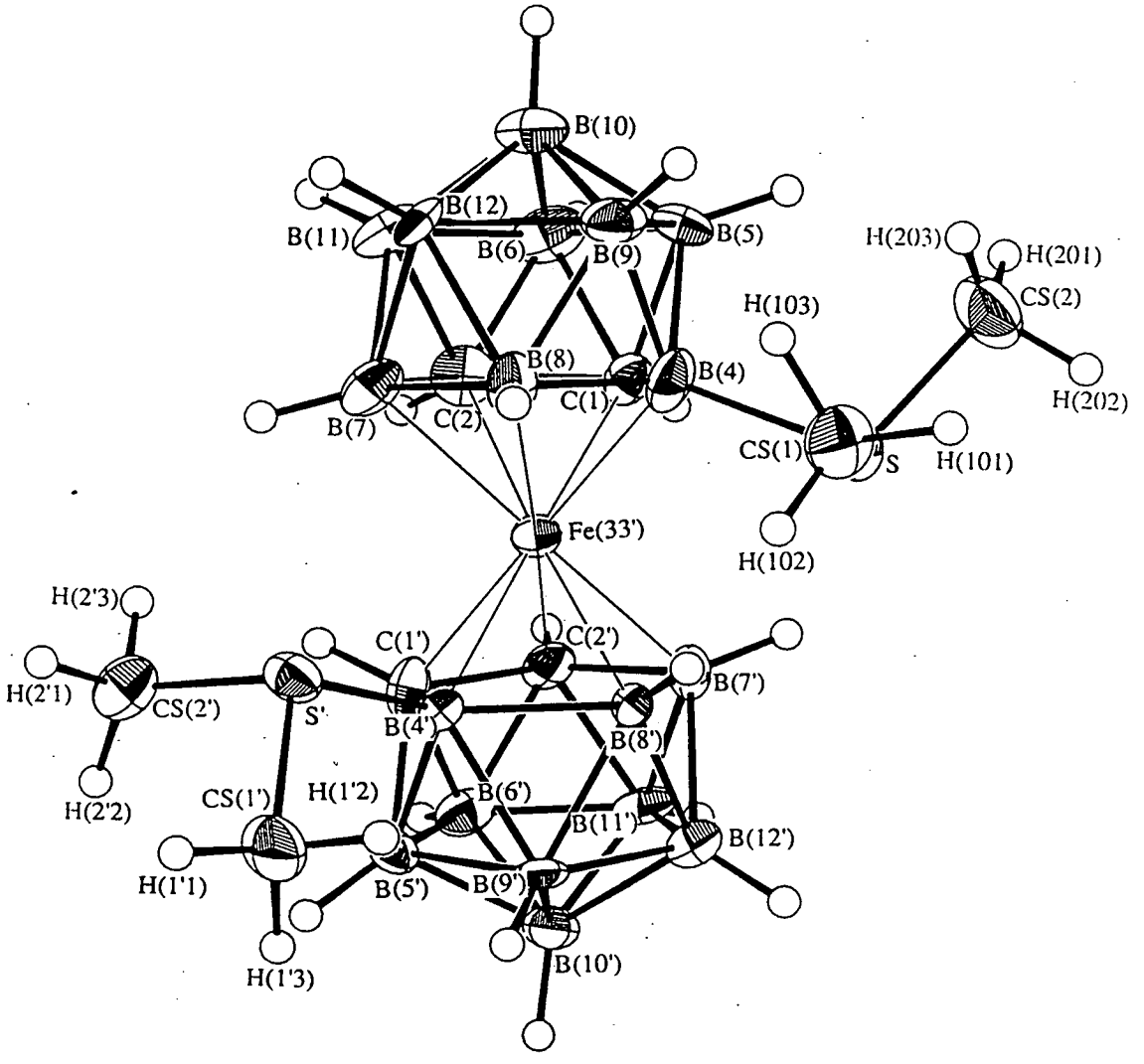

Figure 5.2 Plan View of Central Portion of *E*-[*commo*-3,3'-Fe-4,4'-$(SMe_2)_2$-1,1',2,2',-$(C_2B_9H_{10})_2$], *E*-[Fe(carb')$_2$], **(9)**

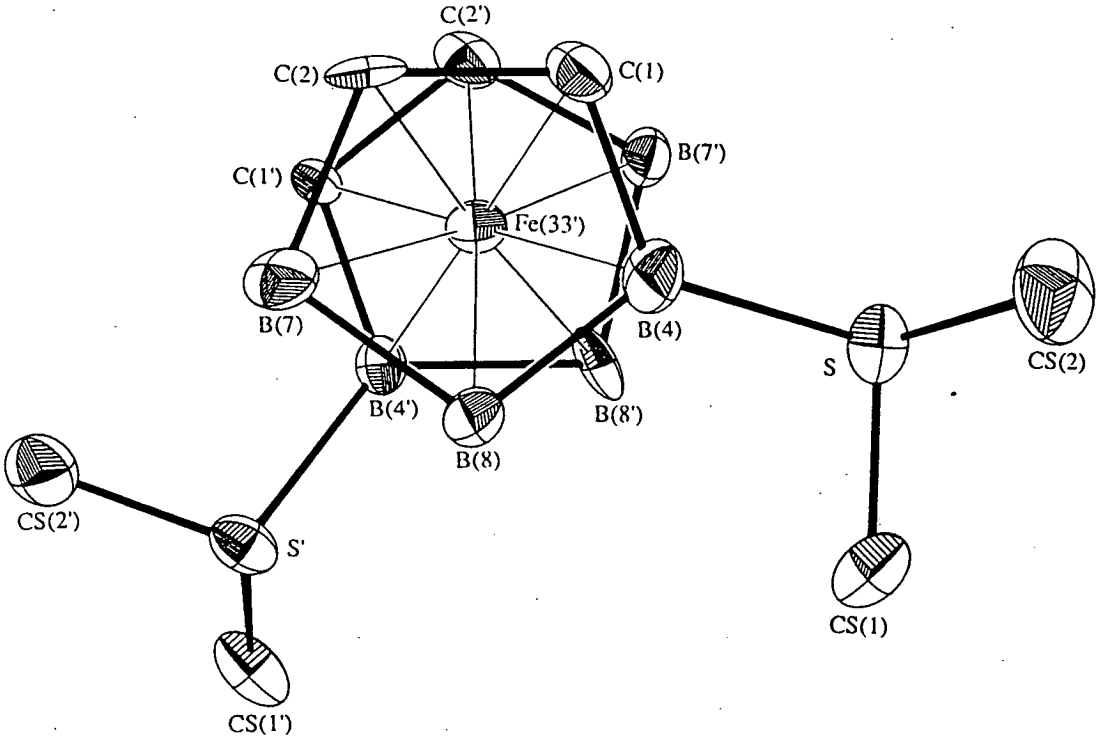

Table 5.1 Coordinates and Equivalent Isotropic Thermal Parameters ($Å^2$) for non-Hydrogen Atoms in *E*-[*commo*-3,3'-Fe-4,4'-$(SMe_2)_2$-1,1',2,2',-$(C_2B_9H_{10})_2$], *E*-[Fe(carb')$_2$], **(8)**

	x	y	z	Ueq
Fe(33')	0.76702(9)	-0.06008(9)	0.79053(8)	0.0212(6)
S	0.79020(18)	0.07364(17)	0.59397(15)	0.0349(14)
CS(1)	0.6568(6)	0.0645(7)	0.4990(5)	0.041(4)
CS(2)	0.8787(7)	0.0734(7)	0.5168(6)	0.059(5)
S'	0.49592(17)	-0.10146(15)	0.77218(14)	0.0286(13)
CS(1')	0.3771(6)	-0.0237(6)	0.7746(6)	0.044(4)
CS(2')	0.4986(7)	-0.1888(6)	0.8703(6)	0.040(4)
C(1)	0.9073(6)	-0.0961(6)	0.7599(6)	0.027(4)
C(2)	0.8683(6)	-0.1889(6)	0.8156(5)	0.028(4)
B(4)	0.8008(8)	-0.0628(8)	0.6572(7)	0.034(4)
B(5)	0.9144(7)	-0.1405(8)	0.6474(7)	0.030(4)
B(6)	0.9532(8)	-0.2180(8)	0.7518(8)	0.041(5)
B(7)	0.7292(8)	-0.2188(7)	0.7592(7)	0.031(5)
B(8)	0.6844(7)	-0.1372(7)	0.6506(7)	0.030(4)
B(9)	0.7757(9)	-0.1668(7)	0.5777(7)	0.034(5)
B(10)	0.8703(8)	-0.2661(8)	0.6386(7)	0.037(5)
B(11)	0.8433(8)	-0.2978(7)	0.7490(7)	0.034(5)
B(12)	0.7289(8)	-0.2688(7)	0.6407(7)	0.030(4)
C(1')	0.7333(6)	-0.0546(6)	0.9231(5)	0.025(4)
C(2')	0.8441(6)	0.0063(6)	0.9254(6)	0.029(4)
B(4')	0.6270(7)	-0.0182(6)	0.8276(6)	0.022(4)
B(5')	0.6415(8)	0.0232(7)	0.9512(6)	0.025(4)
B(6')	0.7871(8)	0.0364(7)	1.0153(7)	0.031(5)
B(7')	0.8183(7)	0.0900(7)	0.8304(7)	0.027(4)
B(8')	0.6729(7)	0.0797(7)	0.7623(6)	0.028(4)
B(9')	0.6040(8)	0.1153(7)	0.8524(7)	0.029(4)
B(10')	0.7067(8)	0.1457(7)	0.9685(7)	0.030(5)
B(11')	0.8384(8)	0.1321(7)	0.9539(7)	0.031(5)
B(12')	0.7259(8)	0.1805(7)	0.8547(7)	0.029(4)

Table 5.2 Internuclear Distances (Å) in *E*-[*commo*-3,3'-Fe-4,4'-$(SMe_2)_2$-1,1',2,2',-$(C_2B_9H_{10})_2$], *E*-[Fe(carb')$_2$], **(8)**

Fe(33') - C(1)	2.018(8)	B(7) -B(12)	1.803(14)
Fe(33') - C(2)	2.071(8)	B(8) - B(9)	1.828(14)
Fe(33') - B(4)	2.073(10)	B(8) -B(12)	1.823(14)
Fe(33') - B(7)	2.134(10)	B(9) -B(10)	1.783(14)
Fe(33') - B(8)	2.166(10)	B(9) -B(12)	1.806(14)
Fe(33') -C(1')	2.062(7)	B(10) -B(11)	1.760(14)
Fe(33') -C(2')	2.035(8)	B(10) -B(12)	1.801(14)
Fe(33') -B(4')	2.081(9)	B(11) -B(12)	1.775(14)
Fe(33') -B(7')	2.079(9)	C(1') -C(2')	1.602(11)
Fe(33') -B(8')	2.140(9)	C(1') -B(4')	1.637(12)
S -CS(1)	1.788(8)	C(1') -B(5')	1.685(12)
S -CS(2)	1.805(9)	C(1') -B(6')	1.732(12)
S - B(4)	1.975(10)	C(2') -B(6')	1.705(12)
S' -CS(1')	1.823(8)	C(2') -B(7')	1.682(12)
S' -CS(2')	1.790(8)	C(2') -B(11')	1.694(13)
S' -B(4')	1.923(9)	B(4') -B(5')	1.786(13)
C(1) - C(2)	1.608(11)	B(4') -B(8')	1.782(12)
C(1) - B(4)	1.687(12)	B(4') -B(9')	1.815(13)
C(1) - B(5)	1.729(12)	B(5') -B(6')	1.778(13)
C(1) - B(6)	1.707(13)	B(5') -B(9')	1.787(13)
C(2) - B(6)	1.660(13)	B(5') -B(10')	1.776(13)
C(2) - B(7)	1.725(13)	B(6') -B(10')	1.749(14)
C(2) -B(11)	1.675(13)	B(6') -B(11')	1.761(14)
B(4) - B(5)	1.801(14)	B(7') -B(8')	1.784(13)
B(4) - B(8)	1.742(14)	B(7') -B(11')	1.775(14)
B(4) - B(9)	1.725(14)	B(7') -B(12')	1.772(13)
B(5) - B(6)	1.727(14)	B(8') -B(9')	1.828(13)
B(5) - B(9)	1.746(14)	B(8') -B(12')	1.823(13)
B(5) -B(10)	1.719(14)	B(9') -B(10')	1.778(14)
B(6) -B(10)	1.725(15)	B(9') -B(12')	1.753(14)
B(6) -B(11)	1.727(15)	B(10')-B(11')	1.755(14)
B(7) - B(8)	1.803(14)	B(10')-B(12')	1.769(14)
B(7) -B(11)	1.818(14)	B(11')-B(12')	1.761(14)

Table 5.3 Interbond Angles (°) in *E*-[*commo*-3,3'-Fe-4,4'-$(SMe_2)_2$-1,1',2,2',-$(C_2B_9H_{10})_2$], *E*-[Fe(carb')$_2$], **(8)**

C(1) -Fe(33')- C(2)	46.3(3)	C(1) - B(5) - B(4)	57.0(5)
C(1) -Fe(33')- B(4)	48.7(3)	C(1) - B(5) - B(6)	59.2(5)
C(1) -Fe(33')-C(1')	131.6(3)	B(4) - B(5) - B(9)	58.2(5)
C(1) -Fe(33')-C(2')	96.7(3)	B(6) - B(5) -B(10)	60.1(6)
C(2) -Fe(33')- B(7)	48.4(3)	B(9) - B(5) -B(10)	61.9(6)
C(2) -Fe(33')-C(1')	100.0(3)	C(1) - B(6) - C(2)	57.0(5)
C(2) -Fe(33')-C(2')	95.9(3)	C(1) - B(6) - B(5)	60.5(5)
B(4) -Fe(33')- B(8)	48.5(4)	C(2) - B(6) -B(11)	59.2(6)
B(7) -Fe(33')- B(8)	49.6(4)	B(5) - B(6) -B(10)	59.8(6)
C(1') -Fe(33')-C(2')	46.0(3)	B(10) - B(6) -B(11)	61.3(6)
C(1') -Fe(33')-B(4')	46.5(3)	Fe(33')- B(7) - C(2)	63.9(4)
C(2') -Fe(33')-B(7')	48.2(3)	Fe(33')- B(7) - B(8)	66.1(4)
B(4') -Fe(33')-B(8')	49.9(3)	C(2) - B(7) -B(11)	56.3(5)
B(7') -Fe(33')-B(8')	50.0(3)	B(8) - B(7) -B(12)	60.7(5)
CS(1) - S -CS(2)	99.4(4)	B(11) - B(7) -B(12)	58.7(5)
CS(1) - S - B(4)	101.0(4)	Fe(33')- B(8) - B(4)	63.0(4)
CS(2) - S - B(4)	108.1(4)	Fe(33')- B(8) - B(7)	64.3(4)
CS(1')- S' -CS(2')	98.3(4)	B(4) - B(8) - B(9)	57.7(5)
CS(1')- S' -B(4')	106.7(4)	B(7) - B(8) -B(12)	59.6(5)
CS(2')- S' -B(4')	104.2(4)	B(9) - B(8) -B(12)	59.3(5)
Fe(33')- C(1) - C(2)	68.6(4)	B(4) - B(9) - B(5)	62.5(6)
Fe(33')- C(1) - B(4)	67.3(4)	B(4) - B(9) - B(8)	58.6(5)
C(2) - C(1) - B(6)	60.0(5)	B(5) - B(9) -B(10)	58.3(6)
B(4) - C(1) - B(5)	63.6(5)	B(8) - B(9) -B(12)	60.2(5)
B(5) - C(1) - B(6)	60.3(5)	B(10) - B(9) -B(12)	60.3(6)
Fe(33')- C(2) - C(1)	65.1(4)	B(5) -B(10) - B(6)	60.2(6)
Fe(33')- C(2) - B(7)	67.7(4)	B(5) -B(10) - B(9)	59.8(6)
C(1) - C(2) - B(6)	63.0(5)	B(6) -B(10) -B(11)	59.4(6)
B(6) - C(2) -B(11)	62.4(6)	B(9) -B(10) -B(12)	60.5(6)
B(7) - C(2) -B(11)	64.6(6)	B(11) -B(10) -B(12)	59.8(6)
Fe(33')- B(4) - S	113.3(5)	C(2) -B(11) - B(6)	58.4(6)
Fe(33')- B(4) - C(1)	64.0(4)	C(2) -B(11) - B(7)	59.0(5)
Fe(33')- B(4) - B(8)	68.6(5)	B(6) -B(11) -B(10)	59.3(6)
S - B(4) - C(1)	122.7(6)	B(7) -B(11) -B(12)	60.2(5)
S - B(4) - B(5)	114.0(6)	B(10) -B(11) -B(12)	61.3(6)
S - B(4) - B(8)	123.0(6)	B(7) -B(12) - B(8)	59.7(5)
S - B(4) - B(9)	115.9(6)	B(7) -B(12) -B(11)	61.1(5)
C(1) - B(4) - B(5)	59.3(5)	B(8) -B(12) - B(9)	60.5(5)
B(5) - B(4) - B(9)	59.3(6)	B(9) -B(12) -B(10)	59.2(5)
B(8) - B(4) - B(9)	63.7(6)	B(10) -B(12) -B(11)	58.9(6)
Fe(33')-C(1') -C(2')	66.1(4)	Fe(33')-B(7') -C(2')	64.5(4)
Fe(33')-C(1') -B(4')	67.3(4)	Fe(33')-B(7') -B(8')	66.8(4)
C(2') -C(1') -B(6')	61.4(5)	C(2') -B(7') -B(11')	58.6(5)
B(4') -C(1') -B(5')	65.0(5)	B(8') -B(7') -B(12')	61.7(5)
B(5') -C(1') -B(6')	62.7(5)	B(11')-B(7') -B(12')	59.5(5)
Fe(33')-C(2') -C(1')	67.9(4)	Fe(33')-B(8') -B(4')	63.3(4)
Fe(33')-C(2') -B(7')	67.2(4)	Fe(33')-B(8') -B(7')	63.2(4)
C(1') -C(2') -B(6')	63.1(5)	B(4') -B(8') -B(9')	60.3(5)
B(6') -C(2') -B(11')	62.4(5)	B(7') -B(8') -B(12')	58.9(5)

B(7') -C(2') -B(11')	63.4(5)	B(9') -B(8') -B(12')	57.4(5)
Fe(33')-B(4') - S'	116.2(4)	B(4') -B(9') -B(5')	59.4(5)
Fe(33')-B(4') -C(1')	66.1(4)	B(4') -B(9') -B(8')	58.6(5)
Fe(33')-B(4') -B(8')	66.8(4)	B(5') -B(9') -B(10')	59.7(5)
S' -B(4') -C(1')	122.8(6)	B(8') -B(9') -B(12')	61.2(5)
S' -B(4') -B(5')	111.7(5)	B(10')-B(9') -B(12')	60.1(5)
S' -B(4') -B(8')	125.1(6)	B(5') -B(10')-B(6')	60.6(5)
S' -B(4') -B(9')	116.6(6)	B(5') -B(10')-B(9')	60.4(5)
C(1') -B(4') -B(5')	58.8(5)	B(6') -B(10')-B(11')	60.3(6)
B(5') -B(4') -B(9')	59.5(5)	B(9') -B(10')-B(12')	59.2(5)
B(8') -B(4') -B(9')	61.1(5)	B(11')-B(10')-B(12')	59.9(5)
C(1') -B(5') -B(4')	56.2(5)	C(2') -B(11')-B(6')	59.1(5)
C(1') -B(5') -B(6')	59.9(5)	C(2') -B(11')-B(7')	57.9(5)
B(4') -B(5') -B(9')	61.1(5)	B(6') -B(11')-B(10')	59.7(5)
B(6') -B(5') -B(10')	59.0(5)	B(7') -B(11')-B(12')	60.2(5)
B(9') -B(5') -B(10')	59.9(5)	B(10')-B(11')-B(12')	60.4(6)
C(1') -B(6') -C(2')	55.6(5)	B(7') -B(12')-B(8')	59.5(5)
C(1') -B(6') -B(5')	57.4(5)	B(7') -B(12')-B(11')	60.3(5)
C(2') -B(6') -B(11')	58.5(5)	B(8') -B(12')-B(9')	61.5(5)
B(5') -B(6') -B(10')	60.5(5)	B(9') -B(12')-B(10')	60.7(5)
B(10')-B(6') -B(11')	60.0(5)	B(10')-B(12')-B(11')	59.7(5)

Table 5.4 Anisotropic Thermal Parameters ($Å^2$) in *E*-[*commo*-3,3'-Fe-4,4'-$(SMe_2)_2$-1,1',2,2',-$(C_2B_9H_{10})_2$], *E*-[Fe(carb')$_2$], **(8)**

	U11	U22	U33	U23	U13	U12
Fe(33')	0.0204(6)	0.0210(6)	0.0194(6)	-0.0023(6)	0.0052(5)	0.0006(7)
S	0.0410(14)	0.0273(13)	0.0337(12)	0.0038(11)	0.0168(11)	-0.0019(11)
CS(1)	0.0449(39)	0.0399(38)	0.0318(36)	0.0104(38)	0.0064(33)	0.0072(40)
CS(2)	0.0517(41)	0.0605(44)	0.0673(42)	0.0144(42)	0.0417(36)	0.0122(41)
S'	0.0223(11)	0.0335(13)	0.0280(12)	-0.0078(10)	0.0112(10)	-0.0046(10)
CS(1')	0.0322(39)	0.0446(42)	0.0537(41)	-0.0122(36)	0.0223(35)	-0.0138(35)
CS(2')	0.0404(41)	0.0313(39)	0.0423(41)	-0.0064(35)	0.0095(36)	-0.0068(36)
C(1)	0.0204(35)	0.0223(37)	0.0353(38)	-0.0010(32)	0.0076(31)	-0.0031(32)
C(2)	0.0144(36)	0.0402(40)	0.0213(36)	0.0022(34)	-0.0087(31)	0.0047(34)
B(4)	0.0336(41)	0.0187(39)	0.0459(42)	0.0123(40)	0.0125(37)	0.0048(40)
B(5)	0.0239(40)	0.0360(43)	0.0294(41)	-0.0049(37)	0.0153(35)	0.0060(38)
B(6)	0.0278(42)	0.0365(44)	0.0496(45)	-0.0060(41)	0.0033(40)	0.0101(40)
B(7)	0.0275(42)	0.0202(41)	0.0387(42)	0.0020(37)	0.0020(37)	0.0061(37)
B(8)	0.0212(40)	0.0285(42)	0.0349(42)	0.0127(37)	0.0064(36)	0.0038(37)
B(9)	0.0500(45)	0.0278(42)	0.0205(40)	-0.0017(36)	0.0132(38)	0.0090(40)
B(10)	0.0316(43)	0.0363(44)	0.0399(43)	-0.0148(39)	0.0122(38)	0.0032(39)
B(11)	0.0344(43)	0.0198(41)	0.0392(43)	-0.0071(38)	-0.0017(38)	0.0064(38)
B(12)	0.0367(43)	0.0093(37)	0.0395(42)	-0.0045(36)	0.0148(37)	-0.0041(36)
C(1')	0.0190(34)	0.0235(36)	0.0251(34)	0.0030(35)	-0.0018(30)	-0.0096(35)
C(2')	0.0179(36)	0.0206(37)	0.0448(40)	-0.0006(34)	0.0112(33)	0.0039(32)
B(4')	0.0252(40)	0.0147(38)	0.0241(38)	-0.0011(33)	0.0106(34)	-0.0004(35)
B(5')	0.0262(41)	0.0296(41)	0.0183(37)	-0.0056(34)	0.0101(34)	-0.0050(36)
B(6')	0.0360(42)	0.0241(43)	0.0265(40)	0.0000(35)	0.0069(36)	0.0073(37)
B(7')	0.0234(38)	0.0237(42)	0.0331(39)	0.0105(35)	0.0123(34)	0.0037(35)
B(8')	0.0332(40)	0.0175(41)	0.0327(38)	-0.0150(36)	0.0207(34)	-0.0180(36)
B(9')	0.0238(39)	0.0188(40)	0.0442(42)	-0.0115(37)	0.0199(36)	0.0011(36)
B(10')	0.0331(42)	0.0282(42)	0.0268(41)	-0.0008(36)	0.0139(36)	0.0066(38)
B(11')	0.0332(42)	0.0236(41)	0.0309(41)	-0.0158(36)	0.0077(37)	0.0009(38)
B(12')	0.0294(42)	0.0208(41)	0.0311(40)	-0.0042(37)	0.0078(36)	0.0005(37)

Table 5.5 Final Hydrogen Atom Coordinates for *E*-[*commo*-3,3'-Fe-4,4'-$(SMe_2)_2$-1,1',2,2',-$(C_2B_9H_{10})_2$], *E*-[Fe(carb')$_2$], **(8)**

	x	y	z
H(1)	0.982(3)	-0.061(4)	0.808(3)
H(2)	0.896(4)	-0.212(4)	0.8918(13)
H(5)	0.962(3)	-0.102(3)	0.608(3)
H(6)	1.0408(12)	-0.220(4)	0.791(4)
H(7)	0.685(4)	-0.262(4)	0.799(3)
H(8)	0.6049(22)	-0.120(4)	0.597(3)
H(9)	0.755(4)	-0.154(4)	0.4995(10)
H(10)	0.905(4)	-0.319(3)	0.600(3)
H(11)	0.875(4)	-0.3652(23)	0.792(3)
H(12)	0.674(3)	-0.3326(24)	0.616(4)
H(1')	0.749(4)	-0.1282(19)	0.958(4)
H(2')	0.9250(20)	-0.019(4)	0.970(3)
H(5')	0.571(3)	0.012(4)	0.975(4)
H(6')	0.837(4)	0.011(4)	1.0876(18)
H(7')	0.882(3)	0.123(4)	0.806(3)
H(8')	0.638	0.092	0.684
H(9')	0.5180(14)	0.134(4)	0.836(4)
H(10')	0.666(4)	0.194(3)	1.007(3)
H(11')	0.9151(23)	0.169(3)	0.994(3)
H(12')	0.714(4)	0.2584(14)	0.830(4)
H(101)	0.6560	0.1149	0.4383
H(102)	0.5816	0.0760	0.5178
H(103)	0.6608	-0.0144	0.4767
H(201)	0.9655	0.0512	0.5381
H(202)	0.8703	0.1531	0.4945
H(203)	0.8301	0.0262	0.4554
H(1'1)	0.2995	-0.0656	0.7567
H(1'2)	0.3755	0.0253	0.7128
H(1'3)	0.3880	0.0226	0.8402
H(2'1)	0.4276	-0.2380	0.8367
H(2'2)	0.4965	-0.1620	0.9417
H(2'3)	0.5748	-0.2313	0.8806

Complexes containing two carbaboranes of different handedness are called *Odd* or *O*. This treatment is sufficient to unambiguously describe the structures of molecules which crystallise in non-polar space groups (*i.e.* containing equal numbers of absolute isomers), such as **(8)** and **(9)** (see later), but has potential limitations in the (relatively unlikely) event of crystallisation in a chiral space group, containing only one absolute isomer.

The central Fe atom is situated at perpendicular distances of 1.5018 and 1.4971Å from the ligating faces of the C(1)-B(12) and C(1')-B(12') cages respectively, with no appreciable slip from a position directly above the centroid of the lower pentagonal plane of either of the carbaborane ligands (Δ 0.05 and 0.04 Å).

Cage C(1')-B(12') is folded into an envelope conformation about the B(4')...B(7') vector, as is common in species of this type. The resulting 3- and 4-atom portions of the upper face are folded away from the Fe atom, giving fold parameters with the lower pentagonal plane of $\phi = 1.50^{o}$ and $\theta = 3.17^{o}$ respectively.

The upper face of the C(1)-B(12) carbaborane is also non-planar, although the nature of the folding is slightly different to that in the above case. Here the folding occurs about the C(1)...B(7) vector. The 4-atom [C(1),B(4),B(8),B(7)] and 3-atom [C(1),C(2),B(7)] portions so created give fold angles with the lower 5B belt of $\theta = 1.61^{o}$ and $\phi = 5.47^{o}$, the positive signs of these parameters denoting folding away from the metal atom.

The orientation of the dimethylsulphide group with respect to the cage geometry has been a feature of the discussion of all of the structures (**(3)**, **(4)**, **(5)**

and (6)) of [carb']-containing species so far presented. In each of these compounds, the SMe_2 function appears to be involved in electrostatic interaction between its (sulphur) lone pair and the relatively protonic H.atom bonded to the adjacent carbon atom [C(1) or C(8), depending on the overall geometry of the cage and numbering scheme consequently employed [36].

In complexes **(4)** and **(5)** there is observed some intramolecular steric crowding which causes the S atom to be depressed by *ca.* 5^{o} from its preferred elevation angle, and it is inferred that this distortion is undergone to preserve the lone pair..$H^{\delta+}$ interaction.

In **(8)** however, we have the first example where this intramolecular electrostatic interaction is not observed, presumably because of unfavourable steric interaction between one of the methyl groups of one ligand and the closest of the (cage) H atoms of the other. Specifically, the following distances are of relevance: H(102)-H(8') = 2.247Å and H(2'3)-H(7) = 2.131Å, *i.e.* less than 2.4Å, which is twice the van der Waal's radius for the hydrogen atom. The torsion observed for each of the SMe_2 groups about the B-S bond is therefore unsurprising, given the (now obvious) steric problems which prevent adoption of an orientation such as that seen in **(3)**, **(4)**, **(5)** and (6)).

Another structural consequence of this steric crowding is the notable degree of depression of the dimethylsulphide groups from their preferred (26^{o}) angle of inclination to the ligating $[C_2B_3]$ faces of the ligands, giving elevation angles of 19.8^{o} (S) and 18.6^{o} (S').

It therefore appears that, unlike the [carb'] complexes discussed earlier, the elevation and orientation of the SMe_2 groups in **(8)** are controlled purely by steric

factors.

Electrochemical Study on (8)

Introduction

Ferrocene, aside from its historic interest, finds a genuine purpose in modern chemistry, namely in electrochemical work, where the ferrocene/ferrocinium ($Fe^{II/III}$) redox couple is widely used as a reference against which other couples may be calibrated.

Given this, together with the results of Chapter 4 (suggesting very similar electronic properties for $[carb']^-$ and Cp^-), it was decided to investigate the electrochemistry of $Fe(carb')_2$.

If, as might seem reasonable, the redox behaviour of ferrocene and its [carb'] analogue, **(8)**, are similar, this would then afford one of the few known examples of vertex-cationic carbametallaboranes [86,87].

Results and Discussion

The techniques employed and equipment used in the electrochemical studies are described in Chapter 6, section 4. A schematic drawing of the experimental set-up comprises **Figure 6.4.1.**

Cyclic voltammetry (c.v.), linear stirred volammetry (s.v.) and alternating current voltammetry (a.c.v.) at a platinum electrode in CH_2Cl_2/0.5M $[TBA]BF_4$ establish that, at 273K, $Fe(carb')_2$ undergoes a reversible oxidation at +0.57V *versus* the Ag/AgCl reference electrode.

Figure 5.3 Cyclic and a.c. Voltammograms for [Fe(carb')$_2$], **(8)**

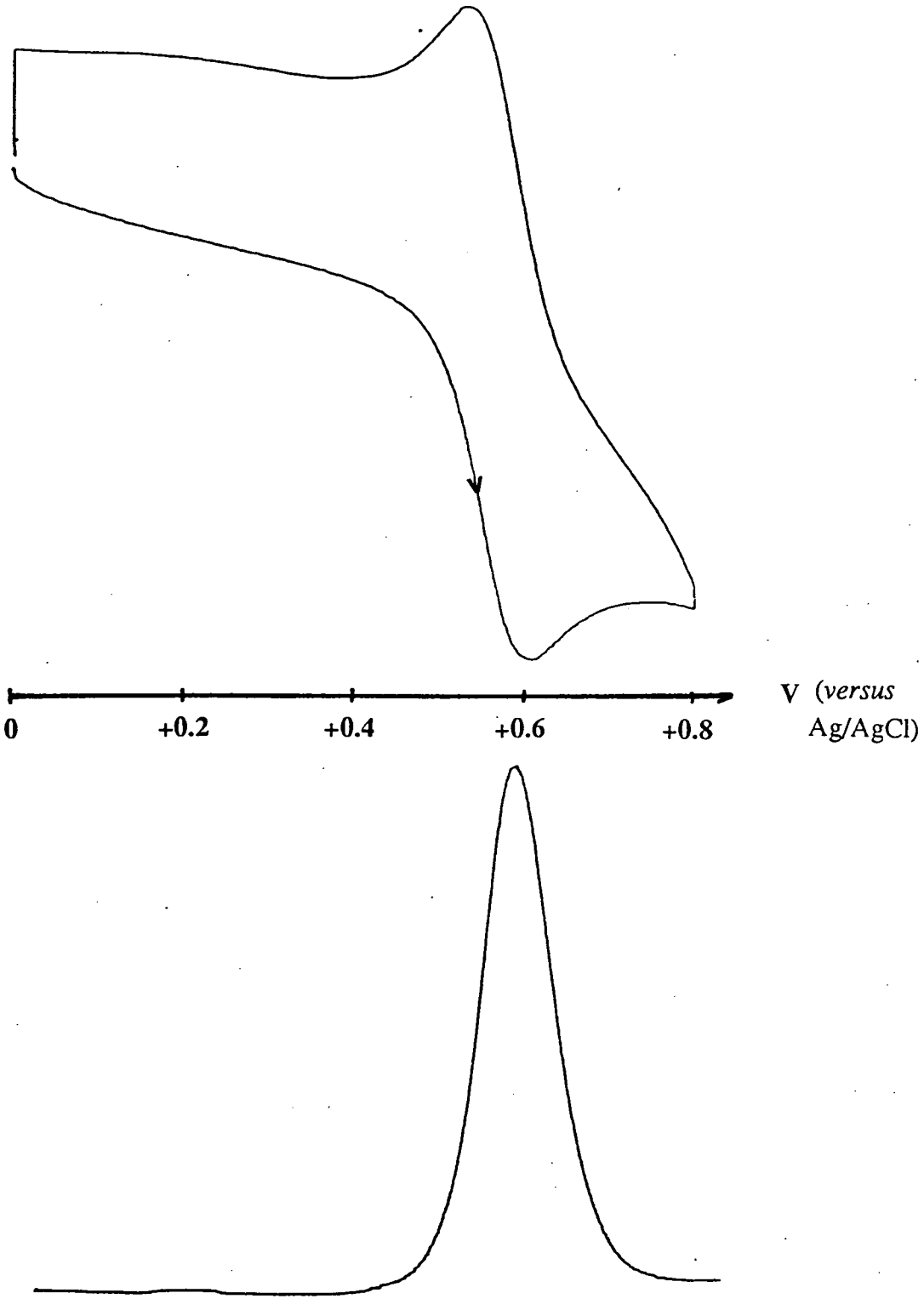

Reversibility criteria are given in Chapter 6, section 4.

The cyclic and a.c. voltammograms are shown in **Figure 5.3.**

The oxidation is a 1-electron process, subsequently confirmed by analysis of data from the spectroelectrochemical experiment (see later). The position of the **(8)**/$[(8)]^+$ oxidation, at only very slightly (*ca.* 10-20mV) higher potential than the Fc/Fc^+ couple, has two obvious implications: (i) the oxidation is iron- and not ligand-based and (ii) the earlier finding of extremely similar net electronic properties for the $[carb']^-$ and Cp^- ligands is again borne out.

An analogous product to **(8)** has been obtained prevoiusly, following protonation of $[Fe(C_2B_9H_{11})_2]^{2-}$ and reaction with diethylsulphide [87]. The oxidation potential for this SEt_2 analogue (in CH_3CN/0.1N $[NEt_4]ClO_4$) is quoted as +0.48V *versus* the saturated calomel electrode (sce), which is equivalent to approximately +0.52V *versus* Ag/AgCl. It is reassuring that the potentials for this complex and for **(8)** are highly similar, despite the fact that the conditions of the electrochemical experiments were different. In view of this, it is difficult to say whether the apparent small difference between the measured potentials is significant.

Chemical Oxidation of (8)

Introduction

Following the electrochemical work on **(8)**, yielding a cationic carbametallaborane, it was clearly of value to effect chemical oxidation of the complex. Given that the oxidation of **(8)** has been shown to be a relatively facile process, chemical oxidation might be expected to be achieved by relatively mild

oxidising agents.

Discussion

The pink $Fe(carb')_2$ species does in fact react with mild inorganic oxidising agents such as Ag^+, Cl_2 and $FeCl_3$, to give deep red/brown species, indicative of the Fe^{III} oxidation state (see Chapter 6, section 1 for experimental details). Attempts to grow crystals of these products for structural work were unfortunately unsuccessful. Although deep red crystals were grown by solvent evaporation from the products of the reactions of **(8)** with $AgBF_4$ and $AgPF_6$, these were, in both cases, too small for use in *X*-ray work.

An electrochemical study was carried out on the product of oxidation of $Fe(carb')_2$ by excess $FeCl_3$, assumed to be **(8)**$[FeCl_4]$.

In the absence of other evidence for the postulated formula, this study proved invaluable in the identification of the product.

Cyclic, alternating current and linear stirred voltammetry at a platinum electrode in CH_2Cl_2/0.5M $[TBA]BF_4$, reveal the presence of two electroactive species, both of which undergo reversible reductions ($Fe^{III/II}$). The potentials of these reductions are identical to those of the **(8)**/$[(8)]^+$ oxidation (see before) and the reduction of an authentic sample of $[FeCl_4]^-$. Thus the product is confirmed as $[Fe(carb')_2][FeCl_4]$.

Spectroelectrochemical Study on $Fe(carb')_2$, (8)

Introduction

Spectroelectrochemical studies were carried out using the Optically Transparent Thin Layer Electrode (O.T.T.L.E.) cell (which is described more fully in Chapter 6, section 4, and shown schematically in **Figure 6.4.2**) and a solution of the complex in CH_2Cl_2/0.5M $[TBA]BF_4$ at 273K.

Results and Discussion

The spectral progression obtained is shown in **Figure 5.4**, illustrating the isosbestic conversion of neutral $Fe(carb')_2$ to its monocation. The bands at 32900 and 36600cm^{-1} grow in intensity and the ill-defined band at *ca.* 42000cm^{-1} collapses as the Fe^{III} species is formed.

The spectroelectrochemical result fully supports that of the electrochemical study, giving (by application of the Nernst equation, see Chapter 6, section 4) a potential for the $Fe(carb')_2/[Fe(carb')_2]^+$ couple of +0.66V *versus* the Ag/AgCl electrode.

The aforementioned application of the Nernst equation to the spectroelectrochemical data yields a second parameter, **n**, the number of electrons transferred per molecule. In this case, the oxidation of **(8)** is shown to be a 1 electron process, with $\mathbf{n} = 1.06 \pm 0.1e^-$. This is, of course, entirely analogous to the $Fe^{II/III}$ couple in the Fc/Fc^+ system.

Figure 5.4 Electronic Absorption Spectra Showing Conversion of $[Fe(carb')_2]$ to $[Fe(carb')_2]^+$

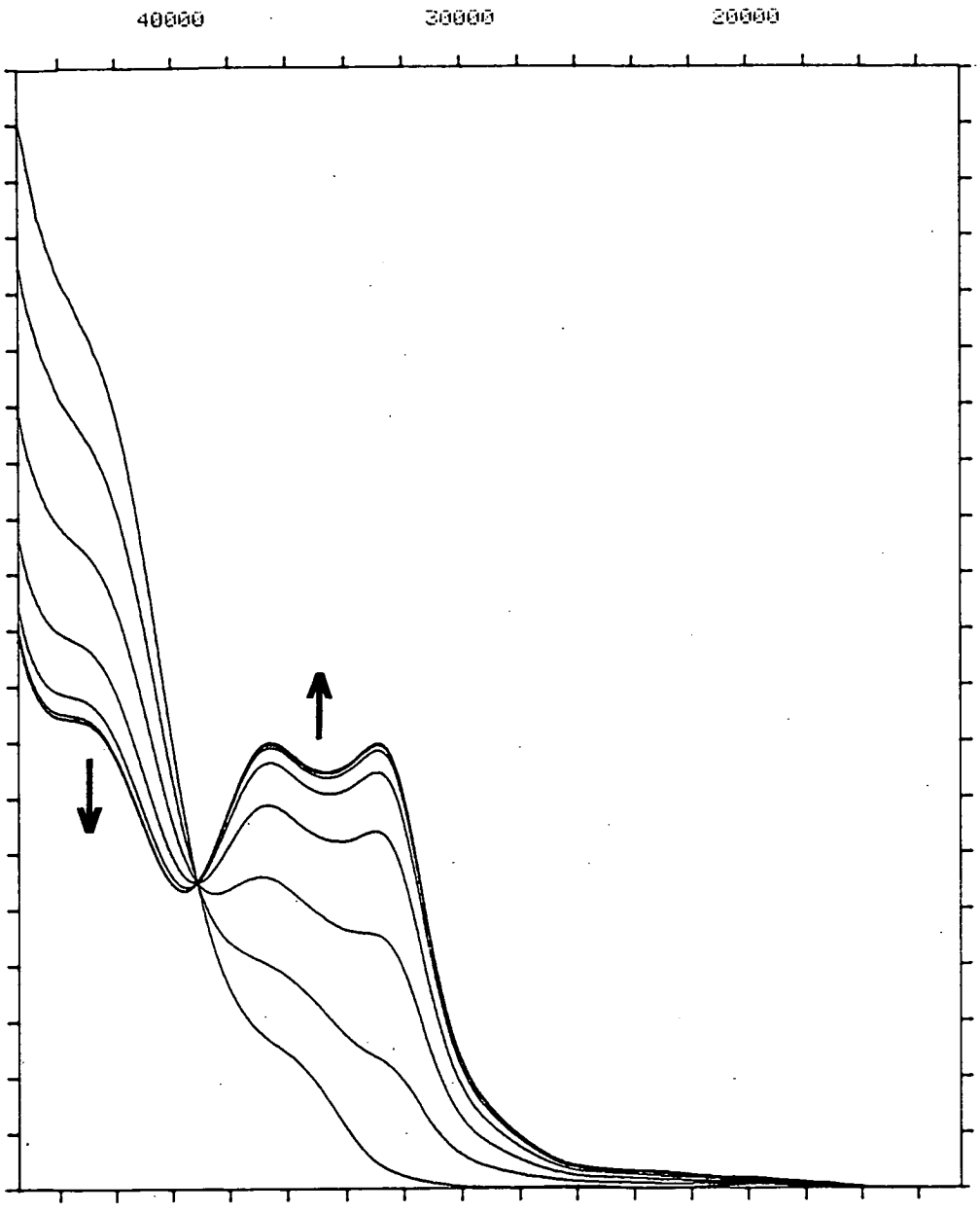

It has been conclusively shown that the bis[carb'] analogue of ferrocene, $Fe(carb')_2$, may be oxidised by electrochemical and chemical means, the oxidation being only very slightly more difficult than that of ferrocene itself. This very small difference (of the order of tens of millivolts) would tend to suggest (as already seen in Chapter 4) that the net electronic properties of $[carb']^-$ and Cp^- are highly similar and lend further support to the analogy between the two ligands.

[*commo*-3,3'-Fe-4-SMe_2-4'-SMe-1,1',2,2'-$(C_2B_9H_{10})_2$],

[Fe(carb')($C_2B_9H_{10}$SMe)], (9)

Introduction

During the course of the work on $Fe(carb')_2$, **(8)**, there was also isolated a second, closely related species, [*commo* -3,3'-Fe-4-SMe_2-4'-SMe-1,1',2,2'-$(C_2B_9H_{10})_2$], **(9)**. The identification and structural characterisation of this species were of immense use in illumination of the nature of isomerism in **(8)**.

The synthesis, chemical characterisation and *X*-ray crystal structure of **(9)** are presented, along with the results of electrochemical and spectroelectrochemical experiments. Conversion of **(9)** into **(8)** is also discussed. This conversion, allied to the principle of microscopic reversibility, allows us to propose a possible mechanism for the formation of **(9)** from **(8)**.

Synthesis and Characterisation of (9)

Complex **(9)** was synthesised as a by-product in one (Method 1, see earlier) particular preparation of **(8)** (experimental details of which are reported in Chapter 6, section 1), in which the extremely finely-divided pink precipitate was collected by filtration over an extended (*ca.* 40 minutes) period of time. Over this interval the pink colour indicative of $Fe(carb')_2$ slowly changed to brown. Redissoluton of the resulting solid in dichloromethane, followed by thin layer chromatography, gave 4 mobile bands, the first two of which were dark brown **(9)** and pink/purple **(8)**. These were followed by a second pair of similarly coloured bands (presumably isomeric with the first pair, and in much lower yields) at lower R_f values, and were not collected.

(9) was characterised by elemental (C,H) microanalysis, the results of which were consistent with the $C_7H_{29}B_{18}S_2Fe$ formulation of the complex, and ^1H, ^{11}B, $^{11}B\text{-}\{^1H\}$ and $^1H\text{-}\{^{11}B$ selective$\}$ n.m.r. spectroscopic studies.

The n.m.r. spectra of **(9)** are of particular interest, as the presence of paramagnetic (d^5) Fe^{III} results in unusual chemical shifts, especially for nearby nuclei, *e.g.* the carbaborane facial boron atoms and their associated protons. Although unusual, this type of effect has been observed previously in Fe^{III} carbaborane species, such as $Fe(C_5H_5)(C_2B_9H_{11})$ [88].

The ^1H spectrum of **(9)** is best discussed in terms of 3 distinct classes of H atom, namely: (i) methyl H's, (ii) H atoms bonded to carbaborane facial B atoms and (iii) other (unassigned) C-H and B-H's.

(i) The three methyl groups in **(9)** each display the expected singlet, and these

occur at δ -0.50, -3.32 and -8.25 p.p.m..

(ii) The six protons bonded to the facial boron atoms give very high positive chemical shifts (δ 127.09, 93.18, 81.17, 49.90, 32.08 and 24.44 p.p.m.) and are assigned as such because of the extreme broadness (*ca.* 1500Hz) of the signals.

(iii) The remaining signals in the ^{1}H spectrum are broad (*ca.* 500Hz) and arise from boron- and carbon-bonded H atoms, although further assignment has not been attempted. Some of these signals are also observed in the ^{1}H-{^{11}B selective} spectra, where they may at least be assigned to a boron nucleus giving a particular chemical shift.

The ^{11}B-{^{1}H} spectrum shows 18 separate peaks, as expected, although these occur over a δ range of approximately 600 p.p.m.. There are six very broad resonances at extremely low frequency (δ -322.07, -379.10, -385.59, -435.63, -462.44 and -491.73 p.p.m.) which are assigned to the six facial boron atoms. The other 12 resonances (δ between 108.33 and -52.44 p.p.m.) are much sharper (being associated less with the paramagnetic Fe^{III} centre) and also display doublet coupling (J_{BH} in the range 80-110Hz) in the ^{11}B spectrum. The six lowest frequency resonances do not (on account of their extreme broadness) appear significantly different in the ^{11}B and ^{11}B-{^{1}H} spectra.

In a series of ^{1}H-{^{11}B selective} experiments, decoupling at the 12 sharp (highest frequency) boron sites results in enhancement of 12 separate proton environments, consistent with the proposed structure.

Structural Study of (9)

Introduction

In order to shed further light on the bonding of [carb']$^-$ to iron, a structural study was carried out on [Fe(carb')($C_2B_9H_{10}$SMe)], **(9)**.

Chemical characterisation has shown the identity of the complex, but offers no information upon the relative handedness of the chiral carbaborane ligands, *i.e.* do the two cages possess the same (*E*) or different (*O*) handedness within the complex?

As has been discussed earlier, the only form of **(8)** which afforded crystals of suitable quality for structural analysis was the *even* (*E*) isomer, in which both ligands are of the same optical isomer, this being the sole product obtained by the second (Method 2) synthetic route. There are, of course equal numbers of both *total* isomers, in the (centrosymmetric) crystal lattice.

High-quality crystals of *O*-[*commo*-3,3'-Fe-4-SMe_2-4'-SMe-1,1',2,2'-$(C_2B_9H_{10})_2$], **(9)**, were grown by slow diffusion of n-hexane into a dichloromethane solution at -30°C. Crystal data, details of data collection and processing, and crystallographic methods used in solution and refinement of the structure may be found in Chapter 6, section 2.

Discussion

8 (2 independent) molecules of **(9)** crystallise in the monoclinic four-fold space group $P2_1/c$. As is apparent from **Figures 5.5A** and **5.5B**, the two independent molecules, *A* and *B* are enantiomers, thus begging the question of why this

symmetry relationship is not utilised in the crystal lattice, allowing a smaller unit cell to be chosen.

Perspective views of molecules *A* and *B* are shown in **Figures 5.5A** and **5.5B** respectively, along with the molecular numbering scheme employed. Cage H atoms are numbered as the vertices to which they are bonded. Plan views of the ligating $[C_2B_3]$ faces of the cages and the Fe, S and methyl C atoms of both molecules are shown in **Figure 5.6**.

Final coordinates of refined atoms are given in **Tables 5.6A** and **5.6B**, including equivalent isotropic thermal parameters for non-hydrogen atoms. **Tables 5.7A** and **5.7B** give internuclear distances within each of the molecules, while relevant interbond angles are presented in **Tables 5.8A** and **5.8B**. Anisotropic thermal vibration parameters for each of the molecules are given in **Tables 5.9A** and **5.9B**. Calculated positions of (non-refined) hydrogen atoms comprise **Table 5.10**.

Upon initial inspection of **Figures 5.5A** and **5.5B**, the gross geometry of the complex may be seen, namely that of two vertex-fused approximate icosahedra, with the iron atom common to both.

The plan views shown in **Figure 5.6** illustrate the disposition of the facial atoms with respect to each other and also the relative positions of the SMe_2 and SMe substituents. Inspection of these figures clearly shows the stereochemistry of the two cages in each molecule to be different, (*i.e.* the *O* isomer) unlike those in the structurally characterised isomer (*E*) of **(8)**. It is also evident from **Figure 5.6** that the two cages within each molecule are in a relative orientation which is neither fully eclipsed nor fully staggered.

Figure 5.5A Perspective View of Molecule A of *O*-[*commo* -3,3'-Fe-4-SMe_2-4'-SMe-1,1',2,2'-$(C_2B_9H_{10})_2$], *O*-[Fe(carb')$(C_2B_9H_{10}SMe)$], **(9)**

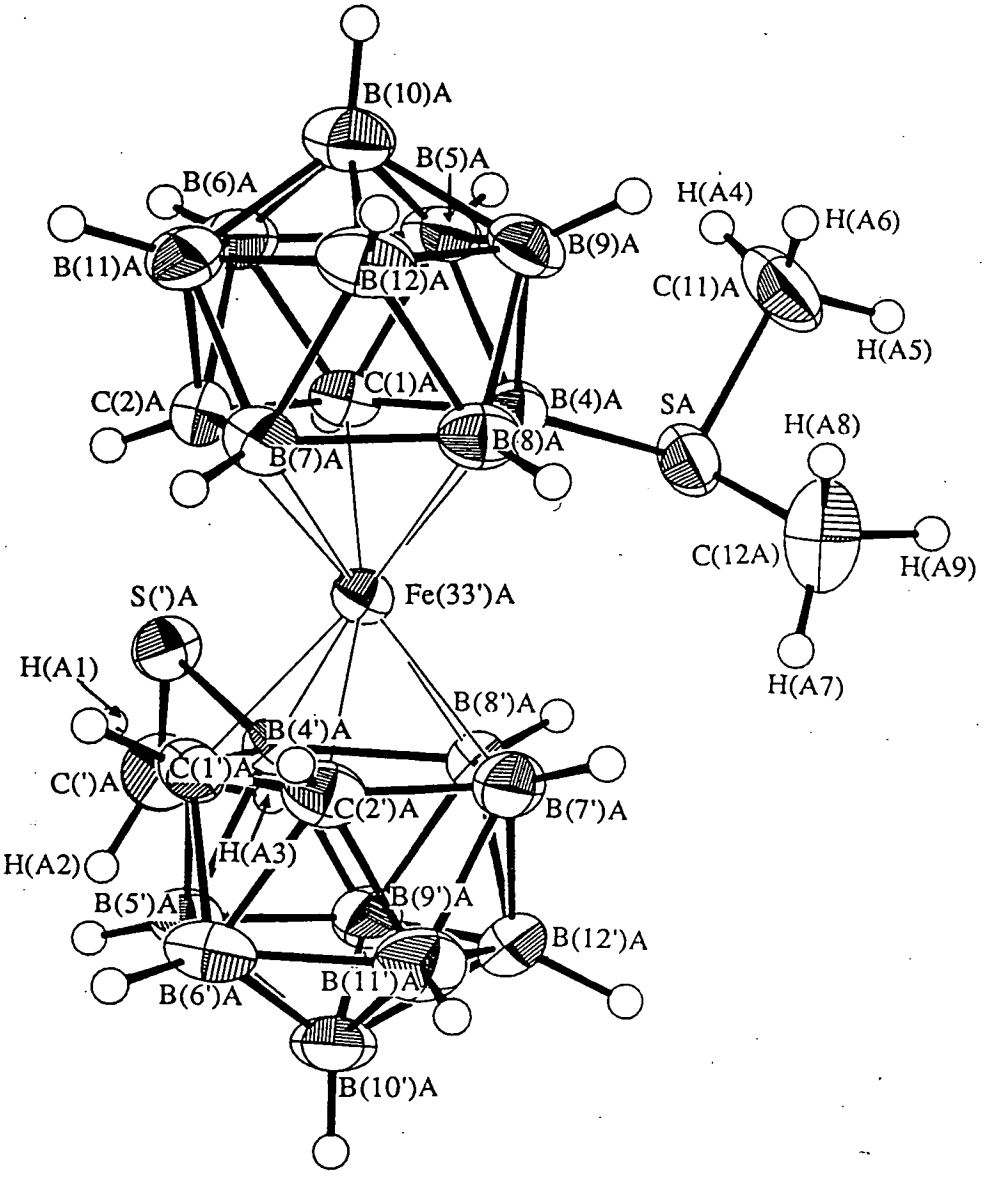

Figure 5.5B Perspective View of Molecule B of *O*-[*commo* -3,3'-Fe-4-SMe_2-4'-SMe-1,1',2,2'-$(C_2B_9H_{10})_2$], *O*-[Fe(carb')($C_2B_9H_{10}SMe$)], **(9)**

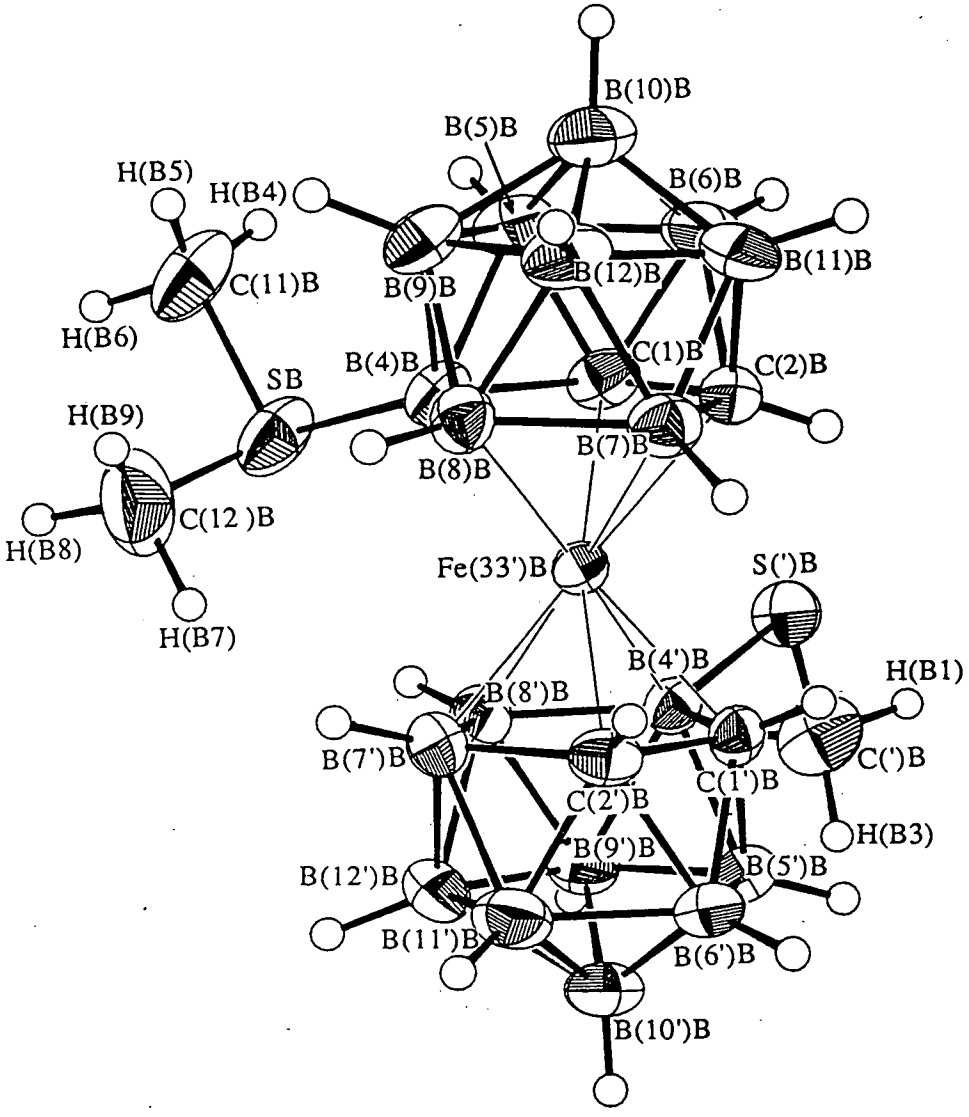

Figure 5.6 Plan Views of Central Portions of Molecules A and B of *O*-[*commo* -3,3'-Fe-4-SMe_2-4'-SMe-1,1',2,2'-$(C_2B_9H_{10})_2$], *O*-[Fe(carb')$(C_2B_9H_{10}SMe]$, **(9)**

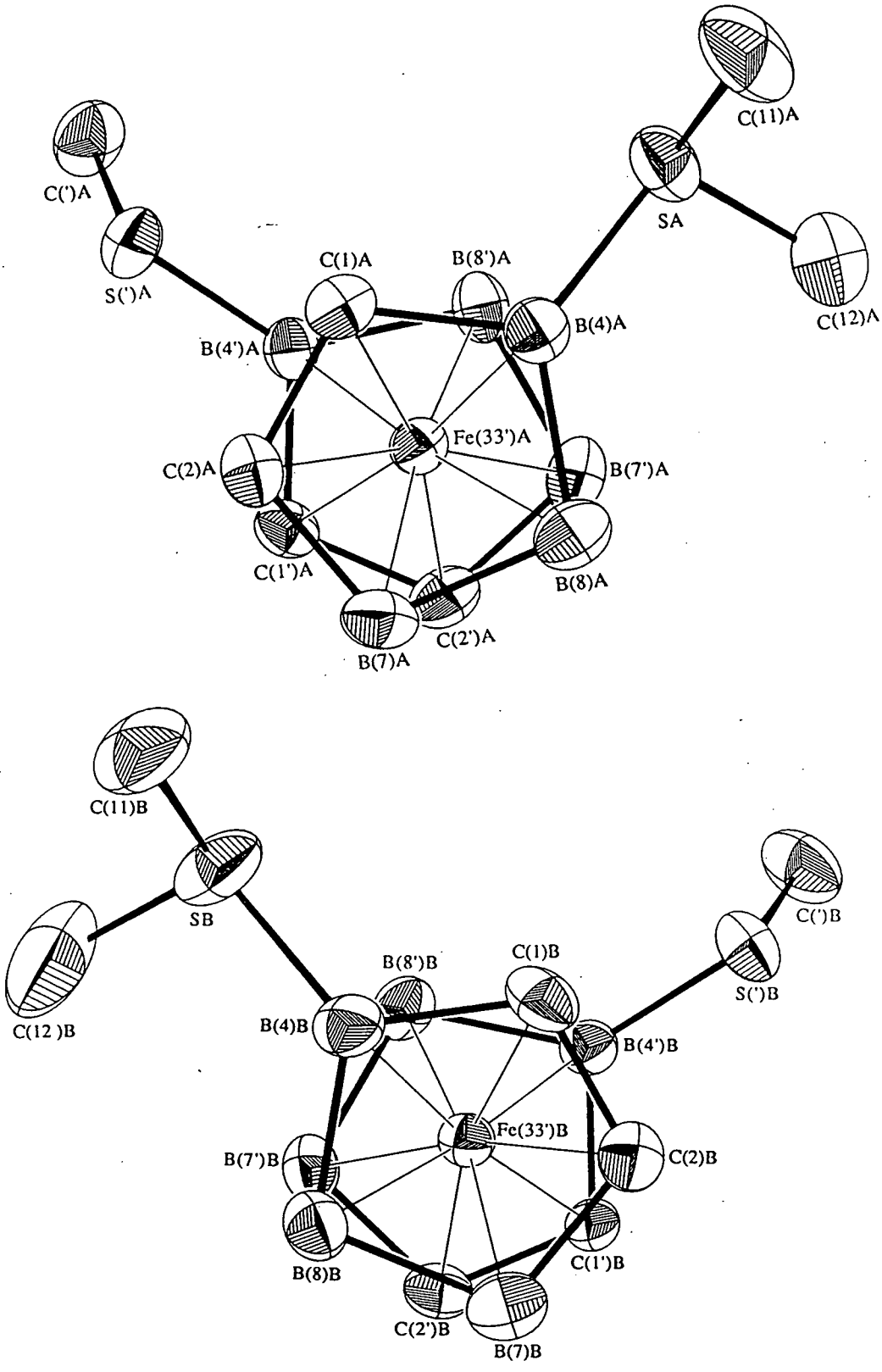

Table 5.6A Coordinates of Refined Atoms and Equivalent Isotropic Thermal Parameters ($Å^2$) for Molecule A of *O*-[*commo*-3,3'-Fe-4-SMe_2-4'-SMe-1,1',2,2'-$(C_2B_9H_{10})_2$], *O*-[Fe(carb')$(C_2B_9H_{10}SMe)$], **(9)**

	x	y	z	Ueq
Fe(33')A	0.23887(4)	0.12374(2)	0.10849(5)	0.0288(4)
S(')A	0.42156(7)	0.05516(4)	0.22989(10)	0.0393(7)
SA	0.08215(8)	0.05176(4)	0.18995(11)	0.0460(8)
C(')A	0.4732(3)	0.00083(16)	0.1868(5)	0.053(3)
C(11)A	0.0226(4)	0.04543(20)	0.3128(6)	0.073(4)
C(12)A	-0.0088(4)	0.06741(21)	0.0509(6)	0.077(4)
C(1')A	0.3408(3)	0.13101(15)	0.0150(4)	0.036(3)
C(2')A	0.2448(3)	0.14878(17)	-0.0758(4)	0.041(3)
B(4')A	0.3375(3)	0.07385(17)	0.0755(4)	0.032(3)
B(5')A	0.3831(4)	0.08627(19)	-0.0578(5)	0.044(4)
B(6')A	0.3258(4)	0.13561(21)	-0.1508(5)	0.049(4)
B(7')A	0.1636(4)	0.10730(20)	-0.0884(5)	0.043(3)
B(8')A	0.2217(3)	0.05540(19)	0.0056(5)	0.036(3)
B(9')A	0.3066(3)	0.03815(20)	-0.0710(5)	0.039(3)
B(10')A	0.2997(4)	0.07559(21)	-0.2081(5)	0.049(4)
B(11')A	0.2130(4)	0.11805(21)	-0.2175(5)	0.052(4)
B(12')A	0.2001(4)	0.05759(21)	-0.1706(5)	0.046(4)
C(1)A	0.2597(3)	0.10883(16)	0.3105(4)	0.034(3)
C(2)A	0.3111(3)	0.15705(16)	0.2875(4)	0.037(3)
B(4)A	0.1507(3)	0.11108(17)	0.2257(5)	0.034(3)
B(5)A	0.1868(4)	0.12199(19)	0.3986(5)	0.045(4)
B(6)A	0.2930(4)	0.15034(20)	0.4371(5)	0.048(4)
B(7)A	0.2418(4)	0.19607(18)	0.1840(5)	0.039(3)
B(8)A	0.1325(4)	0.16831(19)	0.1417(5)	0.041(3)
B(9)A	0.1056(4)	0.16137(20)	0.2946(5)	0.047(4)
B(10)A	0.1948(4)	0.18501(21)	0.4250(5)	0.053(4)
B(11)A	0.2782(4)	0.20679(19)	0.3557(5)	0.046(4)
B(12)A	0.1637(4)	0.21331(21)	0.2691(5)	0.053(4)
H(1')A	0.381(3)	0.1582(16)	0.059(4)	
H(2')A	0.238(3)	0.1777(17)	-0.076(5)	
H(5')A	0.453(3)	0.0782(15)	-0.028(4)	
H(6')A	0.361(3)	0.1665(16)	-0.178(4)	
H(7')A	0.094(3)	0.1207(14)	-0.123(4)	
H(8')A	0.190(3)	0.0265(15)	0.046(4)	
H(9')A	0.324(3)	0.0042(16)	-0.067(4)	
H(10')A	0.313(3)	0.0624(15)	-0.285(4)	
H(11')A	0.179(3)	0.1378(16)	-0.292(4)	
H(12')A	0.148(3)	0.0327(15)	-0.235(4)	
H(1)A	0.289(3)	0.0846(17)	0.336(5)	
H(2)A	0.372(3)	0.1554(16)	0.300(4)	
H(5)A	0.173(3)	0.0969(16)	0.455(4)	
H(6)A	0.347(3)	0.1405(16)	0.517(4)	
H(7)A	0.264(3)	0.2208(16)	0.136(4)	
H(8)A	0.081(3)	0.1792(15)	0.060(4)	
H(9)A	0.039(3)	0.1631(15)	0.291(4)	
H(10)A	0.175(3)	0.2000(15)	0.498(4)	
H(11)A	0.328(3)	0.2326(16)	0.393(4)	
H(12)A	0.130(3)	0.2459(16)	0.255(4)	

Table 5.6B Coordinates of Refined Atoms and Equivalent Isotropic Thermal Parameters ($Å^2$) for Molecule B of *O*-[*commo*-3,3'-Fe-4-SMe_2-4'-SMe-1,1',2,2'-$(C_2B_9H_{10})_2$], *O*-[Fe(carb')($C_2B_9H_{10}$SMe)], **(9)**

	x	y	z	Ueq
Fe(33')B	0.71621(4)	0.37332(2)	-0.13408(5)	0.0278(4)
S(')B	0.54371(8)	0.29464(4)	-0.18671(11)	0.0447(7)
SB	0.87660(9)	0.31513(4)	0.10922(12)	0.0551(8)
C(')B	0.4996(4)	0.24150(18)	-0.2823(5)	0.062(4)
C(11)B	0.9215(4)	0.31228(20)	0.2849(4)	0.069(4)
C(12)B	0.9730(4)	0.3356(3)	0.0701(6)	0.105(5)
C(1')B	0.6264(3)	0.37242(15)	-0.3253(4)	0.032(3)
C(2')B	0.7219(3)	0.39547(17)	-0.3198(4)	0.038(3)
B(4')B	0.6364(3)	0.31654(17)	-0.2507(4)	0.032(3)
B(5')B	0.6036(4)	0.32361(19)	-0.4263(5)	0.040(3)
B(6')B	0.6553(4)	0.37468(19)	-0.4701(5)	0.041(3)
B(7')B	0.8081(4)	0.35879(20)	-0.2422(5)	0.040(3)
B(8')B	0.7567(3)	0.30603(18)	-0.1988(5)	0.038(3)
B(9')B	0.6876(4)	0.28112(19)	-0.3513(5)	0.042(3)
B(10')B	0.6979(4)	0.31615(21)	-0.4833(5)	0.051(4)
B(11')B	0.7733(4)	0.36445(22)	-0.4169(5)	0.050(4)
B(12')B	0.7938(4)	0.30672(20)	-0.3437(5)	0.046(4)
C(1)B	0.6835(3)	0.35895(17)	0.0407(4)	0.040(3)
C(2)B	0.6249(3)	0.40227(16)	-0.0399(4)	0.037(3)
B(4)B	0.7941(4)	0.36866(18)	0.0650(5)	0.037(3)
B(5)B	0.7416(4)	0.37771(21)	0.1926(5)	0.050(4)
B(6)B	0.6317(4)	0.39818(23)	0.1211(5)	0.054(4)
B(7)B	0.6910(4)	0.44537(19)	-0.0795(5)	0.043(3)
B(8)B	0.8049(4)	0.42574(18)	-0.0075(5)	0.039(3)
B(9)B	0.8185(4)	0.42177(19)	0.1656(5)	0.046(4)
B(10)B	0.7172(4)	0.44024(21)	0.1990(5)	0.055(4)
B(11)B	0.6386(4)	0.45455(21)	0.0464(5)	0.053(4)
B(12)B	0.7535(4)	0.46910(21)	0.0750(5)	0.051(4)
H(1')B	0.584(3)	0.3943(17)	-0.331(4)	
H(2')B	0.720(3)	0.4263(17)	-0.312(4)	
H(5')B	0.537(3)	0.3163(16)	-0.474(4)	
H(6')B	0.622(3)	0.4043(16)	-0.543(4)	
H(7')B	0.875(3)	0.3738(15)	-0.204(4)	
H(8')B	0.787(3)	0.2769(16)	-0.130(4)	
H(9')B	0.679(3)	0.2403(17)	-0.357(4)	
H(10')B	0.693(3)	0.3042(16)	-0.569(4)	
H(11')B	0.817(3)	0.3832(15)	-0.456(4)	
H(12')B	0.855(3)	0.2854(15)	-0.341(4)	
H(1)B	0.662(3)	0.3337(18)	0.045(5)	
H(2)B	0.564(3)	0.3980(16)	-0.090(4)	
H(5)B	0.758(3)	0.3522(16)	0.275(4)	
H(6)B	0.575(3)	0.3836(15)	0.147(4)	
H(7)B	0.666(3)	0.4653(15)	-0.172(4)	
H(8)B	0.868(3)	0.4392(16)	-0.018(4)	
H(9)B	0.886(3)	0.4280(15)	0.227(4)	
H(10)B	0.716(3)	0.4566(15)	0.287(4)	
H(11)B	0.580(3)	0.4761(16)	0.033(4)	
H(12)B	0.776(3)	0.5055(17)	0.073(4)	

Table 5.7A Interatomic Distances (Å) in Molecule A of *O*-[*commo*-3,3'-Fe-4-SMe_2-4'-SMe-1,1',2,2'-$(C_2B_9H_{10})_2$], *O*-[Fe(carb')$(C_2B_9H_{10}SMe)$], **(9)**

Fe(33') - C(1')	2.103(4)	B(9') - H(9')	0.97(5)
Fe(33') - C(2')	2.107(5)	B(10')-B(11')	1.760(8)
Fe(33') - B(4')	2.155(5)	B(10')-B(12')	1.769(8)
Fe(33') - B(7')	2.131(5)	B(10')-H(10')	0.97(4)
Fe(33') - B(8')	2.155(5)	B(11')-B(12')	1.765(8)
Fe(33') - C(1)	2.121(4)	B(11')-H(11')	0.98(5)
Fe(33') - C(2)	2.119(5)	B(12')-H(12')	1.13(4)
Fe(33') - B(4)	2.126(5)	C(1) - C(2)	1.602(6)
Fe(33') - B(7)	2.143(5)	C(1) - B(4)	1.667(7)
Fe(33') - B(8)	2.161(5)	C(1) - B(5)	1.701(7)
S(') - C(')	1.815(5)	C(1) - B(6)	1.728(7)
S(') - B(4')	1.849(5)	C(1) - H(1)	0.80(5)
S - C(11)	1.812(6)	C(2) - B(6)	1.705(7)
S - C(12)	1.775(6)	C(2) - B(7)	1.684(7)
S - B(4)	1.924(5)	C(2) - B(11)	1.695(7)
C(1') - C(2')	1.595(6)	C(2) - H(2)	0.91(5)
C(1') - B(4')	1.707(6)	B(4) - B(5)	1.788(7)
C(1') - B(5')	1.684(7)	B(4) - B(8)	1.793(7)
C(1') - B(6')	1.717(7)	B(4) - B(9)	1.799(8)
C(1') - H(1')	1.00(5)	B(5) - B(6)	1.756(8)
C(2') - B(6')	1.707(7)	B(5) - B(9)	1.782(8)
C(2') - B(7')	1.674(7)	B(5) -B(10)	1.756(8)
C(2') -B(11')	1.674(8)	B(5) - H(5)	0.98(4)
C(2') - H(2')	0.80(5)	B(6) -B(10)	1.767(8)
B(4') - B(5')	1.790(7)	B(6) -B(11)	1.762(8)
B(4') - B(8')	1.802(7)	B(6) - H(6)	1.04(5)
B(4') - B(9')	1.788(7)	B(7) - B(8)	1.789(8)
B(5') - B(6')	1.762(8)	B(7) -B(11)	1.775(8)
B(5') - B(9')	1.754(8)	B(7) -B(12)	1.770(8)
B(5') -B(10')	1.765(8)	B(7) - H(7)	0.97(4)
B(5') - H(5')	1.06(4)	B(8) - B(9)	1.803(8)
B(6') -B(10')	1.767(8)	B(8) -B(12)	1.797(8)
B(6') -B(11')	1.750(8)	B(8) - H(8)	1.04(4)
B(6') - H(6')	1.09(4)	B(9) -B(10)	1.774(8)
B(7') - B(8')	1.825(8)	B(9) -B(12)	1.752(8)
B(7') -B(11')	1.779(8)	B(9) - H(9)	1.03(4)
B(7') -B(12')	1.801(8)	B(10) -B(11)	1.767(8)
B(7') - H(7')	1.09(4)	B(10) -B(12)	1.770(8)
B(8') - B(9')	1.797(7)	B(10) -H(10)	1.00(4)
B(8') -B(12')	1.809(8)	B(11) -B(12)	1.752(8)
B(8') - H(8')	1.09(4)	B(11) -H(11)	1.04(4)
B(9') -B(10')	1.765(8)	B(12) -H(12)	1.02(4)
B(9') -B(12')	1.765(8)		

Table 5.7B Interatomic Distances (Å) in Molecule B of *O*-[*commo*-3,3'-Fe-4-SMe_2-4'-SMe-1,1',2,2'-$(C_2B_9H_{10})_2$], *O*-[Fe(carb')$(C_2B_9H_{10}SMe)$], **(9)**

Fe(33') - C(1')	2.107(4)	B(9') -H(9')	1.13(4)
Fe(33') - C(2')	2.095(5)	B(10')-B(11')	1.775(8)
Fe(33') - B(4')	2.150(5)	B(10')-B(12')	1.789(8)
Fe(33') - B(7')	2.109(5)	B(10')-H(10')	0.95(5)
Fe(33') - B(8')	2.133(5)	B(11')-B(12')	1.758(8)
Fe(33') - C(1)	2.102(5)	B(11')-H(11')	1.03(5)
Fe(33') - C(2)	2.110(5)	B(12')-H(12')	1.11(4)
Fe(33') - B(4)	2.117(5)	C(1) - C(2)	1.590(6)
Fe(33') - B(7)	2.134(5)	C(1) - B(4)	1.674(7)
Fe(33') - B(8)	2.171(5)	C(1) - B(5)	1.688(8)
S(') - C(')	1.800(5)	C(1) - B(6)	1.713(8)
S(') - B(4')	1.856(5)	C(1) - H(1)	0.78(5)
S - C(11)	1.799(6)	C(2) - B(6)	1.690(8)
S - C(12)	1.751(7)	C(2) - B(7)	1.697(7)
S - B(4)	1.917(5)	C(2) - B(11)	1.688(8)
C(1') - C(2')	1.592(6)	C(2) - H(2)	0.94(5)
C(1') - B(4')	1.717(6)	B(4) - B(5)	1.789(8)
C(1') - B(5')	1.694(7)	B(4) - B(8)	1.780(7)
C(1') - B(6')	1.726(7)	B(4) - B(9)	1.787(8)
C(1') - H(1')	0.88(5)	B(5) - B(6)	1.742(8)
C(2') - B(6')	1.731(7)	B(5) - B(9)	1.779(8)
C(2') - B(7')	1.686(7)	B(5) -B(10)	1.768(8)
C(2') -B(11')	1.704(8)	B(5) - H(5)	1.10(5)
C(2') - H(2')	0.86(5)	B(6) -B(10)	1.772(9)
B(4') - B(5')	1.800(7)	B(6) -B(11)	1.761(9)
B(4') - B(8')	1.804(7)	B(6) - H(6)	1.07(5)
B(4') - B(9')	1.793(7)	B(7) - B(8)	1.789(8)
B(5') - B(6')	1.745(8)	B(7) -B(11)	1.773(8)
B(5') - B(9')	1.758(8)	B(7) -B(12)	1.774(8)
B(5') -B(10')	1.745(8)	B(7) - H(7)	1.09(5)
B(5') - H(5')	1.03(5)	B(8) - B(9)	1.797(8)
B(6') -B(10')	1.762(8)	B(8) -B(12)	1.797(8)
B(6') -B(11')	1.769(8)	B(8) - H(8)	1.07(5)
B(6') - H(6')	1.14(5)	B(9) -B(10)	1.777(8)
B(7') - B(8')	1.779(8)	B(9) -B(12)	1.754(8)
B(7') -B(11')	1.787(8)	B(9) - H(9)	1.07(5)
B(7') -B(12')	1.770(8)	B(10) -B(11)	1.769(8)
B(7') - H(7')	1.08(5)	B(10) -B(12)	1.766(8)
B(8') - B(9')	1.801(7)	B(10) -H(10)	1.04(5)
B(8') -B(12')	1.794(8)	B(11) -B(12)	1.759(8)
B(8') - H(8')	1.10(4)	B(11) -H(11)	1.05(5)
B(9') -B(10')	1.749(8)	B(12) -H(12)	1.06(5)
B(9') -B(12')	1.767(8)		

Table 5.8A Selected Interbond Angles (°) in Molecule A of *O*-[*commo* -3,3'-Fe-4-SMe_2-4'-SMe-1,1',2,2'-$(C_2B_9H_{10})_2$], *O*-[Fe(carb')$(C_2B_9H_{10}SMe)$], **(9)**

C(1')	- Fe(33')- C(2')	44.54(17)	C(2')	- B(6') - B(11')	57.9(3)
C(1')	- Fe(33')- B(4')	47.25(17)	B(5')	- B(6') - B(10')	60.0(3)
C(2')	- Fe(33')- B(7')	46.53(19)	B(10')	- B(6') - B(11')	60.0(3)
B(4')	- Fe(33')- B(8')	49.43(19)	Fe(33')	- B(7') - C(2')	65.97(24)
B(7')	- Fe(33')- B(8')	50.39(20)	Fe(33')	- B(7') - B(8')	65.48(24)
C(1)	- Fe(33')- C(2)	44.39(17)	C(2')	- B(7') - B(11')	57.9(3)
C(1)	- Fe(33')- B(4)	46.25(18)	B(8')	- B(7') - B(12')	59.8(3)
C(1')	- Fe(33')- C(1)	125.70(17)	B(11')	- B(7') - B(12')	59.1(3)
C(1')	- Fe(33')- C(2)	96.46(17)	Fe(33')	- B(8') - B(4')	65.29(22)
C(2')	- Fe(33')- C(1)	166.69(18)	Fe(33')	- B(8') - B(7')	64.13(23)
C(2')	- Fe(33')- C(2)	122.86(18)	B(4')	- B(8') - B(9')	59.6(3)
C(2)	- Fe(33')- B(7)	46.53(18)	B(7')	- B(8') - B(12')	59.4(3)
B(4)	- Fe(33')- B(8)	49.45(20)	B(9')	- B(8') - B(12')	58.6(3)
B(7)	- Fe(33')- B(8)	49.11(20)	B(4')	- B(9') - B(5')	60.7(3)
C(')	- S(') - B(4')	104.59(22)	B(4')	- B(9') - B(8')	60.3(3)
C(11)	- S - C(12)	100.4(3)	B(5')	- B(9') - B(10')	60.2(3)
C(11)	- S - B(4)	107.72(24)	B(8')	- B(9') - B(12')	61.0(3)
C(12)	- S - B(4)	102.52(25)	B(10')	- B(9') - B(12')	60.2(3)
Fe(33')	- C(1') - C(2')	67.87(23)	B(5')	- B(10') - B(6')	59.8(3)
Fe(33')	- C(1') - B(4')	67.99(22)	B(5')	- B(10') - B(9')	59.6(3)
C(2')	- C(1') - B(6')	61.9(3)	B(6')	- B(10') - B(11')	59.5(3)
B(4')	- C(1') - B(5')	63.7(3)	B(9')	- B(10') - B(12')	59.9(3)
B(5')	- C(1') - B(6')	62.4(3)	B(11')	- B(10') - B(12')	60.0(3)
Fe(33')	- C(2') - C(1')	67.58(23)	C(2')	- B(11') - B(6')	59.7(3)
Fe(33')	- C(2') - B(7')	67.50(25)	C(2')	- B(11') - B(7')	57.9(3)
C(1')	- C(2') - B(4')	62.6(3)	B(6')	- B(11') - B(10')	60.5(3)
B(6')	- C(2') - B(11')	62.4(3)	B(7')	- B(11') - B(12')	61.1(3)
B(7')	- C(2') - B(11')	64.2(3)	B(10')	- B(11') - B(12')	60.3(3)
Fe(33')	- B(4') - S(')	112.37(23)	B(7')	- B(12') - B(8')	60.7(3)
Fe(33')	- B(4') - C(1')	64.76(21)	B(7')	- B(12') - B(11')	59.8(3)
Fe(33')	- B(4') - B(8')	65.28(22)	B(8')	- B(12') - B(9')	60.4(3)
S(')	- B(4') - C(1')	120.1(3)	B(9')	- B(12') - B(10')	59.9(3)
S(')	- B(4') - B(5')	114.9(3)	B(10')	- B(12') - B(11')	59.7(3)
S(')	- B(4') - B(8')	130.4(3)	Fe(33')	- C(1) - C(2)	67.77(22)
S(')	- B(4') - B(9')	124.4(3)	Fe(33')	- C(1) - B(4)	67.04(23)
C(1')	- B(4') - B(5')	57.5(3)	C(2)	- C(1) - B(6)	61.4(3)
B(5')	- B(4') - B(9')	58.7(3)	B(4)	- C(1) - B(5)	64.1(3)
B(8')	- B(4') - B(9')	60.1(3)	B(5)	- C(1) - B(6)	61.6(3)
C(1')	- B(5') - B(4')	58.8(3)	Fe(33')	- C(2) - C(1)	67.85(22)
C(1')	- B(5') - B(6')	59.7(3)	Fe(33')	- C(2) - B(6)	67.48(23)
B(4')	- B(5') - B(9')	60.6(3)	C(1)	- C(2) - B(11)	62.9(3)
B(6')	- B(5') - B(10')	60.1(3)	B(6)	- C(2) - B(11)	62.4(3)
B(9')	- B(5') - B(10')	60.2(3)	B(7)	- C(2) - B(11)	63.4(3)
C(1')	- B(6') - C(2')	55.5(3)	Fe(33')	- B(4) - S	115.65(24)
C(1')	- B(6') - B(5')	57.9(3)	Fe(33')	- B(4) - C(1)	66.72(23)

Fe(33')- B(4) - B(8)	66.29(24	Fe(33')- B(8) - B(7)	64.93(24)
S - B(4) - C(1)	119.2(3)	B(4) - B(8) - B(9)	60.0(3)
S - B(4) - B(5)	109.6(3)	B(7) - B(8) - B(12)	59.1(3)
S - B(4) - B(8)	130.5(3)	B(9) - B(8) - B(12)	58.2(3)
S - B(4) - B(9)	118.6(3)	B(4) - B(9) - B(5)	59.9(3)
C(1) - B(4) - B(5)	58.9(3)	B(4) - B(9) - B(8)	59.7(3)
B(5) - B(4) - B(9)	59.5(3)	B(5) - B(9) - B(10)	59.2(3)
B(8) - B(4) - B(9)	60.3(3)	B(8) - B(9) - B(12)	60.7(3)
C(1) - B(5) - B(4)	57.0(3)	B(10) - B(9) - B(12)	60.3(3)
C(1) - B(5) - B(6)	60.0(3)	B(5) - B(10) - B(6)	59.8(3)
B(4) - B(5) - B(9)	60.5(3)	B(5) - B(10) - B(9)	60.6(3)
B(6) - B(5) - B(10)	60.4(3)	B(6) - B(10) - B(11)	59.8(3)
B(9) - B(5) - B(10)	60.2(3)	B(9) - B(10) - B(12)	59.2(3)
C(1) - B(6) - C(2)	55.6(3)	B(11) - B(10) - B(12)	59.4(3)
C(1) - B(6) - B(5)	58.4(3)	C(2) - B(11) - B(6)	59.0(3)
C(2) - B(6) - B(11)	58.5(3)	C(2) - B(11) - B(7)	58.0(3)
B(5) - B(6) - B(10)	59.8(3)	B(6) - B(11) - B(10)	60.1(3)
B(10) - B(6) - B(11)	60.1(3)	B(7) - B(11) - B(12)	60.2(3)
Fe(33')- B(7) - C(2)	65.99(23)	B(10) - B(11) - B(12)	60.4(3)
Fe(33')- B(7) - B(8)	65.96(24)	B(7) - B(12) - B(8)	60.2(3)
C(2) - B(7) - B(11)	58.6(3)	B(7) - B(12) - B(11)	60.5(3)
B(8) - B(7) - B(12)	60.7(3)	B(8) - B(12) - B(9)	61.1(3)
B(11) - B(7) - B(12)	59.3(3)	B(9) - B(12) - B(10)	60.5(3)
Fe(33')- B(8) - B(4)	64.25(23)	B(10) - B(12) - B(11)	60.2(3)

Table 5.8B Selected Interbond Angles (°) in Molecule B of *O*-[*commo*-3,3'-Fe-4-SMe_2-4'-SMe-1,1',2,2'-$(C_2B_9H_{10})_2$], *O*-[Fe(carb')$(C_2B_9H_{10}SMe)$], **(9)**

C(1')	- Fe(33')- C(2')	44.54(17)	C(2')	- B(6') - B(11')	58.3(3)
C(1')	- Fe(33')- B(4')	47.58(17)	B(5')	- B(6') - B(10')	59.7(3)
C(1')	- Fe(33')- C(1)	126.37(17)	B(10')	- B(6') - B(11')	60.3(3)
C(1')	- Fe(33')- C(2)	96.84(17)	Fe(33')	- B(7') - C(2')	65.92(24)
C(2')	- Fe(33')- B(7')	47.28(19)	Fe(33')	- B(7') - B(8')	65.90(24)
C(2')	- Fe(33')- C(1)	167.58(18)	C(2')	- B(7') - B(11')	58.7(3)
C(2')	- Fe(33')- C(2)	123.70(17)	B(8')	- B(7') - B(12')	60.7(3)
B(4')	- Fe(33')- B(8')	49.81(19)	B(11')	- B(7') - B(12')	59.2(3)
B(7')	- Fe(33')- B(8')	49.60(20)	Fe(33')	- B(8') - B(4')	65.59(22)
C(1)	- Fe(33')- C(2)	44.37(18)	Fe(33')	- B(8') - B(7')	64.50(24)
C(1)	- Fe(33')- B(4)	46.76(19)	B(4')	- B(8') - B(9')	59.6(3)
C(2)	- Fe(33')- B(7)	47.14(19)	B(7')	- B(8') - B(12')	59.4(3)
B(4)	- Fe(33')- B(8)	49.03(19)	B(9')	- B(8') - B(12')	58.9(3)
B(7)	- Fe(33')- B(8)	49.09(20)	B(4')	- B(9') - B(5')	60.9(3)
C(')	- S(') - B(4')	105.26(23)	B(4')	- B(9') - B(8')	60.2(3)
C(11)	- S - C(12)	99.3(3)	B(5')	- B(9') - B(10')	59.7(3)
C(11)	- S - B(4)	108.55(24)	B(8')	- B(9') - B(12')	60.4(3)
C(12)	- S - B(4)	104.2(3)	B(10')	- B(9') - B(12')	61.2(3)
Fe(33')	- C(1') - C(2')	67.34(22)	B(5')	- B(10') - B(6')	59.7(3)
Fe(33')	- C(1') - B(4')	67.53(21)	B(5')	- B(10') - B(9')	60.4(3)
C(2')	- C(1') - B(6')	62.7(3)	B(6')	- B(10') - B(11')	60.0(3)
B(4')	- C(1') - B(5')	63.7(3)	B(9')	- B(10') - B(12')	59.9(3)
B(5')	- C(1') - B(6')	61.4(3)	B(11')	- B(10') - B(12')	59.1(3)
Fe(33')	- C(2') - C(1')	68.12(22)	C(2')	- B(11') - B(6')	59.7(3)
Fe(33')	- C(2') - B(7')	66.79(24)	C(2')	- B(11') - B(7')	57.7(3)
C(1')	- C(2') - B(6')	62.4(3)	B(6')	- B(11') - B(10')	59.6(3)
B(6')	- C(2') - B(11')	62.0(3)	B(7')	- B(11') - B(12')	59.9(3)
B(7')	- C(2') - B(11')	63.6(3)	B(10')	- B(11') - B(12')	60.8(3)
Fe(33')	- B(4') - S(')	113.52(23)	B(7')	- B(12') - B(8')	59.9(3)
Fe(33')	- B(4') - C(1')	64.89(21)	B(7')	- B(12') - B(11')	60.9(3)
Fe(33')	- B(4') - B(8')	64.60(22)	B(8')	- B(12') - B(9')	60.8(3)
S(')	- B(4') - C(1')	119.0(3)	B(9')	- B(12') - B(10')	58.9(3)
S(')	- B(4') - B(5')	113.7(3)	B(10')	- B(12') - B(11')	60.0(3)
S(')	- B(4') - B(8')	132.2(3)	Fe(33')	- C(1) - C(2)	68.07(23)
S(')	- B(4') - B(9')	124.3(3)	Fe(33')	- C(1) - B(4)	67.09(24)
C(1')	- B(4') - B(5')	57.5(3)	C(2)	- C(1) - B(6)	61.4(3)
B(5')	- B(4') - B(9')	58.6(3)	B(4)	- C(1) - B(5)	64.3(3)
B(8')	- B(4') - B(9')	60.1(3)	B(5)	- C(1) - B(6)	61.6(3)
C(1')	- B(5') - B(4')	58.8(3)	Fe(33')	- C(2) - C(1)	67.57(23)
C(1')	- B(5') - B(6')	60.2(3)	Fe(33')	- C(2) - B(7)	67.18(24)
B(4')	- B(5') - B(9')	60.5(3)	C(1)	- C(2) - B(6)	62.9(3)
B(6')	- B(5') - B(10')	60.7(3)	B(6)	- C(2) - B(11)	62.9(3)
B(9')	- B(5') - B(10')	59.9(3)	B(7)	- C(2) - B(11)	63.2(3)
C(1')	- B(6') - C(2')	54.9(3)	Fe(33')	- B(4) - S	116.0(3)
C(1')	- B(6') - B(5')	58.4(3)	Fe(33')	- B(4) - C(1)	66.16(24)

Fe(33')- B(4) - B(8)	67.05(24)	Fe(33')- B(8) - B(7)	64.39(24)
S - B(4) - C(1)	119.5(3)	B(4) - B(8) - B(9)	60.0(3)
S - B(4) - B(5)	109.6(3)	B(7) - B(8) - B(12)	59.3(3)
S - B(4) - B(8)	130.2(3)	B(9) - B(8) - B(12)	58.4(3)
S - B(4) - B(9)	118.1(3)	B(4) - B(9) - B(5)	60.2(3)
C(1) - B(4) - B(5)	58.2(3)	B(4) - B(9) - B(8)	59.6(3)
B(5) - B(4) - B(9)	59.7(3)	B(5) - B(9) - B(10)	59.6(3)
B(8) - B(4) - B(9)	60.5(3)	B(8) - B(9) - B(12)	60.8(3)
C(1) - B(5) - B(4)	57.5(3)	1(0) - B(9) - B(12)	60.0(3)
C(1) - B(5) - B(6)	59.9(3)	B(5) - B(10) - B(6)	58.9(3)
B(4) - B(5) - B(9)	60.1(3)	B(5) - B(10) - B(9)	60.2(3)
B(6) - B(5) - B(10)	60.6(3)	B(6) - B(10) - B(11)	59.7(3)
B(9) - B(5) - B(10)	60.1(3)	B(9) - B(10) - B(12)	59.4(3)
C(1) - B(6) - C(2)	55.7(3)	B(11) - B(10) - B(12)	59.7(3)
C(1) - B(6) - B(5)	58.5(3)	C(2) - B(11) - B(6)	58.6(3)
C(2) - B(6) - B(11)	58.5(3)	C(2) - B(11) - B(7)	58.7(3)
B(5) - B(6) - B(10)	60.4(3)	B(6) - B(11) - B(10)	60.3(3)
B(10) - B(6) - B(11)	60.1(3)	B(7) - B(11) - B(12)	60.3(3)
Fe(33')- B(7) - C(2)	65.68(24)	B(10) - B(11) - B(12)	60.1(3)
Fe(33')- B(7) - B(8)	66.52(24)	B(7) - B(12) - B(8)	60.1(3)
C(2) - B(7) - B(11)	58.1(3)	B(7) - B(12) - B(11)	60.2(3)
B(8) - B(7) - B(12)	60.6(3)	B(8) - B(12) - B(9)	60.8(3)
B(11) - B(7) - B(12)	59.5(3)	B(9) - B(12) - B(10)	60.6(3)
Fe(33')- B(8) - B(4)	63.92(23)	B(10) - B(12) - B(11)	60.2(3)

Table 5.9A Anisotropic Thermal Parameters ($Å^2$) for Molecule A of *O*-[*commo* -3,3'-Fe-4-SMe_2-4'-SMe-1,1',2,2'-$(C_2B_9H_{10})_2$], *O*-[Fe(carb')($C_2B_9H_{10}$SMe)], **(9)**

	U11	U22	U33	U23	U13	U12
Fe(33')A	0.0275(4)	0.0293(4)	0.0277(3)	0.0008(3)	0.0099(3)	0.0023(3)
S(')A	0.0330(7)	0.0430(7)	0.0372(6)	-0.0020(5)	0.0054(5)	0.0086(5)
SA	0.0366(7)	0.0415(7)	0.0582(7)	-0.0058(6)	0.0226(6)	-0.0058(5)
C(')A	0.0458(31)	0.0462(31)	0.0620(31)	-0.0029(24)	0.0116(25)	0.0136(23)
C(11)A	0.0579(36)	0.0725(39)	0.0917(41)	-0.0012(31)	0.0520(33)	-0.0120(28)
C(12)A	0.0503(34)	0.0781(41)	0.0922(45)	0.0066(34)	0.0051(31)	-0.0117(30)
C(1')A	0.0349(27)	0.0324(27)	0.0402(25)	-0.0006(20)	0.0182(22)	-0.0020(21)
C(2')A	0.0453(29)	0.0427(29)	0.0331(24)	0.0081(24)	0.0139(22)	0.0083(25)
B(4')A	0.0265(27)	0.0350(29)	0.0321(26)	-0.0039(22)	0.0099(23)	0.0002(23)
B(5')A	0.0437(34)	0.0416(33)	0.0439(30)	-0.0104(25)	0.0210(27)	0.0011(26)
B(6')A	0.0610(39)	0.0467(34)	0.0381(29)	0.0014(26)	0.0267(29)	0.0061(30)
B(7')A	0.0323(32)	0.0585(37)	0.0330(28)	-0.0028(26)	0.0056(25)	0.0057(28)
B(8')A	0.0300(30)	0.0457(33)	0.0302(26)	-0.0091(24)	0.0079(23)	-0.0052(24)
B(9')A	0.0371(32)	0.0385(33)	0.0377(28)	-0.0053(25)	0.0113(25)	0.0044(26)
B(10')A	0.0519(36)	0.0623(39)	0.0317(29)	-0.0051(26)	0.0191(27)	0.0055(29)
B(11')A	0.0570(39)	0.0603(40)	0.0346(30)	0.0113(27)	0.0109(29)	0.0108(30)
B(12')A	0.0392(33)	0.0631(39)	0.0326(28)	-0.0128(27)	0.0063(26)	-0.0064(29)
C(1)A	0.0365(28)	0.0346(28)	0.0297(23)	0.0020(20)	0.0135(21)	0.0059(21)
C(2)A	0.0307(25)	0.0422(29)	0.0344(24)	-0.0039(20)	0.0075(22)	-0.0049(22)
B(4)A	0.0314(30)	0.0311(29)	0.0373(27)	-0.0033(23)	0.0117(24)	0.0011(23)
B(5)A	0.0551(38)	0.0445(37)	0.0337(28)	-0.0021(24)	0.0251(28)	-0.0017(27)
B(6)A	0.0587(38)	0.0456(36)	0.0369(30)	-0.0061(26)	0.0220(29)	-0.0055(29)
B(7)A	0.0430(32)	0.0274(30)	0.0443(30)	0.0015(24)	0.0198(26)	0.0006(24)
B(8)A	0.0443(33)	0.0377(32)	0.0379(30)	0.0000(25)	0.0144(27)	0.0099(26)
B(9)A	0.0425(34)	0.0464(36)	0.0536(34)	-0.0090(27)	0.0290(29)	0.0038(28)
B(10)A	0.0637(40)	0.0461(36)	0.0486(33)	-0.0067(27)	0.0290(31)	0.0033(29)
B(11)A	0.0540(36)	0.0359(33)	0.0451(31)	-0.0144(26)	0.0207(28)	-0.0071(27)
B(12)A	0.0635(40)	0.0412(36)	0.0530(33)	-0.0007(27)	0.0286(31)	0.0138(30)

Table 5.9B Anisotropic Thermal Parameters ($Å^2$) for Molecule B of *O*-[*commo*-3,3'-Fe-4-SMe_2-4'-SMe-1,1',2,2'-$(C_2B_9H_{10})_2$], *O*-[Fe(carb')$(C_2B_9H_{10}SMe)$], **(9)**

	U11	U22	U33	U23	U13	U12
Fe(33')B	0.0282(4)	0.0265(4)	0.0261(3)	-0.0006(2)	0.0070(3)	-0.0013(3)
S(')B	0.0392(7)	0.0471(7)	0.0449(6)	-0.0043(5)	0.0150(6)	-0.0141(6)
SB	0.0596(8)	0.0457(8)	0.0466(7)	0.0014(6)	-0.0116(6)	0.0099(6)
C(')B	0.0628(33)	0.0530(33)	0.0633(33)	-0.0050(26)	0.0132(28)	-0.0281(27)
C(11)B	0.0689(38)	0.0677(38)	0.0534(32)	0.0102(28)	-0.0174(29)	0.0017(30)
C(12)B	0.0596(41)	0.1670(69)	0.0829(45)	0.0368(46)	0.0197(34)	0.0452(44)
C(1')B	0.0290(27)	0.0344(28)	0.0291(22)	0.0076(19)	0.0078(21)	0.0028(19)
C(2')B	0.0464(29)	0.0345(26)	0.0298(23)	0.0030(21)	0.0162(21)	-0.0009(23)
B(4')B	0.0328(29)	0.0299(29)	0.0309(26)	-0.0002(22)	0.0072(23)	0.0000(23)
B(5')B	0.0378(32)	0.0482(35)	0.0298(27)	-0.0056(24)	0.0048(25)	0.0000(26)
B(6')B	0.0454(35)	0.0479(36)	0.0263(26)	-0.0027(24)	0.0102(26)	0.0026(26)
B(7')B	0.0297(31)	0.0481(34)	0.0400(29)	-0.0005(25)	0.0131(26)	-0.0014(26)
B(8')B	0.0361(30)	0.0331(30)	0.0409(29)	-0.0059(25)	0.0085(25)	0.0050(24)
B(9')B	0.0475(34)	0.0370(32)	0.0390(28)	-0.0093(25)	0.0159(26)	-0.0047(26)
B(10')B	0.0562(37)	0.0602(39)	0.0324(29)	-0.0097(27)	0.0170(28)	-0.0010(30)
B(11')B	0.0494(37)	0.0606(38)	0.0383(30)	-0.0069(27)	0.0221(29)	-0.0095(29)
B(12')B	0.0426(33)	0.0490(35)	0.0446(31)	-0.0032(26)	0.0187(27)	0.0098(28)
C(1)B	0.0435(30)	0.0435(29)	0.0300(23)	0.0032(23)	0.0129(22)	-0.0117(24)
C(2)B	0.0345(26)	0.0426(28)	0.0314(23)	-0.0007(21)	0.0104(21)	0.0008(22)
B(4)B	0.0392(32)	0.0354(31)	0.0313(27)	0.0028(22)	0.0017(25)	-0.0023(24)
B(5)B	0.0594(39)	0.0567(39)	0.0304(29)	-0.0044(26)	0.0103(28)	-0.0051(29)
B(6)B	0.0535(37)	0.0664(41)	0.0396(30)	-0.0148(28)	0.0210(29)	-0.0048(32)
B(7)B	0.0509(36)	0.0353(32)	0.0374(29)	-0.0028(25)	0.0124(27)	0.0043(26)
B(8)B	0.0323(31)	0.0398(32)	0.0401(30)	-0.0012(24)	0.0091(25)	-0.0054(25)
B(9)B	0.0507(36)	0.0417(34)	0.0370(30)	-0.0060(25)	-0.0003(28)	-0.0101(28)
B(10)B	0.0681(41)	0.0545(38)	0.0377(31)	-0.0122(28)	0.0137(30)	0.0002(31)
B(11)B	0.0594(39)	0.0519(38)	0.0445(32)	-0.0161(27)	0.0206(30)	0.0100(30)
B(12)B	0.0679(40)	0.0351(33)	0.0423(31)	-0.0128(26)	0.0107(30)	-0.0055(29)

Table 5.10 Calculated Hydrogen Atom Coordinates in *O*-[*commo*-3,3'-Fe-4-SMe_2-4'-SMe-1,1',2,2'-$(C_2B_9H_{10})_2$], *O*-[Fe(carb')$(C_2B_9H_{10}SMe)$], **(9)**

Molecule A

	x	y	z
H(A1)	0.5208	-0.0142	0.2731
H(A2)	0.5072	0.0084	0.1135
H(A3)	0.4193	-0.0249	0.1482
H(A4)	0.0672	0.0370	0.4087
H(A5)	-0.0269	0.0168	0.2819
H(A6)	-0.0115	0.0794	0.3169
H(A7)	0.0094	0.0693	-0.0395
H(A8)	-0.0340	0.1023	0.0707
H(A9)	-0.0606	0.0403	0.0421

Molecule B

	x	y	z
H(B1)	0.4325	0.2343	-0.2750
H(B2)	0.5439	0.2118	-0.2390
H(B3)	0.4971	0.2451	-0.3842
H(B4)	0.8709	0.2987	0.3279
H(B5)	0.9459	0.3470	0.3279
H(B6)	0.9770	0.2869	0.3034
H(B7)	0.9441	0.3339	-0.0350
H(B8)	1.0276	0.3097	0.1002
H(B9)	0.9985	0.3717	0.0981

The ligating faces of the two carbaboranes are rotated by *ca.* 23^{o} with respect to one another about the vector connecting their centres of gravity. This is, of course, nearer to a fully staggered situation (36^{o}) than fully eclipsed (0^{o}).

The chief features of molecules *A* and *B* of **(9)** are highly similar, and therefore will be discussed together, the values of each parameter for molecule *A* given first, with those for *B* in parentheses.

The Fe(33') atom sits almost symmetrically above the 5 atom open face of the [carb']$^{-}$ ligand, with the slip parameter, Δ = 0.04Å [0.01Å], and the metal a perpendicular distance of 1.564Å [1.555Å] from the [C_2B_3] face. These distances are approximately 0.06Å longer than the corresponding distances in **(8)**, where the central Fe atom is formally in the +II oxidation state, which is a little surprising.

The [carb']$^{-}$ ligand in both molecules *A* and *B* is folded about the B(4')...B(7') vector, as is the case in the majority of complexes of this type, giving fold parameters of θ = 2.55^{o} [2.93^{o}] and ϕ = 0.64^{o} [0.42^{o}].

The Fe atom is again reasonably symmetrically disposed with respect to the ligating [C_2B_3] face of the [SMe-$C_2B_9H_{10}$]$^{2-}$ cage, with Δ = 0.03Å [0.06Å]. The iron atom is closer to the ligating face of this ligand than to that of the [carb']$^{-}$, at a perpendicular distance of 1.548Å [1.536Å].

This [C_2B_3] face is folded similarly to that of the [carb']$^{-}$ ligand, about B(4)...B(7), resulting in fold angles of θ = 3.13^{o} [1.55^{o}] and ϕ = 0.12^{o} [0.27^{o}].

The SMe_2 and SMe substituents on the ligands are depressed from their preferred elevation angles of 26^{o} to 17.5^{o} [17.5^{o}] and 22.7^{o} [21.7^{o}] respectively. In the case of the SMe_2 group, this rather large depression can be traced to steric

crowding between HA7 [HB7] of the C12A [C12B] methyl group and H7'A [H7'B] on the SMe-substituted cage. Specifically, HA7..H7'A = 2.27Å and HB7..H7'B = 2.11Å, rendering unattainable an orientation of the SMe_2 function such as that observed in **(3)**, **(4)**, **(5)** and (6) (see earlier).

The situation involving the SMe substituent is rather more difficult to explain than that for the dimethylsulphide group. As is obvious from **Figure 5.6**, the sulphur atom of the SMe group lies between the two C-H's of the [carb'] ligand opposite. This might then be expected to result in lone pair..$H^{\delta+}$ attractive interactions of the type described in Chapters 3 & 4, leading to an elevation angle for the SMe substituent of greater than the preferred 26^{o}. This is not observed, however, although it is of note that the elevation angle is greater for the SMe function than for the SMe_2 group.

Electrochemical Study on (9)

Introduction

The electrochemical study on **(9)** was performed in order to find the position of the $Fe^{III/II}$ couple relative to the $Fe^{II/III}$ couple in the bis[carb'] species, **(8)**. This was also carried out using the experimental set-up shown in **Figure 6.4.1**.

Results and Discussion

Cyclic voltammetry (c.v.), alternating current voltammetry (a.c.v.) and linear stirred voltammetry (s.v.) at a platinum electrode in CH_2Cl_2/0.5M [TBA]BF_4 at 273K show that **(9)** undergoes a reversible reduction ($Fe^{III/II}$) at +0.305V with respect to the Ag/AgCl electrode. The cyclic and a.c. voltammograms for **(9)** are

shown in **Figure 5.7**.

The position of this couple illustrates the greater degree of stabilisation afforded to the Fe^{III} oxidation state by the ligand set in **(9)** than by that in **(8)**. This is unsurprising, in that the ligands in **(9)** have a total nominal charge of 3^-, and therefore might be expected to stabilise Fe^{III} species more efficiently than the nominally 2^- ligand set in the $Fe(carb')_2$ and $FeCp_2$ systems.

Reaction of (9) with $[Me_3O]BF_4$

Introduction

In order to determine a possible mechanism for the formation of **(9)** from the intended preparation of $Fe(carb')_2$, **(8)**, an investigation of its reaction with a source of $\{Me^+\}$, $[Me_3O]BF_4$, was carried out, using electrochemical techniques to follow the course of the reaction.

Results and Discussion

A quantity of the complex was dissolved in CH_2Cl_2/0.5M $[TBA]BF_4$ and to this was added excess $[Me_3O]BF_4$. Cyclic voltammetry and linear stirred voltammetry at a platinum electrode, using the equipment and methods described in Chapter 6, section 4 show a reversible reduction at +0.57V with respect to the Ag/AgCl reference electrode. The potential of this couple is identical to that of the $Fe^{II/III}$ couple observed for an authentic sample of $Fe(carb')_2$. A reduction was also observed at +0.16V w.r.t. Ag/AgCl, corresponding to that of the excess $[Me_3O]^+$ species.

Figure 5.7 Cyclic and a.c. Voltammograms for **(9)**

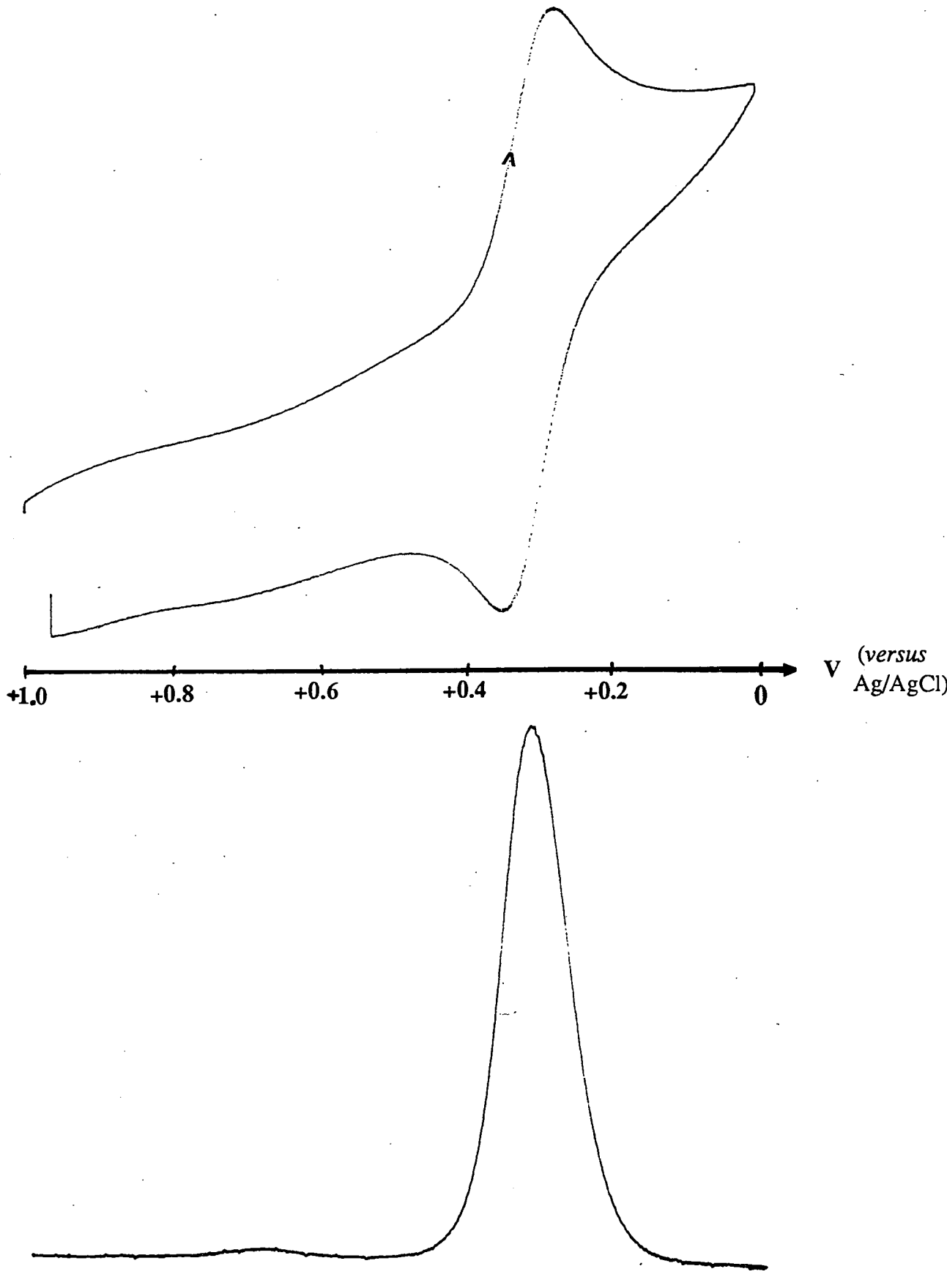

The suggestion of this finding is that complex **(9)** reacts with $\{Me^+\}$ to form $[Fe(carb')_2]^+$, which undergoes a reversible reduction at +0.57V *versus* Ag/AgCl to form **(8)**.

By application of the law of microscopic reversibility, this suggests that a possible mechanism for the formation of **(9)** is by loss of $\{Me^+\}$ from $[Fe(carb')_2]^+$, itself presumably a product of aerial oxidation of **(8)** during the extended period of aerobic work-up of the reaction mixture. It is, however, notable that there is no evidence for expulsion of $\{Me^+\}$ from the chemically or electrochemically prepared samples of $[Fe(carb')_2]^+$ discussed previously, and therefore the implication is that the *particular* conditions in the sole preparation which led to the isolation of **(9)** were also in some way responsible for its formation.

A final important point arising from this result is that, assuming the proposed mechanism for formation of **(9)** is correct, this suggests that the major (not structurally characterised) isomer of **(8)** from the first method of synthesis (Method 1, see Chapter 6, section 1) is of the same isomer type (*odd*, *O*) as the major (structurally characterised) isomer of **(9)**. This, in turn, means that the two synthetic methods devised for **(8)** do not yield identical products, the first giving predominantly the *O* isomer, whereas the second method, involving Tl[carb'], gives solely the *E* isomer, as determined by *X*-ray structural analysis. Presumably there is only a slight thermodynamic difference between formation of the two isomers, and the observed results are directed by kinetic, as well as these thermodynamic factors.

Spectroelectrochemical Study on (9)

Results and Discussion

A spectroelectrochemical study was carried out upon **(9)** in CH_2Cl_2/0.5M [TBA]BF_4, using techniques described in Chapter 6, section 4.

The progression of spectra obtained is presented in **Figure 5.8**, showing the growth of the band at 40000cm^{-1} and collapse of the band at 33300cm^{-1} as the Fe^{III} species is reduced to an Fe^{II} one. The isosbestic point in the spectral progression indicates that the conversion occurs directly, *i.e.* without involvement of an intermediate species, as is perfectly reasonable for a simple $Fe^{III/II}$ reduction.

Application of the Nernst equation to the experimental data (see Chapter 6, section 4) affords a value for the reduction potential of +0.325 $\pm$ 0.009V, in reasonable agreement with the value obtained from a.c. voltammetry (see earlier). This analysis also yields a value for **n**, the number of electrons transferred per molecule, of 1.09 $\pm$ 0.21e^-, thus confirming the 1-electron nature of the process.

Also observed in the progression of spectra were weaker ("d-d") bands at lower frequency than for the charge-transfer bands described above. Both oxidised and reduced species show (at least) one of these weak bands, which shift to higher energy (to *ca.* 17500cm^{-1} from *ca.* 13500cm^{-1}) on reduction of the Fe^{III} complex to the anionic Fe^{II} species. The shift to higher energy of the "d-d" band(s) is consistent with full occupation of the slightly bonding levels (Fe^{II} in a *pseudo* -octahedral environment).

Figure 5.8 Electronic Spectra Showing Conversion of **(9)** to $[(9)]^-$

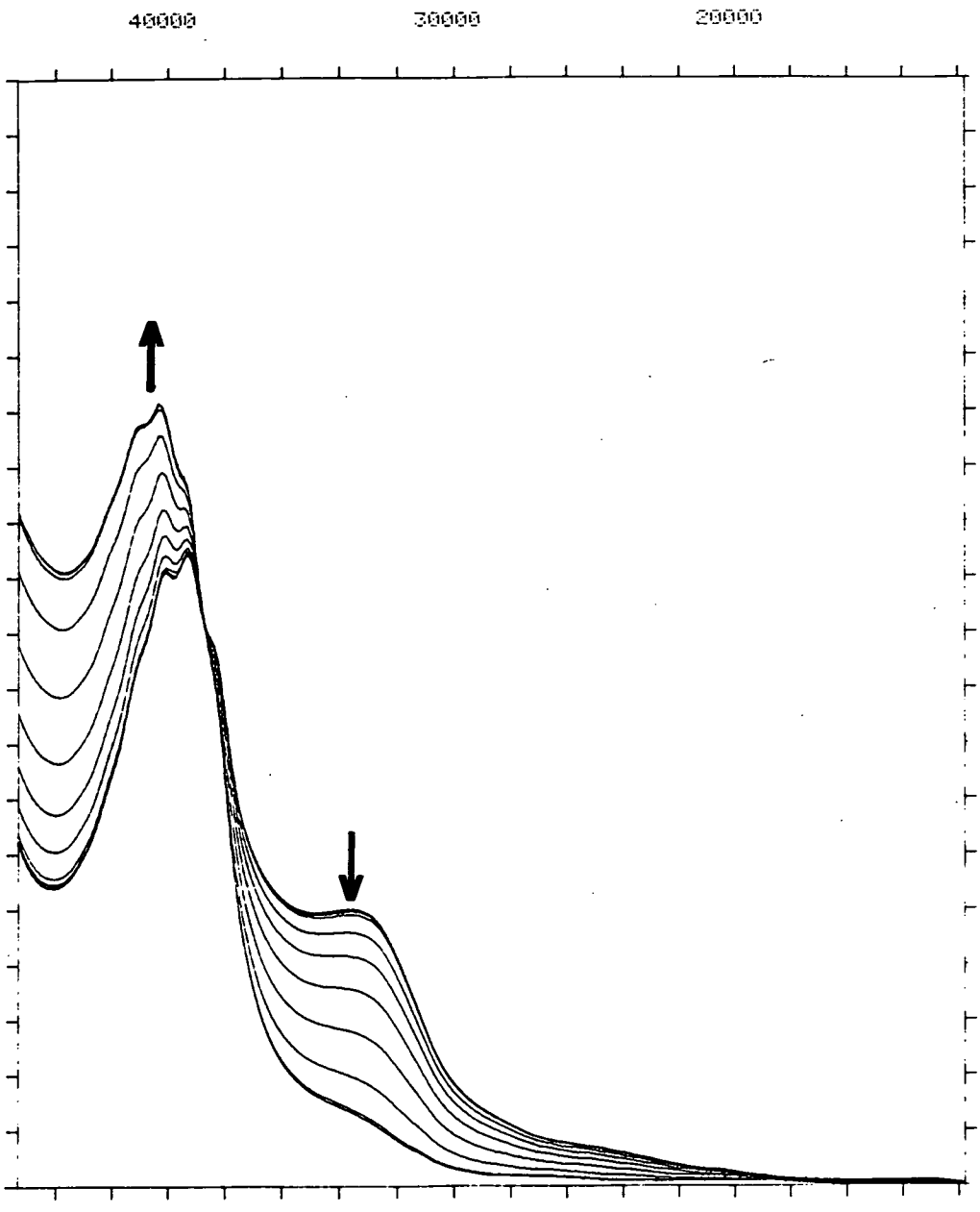

Conclusions

The bis(carb') analogue of ferrocene, $Fe(carb')_2$, **(8)**, has been structurally characterised as the *E* isomer, in which both (chiral) carbaborane ligands have the same handedness. The overall isomeric nature of $Fe(carb')_2$ has been shown to be dependent on the synthetic route employed.

Electrochemical study of **(8)** again shows the net electron-donating properties of [carb'] to be comparable to those of Cp. $Fe(carb')_2$ may be readily oxidised by electrochemical or chemical means to give the monocation $[Fe(carb')_2]^+$.

A second product, $Fe(carb')(C_2B_9H_{10}SMe)$, **(9)**, was also isolated, and structurally characterised as the *O*-isomer. This, allied to the results of electrochemical work, allow a mechanism for the formation of **(9)** to be proposed, involving loss of $\{Me^+\}$ from $[Fe(carb')_2]^+$.

Chapter 6

Experimental

Introduction

This chapter details the experimental procedures leading to the results described in the body of the text. For ease of reference, the chapter comprises 4 sections, each concerned with a particular branch of the work, *viz*:

Section 1 gives details of the synthetic methods employed in preparation of the compounds discussed. Also included in this section are spectral and microanalytical data for each complex.

Section 2 describes the crystallographic techniques employed in determination of the structures of complexes **(1)** to **(9)**, presented in Chapters 2-5.

Section 3 comprises idealised models used in extended Hückel and extended Hückel/fragment molecular orbital calculations, along with (where appropriate) non-default orbital parameters employed.

Section 4 gives experimental details of the electrochemical and spectroelectrochemical studies presented in Chapter 5.

Section 1: Synthetic Methods and Spectral Data

General Techniques

All reactions were carried out under an atmosphere of dry, oxygen-free nitrogen using standard Schlenk techniques, with some subsequent manipulations in the air.

Dichloromethane, tetrahydrofuran, ethanol and n-hexane were dried and distilled immediately prior to use, other solvents were used as received.

Infra-red spectra were recorded as KBr discs or solutions (referenced against the appropriate solvent) on a Perkin-Elmer 598 spectrophotometer.

N.m.r. spectra were recorded at ambient temperature (unless otherwise specified) on Bruker WP360 (^{11}B, ^{11}B(COSY), ^{11}B-{^{1}H} and ^{1}H-{^{11}B}), Bruker WP200SY (^{11}B, ^{11}B-{^{1}H}, ^{1}H and ^{13}C), Bruker WY80SY (^{1}H) and Jeol FX90 (^{31}P) spectrometers. Techniques for recording ^{1}H-{^{11}B selective} and ^{11}B(COSY) spectra have been published previously [89-91]. Chemical shifts are reported relative to external $SiMe_4$ (^{1}H, ^{13}C), BF_3OEt_2 (^{11}B) and 85% H_3PO_4 (^{31}P), positive shifts to high frequency.

Starting Materials

The starting materials $K[C_2B_9H_{12}]$ [35], $Tl[TlC_2B_9H_{11}]$ [92], PPh_3AuCl [93], $[PPh_3CuBr]_4$ [94], $Mn(CO)_5Br$ [95] and $[Mn(CO)_3(NCMe)_3]BPh_4$ [96] were prepared by published methods. All other materials used are commercially available and were used as supplied.

[BTMA][7,8-$C_2B_9H_{12}$], [BTMA](1)

Synthesis

To a solution of K[7,8-$C_2B_9H_{12}$] (0.129g, 0.75mmol) in H_2O (8ml) was added an aqueous solution (6ml) of [BTMA]Br (0.178g, 0.75mmol). The resulting precipitate was filtered off and washed with H_2O (2 x 15ml) then a little Et_2O. The colourless solid produced was crystallised by slow diffusion of n-hexane into a dichloromethane solution at -30°C.

Microanalysis

CALCULATED (for $C_{12}H_{28}B_9N$) 50.81%C 9.95%H 4.94%N FOUND 50.2%C 9.87%H 4.78%N

N.m.r. Data/p.p.m. ($CDCl_3$)

^{1}H δ 7.50-7.65 (5H, C_6H_5), 4.43 (2H, CH_2), 3.13 (9H, CH_3), 1.90 (br, 2H, CH)

^{11}B-{^{1}H} δ -10.38 [B(9),B(11)], -16.46 [B(3),B(5),B(6)], -21.29 [B(2),B(4)], -32.54 [B(10)], -37.17 [B(1)]

^{1}H-{^{11}B selective} δ 1.94 [H(9),H(11)], 1.77 [H(3)], 1.26 [H(2),H(4)], 1.24 [H(5),H(6)], 0.55 [H(1)], 0.11 [H(10)], -0.26 [H(12)]

[dmsoH.dmso][7,8-$C_2B_9H_{12}$], [dmsoH.dmso](1)

Synthesis

To a solution of K[7,8-$C_2B_9H_{12}$] (1.7959g, 10.41mmol) and dimethylsulphoxide (3.2059g, 41.04mmol) in H_2O (15ml) at 0°C was added dropwise conc. H_2SO_4 (10.5ml) over a period of *ca.* 30 minutes. A colourless solid product formed which was left overnight, after which time it was filtered from the mixture. The solid was dried *in vacuo*, then crystallised by slow diffusion of n-hexane into a

dichloromethane solution at -30°C, yielding large crystals. Yield = 70%.

Microanalysis

CALCULATED (for $C_6H_{25}B_9S_2O_2$) 24.8%C 8.67%H FOUND 24.1%C 8.53%H

N.m.r.Data/p.p.m. ($CDCl_3$)

^{1}**H** δ 6.5-7.0 (v. br, solvated H^+), 2.73 (12H, CH_3), 1.88 (br, 2H, CH)

^{11}**B-{^{1}H}** As for [BTMA](1)

[BTMA][10-*endo*-(PPh_3)Au-7,8-*nido*-$C_2B_9H_{11}$]$^-$, [BTMA](2)

Synthesis

To a mixture of solid Tl[Tl-7,8-$C_2B_9H_{11}$] (0.2466g, 0.489mmol), PPh_3AuCl (0.2422, 0.490mmol) and [$PhCH_2NMe_3$]Cl (0.0908g, 0.489mmol) in a foil-covered vessel was added dichloromethane (10ml) with stirring. The reaction mixture was stirred overnight, then filtered and reduced to dryness *in vacuo* to give a pale orange microcrystalline solid. The compound was purified by slow diffusion of n-hexane into a dichloromethane solution at -30°C, giving colourless needle-shaped crystals. Yield = 45%.

Microanalysis

CALCULATED (for $C_{30}H_{42}B_9NPAu.CH_2Cl_2$) 45.03%C 5.36%H 1.69%N FOUND 44.6%C 5.31%H 1.83%N

N.m.r. Data/p.p.m. (CD_2Cl_2)

^{1}**H** δ 7.40-7.75 (20H, C_6H_5), 4.41 (2H, CH_2), 3.05 (9H, CH_3)

^{11}**B-{^{1}H}** δ -16.19 (3B), -17.85 (2B), -21.94 (1B), -22.62 (2B), -35.94 (1B)

^{31}**P** δ 41.3

Infra-red Data (KBr Disc)

ν_{max} (cm^{-1}) 2540 (B-H)

[10,11-μ-H-9-SMe_2-7,8-$C_2B_9H_{10}$], carb'H, (3)

Synthesis

(3) was prepared by a modified version of a published method [6]. Dimethylsulphoxide (2.1451g, 27.5mmol) was added to 6.9ml of a 1M aqueous solution of K[7,8-$C_2B_9H_{12}$] and to this mixture was added conc. H_2SO_4 (10ml) dropwise with stirring over a period of *ca.* 45 minutes, taking care not to allow the temperature of the mixture to exceed 30°C. The mixture was left to stand overnight, after which time two layers were visible. The top layer, containing the product, was extracted into dichloromethane (4 x 20ml). Removal of the solvent from this extract *in vacuo* gave an off-white solid, carb'H, **(3)**. Yield = 50%.

Microanalysis

CALCULATED (for $C_4H_{17}B_9S$) 24.70%C 8.81%H FOUND 24.30%C 8.92%H

N.m.r. Data/p.p.m. ($(CD_3)_2CO$)

^{1}**H** δ 2.87 (CH_3), 2.74 (CH_3), 2.77 (CH), 2.07 (CH), -3.25 (br, B-H-B)

^{11}**B-{^{1}H}** δ -3.33, -6.46[B(9)], -10.71, -15.71, -17.45, -22.44, -25.60, -28.70, -35.67

Tl[9-SMe_2-7,8-$C_2B_9H_{10}$], Tl[carb']

Synthesis

To a solution of carb'H , **(3)**, (0.3006g, 1.545mmol) in dimethylsulphoxide (8ml) was added dropwise a solution of KOH (0.5268g, 9.37mmol) in H_2O (8ml). After a few minutes, when the reaction mixture had cooled, a solution of thallous acetate (0.4702g, 1.78mmol) in H_2O (10ml) was added, giving a dull yellow

precpitate which was collected by filtration and washed with Et_2O (4 x 15ml). Yield = 93%.

[10,11-μ-PPh_3Au-9-SMe_2-7,8-$C_2B_9H_{10}$], PPh_3Au(carb'), (4)

Synthesis

To a suspension of Tl[carb'] (0.1111g, 0.279mmol) in dichloromethane (5ml) in a foil-covered vessel was added a solution of PPh_3AuCl (0.1381g, 0.279mmol) in CH_2Cl_2 (10ml). The mixture was stirred overnight then filtered through Celite filter-aid to give an orange solution, the colour of which is presumably due to a minor Au^{III} co-product. Crystallisation by slow diffusion of n-hexane into a dichloromethane solution at -30°C yielded diffraction quality colourless crystals of the dichloromethane solvate of **(4)**. Yield = 70%.

Microanalysis

CALCULATED (for $C_{22}H_{31}B_9PSAu$) 37.45%C 4.51%H FOUND 37.6%C 4.56%H

N.m.r. Data/p.p.m. (CD_2Cl_2)

^{1}**H** δ 7.4-7.7 (15H, C_6H_5), 2.39 (3H, CH_3), 2.35 (3H, CH_3)

^{11}**B-{^{1}H}** δ -10.31 [1B,B(9)], -14.20 [1B], -16.72 [2B], -17.80 [1B], -18.35 [1B], -21.12 [1B], -23.55 [1B], -35.57 [1B]

^{31}**P** δ 41.0 (br)

Infra-red Data (KBr Disc)

ν_{max} (cm^{-1}) 2540 (B-H), 535 (Au-P)

[3-PPh_3-4-SMe_2-3,1,2-$CuC_2B_9H_{10}$], PPh_3Cu(carb'), (5)

Synthesis

To a suspension of Tl[carb'] (0.4045g, 1.12mmol) in dichloromethane (5ml) in a foil-covered vessel was added a suspension of $[PPh_3CuBr]_4$ (0.4545g, 0.28mmol) in CH_2Cl_2 (10ml) with stirring. The mixture was stirred overnight then filtered to give a colourless solution. Removal of the solvent *in vacuo* gave an off-white solid. Crystallisation was by means of slow diffusion of n-hexane into a dichloromethane solution at -30°C. Yield = 75%.

Microanalysis

CALCULATED (for $C_{22}H_{31}B_9PSCu$) 50.88%C 6.02%H FOUND 50.6%C 6.13%H

N.m.r. Data/p.p.m. (CD_2Cl_2)

^{1}**H** δ 7.20-7.75 (C_6H_5), 2.33 (CH_3), 2.24 (CH_3), 2.26 (CH), 2.01 (CH)

^{11}**B-{^{1}H}** δ -15.37 [2B], -18.14 [1B], -19.54 [1B], -20.12 [1B], -21.71 [1B], -22.51 [2B], -33.66 [1B]

^{31}**P** δ 9.78 (br), -4.54 (br)

[3,3,3-$(CO)_3$-4-SMe_2-3,1,2-$MnC_2B_9H_{10}$], (carb')$Mn(CO)_3$, (6)

Synthesis

Finely ground KOH (0.1385g, 2.47mmol) and carb'H (0.0910g, 0.47mmol) were stirred in CH_2Cl_2 (10ml) for 15 minutes, after which time was added dropwise a solution/suspension of $[Mn(CO)_3(NCMe)_3]BPh_4$ (0.2731g, 0.47mmol) in CH_2Cl_2 (15ml) over a period of 20 minutes. The colour of the mixture changed from light yellow to orange, and a light coloured flocculate formed; stirring was continued

overnight. The mixture was filtered to give an orange solution which was reduced to dryness *in vacuo*. Redissolution in the minimum of CH_2Cl_2 followed by preparative t.l.c. (Kieselgel 60 F_{254}, CH_2Cl_2) gave a mobile yellow band (R_f 0.80) which was identified as the target product. A second mobile band (orange, R_f 0.68) was also collected. Yield of **(6)** = 30%.

Microanalysis

CALCULATED (for $C_7H_{16}B_9O_3SMn$) 25.3%C 4.85%H FOUND 25.5%C 4.72%H

N.m.r.Data/p.p.m (CD_2Cl_2)

^{1}**H** δ 2.72 (CH_3), 2.50 (CH_3)

^{11}**B-{^{1}H}** δ -0.73, -4.05 [B(4)], -7.13, -7.97, -11.69, -13.07, -17.44, -19.77, -25.23

^{13}**C** δ 221.9 (CO)

Infra-red Data (KBr Disc)

ν_{max} (cm^{-1}) 2525 (B-H), 2020, 1950 and 1925 (all C-O)

Infra-red Data for Orange Co-product (CH_2Cl_2 solution)

ν_{max} (cm^{-1}) 2540 (s, B-H), 2015 (w, Mn-H), 1937 and 1865 (both s, C-O)

(η-C_5H_5)Mn(CO)$_3$, CpMn(CO)$_3$, (7)

Synthesis

The complex was prepared in an analogous manner to that published for the syntheses of fluorenyl and indenyl derivatives of manganese tricarbonyl [81].

$Mn(CO)_5Br$ (1.1163g, 4.06mmol) and $Tl[C_5H_5]$ (1.0943g, 4.06mmol) were placed in a foil-covered vessel fitted with a dropping funnel. Tetrahydrofuran

(THF) (25ml) was added dropwise with stirring and the mixture was stirred for 3 days at room temperature. The resulting brown mixture was filtered and evaporated to dryness *in vacuo*. Redissolution in the minimum amount of dichloromethane followed by elution (CH_2Cl_2) through a Florisil column (20 x 2cm) gave two bands, the first, a fast-moving yellow band, being collected. The solvent was removed *in vacuo* to give a yellow solid, which was crystallised by slow diffusion of n-hexane into a CH_2Cl_2 solution at -30°C. Yield = 34%.

Microanalysis

CALCULATED (for $C_8H_5O_3Mn$) 47.09%C 2.47%H FOUND 46.30%C 2.35%H

N.m.r. Data/p.p.m. ($CDCl_3$)

^{1}**H** δ 4.75 (C_5H_5)

^{13}**C** δ 225.0 (CO), 83.0 (C_5H_5)

Infra-red Data (KBr Disc)

ν_{max} (cm^{-1}) 2910-2840 (C-H), 2025, 1945 (both C-O)

[*commo*-3,3'-Fe-4,4'-$(SMe_2)_2$-1,1',2,2',-$(C_2B_9H_{10})_2$], Fe(carb')$_2$, (8)

Synthesis (Method 1)

Finely ground KOH (0.1570g, 2.80mmol) was dissolved/suspended in dimethylsulphoxide (10ml) and to this was added dropwise a solution of carb'H (0.1035, 0.53mmol) in dmso (10ml). After *ca.* 5 minutes a solution of $FeCl_2.4H_2O$ (0.0557g, 0.26mmol) in dmso (8ml), giving an immediate purple colouration to the mixture. Stirring was continued for a further 10 minutes, after which time the mixture was poured into ice/2M HCl to afford a pink/purple solid material which was collected by filtration and dried *in vacuo*. Preparative t.l.c. (Kieselgel 60

F_{254}, CH_2Cl_2) gave 2 mobile pink bands, with R_f values 0.80 and 0.75. The highest R_f (major) band was collected, but the minor band was present in insufficient amount for further study. Yield of major band of **(8)** = 37%.

Microanalysis

CALCULATED (for $C_8H_{32}B_{18}S_2Fe$) 21.70%C 7.28%H FOUND 21.90%C 7.53%H

N.m.r. Data/p.p.m. ($(CD_3)_2CO$)

^{1}H δ 2.82 (CH_3), 2.86 (CH_3)

^{11}B-{^{1}H} δ -2.56 [2B, B(4),B(4')], -4.02 [2B], -7.76 [4B], -9.75 [2B], -13.30 [2B], -19.40 [2B], -23.18 [2B], -25.48 [2B]

^{1}H-{^{11}B selective} δ 2.59, 2.47, 2.42, 1.65, 1.54, 1.19, 1.35, 1.37

Synthesis (Method 2)

Solid Tl[carb'] (0.2995g, 0.753mmol) and $FeCl_2.4H_2O$ (0.0471g, 0.376mmol) were placed in a foil-covered vessel and to this was added dichloromethane (10ml) with stirring. A pink colouration formed and stirring was continued for 1 hour. Filtration followed by reduction in volume *in vacuo* gave a pink/purple oil, which was solidified by trituration with Et_2O. Preparative t.l.c. (Kieselgel 60 F_{254}, CH_2Cl_2) gave only 1 mobile pink band (R_f 0.80) which was collected from the silica with CH_2Cl_2, and the solvent removed *in vacuo*. Yield = 30%. Crystals suitable for *X*-ray analysis were grown by slow diffusion of n-hexane into a dichloromethane solution at -30°C.

Oxidation of (8) by $FeCl_3$

To a solution of Fe(carb')$_2$, **(8)**, in dichloromethane was added excess $FeCl_3$, with stirring, giving an immediate colour change from pink/purple to deep red/brown. Stirring was continued for a few minutes, after which the mixture was filtered to remove excess $FeCl_3$ and the $FeCl_2$ by-product. The deep red product was identified as [**(8)**]$FeCl_4$ by electrochemical methods (see section 4 of this chapter).

Similar colour changes (indicative of formation of the Fe^{III} oxidation state) occur on reaction of **(8)** with other inorganic oxidants such as $AgBF_4$, $AgPF_6$ and Cl_2, although the species formed by these reactions were not further characterised.

[*commo*-3,3'-Fe-4-SMe_2-4'-SMe-1,1',2,2'-($C_2B_9H_{10}$)$_2$], Fe(carb')($C_2B_9H_{10}$SMe), (9)

Synthesis

To a solution/suspension of finely ground KOH (0.4186g, 7.46mmol) in dimethylsulphoxide (10ml) was added dropwise a solution of carb'H (0.2434g, 1.25mmol) in dmso (10ml). After a few minutes, a solution of $FeCl_2.4H_2O$ (0.1246g, 0.627mmol) in dmso (5ml) was added dropwise, giving a purple solution. Addition of this solution to ice/2M HCl gave a pink solid which slowly became more brown in colour whilst being collected by filtration. Redissolution in the minimum of CH_2Cl_2 followed by preparative t.l.c. (Kieselgel 60 F_{254}, CH_2Cl_2) gave 4 mobile bands, in the order Brown (major) (R_f 0.87), Pink (major) (R_f 0.74), Brown (minor) (R_f 0.68) and Pink (minor) (R_f 0.63). The first two (major) bands were collected and identified as **(9)** and Fe(carb')$_2$, **(8)**. The minor bands were present in insufficient quantities for further study. Yield of **(9)** = 42%.

Microanalysis

CALCULATED (for $C_7H_{29}B_{18}S_2Fe$) 19.65%C 6.83%H FOUND 20.0%C 6.98%H

N.m.r. Data/p.p.m. ($(CD_3)_2CO$)

^{1}H δ -0.50 (3H, CH_3), -3.32 (3H, CH_3), -8.25 (3H,CH_3)

δ 127.09, 93.18, 81.17, 49.90, 32.08, 24.44 (all 1H, v.br, B-H$_{facial}$)

δ 38.82, 36.90, 34.58, 33.06, -11.8, -25.8 (all 1H, br, unassigned B-H, C-H)

^{11}B-{^{1}H} δ 108.33, 94.99, 50.97, 26.10, 20.75, 16.52, 9.46, 7.68, 2.33, -4.44, -34.42, -52.44, -322.07 (v. br), -379.10 (v. br), -385.59 (v. br), -435.63 (v. br), -462.44 (v. br), -491.7 (v. br)

^{1}H-{^{11}B selective} (for 12 non-facial B-H) δ -25.7, -6.9, 0.6, -3.6, -4.6, -11.9, 3.4, 2.2, -1.8, 1.5, 38.2, 36.9

Reaction of (9) with $[Me_3O]BF_4$

To a solution of **(9)** in CH_2Cl_2/0.5M $[TBA]BF_4$ was added excess $[Me_3O]BF_4$, and the mixture was well shaken. Electrochemical studies on this solution (see section 4 of this chapter), confirm that the reaction taking place is a sulphur-methylation of **(9)** to give **$[(8)]^+$**.

Section 2: Crystallographic Techniques

This section describes the experimental procedures involved in data collection and processing, and structure solution and refinement for each of the structures presented in the main body of the work. All data were collected on an Enraf-Nonius CAD4 diffractometer, fitted with a ULT-1 low-temperature device. Diffraction quality crystals of all complexes were grown by slow diffusion of n-hexane into dichloromethane solutions at -30^{0}C.

Data were corrected for Lorentz and polarisation effects, and (where necessary) for decay during data reduction (*CADABS* [97]). Heavy atoms were located by automatic direct methods (*SHELX86* [98]) or by inspection of a Patterson map (*SHELX76* [99]), see individual complexes. Subsequent atom location was by Δ_F syntheses and iterative full-matrix least-squares refinement [99]. Scattering factors for C, H, B, S, P, N, O and Cl were those inlaid in the programs. Those for Au, Cu, Mn and Fe were from *International Tables for X-ray Crystallography* [100].

After isotropic convergence, data were corrected empirically for absorption [101]. Geometrical calculations were performed using *CALC* [66] and the molecular drawing facility used was *EASYORTEP* [102], a modification of *ORTEP-II* [103].

The isotropic thermal parameter takes the form $\exp[-8\pi^2 U(\sin^2\theta)/\lambda^2]$

For anisotropic thermal parameters Uij = $\exp[-2\pi^2(U11a^{*2}h^2 + U22b^{*2}k^2 + U33c^{*2}l^2 + 2U23b^*c^*kl + 2U13a^*c^*hl + 2U12a^*b^*hk)]$

The equivalent isotropic thermal parameter is defined as Ueq = $[\Sigma_i\Sigma_j Uija_i^* a_j^* \mathbf{a}_i.\mathbf{a}_j]/3$

[BTMA][7,8-$C_2B_9H_{12}$], [BTMA](1)

Crystal Data

$C_{12}H_{28}B_9N$, M = 283.65, triclinic, space group $P\bar{1}$, a = 11.833(5), b = 11.915(5), c = 13.723(7)Å, α = 110.692(15), β = 91.954(13), γ = 93.480(13)^0, V = 1803.5Å^3, by the least-squares refinement of 25 centred reflections, $11<\theta<12^0$, Z = 4 ion pairs, D_c = 1.045 gcm^{-3}, μ(Mo-$K_{\bar{\alpha}}$) = 0.49 cm^{-1}, F (000) = 608.

Data collection and processing

CAD4 diffractometer, graphite-monochromated Mo-$K_{\bar{\alpha}}$ X-radiation, $\bar{\lambda}$ = 0.71069, ω-2θ scans in 96 steps, with ω scan width 0.8 + 0.34tanθ. Variable scan speeds between 1.37 and 5.49^0 min^{-1}. 3578 unique data measured ($1<\theta<20^0$, +h $\pm$k $\pm$l) yielding 2190 with $F > 2.0\sigma(F)$. No measurable crystal decay or detectable movement.

Structure solution

All non-H atoms found by direct methods and refined with individual isotropic thermal parameters by full-matrix least-squares. Atoms of both crystallographically independent $[PhCH_2NMe_3]^+$ ions ordered. However, in both $[C_2B_9H_{12}]^-$ ions disorder noted over all 12 vertices of approximate icosahedra. Impossible to satisfactorily model disorder and unambiguously identify cage carbon atoms (all cage atoms modelled as B). Refinement terminated at R = 0.1575, unit weights.

[dmsoH.dmso][7,8-$C_2B_9H_{12}$], [dmsoH.dmso](1)

Crystal data

$C_6H_{25}B_9O_2S_2$, M = 290.66, monoclinic, space group $P2_1/n$, a = 8.2919(14), b = 11.0802(21), c = 18.128(5)Å, β = 100.135(18)°, V = 1639.5Å^3, from the least-squares refinement of 25 centred reflections ($14<\theta<15^o$) at 185±1K, Z = 4 ion pairs, D_c = 1.177 gcm^{-3}, μ(Mo-$K_{\bar{\alpha}}$) = 2.98 cm^{-1}, F(000) = 616.

Data collection and processing

CAD4 diffractometer, graphite-monochromated Mo-$K_{\bar{\alpha}}$ X-radiation, $\bar{\lambda}$ = 0.71069Å, ω-2θ scans in 96 steps, with ω scan width 0.8 + 0.34tanθ. Variable scan speeds between 0.82 and 2.35°min^{-1}. 2719 unique data measured ($1<\theta<25^o$, +h +k ±l) yielding 2355 reflections with $F > 2.0\sigma(F)$. No crystal decay or movement.

Structure solution and refinement

Direct methods for all non-H atoms. H atoms from ΔF syntheses following full-matrix least-squares refinement. Empirical absorption correction after isotropic convergence. Thereafter all non-H atoms allowed anisotropic thermal motion. H atoms positionally refined but with common isotropic thermal parameter [U = 0.0462(16)Å^2 at convergence]. Weights applied according to w^{-1} = [$\sigma^2(F)$ + 0.008711F^2]. R = 0.0436, R_w = 0.0698, S = 0.734. Max. and min. residues in final ΔF map 0.38 and 0.62 eÅ^{-3} respectively.

[BTMA][10-*endo*-(PPh_3Au)-7,8-$C_2B_9H_{11}$]$^-$, [BTMA](2)

Crystal data

$C_{30}H_{42}B_9PNAu.CH_2Cl_2$, M = 826.84, monoclinic, space group $P2_1/c$, a = 9.5509(17), b = 19.232(3), c = 19.813(3)Å, β = 90.742(13)°, V = 3639.0Å^3, from least-squares refinement of 25 centred reflections ($12<\theta<13^o$) at 291K, Z = 4, D_{calc} = 1.509 gcm^{-3}, μ(Mo-$K_{\bar{\alpha}}$) = 42.5cm^{-1}, F(000) = 1640.

Data collection and processing

CAD4 diffractometer, graphite-monochromated Mo-$K_{\bar{\alpha}}$ X-radiation, $\bar{\lambda}$ = 0.71069Å, ω-2θ scans in 96 steps, with ω scan width 0.8 + 0.34tanθ. Variable scan speeds between 1.03 and 2.75°min^{-1}. 5307 unique data measured ($1<\theta<25^o$, +h +k ±l) of which 4667 had $F > 2.0\sigma(F)$. Intensities of 2 check reflections decayed to *ca.* 89% of their original values over the period (194 hrs) of data collection, and the data were corrected appropriately.

Structure solution and refinement

Au position from Patterson synthesis, P, C, B, N, Cl, H_{cage} from full-matrix least-squares refinement/ΔF syntheses. Cage C atoms identified by combination of refined (as B) isotropic thermal parameters and interatomic distances. Phenyl rings modelled as rigid, planar hexagons (C-C 1.395Å). Cage H atoms refined positionally, all other H atoms set in fixed positions (C-H 1.08Å). Empirical absorption correction applied after isotropic convergence; therafter, all non-H atoms allowed anisotropic thermal motion, H atoms refined with common isotropic thermal parameter (U_H = 0.108Å^2 at convergence). Data weighted according to $w^{-1} = [\sigma^2(F) + 0.000513F^2]$. R = 0.0487, R_w = 0.0482, S = 1.214. Max. and min. residues in final ΔF map +0.94 (near Au) and -1.09 eÅ^{-3}.

[10,11-μ-H-9-SMe_2-7,8-$C_2B_9H_{10}$], carb'H, (3)

Crystal data

$C_4H_{17}B_9S$, M = 194.53, triclinic, space group $P\bar{1}$, a = 8.7912(14), b = 12.093(5), c = 12.5617(19)Å, α = 107.53(3), β = 101.019, γ = 106.10(3)°, V = 1167.2(8)Å^3, by the least-squares refinement of 25 centred reflections ($14<\theta<15^o$) at 291K, Z = 4, D_c = 1.107 gcm^{-3}, μ(Mo-$K_{\bar{\alpha}}$) = 2.13 cm^{-1}, F (000) = 408.

Data collection and processing

CAD4 diffractometer, graphite-monochromated Mo-$K_{\bar{\alpha}}$ X-radiation, $\bar{\lambda}$ = 0.71069Å, ω-2θ scans in 96 steps, with ω scan width 0.8 + 0.34tanθ. Variable scan speeds between 1.O3 and 3.30°min^{-1}. 4390 unique data measured ($1<\theta<25^o$, +h ±k ±l) yielding 3580 reflections with $F > 2.0\sigma(F)$. No crystal decay or detectable movement during data collection.

Structure solution and refinement

Solution obtained by combination of automatic direct methods and least-squares refinement/ΔF syntheses. Cage C atoms identified by isotropic thermal parameters (after refinement as B) and internuclear distances. All non-H atoms allowed anisotropic thermal motion. Cage H atoms positionally refined, methyl H's treated as part of rigid groups (giving sensible S-C-H angles). All H atoms given a common isotropic thermal parameter, U_H = 0.095(16)Å^2 at convergence. Weighting scheme w^{-1} = [$\sigma^2(F)$ + 0.00002F^2]. R = 0.0480, R_w = 0.0650, S = 1.714. Max. and min. residues in final ΔF synthesis 0.522 and -0.233 eÅ^{-3}.

[10,11-μ-(PPh_3Au)-9-SMe_2-7,8-$C_2B_9H_{10}$], PPh_3Au(carb'), (4)

Crystal data

$C_{22}H_{31}B_9AuPS.CH_2Cl_2$, M = 737.72, monoclinic, space group $P2_1/a$, a = 15.323(6), b = 12.291(3), c = 17.023(11)Å, β = 112.45(4)°, V = 2962.8Å^3, from least-squares refinement of 25 centred reflections ($14<\theta<15^o$) at 185±1K, Z = 4, D_c = 1.654 gcm^{-3}, μ(Mo-$K_{\bar{\alpha}}$) = 52.73 cm^{-1}, F(000) = 1440.

Data collection and processing

CAD4 diffractometer, graphite-monochromated Mo-$K_{\bar{\alpha}}$ X-radiation, $\bar{\lambda}$ = 0.71069Å, ω-2θ scans in 96 steps, with ω scan width 0.8 + 0.34tanθ. Variable scan speeds between 1.10 and 2.75°min^{-1}. 5704 independent reflections measured ($1<\theta<25^o$, +h +k ±l), yielding 4710 with $F > 2.0\sigma(F)$. No crystal movement or decay noted.

Structure solution and refinement

Au position from Patterson synthesis; P, S, C, B, $H_{(cage)}$, Cl atoms from iterative full-matrix least-squares refinement/ΔF syntheses. Cage C atoms identified by refined (as B) isotropic thermal parameters and internuclear distances. Empirical absorption correction applied after isotropic convergence. All non-H atoms allowed anisotropic thermal motion. Phenyl C atoms treated as regular, planar hexagon (C-C = 1.395Å). Phenyl and methylene H atoms set in idealised positions. All H's refined with group thermal parameter, U_H = 0.071(4)Å^2 at convergence. Weighting scheme $w^{-1} = [\sigma^2(F) + 0.000469F^2]$. R = 0.0310, R_w = 0.0400, S = 1.179. Max. and min. residues in final ΔF map 2.38 (near Cl) and -1.29 eÅ^{-3}.

[3-PPh_3-4-SMe_2-3,1,2-$CuC_2B_9H_{10}$], PPh_3Cu(carb'), (5)

Crystal data

$C_{22}H_{31}B_9SPCu$, M = 519.36, triclinic, space group $P\bar{1}$, a = 9.100(8), b = 11.344(4), c = 14.171(7)Å, α = 66.85(3), β = 89.11(5), γ = 82.85(5)°, V = 1333.8Å^3, from the least-squares refinement of 25 centred reflections ($10<\theta<11°$) at 291K, Z = 2, D_c = 1.293 gcm^{-3}, μ(Mo-$K_{\bar{\alpha}}$) = 9.65 cm^{-1}, F (000) = 536.

Data collection and processing

CAD4 diffractometer, graphite-monochromated Mo-$K_{\bar{\alpha}}$ X-radiation, $\bar{\lambda}$ = 0.71069Å, ω-2θ scans in 96 steps, with ω scan width 0.8 + 0.34tanθ. Variable scan speeds between 0.97 and 3.30° min^{-1}. 5015 unique data measured ($1<\theta<25°$, +h ±k ±l), yielding 3748 with $F > 2.0\sigma(F)$. No crystal movement or decay noted over period of data collection.

Structure solution and refinement

Structure solved by automatic direct methods (Cu, P, S) and $F/\Delta F$ syntheses (C, B, H_{cage}). Carbaborane C atoms identified by refined (as B) isotropic thermal parameters along with interatomic distances. Phenyl rings modelled as regular hexagons, with C-C = 1.395Å. Cage and methyl hydrogens positionally refined, phenyl H's set in idealised positions, with C-H = 1.08Å. Empirical absorption correction applied after isotropic convergence. Thereafter, all non-H's allowed anisotropic thermal motion. Phenyl and carbaborane H atoms refined with group isotropic thermal parameters, 0.1096 and 0.0617Å^2 respectively at convergence. Weighting according to $w^{-1} = [\sigma^2(F) + 0.000284F^2]$. R = 0.0410, R_w = 0.0419, S = 1.289. Max. and min. residues in final ΔF map +0.35 and -0.28 eÅ^{-3}.

$[3,3,3\text{-}(CO)_3\text{-}4\text{-}SMe_2\text{-}3,1,2\text{-}MnC_2B_9H_{10}]$, (carb')$Mn(CO)_3$, (6)

Crystal data

$C_7H_{16}B_9MnO_3S$, M = 322.47, triclinic, space group $P\bar{1}$, a = 7.154(4), b = 8.7890(21), c = 13.366(3)Å, α = 91.438(19), β = 101.21(3), γ = 110.69(3)°, V = 764.5Å^3, from the least-squares refinement of 25 centred reflections ($13<\theta<15^o$) at 185±1K, Z = 2, D_c = 1.444 gcm^{-3}, μ(Mo-$K_{\bar{\alpha}}$) = 9.55 cm^{-1}, $F(000)$ = 336.

Data collection and processing

CAD4 diffractometer, graphite-monochromated Mo-$K_{\bar{\alpha}}$ X-radiation, $\bar{\lambda}$ = 0.71069Å, ω-2θ scans in 96 steps, with ω scan width 0.8 + 0.34tanθ. Variable scan speeds between 0.82 and 2.35°min^{-1}. 4814 unique data measured ($1<\theta<30^o$, +h ±k ±l) 3859 of which had $F > 2.0\sigma(F)$. No crystal decay or movement detected during data collection.

Structure solution and refinement

Mn position from Patterson synthesis, all other atoms from iterative full-matrix least-squares refinement/ΔF syntheses. Cage C atoms identified by refined (initially as B) isotropic thermal parameters and by internuclear distances. Empirical absorption correction applied after isotropic convergence. All non-H atoms then allowed anisotropic thermal motion. H atoms refined with individual isotropic thermal parameters. Weighting scheme $w^{-1} = [\sigma^2(F) + 0.000967F^2]$. R = 0.0352, R_w = 0.045, S = 1.059. Max. and min. residues in final ΔF map 0.47 and -0.53 eÅ^{-3}.

$(\eta\text{-}C_5H_5)Mn(CO)_3$, $CpMn(CO)_3$, (7)

Crystal data

$C_8H_5MnO_3$, M = 204.05, monoclinic, space group $P2_1/a$, a = 11.941(7), b = 6.981(5), c = 10.798(7)Å, β = 117.97(5)°, V = 795.03Å^3, from least-squares refinement of 25 centred reflections ($15<\theta<17^o$) at 185 ± 1K, Z = 4, D_c = 1.705 gcm^{-3}, μ(Mo-$K_{\bar{\alpha}}$) = 15.53 cm^{-1}, $F(000)$ = 408.

Data collection and processing

CAD4 diffractometer, graphite-monochromated Mo-$K_{\bar{\alpha}}$ X-radiation, $\bar{\lambda}$ = 0.71069, ω-2θ scans in 96 steps, with ω scan width 0.8 + 0.34tanθ. Variable scan speeds between 0.82 and 2.35°min^{-1}. 2591 independent reflections measured ($1<\theta<30^o$, +h +k ±l) of which 1960 had $F > 2.0\sigma(F)$.

Structure refinement

Starting point for refinement was non-H atom coordinates previously published[78]. After isotropic convergence following full-matrix least-squares refinement, empirical absorption correction applied. Thereafter all non-H atoms allowed anisotropic thermal motion. H atoms located by ΔF synthesis and all except H(8) satisfactorily refined. H(8) unstable under refinement and therefore set in fixed position. H atoms refined with common isotropic thermal parameter, U_H = 0.080(6)Å^2 at convergence. Weighting scheme $w^{-1} = [\sigma^2(F) + 0.0011057 F^2]$. R = 0.0418, R_w = 0.0600, S = 1.153. Max. and min. residues in final ΔF map 0.50 (near Mn) and -1.06 eÅ^{-3}.

E-[*commo*-3,3'-Fe-4,4'-$(SMe_2)_2$-1,1',2,2',-$(C_2B_9H_{10})_2$], *E*-[Fe(carb')$_2$], (8)

Crystal data

$C_8H_{32}B_{18}S_2Fe$, M = 442.89, monoclinic, space group $P2_1/c$, a = 12.667(3), b = 13.017(3), c = 14.193(3)Å, β = 109.08(2)°, V = 2212.41Å^3, from least-squares refinement of 25 centred reflections ($11<\theta<12°$) at 291K, Z = 4, D_c = 1.330 gcm^{-3}, μ(Mo-$K_{\bar{\alpha}}$) = 8.57 cm^{-1}, F(000) = 912.

Data collection and processing

CAD4 diffractometer, graphite-monochromated Mo-$K_{\bar{\alpha}}$ X-radiation, $\bar{\lambda}$ = 0.71069Å, ω-2θ scans in 96 steps, with ω scan width 0.8 + 0.34tanθ. Variable scan speeds between 0.82 and 2.35°min^{-1}. 8537 data measured ($1<\theta<25°$, $\pm$h +k $\pm$l), yielding 3881 having $F > 4.0\sigma(F)$. No crystal movement or decay noted.

Structure solution and refinement

Solution *via* automatic direct methods (Fe, S positions) and full-matrix least-squares refinement/ΔF syntheses. Carbaborane C atoms identified by refined (as B) isotropic thermal parameters and interatomic distances. Empirical absorption correction applied after isotropic convergence. All non-H atoms subsequently allowed anisotropic thermal motion, H atoms refined with group isotropic thermal parameter, U_H = 0.051(4)Å at convergence. B-H and (cage) C-H bonds constrained to be equal in length, and H(8') set in idealised position, after being found to be unstable under refinement. Methyl H atoms set in calculated positions. Data weighted according to $w^{-1} = [\sigma^2(F) + 0.000310F^2]$. R = 0.0830, R_w = 0.0701, S = 1.100. Max. and min. residues in final ΔF map 1.08 and -1.29 eÅ^{-3} respectively.

O-[*commo*-3,3'-Fe-4-SMe_2-4'-SMe-1,1',2,2'-$(C_2B_9H_{10})_2$], O-[Fe(carb')($C_2B_9H_{10}$SMe)], (9)

Crystal data

$C_7H_{29}B_{18}S_2Fe$, M = 427.86, monoclinic, space group $P2_1/c$, a = 15.4546(13), b = 27.532(4), c = 10.6464(13)Å, β = 106.80(1)°, V = 4336.46Å^3, from the least-squares refinement of 25 centred reflections ($14<\theta<15^o$) at 185 ± 1K, Z = 8 (2 crystallographically independent molecules), D_c = 1.311 gcm^{-3}, μ(Mo-$K_{\bar{\alpha}}$) = 8.72 cm^{-1}, F(000) = 1752.

Data collection and processing

CAD4 diffractometer, graphite-monochromated Mo-$K_{\bar{\alpha}}$ X-radiation, $\bar{\lambda}$ = 0.71069Å, ω-2θ scans in 96 steps, ω scan width 0.8 + 0.34tanθ. Variable scan speeds between 1.03 and 3.30 °min^{-1}. 4586 unique data measured ($1<\theta<20^o$, +h +k ±l), yielding 3612 having $F > 2.0\sigma(F)$. No detectable decay or crystal movement during data collection.

Structure solution and refinement

Fe and S from automatic direct methods. B, C, and H_{cage} from least-squares refinement/ΔF syntheses. Cage C atoms identified by refined (as B) isotropic thermal parameters and interatomic distances. Methyl H atoms set in fixed positions. Empirical absorption correction applied after isotropic convergence. All non-H atoms allowed anistropic thermal motion. Independent molecules refined in alternate cycles (324 variables in each cycle). H atoms within each molecule A, B refined with common isotropic thermal parameters, $U_{H(A)}$ and $U_{H(B)}$, 0.0591(24) and 0.063(3)Å^2 respectively at convergence. Weighting scheme w^{-1} = [σ^2F + 0.000288F^2]. R = 0.0378, R_w = 0.0559, S = 1.010. Max. and min.

residues in final ΔF map 0.29 and -0.30 eÅ^{-3}.

Section 3: Molecular Orbital Calculations

The extended Hückel method [104,105] is based on the LCAO (linear combination of atomic orbitals) methodology:

$$\Psi = c_i\psi_i + c_j\psi_j$$

where Ψ is an MO; ψ_i, ψ_j are AO's; and c_i, c_j are their coefficients

In the EHMO method, the basis set of atomic orbitals used is the set of valence orbitals for all atoms in the molecule, and simple 1-electron Hamiltonian operators are employed

A set of secular equations may be derived:

$$\sum c_{ij} (H_{ij} - S_{ij}E) = 0$$

where $H_{ii} = \int \psi_i H \psi_i$

$H_{ij} = \int \psi_i H \psi_j = \int \psi_j H \psi_i$

$S_{ij} = \int \psi_i \psi_j$

Solution of the secular determinant leads to energies and contributions to each MO from each AO. The orbitals so produced then may be represented pictorially, or analysed in terms of their energies and occupations.

A value for the total energy of the complex may be calculated, by summation of the energies for all electrons in the molecule, known as the sum of one-electron energies. While the energies given by extended Hückel calculation are not particularly accurate on an absolute scale, they may be used successfully in probing, for example, conformational preferences.

In practice [106,107], single Slater-type orbitals (STO's) are used for each AO, and these take the form:

$$R(r) = r^{n^*-1} e^{-\zeta r}$$

where $\zeta = (Z - \Sigma S) / n^*$, and Z = atomic number
S = screening constant
n* = effective quantum number

H_{ii}'s used are the valence shell ionisation energies (VSIE's), although these may be optimised by charge-iteration procedures (see below).

H_{ij}'s are calculated using the modified Wolfsberg-Helmholtz formula:

$$H_{ij} = K' S_{ij} (H_{ii} + H_{jj}) / 2$$

where $K' = K + \Delta^2 + \Delta^4 (1-K)$
and $\Delta = (H_{ii} - H_{jj}) / (H_{ii} + H_{jj})$

Charge Iteration Procedures (Optimisation of H_{ii}'s)

2 differerent charge iteration procedures were used. The first, METHOD1, is a simple function which may be represented thus:

$$H_{ii} = H_{ii}^0 + (\text{sense x charge})$$

The second, METHOD2, is a more complex function, of the form

$$H_{ii} = -\text{VSIE}(Q)$$

$$\text{where VSIE}(Q) = AQ^2 + BQ + C$$

For manganese, three configurations were used, as follows:

s:	$d^{n-1} s$	p:	$d^{n-1} p$	d:	d^n
	$d^{n-2} s^2$		$d^{n-2} p^2$		$d^{n-1}s$
	$d^{n-2} sp$		$d^{n-2} sp$		$d^{n-1} p$

Net Atomic Charges

Net atomic charges are calculated in the extended Hückel method by the formula:

$$q(i) = \sum_j \sum_n (N\, c_{in}^2 + N\, c_{in}\, c_{jn}\, S_{ij})$$

where N = number of electrons in the orbital (N = 0, 1, or 2)

The atomic charge, q, is then given by:

$$q = \sum_i q(i)$$

If the atomic number is Z, then the net atomic charge equals q-Z.

Bond Overlap Populations

The bond overlap poulation, which is a measure of the bond strength between two atoms, r and s, is given by:

$$P_{rs} = 2 \sum_{ij} \sum_n N\, c_{in}\, c_{jn}\, S_{ij}$$

The above deals with combination of AO's to form MO's, but there is another approach possible with the locally-available software, which involves MO's derived from basis sets of *fragment* orbitals, rather than atomic orbitals. The method essentially involves partitioning of a molecule into notional fragments, and looking at the interaction of the fragment molecular orbitals (FMO's) on combination to form the MO's of the complete molecule. Of particular interest in such cases is to determine which fragment orbitals incur the largest changes in population (greater or lesser) on going to the full molecular environment.

In the calculations carried out in this work, the models used are either derived from the crystallographically determined geometry, or are idealised. Where idealised models have been used, their coordinates are given below. In the case of the fragment molecular orbital calculations, the models used are constructed by positioning an idealised $\{Mn(CO)_3^+\}$ fragment above a ligand model derived crystallographically.

Distances and angles used in idealised models were: B-B = B-C = C-C = 1.75Å, B-H = C-H = 1.20Å, B-S = 1.88Å, S-H = 1.28Å, Mn-C = 1.78Å and C-O = 1.14Å. Carbaborane cages were icosahedral fragments, tetrahedral geometry was assumed around S, C-Mn-C = 90° and Mn-C-O = 180°.

Idealised Model of $[7,8\text{-}nido\text{-}C_2B_9H_{11}]^{2-}$

	x	y	z
B1	0.9143	0.0000	-1.4886
B2	1.8343	0.0000	0.0000
B3	0.9143	-1.4158	-0.4600
B4	-0.5743	-0.8750	-1.2043
B5	-0.5743	0.8750	-1.2043
B6	0.9143	1.4158	-0.4600
C7	0.9143	-0.8750	1.2043
C8	-0.5744	-1.4158	0.4600
B9	-1.4943	0.0000	0.0000
B10	-0.5743	1.4158	0.4600
B11	0.9143	0.8750	1.2043
H1	1.4509	0.0000	-2.5619
H2	3.0344	0.0000	0.0000
H3	1.4510	-2.4366	-0.7917
H4	-1.1110	-1.5058	-2.0727
H5	-1.1109	1.5059	-2.0727
H6	1.4510	2.4366	-0.7917
H7	1.4509	-1.5059	2.0727
H8	-1.1110	-2.4366	0.7917
H9	-2.6943	0.0000	0.0000
H10	-1.1110	2.4366	0.7917
H11	1.4510	1.5059	2.0727

Idealised (Minimum Energy) Model of [9-SH_2-7,8-*nido*-$C_2B_9H_{10}$]$^-$

	x	y	z
HS2	-3.8009	0.8968	0.8077
HS3	-3.8010	0.2509	-1.1804
S	-3.3744	0.0000	0.0000
B1	0.9143	0.0000	-1.4886
B2	1.8343	0.0000	0.0000
B3	0.9143	-1.4158	-0.4600
B4	-0.5743	-0.8750	-1.2043
B5	-0.5743	0.8750	-1.2043
B6	0.9143	1.4158	-0.4600
C7	0.9143	-0.8750	1.2043
C8	-0.5744	-1.4158	0.4600
B9	-1.4943	0.0000	0.0000
B10	-0.5743	1.4158	0.4600
B11	0.9143	0.8750	1.2043
H1	1.4509	0.0000	-2.5619
H2	3.0344	0.0000	0.0000
H3	1.4510	-2.4366	-0.7917
H4	-1.1110	-1.5058	-2.0727
H5	-1.1109	1.5059	-2.0727
H6	1.4510	2.4366	-0.7917
H7	1.4509	-1.5059	2.0727
H8	-1.1110	-2.4366	0.7917
H10	-1.1110	2.4366	0.7917
H11	1.4510	1.5059	2.0727

{$C_2B_9H_{10}S$} fragment as above. HS2, HS3 vary with torsion angle.

THETA		x	y	z
-180	HS2	-3.8009	0.8968	-0.8077
	HS3	-3.8010	-0.2509	1.1804
-150	HS2	-3.8009	-1.1805	-0.2511
	HS3	-3.8010	0.3729	1.1477
-120	HS2	-3.8009	-1.1479	0.3728
	HS3	-3.8010	0.8968	0.8075
-90	HS2	-3.8009	-0.8077	0.8968
	HS3	-3.8010	1.1804	0.2509
-60	HS2	-3.8009	-0.2511	1.1805
	HS3	-3.8010	-0.2511	1.1805
-30	HS2	-3.8009	0.3728	1.1479
	HS3	-3.8010	0.8075	-0.8968
0	HS2	-3.8009	0.8968	0.8077
	HS3	-3.8010	0.2509	-1.1804
30	HS2	-3.8009	1.1805	0.2511
	HS3	-3.8010	-0.3729	-1.1477
60	HS2	-3.8009	1.1479	-0.3728
	HS3	-3.8010	-0.8968	-0.8075
90	HS2	-3.8009	0.8077	-0.8968
	HS3	-3.8010	-1.1804	-0.2509
120	HS2	-3.8009	0.2511	-1.1805
	HS3	-3.8010	-1.1477	0.3729
150	HS2	-3.8009	-0.3728	-1.1479
	HS3	-3.8010	-0.8075	0.8968
180	HS2	-3.8009	0.8968	-0.8077
	HS3	-3.8010	-0.2509	1.1804

Orbital Parameters used in EHMO/FMO Calculations

Orbital	H_{ii}(eV)	ζ_1	ζ_2	c_1	c_2
H(1s)	-13.30	1.30			
B(2s)	-15.40	1.30			
B(2p)	-8.68	1.30			
C(2s)	-20.90	1.625			
C(2p)	-11.10	1.625			
O(2s)	-29.10	2.275			
O(2p)	-12.50	2.275			
S(3s)	-25.10	1.817			
S(3p)	-14.50	1.817			
Mn(3d)	-11.00	5.15	1.90	0.53108	0.64788
Mn(4s)	-9.11	1.80			
Mn(4p)	-4.68	1.80			

$[(\eta\text{-}C_5H_5)Mn(CO)_3]$ Model for EHMO/FMO Calculation

	x	y	z
H4	1.26856	1.54833	0.11910
H5	-1.01988	1.65278	0.04760
H6	-1.94373	-0.61550	0.13630
H7	-0.10949	-2.05726	0.04860
H8	2.04468	-0.64135	0.11300
C4	0.77071	0.91511	-0.00070
C5	-0.64228	1.00653	0.00030
C6	-1.16788	-0.28432	0.00020
C7	-0.07097	-1.19526	-0.00060
C8	1.11040	-0.44216	0.00080
Mn	0.00000	0.00000	1.77180
CA	1.25865	0.72662	2.79950
OA	2.06475	1.19204	3.45770
CB	0.00000	-1.45339	2.79950
OB	0.00000	-2.38422	3.45770
CC	-1.25865	0.72662	2.79950
OC	-2.06475	1.19204	3.45770

[(carb')Mn(CO)$_3$] Model for EHMO/FMO Calculation

	x	y	z
H1	1.06291	-1.95672	0.32830
H2	2.23879	0.19627	0.33590
H5	-0.30493	-2.52714	-1.78870
H6	2.33867	-1.21843	-1.72280
H7	0.60922	2.43163	0.34930
H8	-2.29039	1.13984	0.23330
H9	-2.32914	-0.46163	-2.05700
H10	0.18756	-0.09015	-3.40170
H11	1.95609	1.58192	-1.88780
H12	-0.88465	2.19952	-2.05100
HS11	-2.42383	-3.51288	-1.20840
HS12	-3.39185	-2.54994	-1.14810
HS13	-3.56882	-3.67777	-0.39340
HS21	-3.17641	-1.37102	2.27240
HS22	-3.83922	-1.04168	1.05350
HS23	-3.94051	-2.22036	1.71120
S	-2.09825	-2.47172	0.66580
CS1	-2.99848	-3.14163	-0.73100
CS2	-3.43764	-1.66171	1.53910
C1	0.64609	-1.25810	0.00300
C2	1.39237	0.14044	-0.01050
B4	-1.02763	-1.04838	0.00550
B5	-0.17866	-1.53591	-1.46990
B6	1.41565	-0.77691	-1.45730
B7	0.31108	1.45751	0.01280
B8	-1.32182	0.70856	-0.01080
B9	-1.40806	-0.26103	-1.53070
B10	0.10911	-0.08242	-2.43830
B11	1.16831	0.96636	-1.48150
B12	-0.56345	1.29683	-1.52970
Mn	0.00000	0.00000	1.64340
CA	1.25865	0.72662	2.67110
OA	2.06475	1.19204	3.32930
CB	0.00000	-1.45339	2.67110
OB	0.00000	-2.38422	3.32930
CC	-1.25865	0.72662	2.67110
OC	-2.06475	1.19204	3.32930

Section 4: Electrochemical and Spectroelectrochemical Techniques

In this section, an outline of the experimental techniques and description of the equipment used in the electrochemical and spectroelectrochemical studies are given [108].

Electrochemical Studies

The experiments described in Chapter 5 were performed on CH_2Cl_2/0.5M $[TBA]BF_4$ solutions of the complexes under study, using a conventional three-electrode configuration, represented schematically in **Figure 6.4.1**.

This comprises a working electrode (w.e.), a reference electrode (r.e.) and a counter (auxiliary) electrode (c.e.). A potential difference is measured between the r.e. and the w.e., and a current monitored between the w.e. and c.e. The r.e. maintains a constant reference potential throughout the experiment and any change in applied potential appears across the w.e./solution interface. No current flows to the r.e., which is therefore left unpolarised and stable. The reference electrode used in these studies was Ag/AgCl, while both working and counter electrodes were of Pt.

Cyclic voltammetry, linear stirred voltammetry and alternating current voltammetry were each performed, the results of which are presented in the approriate discussions in Chapter 5.

Figure 6.4.1 Typical Cell Arrangement for Conventional Electrochemistry

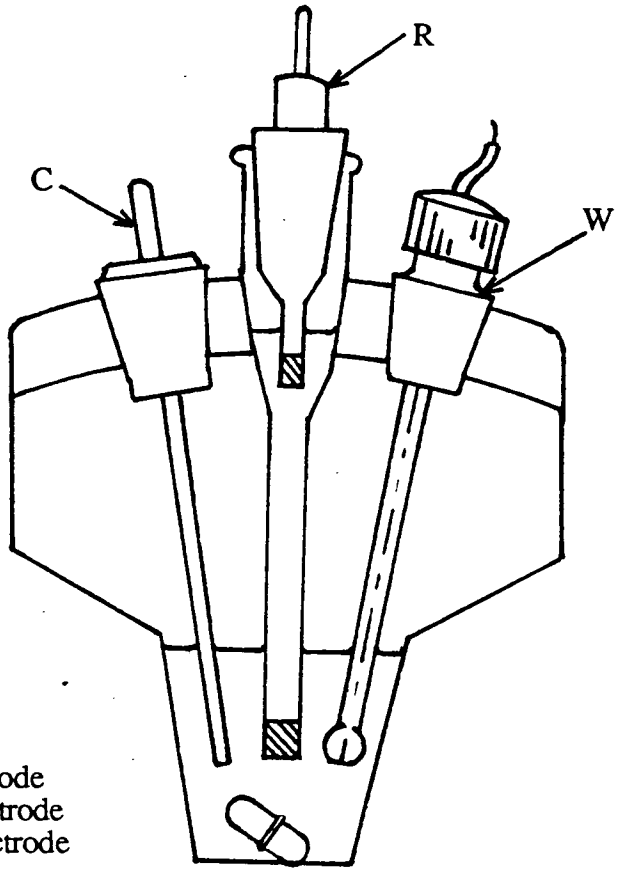

Key

C: Counter electrode
W: Working electrode
R: Reference electrode

Reversibility criteria for cyclic voltammetry (c.v.) and alternating current voltammetry (a.c.v.) are given below:

Cyclic Voltammetry

E_p is independent of ν

$E_p^F - E_p^R = 59/n$ mV and is independent of ν

$0.5[E_p^F + E_p^R] = E_{1/2}$, independent of concentration

$i_p/\nu^{1/2}$ (current function) is independent of ν

$i_p^R/i_p^F = 1$ and is independent of n

where ν = scan rate

E_p^F, E_p^R = potential at maximum of forward and reverse curves

i_p^F, i_p^R = peak current at maximum of forward and reverse curves

A.C. Voltammetry

(a) Potential

E_p is independent of ω

$W_{1/2} = 90/n$ mV at 25° and is independent of ω

where E_p = potential of peak maximum

ω = a.c. frequency

$W_{1/2}$ = peak width at half height

(b) Current

A plot of i_p *versus* $\omega^{1/2}$ gives a straight line through the origin

where i_p = maximum of peak current

These experiments were carried out using the O.T.T.L.E. cell, shown schematically in **Figure 6.4.2.** This consists of a fine Pt/Rh gauze working electrode (transparency *ca.* 40%) fitted into a quartz *UV/VIS/NIR* cell of pathlength 0.05 cm. At the top of the cell is a quartz extension which functions as a reservoir for the solution. Into this are placed a Pt wire counter electrode and Ag/AgCl reference electrode, both protected from the bulk solution by a porous frit.

The cell, together with the electrodes and solution containing the species of interest are fitted into a gas-tight PTFE block. Temperature control is maintained by passing dry, pre-cooled nitrogen gas between an inner set of quartz windows in the block and the quartz cell. To prevent fogging of the inner windows, dry N_2 gas is passed between these and a set of outer quartz windows.

The temperature is monitored by a thermocouple and digital thermometer. A Perkin-Elmer Lambda-9 spectrophotometer was employed.

Figure 6.4.2 Schematic Diagram of the O.T.T.L.E. Cell

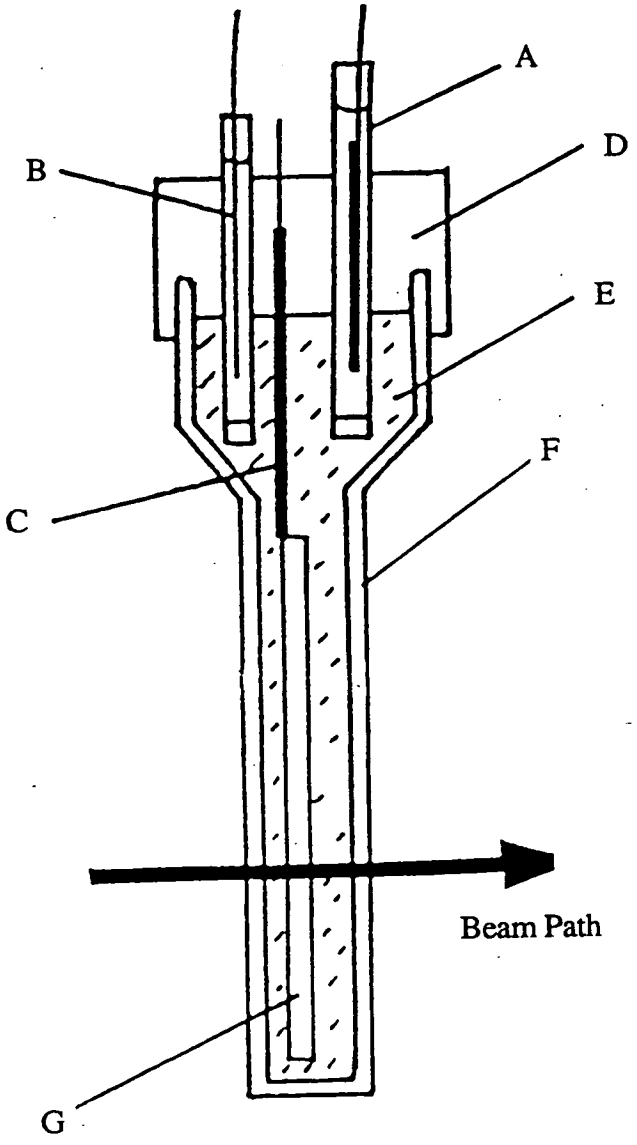

Key

A: Counter electrode
B: Reference electrode
C: Working electrode connection protected from bulk solution by PTFE sleeve
D: PTFE cell cap
E: Test solution
F: 0.1cm Infrasil quartz cell containing Pt grid working electrode
G: Pt grid working electrode

Application of the Nernst Equation to the Spectroelectrochemical Data

The Nernst equation may be applied to data obtained from controlled-potential spectroelectrochemical experiments, to yield two useful parameters, n, the number of electrons involved in the electrochemical process, and E^o, the potential at which the process occurs. The method employed is outlined below, followed by relevant data for complexes **(8)** and **(9)**.

$$E = E^0 + RT/nF \ln[O]/[R] \qquad \text{- Nernst equation}$$

Usually the experimentally measured absorbance ratio r(E) is equal to the ratio [O]/[R]

$$r(E) = [A(E) - A_R]/[A_O - A(E)]$$

where $A(E)$ = absorbance at chosen wavelength, λ, at the applied potential
A_R = absorbance at chosen wavelength, λ, of fully reduced material
A_O = absorbance at chosen wavelength, λ, of fully oxidised material

Thus a plot of E *versus* ln r(E) should give a straight line with an intercept at ln r(E) = 0, giving E^0 and a slope giving n.

For complex **(8)**, band at ν_{max} = 32900 cm^{-1}

E_{app}	r(E)	ln r(E)
0.700	4.263	1.45
0.648	0.667	-0.42
0.624	0.194	-1.64
0.600	0.046	-3.08

This data yields a value for E^0 of +0.66V *versus* Ag/AgCl and a value for n of 1.06±0.1e.

For complex **(9)**, band at ν_{max} = 33300cm^{-1}

Eapp	r(E)	ln r(E)
0.400	8.585	2.15
0.350	3.525	1.26
0.324	1.649	0.50
0.300	0.711	-0.34
0.276	0.224	-1.50
0.250	0.013	-4.34

This data yields a value for E^0 of +0.325V *versus* Ag/AgCl and a value for n of 1.09±0.21e.

References

1. M.F. Hawthorne, D.C.Young and P.A. Wegner, *J. Am. Chem. Soc.*, 1965, **87**, 1818.

2. M.F. Hawthorne, D.C. Young, T.D. Andrews, D.V. Howe, R.L. Pilling, A.D. Pitts, M. Reintjes, L.F. Warren Jnr. and P.A. Wegner, *J. Am. Chem. Soc.*, 1968, **90**, 879.

3. T.P Hanusa, *Polyhedron*, 1982, **1**, 663.

4. W.L. Jørgenson and L. Salem, *"The Organic Chemist's Book of Orbitals"*, Academic Press, New York, 1973.

5. D.M.P. Mingos, *J. Chem. Soc., Dalton Trans.*, 1977, 602

6. J. Plesek, Z. Hanousek and S. Hermanek, *Collect. Czech. Chem. Commun.*, 1978, **43**, 2862.

7. D.C. Young, D.V. Howe and M.F. Hawthorne, *J. Am. Chem. Soc.*, 1969, **91**, 859.

8. S.A. Miller, J.A. Tebboth and J.F. Tremaine, *J. Chem. Soc.*, 1952, 632.

9. T.J. Kealy and P.L. Pauson, *Nature*, 1951, **168**, 1039.

10. A.N. Nesmeyanov and N.S. Kochetkova, *Russ. Chem. Rev. (Engl. Transl.)*, 1974, **43**, 710.

11. N.S. Kochetkova and Yu.K. Kryninka, *Russ. Chem. Rev. (Engl. Transl.)*, 1978, **47**, 486.

12. *e.g. "Comprehensive Organometallic Chemistry"*, Eds. G. Wilkinson, F.G.A. Stone and E.W. Abel, Pergamon, New York, 1982.

13. G. Wilkinson, M. Rosenblum, M.C. Whiting and R.B. Woodward, *J. Am. Chem. Soc.*, 1952, **74**, 2125.

14. E.O. Fischer and W. Pfab, *Z. Naturforsch.*, **7b**, 377,**(1952).**

15. J.M. Birmingham, *Adv. Organomet. Chem.*, 1964, **2**, 365.

16. G. Wilkinson, *J.Am. Chem. Soc.*, 1952, **74**, 6146.

17. G. Wilkinson, P.L. Pauson and F.A. Cotton, *J. Am. Chem. Soc.*, 1954, **76**, 1970.

18. G. Wilkinson, F.A. Cotton and J.M. Birmingham, *J. Inorg. Nucl. Chem.*, 1956, **2**, 95.

19. G. Wilkinson, *J. Am.Chem.Soc.*, 1954, **76**, 209.

20. M.Y. Antipin, E.B. Lobkowskii, K.N. Semenenko, G.L. Soloveichik and Y.T. Struchkov, *Zh. Strukt. Khim.*, 1979, **20**, 942.

21. E. Weiss and E.O. Fischer, *Z. Anorg. Allg. Chem.*, 1956, **284**, 69.

22. W. Bünder and E. Weiss, *J. Organometal. Chem.*, 1975, **92**, 65.

23. P. Seiler and J.D. Dunitz, *Acta Crystallogr.*, 1980, **B36**, 2255.

24. E. Weiss and E.O. Fischer, *Z. Naturforsch.*, 1955, **10b**, 58.

25. E.O. Fischer and H. Wawersik, *J. Organometal. Chem.*, 1966, **5**, 559.

26. E.O. Fischer and H. Grubert, *Chem. Ber.*, 1959, **92**, 2302.

27. F.A. Cotton, *"Chemical Applications of Group Theory", (2nd Edition)*, Interscience, Wiley, New York, 1971.

28. J. Kozikowski, R.E. Maginn and M.S. Klove, *J. Am.Chem. Soc.*, 1959, **81**, 2995.

29. E.O. Fischer and K. Plesske, *Chem. Ber.*, 1960, **93**, 1006.

30. T.S.Piper, F.A. Cotton and G. Wilkinson, *J. Inorg. Nucl. Chem.*, 1955, **1**, 165.

31. G. Huttner, H.H. Britzinger, L.G. Bell, P. Friedrich, V. Bejenke and D. Neugebauer, *J. Organometal. Chem.*, 1978, **145**, 329.

32. M.J. Bennett, F.A. Cotton, A. Davison, J.W. Faller, S.J. Lippard and S.M. Morehouse, *J. Am. Chem. Soc.*, 1966, **88**, 4371.

33. J.W. Faller, *Adv. Orgamometal. Chem.*, 1977, **16**, 211.

34. R.A. Wiesboeck and M.F. Hawthorne, *J. Am. Chem. Soc.*, 1964, **86**, 1642.

35. M.F. Hawthorne, D.C. Young, P.M. Garrett, D.A. Owen, S.G. Schwerin, F.N. Tebbe and P.A. Wegner, *J. Am. Chem. Soc.*, 1968, **90**, 862.

36. J.B. Casey, W.J. Evans and W.H. Powell, *Inorg. Chem.*, 1983, **22**, 2228, 2236.

37. K. Wade, *Adv. Inorg. Chem. Radiochem.*, 1976, **18**, 1.

38. R.E. Williams, *Adv. Inorg. Chem. Radiochem.*, 1976, **18**, 67.

39. A. Zalkin, T.E. Hopkins and D.H. Templeton, *Inorg. Chem.*, 1966, **5**, 1189.

40. D.M.P. Mingos, M.I. Forsyth and A.J. Welch, *J. Chem. Soc., Chem. Commun.*, 1977, 605.

41. H.M. Colquhoun, T.J. Greenhough and M.G.H. Wallbridge, *J. Chem. Soc., Dalton Trans.*, 1976, 1019.

42. H.M. Colquhoun, T.J. Greenhough and M.G.H. Wallbridge, *J, Chem. Soc., Dalton Trans.*, 1979, 619.

43. Y. Do, H.C. Kang, C.B. Knobler and M.F. Hawthorne, *Inorg. Chem.*, 1987, **26**, 2348.

44. M. Green, J.A.K. Howard, A.P. James, A.N. de M. Jelfs, C.M. Nunn and F.G.A. Stone, *J. Chem. Soc., Chem. Commun.*, 1985, 1778.

45. C.B. Knobler, T.B. Marder, E.A. Mizusawa, R.G. Teller, J.A. Long, P.E. Behnken and M.F. Hawthorne, *J. Am. Chem. Soc.*, 1984, **106**, 2990.

46. R.G. Teller, J.J. Wilczynski and M.F. Hawthorne, *J. Chem. Soc., Chem. Commun.*, 1979, 472.

47. H.C. Kang, Y. Do, C.B. Knobler and M.F. Hawthorne, *J. Am. Chem. Soc.*, 1987, **109**, 6530.

48. C.W. Jung, R.T. Baker and M.F. Hawthorne, *J. Am. Chem. Soc.*, 1981, **103**, 810.

49. E.L. Hoel and M.F. Hawthorne, *J. Am. Chem. Soc.*, 1974, **96**, 4676.

50. Proceedings of Third International Symposium on Neutron Capture Therapy, *Strahlenther. Onkol.*, 1989, **165**, 65.

51. J.S. Beck, W. Quintana and L.G. Sneddon, *Organometallics*, 1988, **7**, 1015.

52. T.D. Getman, J.A. Krause and S.G. Shore, *Inorg. Chem.*, 1988, **27**, 2398.

53. J. Emsley, *Chem. Soc. Rev.*, 1980, **9**, 91.

54. D.E. Smith and A.J. Welch, *Acta Crystallogr.*, 1986, **C42**, 1717, and refs. therein.

55. G.F. Mitchell and A.J. Welch, *J. Chem. Soc., Dalton Trans.*, 1987, 1017.

56. R. Hoffmann, *Angew. Chem. Int Ed. Engl.*, 1982, **21**, 711.

57. *e.g.* A.P. Ginsberg, W.E. Lindsell, K.J. M^{c}Cullough, C.R. Sprinkle and A.J. Welch, *J. Am. Chem. Soc.*, 1986, **108**, 403.

58. D.G Evans and D.M.P. Mingos, *J. Organometal. Chem.*, 1982, **232**, 171.

59. R. Hüttel, U. Raffray and H. Reinheimer, *Angew. Chem. Int. Ed. Engl.*, 1967, **6**, 862.

60. G. Ortaggi, *J. Organometal. Chem.*, 1974, **80**, 275.

61. T.V. Baukova, Yu.L. Slovokhotov and Yu.T. Struchkov, *J. Organometal. Chem.*, 1981, **220**, 125.

62. F.A. Cotton and J. Takats, *J. Am. Chem. Soc.*, 1970, **92**, 2353.

63. J. Cowie, E.J.M. Hamilton, J.C.V. Laurie and A.J. Welch, *Acta Crystallogr.*,

1988, **C44**, 1648.

64. *e.g.* N.N. Greenwood and A. Earnshaw, in *"The Chemistry of the Elements"* , Pergamon, Oxford, 1982.

65. V. Subrtova, C. Novak and A. Linek, *Acta Crystallogr.*, 1984, **C40**, 1955.

66. R.O. Gould and P. Taylor, University of Edinburgh, 1986.

67. A.J. Wynd, Ph.D. Thesis, University of Edinburgh, 1988.

68. K.D. Schramm and J.A. Ibers, *Inorg. Chem.*, 1977, **16**, 3287.

69. E. Mizusawa, S.E. Rudnick and K. Eriks, *Inorg. Chem.*, 1980, **19**, 1188.

70. M.F. Hawthorne, A.R. Pitochelli, R.D. Strahm and J.J. Miller, *J. Am. Chem. Soc.*, 1960, **82**, 1825.

71. S.K. Boocock, N.N. Greenwood, J.D. Kennedy, W.S. M^{c}Donald and J. Staves, *J. Chem. Soc., Dalton Trans.*, 1981, 2573.

72. J.D. Kennedy and J. Staves, *Z. Naturforsch., Teil. B*, 1979, **34**, 808.

73. G.K. Barker, N.R. Godfrey, M. Green, H.E. Parge, F.G.A. Stone and A.J. Welch, *J. Chem. Soc., Chem. Commun.*, 1983, 277.

74. N.W. Alcock, L. Parkhill and M.G.H. Wallbridge, *Acta Crystallogr.*, 1985, **C41**, 716.

75. A.J. Wynd, A.J. M^{c}Lennan, D. Reed and A.J. Welch, *J. Chem. Soc., Dalton Trans.*, 1987, 2761.

76. R.V. Parish, L.S. Moore, A.J. Dens, D.M.P. Mingos and D.J. Sherman, *J. Chem. Soc., Dalton Trans.*, 1989, 539.

77. D.M.P. Mingos, M.I. Forsyth and A.J. Welch, *J. Chem. Soc., Dalton Trans.*, 1978, 1363.

78. A.F. Berndt and R.E. Marsh, *Acta Crystallogr.*, 1963, **16**, 118.

79. J.A. Timney, *Inorg Chem.*, 1979, **18**, 2502.

80. F.A. Cotton and R.M. Wing, *Inorg. Chem.*, 1965, **4**, 314.

81. R.B. King and A. Efraty, *J. Organometal.Chem.*, 1970, **23**, 527.

82. M. Elian, M.M.L. Chen, D.M.P. Mingos and R. Hoffmann, *Inorg. Chem.*, 1976, **15**, 1148.

83. H. Haas and T.P. Sheline, *J. Chem. Phys.*, 1967, **47**, 2996.

84. *e.g.* R.N. Grimes in *"Carboranes"*, Academic Press, New York, 1971.

85. W.L. Jolly, *Inorg. Synth.*, **11**, 120.

86. R.J. Wilson, L.F. Warren Jnr. and M.F. Hawthorne, *J.Am. Chem. Soc.*, 1969, **91**, 758.

87. M.F. Hawthorne, L.F. Warren Jnr., K.P. Callahan and N.F. Travers, *J. Am. Chem. Soc.*, 1971, **93**, 2407.

88. R.J. Wiersema and M.F. Hawthorne, *J. Am. Chem. Soc.*, 1974, **96**, 761.

89. J.D. Kennedy and B. Wrackmeyer, *J. Magn. Reson.*, 1980, **38**, 529.

90. A. Bax and R. Freeman, *J. Magn. Reson.*, 1981, **42**, 164; 1981, **44**, 542.

91. T.L. Venable, W.C. Hutton and R.N. Grimes, *J. Am. Chem. Soc.*, 1982, **104**, 4716.

92. M.P. Garcia, M. Green, F.G.A. Stone, R.G. Sommerville, A.J. Welch, C.E. Briant, D.N. Cox and D.M.P. Mingos, *J. Chem. Soc., Dalton Trans.*, 1985, 2343.

93. A.J. Carty and A. Efraty, *Inorg. Chem.*, 1969, **8**, 543.

94. G. Costa, E. Reisenhover and L. Stefani, *J. Inorg. Nucl. Chem.*, 1965, **27**, 2581.

95. M.H. Quick and R.J. Angelici, *Inorg. Synth.*, **19**, 160.

96. R.H. Reimann and E. Singleton, *J. Chem. Soc., Dalton Trans.*, 1974, 808.

97. R.O. Gould and D.E. Smith, University of Edinburgh, 1986.

98. G.M. Sheldrick, University of Gottingen, Federal Republic of Germany, 1986.

99. G.M. Sheldrick, University of Cambridge, 1976.

100. *"International Tables for X-ray Crystallography"*, Kynoch Press, Birmingham, 1974, **4**, 99.

101. N.G. Walker and D. Stuart, *Acta Crystallogr.*, 1983, **A39**, 158.

102. P.R. Mallinson, University of Glasgow, 1982.

103. C.K. Johnson, Report *ORNL-5138*, Oak Ridge National Laboratory, Tennesee, U.S.A., 1976.

104. R. Hoffmann and W.N. Lipscomb, *J. Chem. Phys.*, 1962, **36**, 2179.

105. R. Hoffmann, *J. Chem. Phys.*, 1963, **39**, 1397.

106. J. Howell, A. Rossi, D. Wallace, K. Haraki and R. Hoffmann, *ICON*, Quantum Chemistry Program Exchange, Univ. Indiana, 1977, no. 344.

107. J.H. Ammeter, H.-B. Burgi, J.C. Thibeault and R. Hoffmann, *J. Am. Chem. Soc.*, 1982, **100**, 3686.

108. A.J. Bard and L.R. Faulkner, *"Electrochemical Methods"*, Wiley, New York, 1980.

Appendices

Appendix 1: Lectures and Courses Attended

Recent Advances in Inorganic Chemistry

Drs. A.J. Welch, L.J. Yellowlees, S.K. Chapman and M. Schröder

N.m.r. Spectroscopy

Dr. I.H. Sadler

Solution and Refinement of Crystal Structures (Parts 1 & 2)

Drs. R.O. Gould and A.J. Blake

Departmental Research Seminars and Colloquia

Inorganic Section Meetings

Intraboron VII, VIII and IX, Annual Meetings of British Boron Chemists

University of Strathclyde Inorganic Club (USIC) Meetings, 1987-1989

Scottish *Dalton* Meetings, 1987-1989

B.C.A. Residential Crystallography School, Aston, Birmingham, April 1989

Appendix 2: Published Work

Certain of the results presented in the body of the thesis have been published. The references for these papers are:

J. Cowie, E.J.M. Hamilton, J.C.V. Laurie and A.J. Welch, *Acta Crystallogr.*, 1988, **C44**, 1648.

J. Buchanan, E.J.M. Hamilton, D. Reed and A.J. Welch, *J. Chem. Soc., Dalton Trans.*, 1990, 677.

A reprint of each paper is included.

In addition, the following papers have been accepted for publication:

Structure of 10,11-μ-(Triphenylphosphine)aurio-9-dimethylsulphido-7,8-dicarba-*nido*-undecaborane(10) Methylene Chloride Solvate, E.J.M. Hamilton and A.J. Welch, *Acta Crystallogr., Sect. C*, in press.

The Chemistry of Monoanionic Carbaborane Ligands. Synthesis, and Molecular and Electronic Structure of $[3,3,3\text{-}(CO)_3\text{-}4\text{-}SMe_2\text{-}3,1,2\text{-}MnC_2B_9H_{10}]$, and Order-of-Magnitude Improved Structure of $(\eta\text{-}C_5H_5)Mn(CO)_3$, J. Cowie, E.J.M. Hamilton, J.C.V. Laurie and A.J. Welch, *J. Organometal. Chem.*, in press.

The Structure of $[7,8\text{-}C_2B_9H_{12}]^-$; Correction of a Popular Misconception†

Jill Buchanan, Ewan J. M. Hamilton, David Reed, and Alan J. Welch*
Department of Chemistry, University of Edinburgh, Edinburgh EH9 3JJ

The $[7,8\text{-}C_2B_9H_{12}]^-$ ion has been shown, *via* n.m.r. spectroscopic and *X*-ray crystallographic study, to contain an *endo*-H atom bonded to B(10) and not, as generally thought, a B–H–B bridge. Four ion pairs of $[H(dmso)_2][C_2B_9H_{12}]$ (dmso = dimethyl sulphoxide) crystallise in a unit cell of dimensions $a = 8.2919(14)$, $b = 11.0802(21)$, $c = 18.128(5)$Å, $\beta = 100.135(18)°$, and space group $P2_1/n$. The structure has been refined to $R = 0.0436$, $R' = 0.0698$ for 2 355 reflections measured at 185 ± 1 K. The presence of an *endo*-H atom in $[7,8\text{-}C_2B_9H_{12}]^-$ is rationalised by consideration of the form of the highest occupied molecular orbital of $[7,8\text{-}C_2B_9H_{11}]^{2-}$. Analysis of the results of extended-Hückel molecular orbital calculations confirms that the *endo*-H atom bonds to the cage *via* a four-centre two-electron bond, and allows the relative magnitudes of *endo* and *exo* B–H coupling constants to be understood as well as the observation of weak coupling between the *endo*-H atom and B(9) and B(11).

The $[7,8\text{-}C_2B_9H_{12}]^-$ ion (**1**), easily formed by partial cage degradation of $1,2\text{-}C_2B_{10}H_{12}$ in alcoholic solution,[1,2] has been known for very many years. Indeed, it is (following deprotonation with strong base) the precursor of the ubiquitous $[7,8\text{-}C_2B_9H_{11}]^{2-}$ ion that afforded the first carbametallaboranes nearly 25 years ago.[3,4]

Although it is well accepted[1,2] that (**1**) has a *nido*-icosahedral cage architecture, consistent with the Polyhedral Skeletal Electron Pair Theory,[5,6] its precise structure has never been determined, and in particular the exact nature of the twelfth H atom has never been demonstrated. In spite of the fact that Hawthorne *et al.*[2] considered a number of possible sites for this atom (including what turns out to be the correct one), later authors[7] almost invariably assume a bridge position on one of the two (otherwise symmetry-equivalent) B–B connectivities of the open pentagonal face.

Recent structural studies on *nido*-$[3,4\text{-}Et_2\text{-}3,4\text{-}C_2B_5H_6]^-$ (**2**)[8] and *nido*-$[B_{11}H_{14}]^-$ (**3**)[9] have confirmed the presence of $\{BH_2\}$ units in *nido* boranes and carbaboranes, whereas such groups are more commonly associated with *arachno* and *hypho* polyboranes. This has prompted us to reconsider the possibility of a $\{BH_2\}$ group in (**1**), and to seek confirmation of the exact nature of this anion in both the solid state *via* single-crystal *X*-ray diffraction, and in solution *via* multinuclear, multidimensional n.m.r. spectroscopy.

Experimental

N.m.r. spectra were recorded at room temperature as CD_2Cl_2 solutions on Bruker WP 200 SY or Bruker WH 360 spectrometers, the latter fitted with an Aspect 3000 computer. Techniques for recording ^{1}H-{^{11}B} and ^{11}B (correlation spectroscopy, COSY) spectra have been described previously.[10] Chemical shifts are quoted relative to external $SiMe_4$ (^{1}H) or $BF_3{\cdot}OEt_2$ (^{11}B), with positive values to high frequency. Microanalyses were performed by the departmental service.

The salt $[H(dmso)_2][C_2B_9H_{12}]$ (**1a**) was afforded as a white solid by treatment of $K[C_2B_9H_{12}]$ (3g; *ca.* 10 mmol) in dimethyl sulphoxide (dmso)/water (5 cm^3) with concentrated H_2SO_4 (5 cm^3) and not stirring the product. Recrystallisation by slow diffusion of hexane into a CH_2Cl_2 solution at −30 °C yielded large colourless crystals (Found: C, 24.1; H, 8.55. $C_6H_{25}B_9O_2S_2$ requires C, 24.8; H, 8.65%). ^{1}H N.m.r: δ 6.5—7.0 (vbr, solvated H^+), 2.73 (12 H, CH_3), and 1.88 (br, 2H, cage CH).

Crystallography.—Crystal data. $C_6H_{25}B_9O_2S_2$, $M = 290.66$, monoclinic, space group $P2_1/n$, $a = 8.291\,9(14)$, $b = 11.080\,2(21)$, $c = 18.128(5)$Å, $\beta = 100.135(18)°$, $U = 1\,639.5$Å^3, from the least-squares refinement of 25 centred reflections ($14 < \theta < 15°$) at 185 ± 1K, $Z = 4$ ion pairs, $D_c = 1.177$ g cm^{-3}, μ(Mo-K_α) = 2.98 cm^{-1}, $F(000) = 616$.

Data collection and processing. CAD4 diffractometer, graphite-monochromated Mo-K_α *X*-radiation, λ(bar) = 0.710 69Å, ω—2θ scans in 96 steps, with ω scan width 0.8 + 0.34 tanθ. Variable scan speeds between 0.82 and 2.35° min^{-1}. 2 719 Unique data measured ($1 < \theta < 25°$, $+h + k \pm l$) yielding 2 355 reflections with $F \geq 2.0\sigma(F)$. No measureable crystal decay or detectable movement.

Structure solution and refinement. All non-H atoms found by direct methods.[11] Hydrogen atoms from ΔF syntheses following full-matrix least-squares refinement.[12] Empirical absorption correction[13] after isotropic convergence. Thereafter all non-hydrogen atoms allowed anisotropic thermal motion. Hydrogen atoms positionally refined but with common isotropic thermal parameter [$U_H = 0.046\,2(16)$Å^2 at convergence]. Weights applied according to $w^{-1} = [\sigma^2(F) + 0.008\,711F^2]$. $R = 0.043\,6$, $R' = 0.069\,8$, $S = 0.734$. Maximum and minimum residues in final ΔF map 0.38 and −0.62 e Å^{-3} respectively. Scattering factors for neutral atoms as in SHELX 76.[12] Computer programs used in addition to those already referenced include CADABS,[14] CALC,[15] and EASYORTEP.[16] Co-ordinates of non-hydrogen atoms in Table 1.

Additional material available from the Cambridge Crystallographic Data Centre comprises H-atom co-ordinates, thermal parameters, and remaining bond lengths and angles.

Results and Discussion

Recourse to the crystallographic and relatively sophisticated n.m.r. spectroscopic studies described herein is necessary because conventional spectroscopic techniques applied to anion (**1**) fail to define a unique structure. There is no evidence of a B–H–B bridge in its i.r. spectrum, but this is not conclusive

† Dodecahydro-7,8-dicarba-*nido*-undecaborate.

Supplementary data available: see Instructions for Authors, *J. Chem. Soc., Dalton Trans.*, 1990, Issue 1, pp. xix—xxii.

Table 1. Positional parameters of non-hydrogen atoms in [H-(dmso)$_2$][7,8-$C_2B_9H_{12}$]

Atom	*x*	*y*	*z*
S(1)	0.675 15(6)	0.317 81(4)	0.389 41(3)
S(2)	0.317 87(6)	0.131 83(4)	0.284 30(3)
O(1)	0.528 07(19)	0.387 38(13)	0.344 18(10)
O(2)	0.308 72(16)	0.269 74(13)	0.275 00(9)
C(11)	0.694 4(3)	0.379 84(22)	0.479 88(13)
C(12)	0.846 1(3)	0.385 45(21)	0.359 48(14)
C(21)	0.114 5(3)	0.090 26(25)	0.290 71(14)
C(22)	0.322 1(4)	0.077 56(24)	0.192 65(16)
B(1)	0.350 11(24)	0.281 74(18)	0.589 54(12)
B(2)	0.400 6(3)	0.150 25(20)	0.643 27(14)
B(3)	0.422 2(3)	0.152 21(19)	0.548 49(14)
B(4)	0.260 04(25)	0.237 34(20)	0.497 57(12)
B(5)	0.132 1(3)	0.284 14(18)	0.559 51(13)
B(6)	0.219 7(3)	0.228 31(20)	0.652 11(13)
C(7)	0.321 46(22)	0.036 77(17)	0.583 13(11)
C(8)	0.244 01(23)	0.083 55(17)	0.504 77(11)
B(9)	0.075 8(3)	0.156 04(19)	0.503 37(13)
B(10)	0.041 3(3)	0.160 88(20)	0.599 58(13)
B(11)	0.215 0(3)	0.068 71(20)	0.646 94(13)

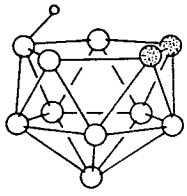

(I)

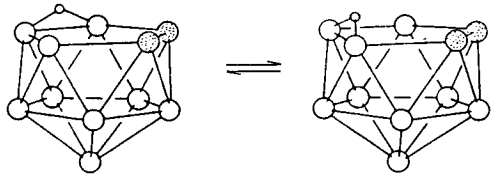

(II)

○ B—H_{exo}
◎ C—H_{exo}
○ H

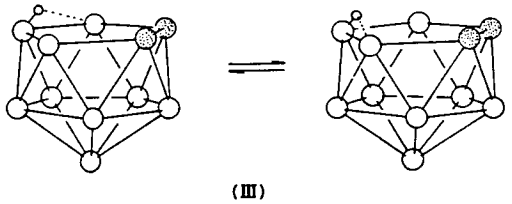

(III)

* Compound (**1b**) was precipitated by mixing aqueous solutions of [$NMe_3(CH_2Ph)$]Br and K[$C_2B_9H_{12}$]^2 and recrystallised by slow diffusion of hexane into a CH_2Cl_2 solution at −30 °C (Found: C, 50.0; H, 10.00; N, 4.95. $C_{12}H_{28}B_9N$ requires C, 50.8; H, 9.95; N, 4.95%).

Table 2. Assignment of ^{11}B and ^{1}H n.m.r. chemical shifts of compound (**1b**)

Position	δ(^{11}B)	δ(^{1}H)
9,11	−10.38	1.94
3(5,6)	−16.46	1.77 (1.24)
2,4	−21.29	1.26
10	−32.54	0.11(*exo*), −2.80(*endo*)
1	−37.17	0.55

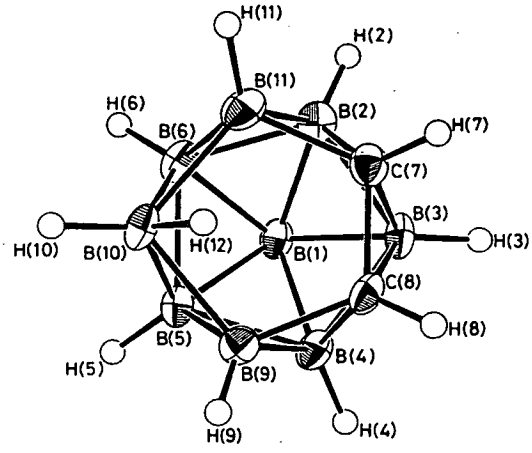

Figure. Plot of the [7,8-$C_2B_9H_{12}$]$^-$ anion (**1**) from above the open face; H(1) is totally obscured by B(1). All atoms drawn with 50% thermal ellipsoids, except H atoms which have been given an artificial radius of 0.1 Å for clarity

evidence that such a bridge does not exist. Similarly, ^{11}B n.m.r. spectroscopy alone fails to distinguish between a {BH_2}-containing form (**I**) and rapidly interconverting hydrogen-bridged forms (**II**).

The ^{11}B-{^{1}H} n.m.r. spectrum of [$NMe_3(CH_2Ph)$][$C_2B_9H_{12}$] (**1b**)* comprises five signals of relative area 2:3:2:1:1, and the ^{11}B n.m.r. spectrum confirms that all nine boron atoms in (**1**) carry *exo*-polyhedral H atoms since all five signals show clear doublet coupling, J_{BH} 125—150(±5) Hz. In addition, the second lowest-frequency signal in the ^{11}B spectrum (δ −32.54 p.p.m.) shows a smaller coupling, 50 ± 5 Hz, thus appearing as a doublet of doublets [doublet of doublets, *apparent* triplet, is surely the correct description of the signal due to B(6) in anion (**2**)[8]]. The additional structure on this resonance was, in fact, noted in an early ^{11}B n.m.r. spectrum of anion (**1**) (Figure 3 of ref. 2).

An ^{11}B(COSY) spectrum of (**1b**) allows assignment of the one-dimensional spectrum (Table 2). The signal with additional coupling in the ^{11}B n.m.r. spectrum arises from B(10), given a conventionally numbered *nido*-icosahedral anion in which the carbon atoms occupy positions 7 and 8. No other signal shows detectable coupling to the twelfth H atom.

A series of ^{1}H n.m.r. spectra with selective ^{11}B decoupling were obtained, and chemical shifts of the *exo*-polyhedral boron-bonded H atoms so determined are included in Table 2. In addition to these, a low-frequency H atom [δ −2.80, H(12)] is significantly enhanced by irradiation at −32.54 p.p.m. [B(10)] and very weakly enhanced by irradiation at −10.38 p.p.m. [B(9), B(11)]. Thus, at ambient temperature, H(12) is strongly bonded to B(10) but only weakly associated with the other (symmetry-equivalent) facial boron atoms, B(9) and B(11).

Evidently this latter association is sufficiently small that no additional structure or even broadening is seen on the doublet centred at −10.38 p.p.m. in the ^{11}B n.m.r. spectrum.

No significant changes in the ^{11}B or ^{11}B-{^{1}H} n.m.r. spectra of compound (**1b**) are observed on cooling to −78 °C. Taken together with the aforementioned data, this implies that the structure of (**I**) is best represented either by the {BH_2}-containing form (**I**) [in which there is a small but detectable interaction between the *endo*-H atom and B(9) and B(11)] or by asymmetrically bridged forms (**III**) in rapid (and, within the limits of our experiment, unstoppable) interconversion.

In an attempt to gain additional information on this system we have studied anions (**I**) in the solid state by *X*-ray diffraction. Initial attempts were frustrated by disorder. Thus good single crystals of compound (**1b**) may be grown, but analysis of the diffraction data obtained* quickly revealed that the cage is randomly disordered, appearing as a closed icosahedron. Disorder of this kind is not uncommon for *nido*-icosahedral cages.[17] Very fortuitously, however, large single crystals of compound (**1a**) are afforded (following recrystallisation) if the synthesis of 9-SMe_2-7,8-$C_2B_9H_{11}$ [10,11] from K[7,8-$C_2B_9H_{12}$] is dmso/water and concentrated H_2SO_4 is attempted without sufficient stirring. The anion in this salt is *not* disordered, allowing the first structural characterisation of [7,8-$C_2B_9H_{12}$]$^-$.

The anion is viewed, from a position above the centre of the open face, in the Figure, and Table 3 lists interatomic distances and important interbond angles derived†. Anion (**I**) has the expected *nido*-icosahedral geometry with an *exo*-polyhedral H atom terminal to each cage atom (B or C). The open face is *not* planar, but is folded into an envelope conformation about the B(9) · · · B(11) vector such that both B(10) and the C(7)–C(8) edge dip towards the B(2)B(3)B(4)B(5)B(6) lower pentagonal belt. This *is* planar (σ = 0.012 6Å) and, with respect to it, the aforementioned three- and four-atom portions of the upper pentagonal face (the latter of which is planar to within 0.004 4Å) make fold angles[19] (φ and 0) of 2.34 and 1.88° respectively. Folding of the upper face in this way is commonly observed in metal complexes of $[C_2B_9H_{11}]^{2-}$ and related ligands.[19]

In the solid state the twelfth H atom of (**I**) clearly occupies a symmetric *endo*-terminal position on B(10), affording the entire anion effective C_s molecular symmetry. We have tested the fact the H(12) is ordered in the crystal [and not, say, disordered about B(9)–B(10) and B(10)–B(11) bridging sites] by a least-squares refinement with H(12) and, for comparison, H(10) omitted from the final model. The two highest maxima in the resultant ΔF synthesis correspond to H(10) (0.83e Å^{-3}) and H(12) (0.53e Å^{-3}) respectively. The next peak [0.39e Å^{-3}, *ca.* 1 Å from S(2)] is assigned to a S lone pair, and all further peaks have an electron density < 0.3e Å^{-3}.

Table 3. Interatomic Distances (Å) and selected interbond angles (°) in [H(dmso)$_2$][7,8-$C_2B_9H_{12}$]

(*a*) Anion

B(1)–B(2)	1.762(3)	B(5)–B(6)	1.816(3)
B(1)–B(3)	1.768(3)	B(5)–B(9)	1.761(3)
B(1)–B(4)	1.772(3)	B(5)–B(10)	1.775(3)
B(1)–B(5)	1.794(3)	B(5)–H(5)	1.09(3)
B(1)–B(6)	1.799(3)	B(6)–B(10)	1.777(3)
B(1)–H(1)	1.122(23)	B(6)–B(11)	1.771(3)
B(2)–B(3)	1.759(3)	B(6)–H(6)	1.07(3)
B(2)–B(6)	1.763(3)	C(7)–C(8)	1.542(3)
B(2)–C(7)	1.717(3)	C(7)–B(11)	1.613(3)
B(2)–B(11)	1.796(3)	C(7)–H(7)	0.95(3)
B(2)–H(2)	1.01(3)	C(8)–B(9)	1.606(3)
B(3)–B(4)	1.764(3)	C(8)–H(8)	0.96(3)
B(3)–C(7)	1.707(3)	B(9)–B(10)	1.817(3)
B(3)–C(8)	1.726(3)	B(9)–H(9)	0.94(3)
B(3)–H(3)	1.09(3)	B(10)–B(11)	1.849(3)
B(4)–B(5)	1.754(3)	B(10)–H(10)	1.10(3)
B(4)–C(8)	1.716(3)	B(10)–H(12)	1.15(3)
B(4)–B(9)	1.793(3)	B(11)–H(11)	1.08(3)
B(4)–H(4)	1.09(3)		

B(2)–B(1)–B(3)	59.76(13)	B(9)–B(5)–B(10)	61.84(13)
B(2)–B(1)–B(6)	59.34(12)	B(1)–B(6)–B(2)	59.27(12)
B(3)–B(1)–B(4)	59.77(12)	B(1)–B(6)–B(5)	59.50(12)
B(4)–B(1)–B(5)	58.90(12)	B(2)–B(6)–B(11)	61.09(13)
B(5)–B(1)–B(6)	60.73(12)	B(5)–B(6)–B(10)	59.20(12)
B(1)–B(2)–B(3)	60.31(13)	B(10)–B(6)–B(11)	62.82(13)
B(1)–B(2)–B(6)	61.40(13)	B(2)–C(7)–B(3)	61.82(13)
B(3)–B(2)–C(7)	58.80(12)	B(2)–C(7)–B(11)	65.18(13)
B(6)–B(2)–B(11)	59.68(13)	B(3)–C(7)–C(8)	63.93(13)
C(7)–B(2)–B(11)	54.61(12)	B(3)–C(8)–B(4)	61.68(12)
B(1)–B(3)–B(2)	59.93(13)	B(3)–C(8)–C(7)	62.68(13)
B(1)–B(3)–B(4)	60.23(12)	B(4)–C(8)–B(9)	65.22(13)
B(2)–B(3)–C(7)	59.38(13)	B(4)–B(9)–B(5)	59.13(12)
B(4)–B(3)–C(8)	58.89(12)	B(4)–B(9)–C(8)	60.35(12)
C(7)–B(3)–C(8)	53.39(11)	B(5)–B(9)–B(10)	59.47(12)
B(1)–B(4)–B(3)	60.00(12)	B(5)–B(10)–B(6)	61.50(13)
B(1)–B(4)–B(5)	61.18(12)	B(5)–B(10)–B(9)	58.69(12)
B(3)–B(4)–C(8)	59.43(12)	B(6)–B(10)–B(11)	58.42(12)
B(5)–B(4)–B(9)	59.53(12)	B(9)–B(10)–H(12)	65.8(13)
C(8)–B(4)–B(9)	54.43(12)	B(11)–B(10)–H(12)	64.5(13)
B(1)–B(5)–B(4)	59.93(12)	H(10)–B(10)–H(12)	109.7(19)
B(1)–B(5)–B(6)	59.77(12)	B(2)–B(11)–B(6)	59.24(13)
B(4)–B(5)–B(9)	61.34(12)	B(2)–B(11)–C(7)	60.21(13)
B(6)–B(5)–B(10)	59.30(12)	B(6)–B(11)–B(10)	58.75(12)

(*b*) Cation

S(1)–O(1)	1.549 8(17)	C(11)–H(113)	1.00(3)
S(1)–C(11)	1.759 4(24)	C(12)–H(121)	0.97(3)
S(1)–C(12)	1.770 8(25)	C(12)–H(122)	0.84(3)
S(2)–O(2)	1.537 7(16)	C(12)–H(123)	0.96(3)
S(2)–C(21)	1.771(3)	C(21)–H(211)	0.94(3)
S(2)–C(22)	1.773(3)	C(21)–H(212)	1.04(3)
O(1)–H(O)	0.95(4)	C(21)–H(213)	0.91(3)
O(2) · · · H(O)	1.45(4)	C(22)–H(221)	0.73(3)
C(11)–H(111)	0.91(3)	C(22)–H(222)	0.94(3)
C(11)–H(112)	0.95(3)	C(22)–H(223)	1.00(3)

O(1)–S(1)–C(11)	103.45(10)	C(21)–S(2)–C(22)	98.58(13)
O(1)–S(1)–C(12)	103.01(10)	S(1)–O(1)–H(O)	113.4(21)
C(11)–S(1)–C(12)	100.03(11)	S(2)–O(2) · · · H(O)	115.2(14)
O(2)–S(2)–C(21)	103.67(11)	O(1)–H(O) · · · O(2)	172.2(35)
O(2)–S(2)–C(22)	104.06(11)		

* *Crystal data.* $C_{12}H_{28}B_9N$, M = 283.65, triclinic, space group $P\bar{1}$, a = 11.833(5), b = 11.915(5), c = 13.723(7)Å, α = 110.692(15), β = 91.954(13), γ = 93.480(13)°, U = 1 803.5Å^3, by the least-squares refinement of 25 centred reflections, 11 < θ < 12°, Z = 4 ion pairs, D_c = 1.045 g cm^{-3}, μ(Mo-K_α) = 0.49 cm^{-1}, F(000) = 608.

Data collection and processing. As for compound (**1a**) except scan speeds between 1.37 and 5.49° min^{-1}, 3 578 Unique data measured (1 < θ < 20°, $+h \pm k \pm l$) yielding 2 190 with $F \geqslant 2.0\ \sigma(F)$. No measureable crystal decay or detectable movement.

Structure solution. All non-H atoms found by direct methods[11] and refined with individual isotropic thermal parameters by full-matrix least squares.[12] Atoms of both crystallographically independent [$NMe_3(CH_2Ph)$]$^+$ ions ordered. However, in both [$C_2B_9H_{12}$]$^-$ ions disorder noted over all 12 vertices of approximate icosahedra. Impossible satisfactorily to model disorder and unambiguously identify cage carbon atoms (all cage atoms modelled as B). Refinement terminated at R = 0.157 5, unit weights. Co-ordinates of refined atoms deposited as Supplementary Data.

† The cation consists of an O-protonated dmso molecule to which a second dmso is hydrogen bonded *via* the O(1)–H(O) · · · O(2) bridge. The hydrogen bond is of a conventional type[18] with O(1)–H(O) 0.95(4), O(2) · · · H(O) 1.45(4)Å, and O(1)–H(O) · · · O(2) 172(4)°. There is a small (0.01Å) but statistically significant difference in the S–O bond lengths, that to the protonated oxygen being the longer. Overall, the cation has effective C_s molecular symmetry.

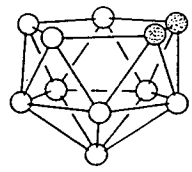

(IV)

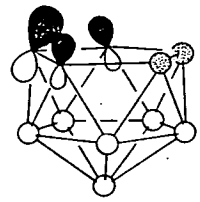

(V)

Consistent with other studies,[8,9] the *endo* B–H bond appears to be a little longer than *exo* B–H bonds involving similarly connected boron atoms, but even though the present study is an accurate one the estimated standard deviations (e.s.d.s) on B–H distances are sufficiently high to preclude further comment. The H(10)–B(10)–H(12) angle, 109.7(19)°, is, within experimental error, the tetrahedral ideal, and H(12) is evenly distanced from B(9) and B(11), 1.71(3)Å in each case. The lengths of the B(9)–B(10) and B(10)–B(11) edges are typical of those of unbridged connectivities.[20]

Thus, the key result from the crystallographic study is that anion (I) has the $\{BH_2\}$-containing structure (I), and therefore by implication that this, and not forms (II) or (III), is the preferred, ground-state structure, at least in the solid.*

This conclusion is fully consistent with the form of the highest occupied molecular orbital (h.o.m.o.) of $[7,8\text{-}C_2B_9H_{11}]^{2-}$. The frontier orbitals of $[C_2B_9H_{11}]^{2-}$, as given by extended-Hückel m.o. calculation, have been reported previously.[21] For the present purposes we have repeated this calculation using the $\{C_2B_9H_{11}\}$ fragment derived crystallographically above [by removal of H(12), line diagram (IV)] and performing the calculation, using the ICON8 program[22] and the weighted H_{ij} formula,[23] with full charge iteration (including Madelung correction) on all atoms. The h.o.m.o., an *a'* m.o., is localised on B(10) (41%) and B(9) and B(11) (13% on each), and these contributions are sketched in (V). The components from these atoms are *s–p* hybrids, outward pointing from the open face. Clearly, the preferred site of protonation of $[7,8\text{-}C_2B_9H_{11}]^{2-}$ is above B(10), slightly inside the upward projection of the pentagonal face, to afford the *endo*-H atom revealed by the crystallographic study.

In addition to affording an understanding of the experimental finding of an *endo*-H atom in anion (I), we find that the results of extended-Hückel m.o. calculations also allow some rationalisation of the relative magnitudes of *endo* and *exo* B–H coupling constants. Thus, a calculation on $[C_2B_9H_{12}]^-$ reveals < B(2*s*)/*exo*-H(1*s*) > overlap integrals in the range 0.520—0.605, whereas that between B(10)(2*s*) and H(12)(1*s*) is only 0.506. Moreover, significant overlap integrals (0.277) are calculated between B(9,11)(2*s*) and H(12)(1*s*), in keeping with the small but real interaction between H(12) and B(9) and B(11) that was detected by the $^1H\text{-}\{^{11}B, \text{selective}\}$ n.m.r. experiments.

* *Note added in proof*: The *endo* terminal position of H(12) in $[7,8\text{-}C_2B_9H_{12}]^-$ has been independently determined (see following paper), *via* n.m.r. spectroscopic studies.

Acknowledgements

We thank the S.E.R.C. and the S.E.D for support, and Dr. S. G. D. Henderson for some spectra.

References

1 R. A. Wiersboeck and M. F. Hawthorne, *J. Am. Chem. Soc.*, 1964, **86**, 1642.
2 M. F. Hawthorne, D. C. Young, P. M. Garrett, D. A. Owen, S. G. Schwerin, F. N. Tebbe, and P. A. Wegner, *J. Am. Chem. Soc.*, 1968, **90**, 862.
3 M. F. Hawthorne, D. C. Young, and P. A. Wegner, *J. Am. Chem. Soc.*, 1965, **87**, 1818.
4 M. F. Hawthorne, D. C. Young, T. D. Andrews, D. V. Howe, R. L. Pilling, A. D. Pitts, M. Reintjes, L. F. Warren, jun., and P. A. Wegner, *J. Am. Chem. Soc.*, 1968, **90**, 879.
5 K. Wade, *Adv. Inorg. Chem. Radiochem.*, 1976, **18**, 1.
6 R. E. Williams, *Adv. Inorg. Chem. Radiochem.*, 1976, **18**, 67.
7 For example; T. P. Onak, 'Comprehensive Organometallic Chemistry,' eds. G. Wilkinson, F. G. A. Stone, and E. W. Abel, Pergamon, Oxford, 1982; N. N. Greenwood and A. Earnshaw, 'Chemistry of the Elements,' Pergamon, Oxford, 1984.
8 J. S. Beck, W. Quintana, and L. G. Sneddon, *Organometallics*, 1988, **7**, 1015.
9 T. D. Getman, J. A. Krause, and S. G. Shore, *Inorg. Chem.*, 1988, **27**, 2398.
10 G. B. Jacobsen, D. G. Meina, J. H. Morris, C. Thomson, S. J. Andrews, D. Reed, A. J. Welch, and D. F. Gaines, *J. Chem. Soc., Dalton Trans.*, 1985, 1645.
11 G. M. Sheldrick, University of Göttingen, 1986.
12 G. M. Sheldrick, University of Cambridge, 1976.
13 N. G. Walker and D. Stuart, *Acta Crystallogr., Sect. A*, 1983, **39**, 158.
14 R. O. Gould and D. E. Smith, University of Edinburgh, 1986.
15 R. O. Gould and P. Taylor, University of Edinburgh, 1986.
16 P. D. Mallinson and K. W. Muir, *J. Appl. Crystallogr.*, 1985, **18**, 51.
17 See, for example, G. K. Barker, N. R. Godfrey, M. Green, H. E. Parge, F. G. A. Stone, and A. J. Welch, *J. Chem. Soc., Chem. Commun.*, 1983, 277.
18 J. Emsley, *Chem. Soc. Rev.*, 1980, **9**, 91.
19 D. E. Smith and A. J. Welch, *Acta Crystallogr., Sect. C*, 1986, **42**, 1717 and refs. therein.
20 G. F. Mitchell and A. J. Welch, *J. Chem. Soc., Dalton Trans.*, 1987, 1017.
21 D. M. P. Mingos, *J. Chem. Soc., Dalton Trans.*, 1977, 602.
22 J. Howell, A. Rossi, D. Wallace, K. Haraki, and R. Hoffmann, Quantum Chemistry Program Exchange, University of Indiana, 1977, no. 344.
23 J. H. Ammeter, H-B. Burgi, J. C. Thibeault, and R. Hoffmann, *J. Am. Chem. Soc.*, 1982, **100**, 3686.

Received 24*th April* 1989; *Paper* 9/01707K

Acta Cryst. (1988). C44, 1648–1650

Structure of 10,11-μ-Hydro-9-dimethylsulfido-7,8-dicarba-*nido*-undecaborane(11)

BY JILL COWIE, EWAN J. M. HAMILTON, JILL C. V. LAURIE AND ALAN J. WELCH

Department of Chemistry, University of Edinburgh, Edinburgh EH9 3JJ, Scotland

(*Received* 7 *March* 1988; *accepted* 10 *May* 1988)

Abstract. $C_4H_{17}B_9S$, $M_r = 194{\cdot}53$, triclinic, $P\bar{1}$, $a = 8{\cdot}7912\ (14)$, $b = 12{\cdot}093\ (5)$, $c = 12{\cdot}5617\ (19)$ Å, $\alpha = 107{\cdot}53\ (3)$, $\beta = 101{\cdot}019\ (13)$, $\gamma = 106{\cdot}10\ (3)°$, $V = 1167{\cdot}2\ (8)$ Å^3, $Z = 4$, $D_x = 1{\cdot}107$ Mg m^{-3}, Mo $K\alpha$, $\lambda = 0{\cdot}71069$ Å, $\mu = 0{\cdot}213$ mm^{-1}, $F(000) = 408$, 291 K, $R = 0{\cdot}0480$ for 3580 observed reflections. There are two crystallographically independent molecules in the asymmetric fraction of the unit cell, which differ in respect of the torsion about the B(9)—S bond. The μ-H atom bridges the B(10)—B(11) connectivity asymmetrically, favouring B(10), the less positively charged boron [average μ-H—B(10) 1·165, average μ-H—B(11) 1·35 Å].

0108-2701/88/091648-03$03.00

Introduction. The synthesis of the title compound (1) was reported ten years ago (Plesek, Janousek & Hermanek, 1978). Spectroscopic study indicated that the SMe_2 unit was bound to B(9) of the *nido*-icosahedral {7,8-C_2B_9} polyhedron, but the position of the bridging H atom (shown to be either 9,10 or 10,11 bridging) was not unambiguously determined.

We are interested in (1) as a precursor of [9-SMe_2-*nido*-7,8-$C_2B_9H_{10}]^-$, a monoanionic carbaborane fully analogous to the ubiquitous $[C_5H_5]^-$ ligand. Since the position of the μ-H atom in (1) may be important in the formation and structure of metal complexes of its anion, we have undertaken the present study.

Table 1. *Coordinates of refined atoms and equivalent isotropic thermal parameters*

$$U_{eq} = \frac{1}{3}\sum_i\sum_j U_{ij} a_i^* a_j^* \mathbf{a}_i.\mathbf{a}_j$$

	x	y	z	U_{eq}(Å²)
S(*a*)	0·28339 (6)	0·50594 (6)	0·74844 (5)	0·0543 (4)
CS(1*a*)	0·4092 (3)	0·5721 (3)	0·89584 (21)	0·0680 (19)
CS(2*a*)	0·3532 (4)	0·6307 (4)	0·7025 (3)	0·125 (4)
B(1*a*)	−0·2536 (3)	0·4679 (3)	0·6394 (3)	0·0592 (19)
B(2*a*)	−0·3199 (3)	0·4313 (3)	0·7506 (3)	0·0651 (21)
B(3*a*)	−0·2555 (3)	0·3274 (3)	0·6577 (3)	0·0676 (21)
B(4*a*)	−0·0869 (3)	0·4149 (3)	0·62429 (25)	0·0571 (19)
B(5*a*)	−0·0453 (2)	0·57396 (25)	0·70139 (22)	0·0502 (17)
B(6*a*)	−0·1908 (3)	0·5851 (3)	0·78330 (25)	0·0562 (18)
C(7*a*)	−0·1847 (3)	0·37267 (25)	0·8065 (3)	0·0729 (21)
C(8*a*)	−0·0531 (3)	0·36857 (23)	0·74344 (24)	0·0630 (18)
B(9*a*)	0·0701 (3)	0·49794 (23)	0·75785 (21)	0·0453 (16)
B(10*a*)	0·0197 (3)	0·6129 (3)	0·85526 (23)	0·0501 (17)
B(11*a*)	−0·1544 (4)	0·5147 (3)	0·8862 (3)	0·0680 (22)
S(*b*)	−0·22948 (7)	0·87045 (6)	0·66900 (6)	0·0658 (5)
CS(2*b*)	−0·3046 (4)	0·9752 (3)	0·6194 (3)	0·0884 (24)
CS(1*b*)	−0·2613 (4)	0·7515 (3)	0·5314 (3)	0·0815 (22)
B(1*b*)	0·2735 (4)	1·1753 (3)	0·8471 (3)	0·0690 (22)
B(2*b*)	0·3982 (4)	1·0923 (3)	0·8717 (3)	0·0773 (24)
B(3*b*)	0·2494 (5)	1·0956 (3)	0·9435 (3)	0·0805 (25)
B(4*b*)	0·0719 (4)	1·0921 (3)	0·8466 (3)	0·0665 (21)
B(5*b*)	0·1156 (3)	1·08273 (25)	0·71294 (24)	0·0551 (18)
B(6*b*)	0·3212 (4)	1·0805 (3)	0·7275 (3)	0·0673 (21)
C(7*b*)	0·2717 (3)	0·9598 (3)	0·8719 (3)	0·0751 (21)
C(8*b*)	0·0923 (3)	0·95489 (24)	0·85366 (21)	0·0628 (18)
B(9*b*)	0·0036 (3)	0·94901 (23)	0·72891 (22)	0·0483 (16)
B(10*b*)	0·1446 (3)	0·9414 (3)	0·64557 (25)	0·0579 (19)
B(11*b*)	0·3233 (4)	0·9442 (3)	0·7531 (4)	0·0776 (25)
H(1*a*)	−0·347 (4)	0·472 (3)	0·564 (3)	
H(2*a*)	−0·444 (4)	0·397 (3)	0·7522 (25)	
H(3*a*)	−0·330 (4)	0·236 (3)	0·601 (3)	
H(4*a*)	−0·064 (4)	0·386 (3)	0·545 (3)	
H(5*a*)	−0·003 (4)	0·644 (3)	0·667 (3)	
H(6*a*)	−0·238 (4)	0·664 (3)	0·800 (3)	
H(7*a*)	−0·219 (4)	0·310 (3)	0·832 (3)	
H(8*a*)	−0·012 (4)	0·285 (3)	0·731 (3)	
H(10*a*)	0·107 (4)	0·709 (3)	0·913 (3)	
H(11*a*)	−0·186 (4)	0·547 (3)	0·965 (3)	
H(**a*)	0·006 (4)	0·545 (3)	0·900 (3)	
H(1*b*)	0·327 (4)	1·274 (3)	0·875 (3)	
H(2*b*)	0·524 (4)	1·127 (3)	0·917 (3)	
H(3*b*)	0·272 (4)	1·130 (3)	1·037 (3)	
H(4*b*)	−0·024 (4)	1·128 (3)	0·883 (3)	
H(5*b*)	0·064 (4)	1·123 (3)	0·653 (3)	
H(6*b*)	0·399 (4)	1·118 (3)	0·670 (3)	
H(7*b*)	0·303 (4)	0·926 (3)	0·922 (3)	
H(8*b*)	0·031 (4)	0·913 (3)	0·893 (3)	
H(10*b*)	0·116 (4)	0·902 (3)	0·548 (3)	
H(11*b*)	0·416 (4)	0·900 (3)	0·727 (3)	
H(**b*)	0·170 (4)	0·860 (3)	0·677 (3)	

Table 2. *Interatomic distances* (Å)

S(*a*)–CS(1*a*)	1·768 (3)	S(*b*)–CS(2*b*)	1·792 (4)
S(*a*)–CS(2*a*)	1·770 (4)	S(*b*)–CS(1*b*)	1·797 (3)
S(*a*)–B(9*a*)	1·879 (3)	S(*b*)–B(9*b*)	1·889 (3)
B(1*a*)–B(2*a*)	1·740 (5)	B(1*b*)–B(2*b*)	1·724 (5)
B(1*a*)–B(3*a*)	1·778 (5)	B(1*b*)–B(3*b*)	1·769 (5)
B(1*a*)–B(4*a*)	1·774 (4)	B(1*b*)–B(4*b*)	1·777 (5)
B(1*a*)–B(5*a*)	1·777 (4)	B(1*b*)–B(5*b*)	1·768 (5)
B(1*a*)–B(6*a*)	1·795 (4)	B(1*b*)–B(6*b*)	1·793 (5)
B(1*a*)–H(1*a*)	1·15 (3)	B(1*b*)–H(1*b*)	1·07 (3)
B(2*a*)–B(3*a*)	1·740 (5)	B(2*b*)–B(3*b*)	1·728 (6)
B(2*a*)–B(6*a*)	1·762 (5)	B(2*b*)–B(6*b*)	1·757 (5)
B(2*a*)–C(7*a*)	1·690 (5)	B(2*b*)–C(7*b*)	1·679 (5)
B(2*a*)–B(11*a*)	1·800 (5)	B(2*b*)–B(11*b*)	1·796 (5)
B(2*a*)–H(2*a*)	1·06 (3)	B(2*b*)–H(2*b*)	1·04 (3)
B(3*a*)–B(4*a*)	1·769 (5)	B(3*b*)–B(4*b*)	1·768 (5)
B(3*a*)–C(7*a*)	1·712 (5)	B(3*b*)–C(7*b*)	1·704 (5)
B(3*a*)–C(8*a*)	1·740 (5)	B(3*b*)–C(8*b*)	1·738 (5)
B(3*a*)–H(3*a*)	1·05 (3)	B(3*b*)–H(3*b*)	1·08 (3)
B(4*a*)–B(5*a*)	1·767 (4)	B(4*b*)–B(5*b*)	1·771 (5)
B(4*a*)–C(8*a*)	1·752 (4)	B(4*b*)–C(8*b*)	1·744 (5)
B(4*a*)–B(9*a*)	1·749 (4)	B(4*b*)–B(9*b*)	1·757 (4)
B(4*a*)–H(4*a*)	1·03 (3)	B(4*b*)–H(4*b*)	1·16 (3)
B(5*a*)–B(6*a*)	1·797 (4)	B(5*b*)–B(6*b*)	1·790 (5)
B(5*a*)–B(9*a*)	1·736 (4)	B(5*b*)–B(9*b*)	1·736 (4)
B(5*a*)–B(10*a*)	1·779 (4)	B(5*b*)–B(10*b*)	1·776 (4)
B(5*a*)–H(5*a*)	1·07 (3)	B(5*b*)–H(5*b*)	1·11 (3)
B(6*a*)–B(10*a*)	1·785 (4)	B(6*b*)–B(10*b*)	1·788 (5)
B(6*a*)–B(11*a*)	1·775 (5)	B(6*b*)–B(11*b*)	1·777 (5)
B(6*a*)–H(6*a*)	1·13 (3)	B(6*b*)–H(6*b*)	1·19 (3)
C(7*a*)–C(8*a*)	1·525 (4)	C(7*b*)–C(8*b*)	1·531 (4)
C(7*a*)–B(11*a*)	1·623 (5)	C(7*b*)–B(11*b*)	1·613 (5)
C(7*a*)–H(7*a*)	0·91 (3)	C(7*b*)–H(7*b*)	0·88 (3)
C(8*a*)–B(9*a*)	1·571 (4)	C(8*b*)–B(9*b*)	1·582 (4)
C(8*a*)–H(8*a*)	1·14 (3)	C(8*b*)–H(8*b*)	0·94 (3)
B(9*a*)–B(10*a*)	1·775 (4)	B(9*b*)–B(10*b*)	1·773 (4)
B(10*a*)–B(11*a*)	1·843 (5)	B(10*b*)–B(11*b*)	1·851 (5)
B(10*a*)–H(10*a*)	1·12 (3)	B(10*b*)–H(10*b*)	1·12 (3)
B(10*a*)–H(**a*)	1·11 (3)	B(10*b*)–H(**b*)	1·22 (3)
B(11*a*)–H(11*a*)	1·07 (3)	B(11*b*)–H(11*b*)	1·14 (3)
B(11*a*)–H(**a*)	1·31 (3)	B(11*b*)–H(**b*)	1·39 (3)

Experimental. Compound prepared according to the literature (Plesek, Janousek & Hermanek, 1978), and purity checked by microanalysis (C, H) and NMR spectroscopies (^{1}H, ^{11}B{^{1}H}); crystals suitable for diffraction study obtained by solvent diffusion (CH_2Cl_2–*n*-hexane) at 291 K; colourless block, *ca* 0·3 × 0·3 × 0·4 mm mounted on glass fibre and set on Enraf–Nonius CAD-4 diffractometer (Mo $K\alpha$ X-radiation, graphite monochromator); cell parameters and orientation matrix from least-squares refinement of θ values ($14 < \theta < 15°$) of 25 centred reflections; data collection by ω–2θ scans in 96 steps with ω scan width $(0{\cdot}8 + 0{\cdot}34\tan\theta)°$; data ($h$:0 to 10, k:−14 to 14, l:−14 to 14) measured for $1 \le \theta \le 25°$ over 92 X-ray hours; no detectable crystal decay or movement; corrections for Lorentz and polarization effects applied (Gould & Smith, 1986), but not for absorption; 4390 independent reflections measured, 3580 $[F \ge 2{\cdot}0\sigma(F)]$ retained; structure solution using automatic direct methods (Sheldrick, 1986), and iterative full-matrix least-squares refinement (on F)/ΔF syntheses (Sheldrick, 1976); cage C atoms assigned by a combination of short C–C distance and low isotropic thermal parameters after refinement as B; weights assigned according to $w^{-1} = [\sigma^2(F) + 0{\cdot}00002F^2]$; all non-H atoms allowed anisotropic thermal motion; cage H atoms positionally refined, and methyl H atoms treated as part of rigid groups (giving sensible S–C–H angles); all H atoms given an overall isotropic thermal parameter, 0·095(16) Å² at convergence; No. of variables 320; data:variable ratio >11:1; $R = 0{\cdot}0480$, $R' = 0{\cdot}0650$, $S = 1{\cdot}714$; max. shift/e.s.d. in final cycle <0·1; max. and min. residues in final ΔF synthesis 0·522 and −0·233 e Å^{-3}; scattering factors inlaid in *SHELX*76; all calculations performed on Amdahl 470 V/8 computer.

Discussion. Table 1* lists final atomic coordinates and (for non-H atoms) equivalent isotropic thermal parameters. Interatomic distances are given as Table 2. There

* Lists of structure factors, idealized H-atom coordinates, anisotropic thermal parameters and bond angles have been deposited with the British Library Document Supply Centre as Supplementary Publication No. SUP 51017 (27 pp.). Copies may be obtained through The Executive Secretary, International Union of Crystallography, 5 Abbey Square, Chester CH1 2HU, England.

are two crystallographically independent molecules in the asymmetric unit, *a* and *b*. The root-mean-square misfit (Gould & Taylor, 1986) of the $\{C_2B_9S\}$ fragments of *a* and *b* is only 0·016 Å, but this increases substantially (0·209 Å) if the C_{methyl} atoms are also included. Hence *a* and *b* differ only in respect of the torsion about the B(9)–S bond. For *a* C(8)–B(9)–S–CS(1) is −100·01 (20)°; for *b* the equivalent torsion is −123·22 (21)°. Plesek *et al.* (1978) noted two CH_3 resonances in the ^1H NMR spectrum of (1), and interpreted this as indicating no free rotation of the SMe_2 unit about the B(9)–S bond. However, the methyl groups of (1) are magnetically inequivalent whatever the torsion about the B–S bond (as long as inversion at S does not occur), so the extent of rotation about this bond in solution remains unknown. It would be surprising, however, if such rotation were restricted at ambient temperature.

In the crystal there are no intermolecular contacts closer than the van der Waals sums of atoms. Fig. 1 presents a perspective view of molecule *a*, and Fig. 2 views the same molecule from a position directly above

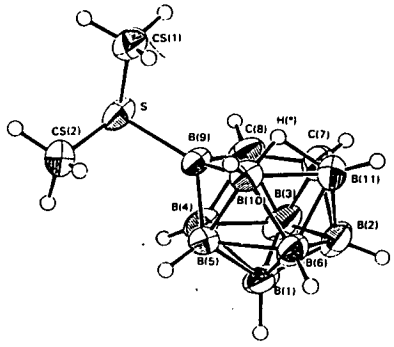

Fig. 1. Perspective view of molecule *a* of $[9\text{-}SMe_2\text{-}nido\text{-}7,8\text{-}C_2B_9H_{11}]$ (1) (Mallinson, 1982) showing the atomic numbering scheme.

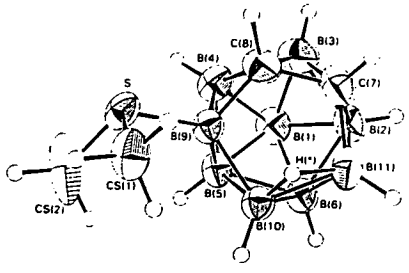

Fig. 2. View of molecule *a* from above the open five-atom face, clearly demonstrating the conformation of the pendant SMe_2 group. In molecule *b* there is a *ca* 23° relative twist about the B(9)–S bond.

the open five-atom face. The crystallographic study clearly defines the H-bridging site as the B(10)–B(11) connectivity. The bridges are significantly asymmetric, favouring B(10) in both independent molecules. Specifically, H(*)–B(10) is 1·11 (3) and H(*)–B(11) 1·31 (3) Å in *a*, and 1·22 (3) and 1·39 (3) Å respectively in *b*. In contrast, the B–H–B bridge in $[8\text{-}SMe_2\text{-}nido\text{-}7,9\text{-}C_2B_9H_{11}]$ [a structural isomer of (1)] is symmetric (Šubrtová, Novák, Linek & Hašek, 1984). The asymmetry in (1) can be readily understood in terms of the protonic nature of bridging H atoms and the relative electronegativity of the (cage) C atoms. Charge-iterated extended Hückel molecular orbital calculations (Howell, Rossi, Wallace, Haraki & Hoffmann, 1977) on idealized models of $[nido\text{-}7,8\text{-}C_2B_9H_{11}]^{2-}$ and $[9\text{-}SH_2\text{-}nido\text{-}7,8\text{-}C_2B_9H_{10}]^-$ suggest that in (1) B(10) is substantially more negative than B(11), but indicate that this arises primarily from the non-adjacency of cage carbon atoms rather than any effect caused by the SMe_2 group pendant to B(9).

All other molecular parameters in (1) are as expected. The B–S distance [ave. 1·884 (4) Å] agrees well with those previously reported (*e.g.* Šubrtová *et al.*, 1984; Schramm & Ibers, 1977; Mizusawa, Rudnick & Eriks, 1980). Future contributions will report the structural consequences of deprotonation and isolobal substitution of the μ-H atom of (1), and the results of synthetic and structural studies on η-bonded transition metal and actinide complexes of $[9\text{-}SMe_2\text{-}nido\text{-}7,8\text{-}C_2B_9H_{10}]^-$.

We thank the SED (JC) and SERC (EJMH) for support.

References

Gould, R. O. & Smith, D. E. (1986). *CADABS*. Program for data reduction. Univ. of Edinburgh, Scotland.

Gould, R. O. & Taylor, P. (1986). *CALC*. Program for molecular geometry calculations. Univ. of Edinburgh, Scotland.

Howell, J., Rossi, A., Wallace, D., Haraki, K. & Hoffmann, R. (1977). *ICON*8. Program for extended Hückel molecular calculations. Quantum Chemistry Program Exchange, Univ. of Indiana, USA.

Mallinson, P. (1982). *EASYORTEP*. An easy-to-use version of *ORTEP*II. Univ. of Glasgow, Scotland.

Mizusawa, E., Rudnick, S. E. & Eriks, K. (1980). *Inorg. Chem.* **19**, 1188–1191.

Plesek, J., Janousek, Z. & Hermanek, S. (1978). *Collect. Czech. Chem. Commun.* **43**, 2862–2868.

Schramm, K. D. & Ibers, J. A. (1977). *Inorg. Chem.* **16**, 3287–3293.

Sheldrick, G. M. (1976). *SHELX*76. Program for crystal structure determination. Univ. of Cambridge, England.

Sheldrick, G. M. (1986). *SHELX*86. Program for crystal structure determination. Univ. of Göttingen, Federal Republic of Germany.

Šubrtová, V., Novák, C., Linek, A. & Hašek, J. (1984). *Acta Cryst.* C**40**, 1955–1956.